HIGH RESOLUTION INFRARED SPECTROSCOPY OF CH_3F, CD_3I, AND CD_3Br AND INFRARED-RADIOFREQUENCY DOUBLE RESONANCE SPECTROSCOPY OF CD_3I AND CD_3Br

By

Han-Gook Cho

A DISSERTATION

Submitted to
Michigan State University
in partial fulfillment of the requirements
for the degree of

DOCTOR OF PHILOSOPHY

Department of Chemistry

1989

ABSTRACT

HIGH RESOLUTION INFRARED SPECTROSCOPY OF CH_3F, CD_3I, AND CD_3Br AND INFRARED-RADIOFREQUENCY DOUBLE RESONANCE SPECTROSCOPY OF CD_3I AND CD_3Br

By

Han-Gook Cho

The $\nu_3+\nu_6-\nu_6$ band of CH_3F and the ν_2 bands of CD_3I and CD_3Br have been recorded by means of an infrared microwave sideband laser (IMSL) spectrometer and analyzed by vibration-rotation theory including coupling with nearby vibrational states. The frequency measurement and analysis were performed in order to obtain frequency information for subsequent double resonance studies as well as to investigate the effect of various energy couplings. It has been possible to record the lineshapes of high J and K transitions at Doppler-limited resolution and to use the measured frequencies to determine molecular constants including high order centrifugal distortion constants for the ground and excited vibrational states. In the infrared spectrum of CH_3F the high resolution allowed, in addition to the measurement of conventional transitions, the observation of 14 ℓ-type doublets between two degenerate vibrational states. As a result, the infrared frequencies in the $\nu_3+\nu_6-\nu_6$ band can be reproduced with the molecular constants to within a few MHz, which is accurate enough for most double resonance studies. In CD_3I and CD_3Br analysis of the ν_2 vibration-rotation

structure also led to molecular constants that can predict the frequencies to within a few MHz. These frequencies were used for double resonance experiments in this work.

Infrared-radiofrequency double resonance, which has already been recognized as a very sensitive and precise method for the observation of various hyperfine energy structures, was used to record pure quadrupole transitions of CD_3I and CD_3Br for the ground and the ν_2 vibrational states. The data were analyzed by means of exact diagonalization of the total Hamiltonian matrix composed of the rotational and quadrupole interaction parts. The IMSL spectrometer employed as the infrared pumping source had sufficient tunability to make it possible to select for study an appropriate set of transitions without having to depend on accidental coincidences with laser lines. Consequently, it was possible to make precise measurements of a large number of transitions and to determine the spin-rotation constants as well as the centrifugal distortion constants for the quadrupole coupling in these molecules.

During the fitting of the frequencies of the pure quadrupole spectra, it became evident that some effect was causing an apparent shift of the transitions, especially at low RF-frequencies. The shift has been traced to a double-resonance effect that appears in calculations when four interacting levels are taken into account, but is not evident in calculations based on the usual three-level system employed for double-resonance theory. An appropriate linear equation was set up in the density matrix formalism for the four-interacting-level system, and solved at each RF-frequency for a sequence of values of the molecular velocity and for a fixed value of the laser frequency. The agreement between the experimental and the calculated spectra

obtained for both the frequency shift and the distorted lineshape strongly confirms the four-interacting-level double-resonance effect.

To the Memory of Bo-Kyoung

ACKNOWLEDGMENTS

I would like to thank Dr. R. H. Schwendeman for his guidance and encouragement throughout the course of this study and the preparation of this thesis. I wish to thank the other members of our group for their cooperation in the laboratory.

The partial support from the National Science Foundation is gratefully acknowledged.

TABLE OF CONTENTS

LIST OF TABLES

LIST OF FIGURES

CHAPTER I

INTRODUCTION

Studies of the vibrational-rotational spectra of polyatomic molecules in the gaseous phase provide considerable information including intermolecular distances and angles, the vibrational frequencies and force constants, dissociation energies, and other data concerning the structures of the molecules. The information attainable from studies of the vibrational-rotational spectra of polyatomic molecules has recently been greatly increased by the advent of laser spectroscopy and by considerable progress in the theoretical and experimental studies of the fine structure of the vibrational-rotational spectra of molecules. For the research reported in this dissertation, high resolution spectroscopy was performed for the purpose of obtaining frequency information for subsequent double resonance studies as well as for examination of the effect of various energy couplings. The purpose of this "Introduction" is to provide an outline of the organization of this dissertation. More details concerning the reasons for carrying out the work, results of previous studies, etc., are given in the chapters describing each project.

Chapter II presents the high resolution infrared spectroscopy of the $\nu_3+\nu_6-\nu_6$ band of $^{12}CH_3F$ by means of an infrared microwave sideband laser (IMSL) spectrometer. This band is located in the vibrational spectrum of CH_3F in the important 10 μm region, which has been the

subject of many high resolution studies. Moreover, this band is of interest because it appears to be the first example of a high-resolution infrared study of an E←E band in a prolate C_{3v} symmetric top. More than 200 transitions with J and K values up to 20 and 10, respectively, have been identified and their frequencies measured to an accuracy of a few MHz. Among the identified transitions are the components of 14 ℓ-type doublets in this hot band of E←E symmetry. The spectra have been fit to experimental accuracy by adjusting rotational parameters including centrifugal distortion constants through the sixth order as well as Coriolis coupling and ℓ-resonance parameters.

In Chapter III, high resolution infrared studies of the ν_2 bands of CD_3I, $CD_3{}^{79}Br$, and $CD_3{}^{81}Br$ are described. About 200 transitions for each species have been recorded and the frequencies have been determined to an accuracy of few MHz. The frequencies in these parallel bands have been fit by least squares to an energy expression containing centrifugal distortion parameters up to the eighth order. The strong Coriolis interaction with the ν_5 band has been taken into account in each case by using previously-reported parameters for the interaction and for the ν_5 band (for CD_3I, interaction with the $2\nu_3$ state has been also included). The resulting combination of the ν_2 parameters obtained in this work and the parameters from previous work is sufficient for each molecule to predict the ν_2-band frequencies up to high J and K (~40 and ~10) within a few MHz.

Radiofrequency spectroscopy is known to be a powerful tool for investigation of various hyperfine energy structures. However, the scope of the technique has been seriously limited by the density of the spectra and the poor signal-to-noise ratio. When infrared-

radiofrequency double resonance was introduced, which involves the simultaneous application of two fields of radiation to the sample, radiofrequency spectroscopy could be performed with greatly enhanced sensitivity and selectivity. In infrared-radiofrequency double resonance, hyperfine resonances are observed as a steady-state change in absorption of laser power simply due to the change in the population difference between the excited and ground states as the RF frequency passes through resonance. A molecular population change is made possible by pumping molecules from the ground state to the upper vibrational state by means of a strong infrared laser field which is resonant with an infrared transition. When the RF-field is resonant with the hyperfine levels, infrared absorption is increased by equilibrating the populations of the hyperfine energy states.

The development of IR-RF double resonance spectroscopy in the last two decades has made it possible to determine the values of a large number of parameters for hyperfine states, and many of these can be used for the investigation of the electron distribution in molecules. These parameters are usually measures of weak interaction occurring between atomic nuclei having electric quadrupole moments and electrons, and as such yield information about the electronic structure of the molecule. As will be seen in Chapter IV, the nuclear quadrupole coupling energy is given as the inner product of the nuclear quadrupole tensor and the electrostatic field-gradient tensor evaluated at the nucleus. Such an inner product depends on the mutual orientation of the two axis systems to which the two tensors are referred; for the nuclear quadrupole tensor, the natural system is one in which one axis coincides with the spin axis of the nucleus. The interest in quadrupole coupling constants

lies in the different values of the field gradient seen by a given nucleus in different molecular environments. The electric field gradient at the nucleus may be extracted from the quadrupole interaction energy represented by the quadrupole coupling constants, by dividing by the appropriate nuclear quadrupole moment.

The IR-RF double resonance technique has been applied to the ν_2 and the ground vibrational states of CD_3I, $CD_3{}^{79}Br$, and $CD_3{}^{81}Br$ by using an IMSL as the infrared laser pump. The tunability of the laser allowed the selection of an appropriate set of transitions with a wide range of J and K quantum numbers without having to depend on accidental coincidences with laser lines; more than 150 pure quadrupole transitions for each species have been observed. To improve the accuracy of the frequency measurement, the RF radiation power was kept as low as is consistent with reasonably good signal-to-noise ratio, because IR-RF spectra are easily RF power broadened. The typical half width at half maximum for the transitions was as low as 70 and 100 kHz for CD_3I and CD_3Br, respectively. As a result, it was possible to determine the spin-rotation constants as well as the centrifugal distortion constants for the quadrupole couplings in these molecules. The theoretical and experimental details are described in Chapter IV.

During the IR-RF double resonance study stated above, it was realized that some effect was causing an apparent shift of the transitions that occur at low RF frequencies. This effect could be easily shown through the adjustment of parameters to fit the frequencies of the pure quadrupole spectra; experimental values for the two lowest radiofrequency transitions were found to be much closer together than predicted by the best values of the parameters. These shifts were

traced to a double-resonance effect that appears in calculations when four interacting levels are taken account, but is not evident in calculations based on the usual three-level system employed for double-resonance theory. The nature of the problem is described in detail in Chapter V. Essentially, it results from the fact that the hyperfine splittings in the upper state are not greatly different from those in the lower state for the double resonances in this work. As a result, quadrupole transitions of the upper and the lower vibrational states are often overlapped, and, generally, the lower frequencies are more seriously overlapped than the higher frequencies. Since both the upper and the lower states of the RF transitions are pumped by the strong infrared radiation and the RF radiation connects the hyperfine levels, the four levels must be considered as a four-interacting-level system.

An appropriate linear equation was set up in the density matrix formalism for the four-interacting-level system, and solved at each RF frequency for a sequence of values of the molecular velocity and a fixed value of the laser frequency; the resulting contributions to the absorption were multiplied by the appropriate Doppler weight and summed. The frequency shifts obtained by fitting the spectra calculated with estimated parameters show good agreement with the shifts observed experimentally. The details are described in Chapter V.

CHAPTER II

HIGH RESOLUTION INFRARED STUDY OF THE $\nu_3 + \nu_6 - \nu_6$ BAND OF $^{12}CH_3F$

II-1 Introduction

Methyl fluoride and ammonia, with their relatively simple rotational structure and strong spectra, have been considered as model compounds in the development of infrared high resolution spectroscopy. Especially, the vibrational spectrum of CH_3F in the 10 μm region has been the subject of a number of recent high-resolution infrared studies because the many strong transitions in this region include several that are in coincidence with CO_2 lasers, and therefore provide pumping sources for far-infrared lasers and for double-resonance effects. For this molecule, a series of spectroscopic works have been performed by means of infrared-microwave two-photon and infrared-microwave laser spectroscopy in our laboratory (1-3). As a result of extensive analyses for the ν_3 fundamental and $2\nu_3 - \nu_3$ hot bands of $^{12}CH_3F$ and $^{13}CH_3F$, transition frequencies can be calculated to within a few MHz with the reported molecular constants. The obtained information has been successfully applied to an infrared-infrared double-resonance study of collisional energy transfer including a determination of the change in velocity upon collision (4).

This chapter is concerned with a high resolution infrared study of the $\nu_3 + \nu_6 - \nu_6$ band (1039.1 cm^{-1}) of $^{12}CH_3F$ carried out with infrared

microwave sideband laser spectroscopy. Like other XYZ_3 type symmetric top molecules, CH_3F has three totally symmetric and three doubly degenerate vibrational bands. Among these, ν_3 is the totally symmetric C-F stretching band (1048.6 cm^{-1}), ν_6 the degenerate CH_3 rocking band (1182.7 cm^{-1}), and $\nu_3+\nu_6$ the combination band (2221.8 cm^{-1}). Although the upper and lower state energy levels of the $\nu_3 + \nu_6 - \nu_6$ band in CH_3F have been studied previously during investigations of other bands by infrared and microwave spectroscopy (5-9), the present work is the first extensive high-resolution study of this hot band.

Values for the vibrational energy and primary rotational parameters (A, B, and $A\zeta$) of the $v_6 = 1$ state were obtained by Smith and Mills from grating spectra taken at 0.2 - 0.4 cm^{-1} resolution (5). Hirota and his co-workers later determined B, $A\zeta\eta_K$, and $|q_6|$ by means of microwave spectroscopy (6,7). Later, Hirota, by means of diode laser spectroscopy, observed Q-branch transitions in the ν_6 band for J and K values up to 14 and 3, respectively (8). The frequencies of these transitions were used together with rotational frequencies to determine A, $A\zeta$, $A\zeta\eta_K$, the band center ($\nu_o + A\zeta^2$), and the sign of q_v for $v_6 = 1$.

A set of constants for the $\nu_3 + \nu_6$ state was determined by Nakagawa *et al.* from grating spectra taken at 0.06 cm^{-1} resolution (9). However, they were unable to assign $\Delta k = -1$ spectra and could not determine an accurate value for the ℓ-doubling constant q_v. A final piece of information on the spectrum of interest in the present work is the assignment of the $^{Q}Q(6,4)$ transition in the $\nu_3 + \nu_6 - \nu_6$ band by an optical-optical double resonance method by Duxbury and Kato (10).

In addition to its importance for double resonance experiments, the $\nu_3 + \nu_6 - \nu_6$ band is also of interest because it appears to be the first

example of a high-resolution infrared study of an E - E band in a prolate C_{3v} symmetric top. Previous high-resolution studies of transitions between doubly-degenerate vibrational states have included analyses of the D_{3h} molecule BF_3 (11) and the oblate C_{3v} molecules CF_3H (12)and CF_3D (13).

In the present study, infrared spectra of the $\nu_3 + \nu_6 - \nu_6$ band in $^{12}CH_3F$ have been recorded at Doppler-limited resolution ($\Delta\nu_D \equiv 34$ MHz) by an infrared microwave sideband laser spectrometer with a White-type long path absorption cell. The frequencies of more than 230 transitions have been measured to an accuracy of a few MHz. The measured frequencies include transition frequencies from 14 ℓ-type doublets which allow the determination of ℓ-type doubling constants for both the upper and the lower vibrational states. For this work, it was first necessary to identify all of the transitions of the fundamental ν_3 bands of $^{12}CH_3F$ and $^{13}CH_3F$ (which occurs in natural abundance) and of the $2\nu_3 - \nu_3$ hot band of $^{12}CH_3F$; the absorption lines in these bands dominate the spectra in this region. All of the observed transitions in the $\nu_3 + \nu_6 - \nu_6$ band that were assigned in the present study follow the selection rule, $\Delta k = 0$, $\Delta\ell = 0$. Spectra obeying other selection rules may also occur as a result of rotational ℓ-type resonances, but they have not yet been identified, probably because of exceedingly weak transition intensities. The spectra were fit to experimental accuracy by adjusting rotational parameters, including centrifugal distortion constants through the 6th order, diagonal Coriolis coupling parameters, and ℓ-doubling constants.

It is expected that the results of the present work will be applied to a subsequent energy transfer study between nearby vibrational states with predicted CO_2 laser coincidences. For this purpose, resolved ℓ-

type doublets may provide ideal two level systems which are similar to ammonia inversion doublets. The general theory for the present study is described briefly in the next section. The experimental details, analysis of the spectra, results of the study, and a discussion of the results follow in subsequent sections.

II-2 Theory

Investigations of the vibration-rotation spectra of polyatomic molecules in the gas phase have been of importance for determining precise molecular geometry and energy structure. With the advent of laser spectroscopy, both the resolution and feasibility of various types of experiments have been greatly improved. As a result, the importance of studies of the rovibrational states of polyatomic molecules has increased.

The quantum mechanical description of the electronic and nuclear motions should yield the vibrational, rotational, and electronic energy levels as well as the corresponding wave functions for the system. Since the electronic motion is so fast in comparison with the nuclear motion, at each point the electronic energy may be considered to have reached its equilibrium value corresponding to the nuclear geometry. Therefore, we are normally justified to employ the Born-Oppenheimer approximation which treats the nuclear and the electronic motion separately.

As a further approximation, the rigid rotor-harmonic oscillator may be employed to divide the Hamiltonian of nuclear motion into the vibrational and rotational parts, as follows:

$$H_n = H_t + H_r + H_v \ , \qquad (2\text{-}1)$$

where H_t is the Hamiltonian for molecular translation, H_r the rotational Hamiltonian, and H_v the vibrational Hamiltonian. With these

approximations, the energy of a molecule may be expressed simply by a sum of electronic, vibrational, rotational, and translational contributions;

$$E = E_e + E_v + E_r + E_t \ , \qquad (2\text{-}2)$$

where E_e, E_v, E_r, and E_t are the electronic, vibrational, rotational, and translational energies. Since this thesis is concerned with the vibration-rotation transitions in one electronic state, the electronic and translational parts will not be discussed further.

The rigid rotor approximation is of course not sufficient to analyze experimental data on vibrational-rotational transitions. Higher-order corrections for the vibrational-rotational interactions, the centrifugal effect of molecular rotation, and the anharmonicity of molecular vibrations must be introduced to utilize fully the wealth of information involved in the data of high resolution experiments.

The theoretical details will be discussed in this section especially for symmetric top molecules.

II-2-1 Hamiltonian for Harmonic Oscillator-Rigid Rotor Approximation

To a good approximation, the electronic and vibrational-rotational motions are normally separated in molecular spectroscopy. However, it is necessary to introduce further approximations because the Schrödinger equation is still too complicated to be solved exactly. Although these approximations are much cruder than the Born-Oppenheimer approximation, they are very important, since the known eigenfunctions will be used to

form the basis vectors for higher variation or perturbation calculations.

As the first approximation, it is assumed that the vibrational displacements of the atomic nuclei in rigid molecules are limited in a small region around the equilibrium configuration. Hence the molecule keeps the equilibrium moment of inertia by neglecting the vibrational dependence:

$$H_{vr} = \sum_{\alpha=x,y,z} (J_\alpha - P_\alpha)^2 / 2I^o_{\alpha\alpha} + \Sigma P_k^2 /2 + V_k \qquad (2\text{-}3)$$

where P_k is vibrational momentum, J_α and P_α are rotational and vibrational angular momenta, and $I^o_{\alpha\alpha}$ is a moment of inertia along a molecular principal axis. As a further approximation, both the vibrational angular momentum and the anharmonicity are neglected. The obtained Hamiltonian operator for this case is

$$H^o_{vr} = \frac{1}{2}\left[\frac{J_x^2}{I^o_{xx}} + \frac{J_y^2}{I^o_{yy}} + \frac{J_z^2}{I^o_{zz}} \right] + \frac{1}{2} \sum_{k=1}^{3N-6} \left[P_k^2 + \lambda_k Q_k^2 \right] . \qquad (2\text{-}4)$$

II-2-1-1 Harmonic Oscillator

The harmonic oscillator leads to a wave equation for the nonlinear molecule that can be written in the form

$$-\frac{1}{2}\sum_{k=1}^{3N-6}\left[\hbar^2\frac{\partial^2\Psi_v^o}{\partial Q_k^2}-\lambda_k Q_k^2\Psi_v^o\right]=E_v^o\,\Psi_v^o \qquad (2\text{-}5)$$

where Q_k is the normal coordinate of the k-th mode of frequency $\nu_k=\lambda_k^{1/2}/2\pi$, E_v^o is the vibrational energy, and Ψ_v^o is the vibrational wave function depending on the normal coordinates.

It is convenient to introduce dimensionless normal coordinates q_k and corresponding operators of linear momenta p_k which are defined by the equations

$$q_k=\left(\frac{\lambda_k}{\hbar^2}\right)^{1/2}Q_k \qquad (2\text{-}6)$$

$$p_k\left(\equiv -i\frac{\partial}{\partial q_k}\right)=\lambda_k^{-1/4}\,\hbar^{-1/2}\,P_k \qquad (2\text{-}7)$$

where $\lambda_k=4\pi^2\nu_k^2$ and $P_k=-i\hbar\partial/\partial Q_k$. So that Eq. (2-5) becomes

$$-\frac{1}{2}\sum_{k=1}^{3N-6}(\hbar\lambda_k^{1/2})(p_k^2+q_k^2)\,\Psi_v^o(q_k)=E_v^o\,\Psi_v^o(q_k)\ . \qquad (2\text{-}8)$$

It is well known that the solutions of Eq. (2-5) are the vibrational energy levels E_v for which

$$E_v^{(k)}=h\nu_k(v_k+1/2)\ .\qquad v=0,1,2,.... \qquad (2\text{-}9)$$

The eigenfunctions of the linear harmonic oscillator equations (Eqs. (2-2)~(2-5)) are

$$\Psi_{v_k} = N_{v_k} e^{-\gamma_k Q_k^2/2} H_{v_k}(\gamma_k^{1/2} Q_k) \qquad (2\text{-}10)$$

where $\gamma_k = 4\pi^2 \nu_k / h$ and $H_{v_k}(\gamma_k^{1/2} Q_k)$ is the hermite polynomial of order of v_k expressed as a function of $\gamma_k^{1/2} Q_k$; N_{v_k} is a normalization constant

$$N_{v_k} = \left[\left(\frac{\gamma_k}{\pi}\right)^{1/2} \frac{1}{2^{v_k}(v_k!)} \right]^{1/2} . \qquad (2\text{-}11)$$

For a doubly degenerate normal vibration, the Schrödinger equation can be written in the form,

$$\frac{1}{2}(\hbar\lambda^{1/2})[(p_a^2+p_b^2)+(q_a^2+q_b^2)]\Psi_v = E_v\Psi_v \quad . \qquad (2\text{-}12)$$

It is convenient to introduce polar coordinates ρ and ϕ by the equations,

$$q_a = \rho\cos\phi \qquad (2\text{-}13)$$

and

$$q_b = \rho\sin\phi \ , \qquad (2\text{-}14)$$

where $0 \leq \rho < \infty$ and $0 \leq \phi < 2\pi$. It holds that

$$p_a = -i[\cos\phi \frac{\partial}{\partial\rho} - \frac{\sin\phi}{\rho} \frac{\partial}{\partial\phi}] , \qquad (2\text{-}15)$$

$$p_b = -i[\sin\phi \frac{\partial}{\partial\rho} + \frac{\cos\phi}{\rho} \frac{\partial}{\partial\phi}] , \qquad (2\text{-}16)$$

and Eq. (2-12) then assumes the form,

$$\left[\frac{\partial^2}{\partial\rho^2} + \frac{1}{\rho} \frac{\partial}{\partial\rho} + \frac{1}{\rho^2} \frac{\partial^2}{\partial\phi^2} + \{ \frac{2E_v}{h\nu} - \rho^2 \} \right] \Psi_v(\rho,\phi) = 0 . \qquad (2\text{-}17)$$

The wave function that is the solution of Eq. (2-17) depends on ρ and ϕ as variables and two vibrational quantum numbers v and ℓ to label the states. It can be shown that this function can be written as a product of radial(ρ) and angular(ϕ) wave functions

$$\Psi_{v,\ell}(\rho,\phi) = N_{v,\ell}\, e^{-\rho^2/2}\, \rho^{|\ell|} [\, L^{|\ell|}_{(v+|\ell|)/2}(\rho)][e^{i\ell\phi}] . \qquad (2\text{-}18)$$

The vibrational quantum number v assumes the values,

$$v = 0,1,2,\ldots , \qquad (2\text{-}19)$$

and the quantum number ℓ assumes the v+1 values,

$$\ell = v, v-2, \ldots, -v+2, -v . \qquad (2\text{-}20)$$

The function $L^{|\ell|}_{(v+|\ell|)/2}(\rho)$ is the associated Laguerre polynomial (14), and N_v is the normalization factor,

$$N_{v,\ell} = [(v-|\ell|)!]^{1/2}/\{[v+|\ell|)/2]!\}^{3/2} \quad . \qquad (2\text{-}21)$$

The expressions for the energy levels of the two dimensional isotropic harmonic oscillator can be written in the form:

$$E_v^{(k)} = h\nu_k(v_k+1) \quad ; \qquad (2\text{-}22)$$

i.e. E_v is independent of ℓ. Each energy level of this oscillator for a given v has (v+1)-fold degeneracy corresponding to the (v+1) values that quantum number ℓ can assume according to Eq. (2-20).

The fact that $\exp(i\ell\phi)$ appears in the expression of the wavefunction $\Psi_{v,\ell}(\rho,\phi)$, Eq. (2-18), indicates the presence of a vibrational angular momentum; ℓ is therefore the so-called vibrational angular momentum quantum number. Classically, the vibrational angular momentum can be interpreted as arising through superposition of the normal vibrations Q_a and Q_b with 90^o phase shift.

II-2-1-2 Rigid Rotor

II-2-1-2-1 Moment of Inertia

The moment of inertia tensor is defined as

$$\tilde{\tilde{I}} = \sum_i m_i(r_i^2 \tilde{\tilde{1}} - \tilde{r}_i\tilde{r}_i) \qquad (2\text{-}23)$$

in which the moment of inertia tensor is written in the notation of a dyadic which is an expression of a second rank tensor. In the three

dimensional Cartesian coordinates,

$$I_{xx} = \sum_i m_i(r_i^2 - x_i^2) = \sum_i m_i(y_i^2 + z_i^2) \ , \qquad (2\text{-}24)$$

where I_{yy} and I_{zz} can be expressed by the permutation of x, y, and z. The off-diagonal elements are given by

$$I_{xy} = -\sum_i m_i x_i y_i . \qquad (2\text{-}25)$$

Since the inertia tensor is real and symmetric, it may be diagonalized through suitable rotations of axes. The diagonal elements of the diagonal form are called principal moments of inertia ($I_a \leq I_b \leq I_c$), and the axis system is termed the principal axis system.

For some molecules, two moments of inertia such as I_a and I_b or I_b and I_c may be the same, in which case the molecule is called a symmetric top molecule. From the point of symmetry, if a molecule has an axis of three or more fold symmetry, then it is always a symmetric top. If a molecule has an axis of symmetry, the axis lies on a principal axis of the molecule.

II-2-1-2-2 Nonvanishing Matrix Elements of Rigid Rotor

From Eq. (2-4), the rotational Hamiltonian operator in the rigid rotor approximation is given by

$$H_r^o = (J_x^2 / I_{xx}^o + J_y^2 / I_{yy}^o + J_z^2 / I_{zz}^o) \tag{2-26}$$

where J_x, J_y, J_z are the angular momentum components along the principal axes x, y, z and I_{xx}^o, I_{yy}^o, I_{zz}^o are the moments of inertia about the principal axes. The matrix elements of operators J_x^2, J_y^2, and J_z^2 can be obtained by matrix multiplication

$$\langle J',k',m'|J_\alpha^2|J,k,m\rangle$$

$$= \sum_{J'',k'',m''} \langle J',k',m'|J_\alpha|J'',k'',m''\rangle\langle J'',k'',m''|J_\alpha|J,k,m\rangle \ . \tag{2-27}$$

Only the diagonal matrix elements of the operator, J_z^2, are nonzero,

$$\langle J,k,m|J_z^2|J,k,m\rangle = \hbar^2 k^2 \ . \tag{2-28}$$

On the other hand, J_x and J_y have diagonal as well as off-diagonal matrix elements. From the relations,

$$\langle J,k\pm1,m|J_x|J,k,m\rangle = (\hbar/2)[(J\mp k)(J\pm k+1)]^{1/2} \tag{2-29}$$

$$\langle J,k\pm1,m|J_y|J,k,m\rangle = \pm(i\hbar/2)[(J\mp k)(J\pm k+1)]^{1/2} \ , \tag{2-30}$$

the diagonal elements of J_x^2 and J_y^2 are

$$\langle J,k,m|J_x^2|J,k,m\rangle = \langle J,k,m|J_y^2|J,k,m\rangle$$

$$= (\hbar^2/2)[J(J+1)-k^2] \tag{2-31}$$

and the off-diagonal elements are

$$\langle J,k\pm2,m|J_x^2|J,k,m\rangle = -\langle J,k\pm2,m|J_y^2|J,k,m\rangle$$
$$= (\hbar^2/4)[J(J+1)-k(k\pm1)]^{1/2}[J(J+1)-(k\pm1)(k\pm2)]^{1/2} . \qquad (2\text{-}32)$$

Hence there are the following nonzero matrix elements of H_r^o in the J, k, m representation:

$$\langle J,k,m|H_r^o|J,k,m\rangle = \frac{\hbar^2}{4}\left[\{\frac{1}{I_{xx}^o} + \frac{1}{I_{yy}^o}\}[J(J+1)-k^2] + \frac{2k^2}{I_{zz}^o}\right] , \qquad (2\text{-}33)$$

$$\langle J,k,m|H_r^o|J,k\pm2,m\rangle$$
$$= \frac{\hbar^2}{8}\left[\frac{1}{I_{xx}^o} - \frac{1}{I_{yy}^o}\right][J(J+1)-k(k\pm1)]^{1/2}[J(J+1)-(k\pm1)(k\pm2)]^{1/2}. \qquad (2\text{-}34)$$

II-2-1-2-3 Rotational Energy Levels of Symmetric Top Molecules

For a symmetric top molecule, $I_{xx}^o = I_{yy}^o$ if the principal axis z lies along the axis of symmetry. As a result, H_r^o has only diagonal nonvanishing matrix elements in the J, k, m representation; that is, the angular momentum quantum number k becomes a good quantum number:

$$\langle J,k,m|H_r^o|J,k,m\rangle = \frac{\hbar^2}{2}\{\frac{J(J+1)}{I_{yy}^o} + \left[\frac{1}{I_{zz}^o} - \frac{1}{I_{yy}^o}\right] k^2\} . \qquad (2\text{-}35)$$

The molecular rotation constants A, B, C can be introduced by the following relations:

$$A = \hbar^2/(4\pi c I_a),\ B = \hbar^2/(4\pi c I_b),\ C = \hbar^2/(4\pi c I_c) , \qquad (2\text{-}36)$$

where c is the speed of light. In terms of the rotational constants, the rotational energy levels of the prolate symmetric top are given by the expression,

$$E_r^o/hc = BJ(J+1) + (A-B)k^2 \ ; \qquad (2\text{-}37)$$

for an oblate top molecule,

$$E_r^o/hc = BJ(J+1) + (C-B)k^2 \ . \qquad (2\text{-}38)$$

Hereafter, we will express all energies in multiples of hc, so that $E_r/hc = E_r$.

II-2-1-2-4 Symmetric Top Rotational Wavefunctions

In terms of the Euler angles e, ϕ, χ, the Schrödinger equation for a rigid prolate symmetric top can be written in the following form

$$\frac{1}{\sin e}\frac{\partial}{\partial e}\left(\sin e \frac{\partial \Psi_r^o}{\partial e}\right) + \frac{1}{\sin^2 e}\frac{\partial^2 \Psi_r^o}{\partial \phi^2} + \left[\frac{\cos^2 e}{\sin^2 e} + \frac{A}{B}\right]\frac{\partial^2 \Psi_r^o}{\partial \chi^2}$$
$$- \frac{2\cos e}{\sin^2 e}\frac{\partial^2 \Psi_r^o}{\partial \phi \partial \chi} + \frac{E_r^o}{B}\Psi_r^o = 0 \ . \qquad (2\text{-}39)$$

Variables in Eq. (2-39) can be separated and the wave function, Ψ_r^o, can

be written as a product

$$\Psi_r^o(\theta,\phi,\chi) = \Theta(\theta)\, e^{im\phi}\, e^{ik\chi} \ . \qquad (2\text{-}40)$$

Since Ψ_r^o must be single valued if ϕ and χ are changed to $\phi+2\pi n$ and $\chi+2\pi n$ ($n=0,1,2,\ldots$), k and m in Eq. (2-39) can assume only integral values $0,\pm1,\pm2,\ldots$

Because variables ϕ and χ occur only in the derivatives in Eq. (2-39), they appear in Eq. (2-40) in simple exponential terms. Function $\Theta(\theta)$ is more complicated because it is the solution of the following equation:

$$\frac{1}{\sin\theta}\frac{\partial}{\partial\theta}\left(\sin\theta\frac{\partial\Theta(\theta)}{\partial\theta}\right) - \left[\frac{m^2}{\sin^2\theta} + \left(\frac{\cos^2\theta}{\sin^2\theta} + \frac{A}{B}\right)k^2 - \frac{2\cos\theta}{\sin^2\theta}km - \frac{E_r^o}{B}\right]\Theta(\theta) = 0 \ . \qquad (2\text{-}41)$$

Physically acceptable solutions of Eq. (2-41) exist only if E_r^o satisfies the following conditions:

$$E_r^o = BJ(J+1) + (A-B)k^2, \qquad (2\text{-}42)$$

where J is a positive integer with $J \geq |k|$ or $|m|$, i.e.,

$$J = 0,1,2,\ldots, \qquad (2\text{-}43)$$

$$k = 0,\pm1,\pm2,\ldots, J, \qquad (2\text{-}44)$$

$$m = 0,\pm1,\pm2,\ldots, J. \qquad (2\text{-}45)$$

Wavefunctions $\Theta_{Jkm}(\theta)$ corresponding to eigenvalues $E_r^o(J,k)$ for $k=m=0$ are the Legendre polynomials $P_J^o(\cos\theta)$, whereas for $m \neq 0$ they are the associated Legendre polynomials (15). The function $\Theta_{J00}(\theta)$ can be written as

$$\Theta_{J00}(\theta) = \left[\frac{[(2J+1)/(8\pi^2)]^{1/2}}{2^J J!}\right] \frac{d^J}{(d\cos\theta)^J} (\cos^2\theta-1)^J \quad . \quad (2\text{-}46)$$

II-2-2 Selection Rules

If the molecule is in a free space, the isotropy of the space makes it possible to consider any one of the three space-fixed principal axes. The electric dipole moment operator is given by

$$\mu_Z = \sum_{i=1}^{N+N_e} e_i(Z_i - Z_i^o) \quad (2\text{-}47)$$

where e_i and Z_i are the charge and space-fixed coordinate of the ith particle in the molecule; Z_i^o is a coordinate of the molecular center of mass. We express μ_Z in terms of the components μ_x, μ_y, μ_z of $\tilde{\mu}$ along the molecule-fixed axes:

$$\mu_Z = \mu_x \lambda_{Zx} + \mu_y \lambda_{Zy} + \mu_z \lambda_{Zz} \quad (2\text{-}48)$$

where λ_{Zx}, λ_{Zy}, λ_{Zz} are the direction cosines.

If the rovibronic wavefunctions are considered in the approximation as the product of electronic, vibrational, and rotational functions, we can write

$$\langle \Psi'_e \Psi'_v \Psi'_r | \mu_Z | \Psi''_e \Psi''_v \Psi''_r \rangle$$
$$= \sum_{\alpha=x,y,z} \langle \Psi'_e \Psi'_v | \mu_\alpha | \Psi''_e \Psi''_v \rangle \langle \Psi'_r | \lambda_{Z\alpha} | \Psi''_r \rangle \qquad (2\text{-}49)$$

because μ_α depends only on the vibronic coordinates and $\lambda_{Z\alpha}$ on the rotational coordinates. We can integrate over the electronic coordinates by writing

$$\langle \Psi'_e \Psi''_v | \mu_\alpha | \Psi''_e \Psi''_v \rangle = \langle \Psi'_v [\langle \Psi'_e | \mu_\alpha | \Psi''_e \rangle] \Psi''_v \rangle = \langle \Psi'_v | \mu_\alpha(e',e'') | \Psi''_v \rangle \qquad (2\text{-}50)$$

where $\mu_\alpha(e',e'')$ depends still on the nuclear coordinates. We expand $\mu_\alpha(e',e'')$ in terms of the normal coordinates of the electronic states about the point of the equilibrium configuration of the atomic nuclei of that state,

$$\mu_\alpha(e',e'') = \mu^o_\alpha(e',e'') + \sum_k (\partial \mu_\alpha(e',e'')/\partial Q_k)_o \, Q_k$$
$$+ (1/2) \sum_{k,l} (\partial^2 \mu_\alpha(e',e'')/\partial Q_k \partial Q_l)_o Q_k Q_l \, . \qquad (2\text{-}51)$$

By substituting the first two terms of Eq. (2-51) into Eq.(2-49), we obtain

$$\langle\Psi'_e\Psi'_v\Psi'_r|\mu_Z|\Psi''_e\Psi''_v\Psi''_r\rangle$$

$$= \sum_\alpha [\mu^o_\alpha(e',e'')\langle\Psi'_v|\Psi''_v\rangle + \Sigma(\partial\mu_\alpha(e',e'')/\partial Q_k)_o\langle\Psi'_v|Q'_k|\Psi''_v\rangle]\langle\Psi'_r|\lambda_{Z\alpha}|\Psi''_r\rangle. \quad (2\text{-}52)$$

The first term is responsible for pure rotational transitions where ($\Psi'_e = \Psi''_e$, $\Psi'_v = \Psi''_v$). The intensities of such spectra are proportional to $[\mu^o_\alpha\langle\Psi'_r|\lambda_{Z\alpha}|\Psi''_r\rangle]^2$, the product of the square of a component of the permanent dipole moment and the square of the corresponding direction-cosine matrix element. Vibrational transitions within a given electronic state are controlled by the second term in the square brackets. From the harmonic oscillator approximation, $\langle\Psi'_v|Q_k|\Psi''_v\rangle \neq 0$ only if $\Delta v_k = \pm 1$.

For the case of vibration-rotation transitions, we must consider the matrix elements of $\lambda_{Z\alpha}$ together to specify selection rules on the rotational quantum numbers J,k. It is convenient to write Eq. (2-49) in the form

$$\begin{aligned}\langle\Psi'_e\Psi'_v\Psi'_r|\mu_Z|\Psi''_e\Psi''_v\Psi''_r\rangle &= \langle\Psi'_v|\mu_z(e',e'')|\Psi''_v\rangle\langle\Psi'_r|\lambda_{Zz}|\Psi''_r\rangle \\ &+ (1/2)\langle\Psi'_v|\mu_x(e',e'')-i\mu_y(e',e'')|\Psi''_v\rangle\langle\Psi'_r|\lambda_{Zx}+i\lambda_{Zy}|\Psi''_r\rangle \\ &+ (1/2)\langle\Psi'_v|\mu_x(e',e'')+i\mu_y(e',e'')|\Psi''_v\rangle\langle\Psi'_r|\lambda_{Zx}-i\lambda_{Zy}|\Psi''_r\rangle \ . \quad (2\text{-}53)\end{aligned}$$

It turns out that the only non-zero elements of λ_{Zz} are

$$\langle\Psi'_r|\lambda_{Zz}|\Psi''_r\rangle \neq 0 \qquad \text{if } \Delta k = k'-k'' = 0 \qquad (2\text{-}54)$$

and

$$\langle\Psi'_r|\lambda_{Zx}\pm i\lambda_{Zy}|\Psi''_r\rangle \neq 0 \qquad \text{if } \Delta k = \pm 1 \ . \qquad (2\text{-}55)$$

The general selection rules may be applied to symmetric top molecules by taking account of the fact that $\mu_x^o = \mu_y^o = 0$, $\mu_z^o \neq 0$. For the pure rotation spectra of non-degenerate vibrational states of symmetric tops:

$$\Delta k = 0, \Delta J = 0, \pm 1. \tag{2-56}$$

Selection rules for the allowed vibration-rotation transitions can be obtained by combining the selection rules for vibrational and rotational transitions. There are two different types of allowed transitions in symmetric top molecules (16). When the electric dipole moment oscillates in a direction which is parallel to the z axis (parallel band),

$$(\partial\mu_z/\partial Q_k)_o \neq 0, \ (\partial\mu_x/Q_k)_o = (\partial\mu_y/\partial Q_k)_o = 0. \tag{2-57}$$

In this case, selection rules for the rotational quantum numbers are

$$\Delta k = 0, \Delta J = 0, \pm 1 \quad \text{for } k \neq 0 , \tag{2-58}$$

$$\Delta k = 0, \Delta J = \pm 1 \quad \text{for } k = 0 . \tag{2-59}$$

When the electric dipole moment oscillates in a direction that is perpendicular to the z axis (perpendicular band),

$$(\partial\mu_z/\partial Q_k)_o = 0, \ (\partial\mu_x/\partial Q_k)_o \neq 0, \ (\partial\mu_y/\partial Q_k)_o \neq 0. \tag{2-60}$$

Selection rules for the rotational quantum numbers are then

$$\Delta k = \pm 1, \ \Delta J = 0, \pm 1 \ . \qquad (2\text{-}61)$$

In addition to the above selection rules for the rotational quantum numbers, there are also selection rules which are concerned with the symmetry properties of the rotational levels. Hougen derived general selection rules for electric dipole transitions by consideration of the fact that rovibronic energy levels can be classified according to certain symmetry species (17). The dipole moment operator is invariant to a permutation of the coordinates of identical particles since the operator μ_Z is simply the sum of the charges e_i of all the particles in the molecule multiplied by their Z coordinates. It may be noticed that the transformation properties of μ_Z are identical with those of the product $T_z R_z$, where T_z and R_z represent a translation and a rotation about the z axis (17).

Selection rules may be formulated from the transformation properties of μ_Z, which lead to the conclusion that the electric dipole transition between two rovibronic states, of species Γ' and Γ'', is allowed if and only if $\Gamma' \times \Gamma''$ contains $\Gamma_{T_z} \times \Gamma_{R_z}$. Here Γ_{T_z} and Γ_{R_z} are the irreducible representations of T_z and R_z for the corresponding permutation-inversion group. Application of this rule to a C_{3v} molecule leads to the consideration that the dipole moment operator is classified under A_2 species from $\Gamma_{T_z} \times \Gamma_{R_z} = A_1 \times A_2 = A_2$. Therefore, the allowed transitions ought to be such that $\Gamma' \times \Gamma''$ contains A_2. As a result, we may add two more selection rules:

$A_1 \leftrightarrow A_2$ and $E \leftrightarrow E$. (2-62)

The principally allowed transitions are shown in Fig. 2-1 and Fig. 2-2.

Hougen (17) introduced a convenient quantum number, $G = G_{ev} - k$ (for the ground electronic state, $G = \ell - k$), which may replace the ℓ-designation originally proposed by Herzberg (16). This quantum number allows influence of the symmetry species of rovibronic energy levels to be specified without additional quantum numbers. The selection rule due to symmetry considerations may be described with the quantum number G as follows: An electric dipole transition between two states is allowed if and only if $G' - G'' \equiv \Delta G = 0 \bmod n$, where n is the highest-fold axis of rotation in the molecule. As a result, the electric dipole transition selection rules, $\Delta k = 0$ for parallel transitions and $\Delta k = \pm 1$ for perpendicular transitions, are proved by the fact that the connected states have the same symmetry as shown in Fig. 2-1.

This rule may also be applied to the additional transitions allowed by Coriolis interactions, which need not obey the selection rules on k. Such transitions will normally be exceedingly weak compared to vibronically allowed transitions. It should be pointed out that the quantum number G by itself contains no more information than is contained in the symmetry species label of the rovibronic level.

II-2-3 Nonrigid Symmetric Top Molecules

II-2-3-1 Centrifugal Distortion

Rotation about any axis in the molecule is accompanied by centrifugal forces which tend to alter the effective moments of inertia.

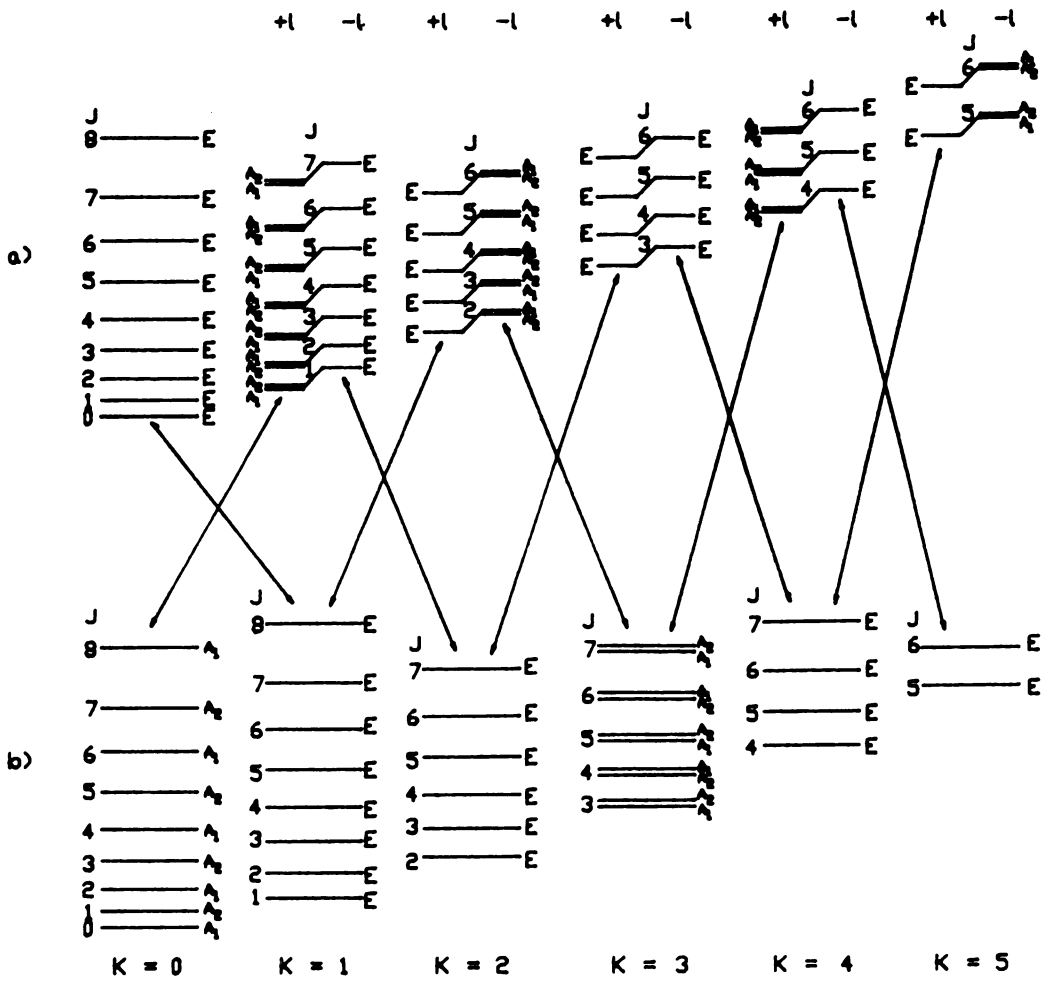

Figure 2-1. Symmetry properties of rotational levels of molecules with a three-fold axis; (a) in a totally symmetric vibrational state, (b) in a degenerate vibrational state. The arrows show allowed transitions.

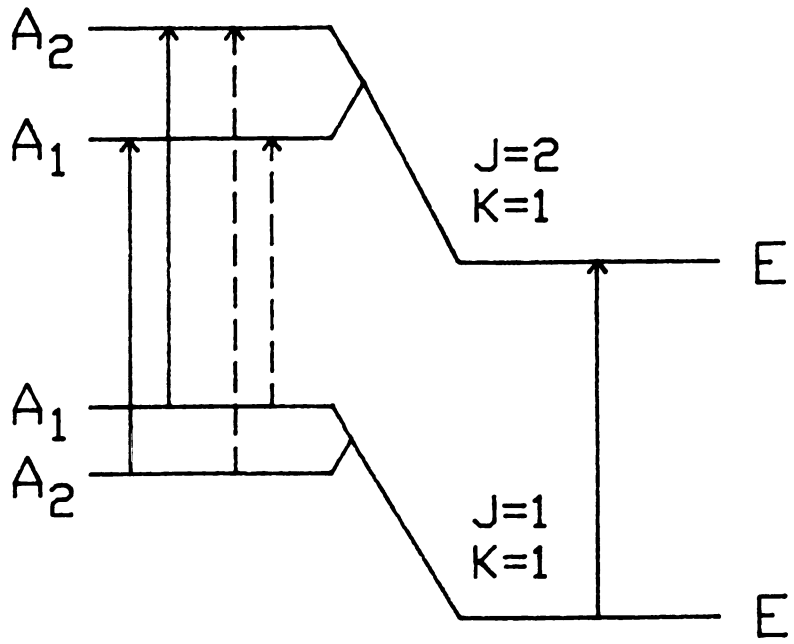

Figure 2-2. The rovibronic levels with K = 1 and J = 1,2 for vibronic E-state of a molecule of symmetry C_{3v}. The transitions indicated by solid arrows are allowed; those indicated by dashed arrows are not.

The resulting dynamic effect forces the atoms away from an axis of rotation and increases the moment of inertia about that axis. The centrifugal effects introduce into the energy level expression terms with high powers of $J(J+1)$ and K^2. For a prolate top molecule,

$$E = BJ(J+1) + (A-B)K^2 - D_J J^2(J+1)^2 - D_K K^4 - D_{JK} J(J+1)K^2 + \dots , \quad (2\text{-}63)$$

where D_J, D_K, and D_{JK} are the quartic centrifugal distortion constants. The correction terms for centrifugal distortion are found to depend only on even powers of the angular momentum because the distortion effects do not depend on the direction of rotation about any axis.

II-2-3-2 Coriolis Interaction

Coriolis resonance interactions in symmetric top molecules have been studied by Nielson and coworkers (18-20) and later by diLauro and Mills (21). According to Jahn's rule (22), if the product of the symmetry species of two vibrational modes contains the species of rotation, $\Gamma(Q_k) \times \Gamma(Q_{k'}) = \Gamma(R_\alpha)$, Coriolis interaction takes place between the vibrational modes (17). The Coriolis force is represented in classical mechanics as the cross product of the linear velocity of the particle relative to the molecule-fixed axis system and the angular velocity of the rotation;

$$\tilde{F}_{cor} = 2m\tilde{v} \times \tilde{\omega} . \quad (2\text{-}64)$$

Fig. 2-3 illustrates the effect of the Coriolis interaction between

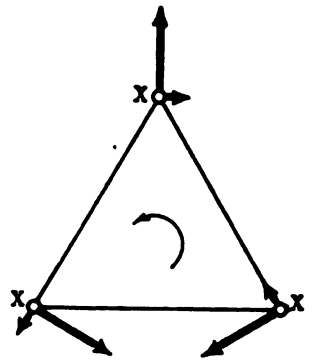

Figure 2-3. Coriolis forces during the degenerate vibration of an X_3 molecule.

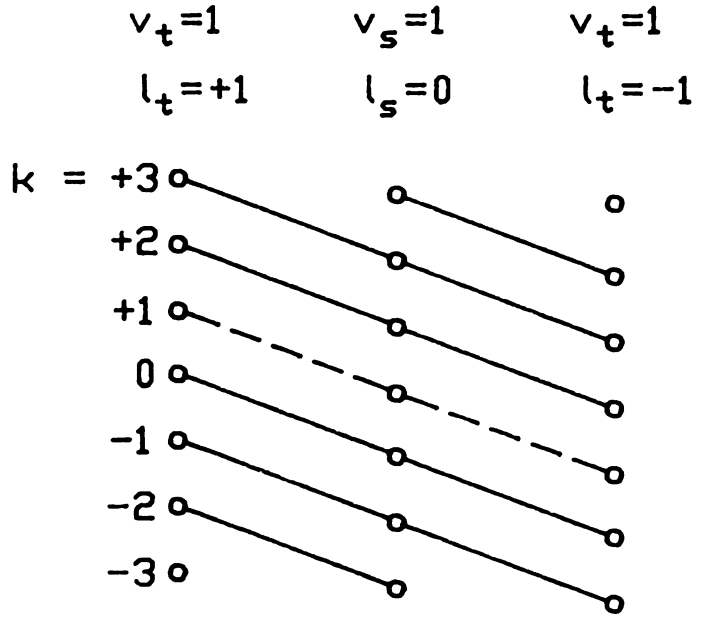

Figure 2-4. Diagrammatic representation of the x,y-Coriolis coupling of the states with J = 3 and with the same k-ℓ_t. The dotted line connects states exhibiting giant ℓ-type doubling.

components of the ν_2 degenerate vibrational mode of the tri-atomic molecule X_3. For a counter-clockwise rotation of the molecule the Coriolis forces are as shown by the short arrows (Fig. 2-3). It is noticed from the figure that they tend to excite the other component of the degenerate vibration. The result of this Coriolis interaction is a splitting of the degenerate vibrational levels into two levels whose separation increases with increasing rotation (K) about the top axis and is zero for K = 0.

Coriolis interaction may be explained in quantum mechanics as the interaction between the vibrational and rotational angular momenta about the appropriate molecular axis:

$$H_{cor} = (2A/\hbar^2)(-p_z J_z) + (2B/\hbar^2)(-p_x J_x - p_y J_y) , \qquad (2\text{-}65)$$

where A,B are the rotational constants of a prolate top molecule and J_x, J_y, J_z and p_x, p_y, p_z denote the components of over-all and vibrational angular momentum about the corresponding molecular axis. Eq. (2-65) indicates that there are basically two kinds of effects: (i) interaction due to the rotation about the top axis z (in a symmetric top molecule, interaction of two degenerate modes ν_t and $\nu_{t'}$), and (ii) interaction due to the rotation about the x, y axes (in a symmetric top molecule, interaction between nondegenerate mode ν_s and the degenerate mode ν_t).

When $\nu_t=\nu_t'$, the z-axis Coriolis coupling contributes to the energy in the first order by the term

$$\Sigma[-2B_z\zeta_t + \eta^z_{tJ}J(J+1) + \eta_{tK}k^2]\ell_t k \qquad (2\text{-}66)$$

where the term $-2B_z\zeta^z_t\ell_t k$ represents the primary effect of the Coriolis interaction and the other terms describe the rotational dependence of the Coriolis coupling. The subscript t denotes a degenerate vibrational state. The result of this strong Coriolis interaction is a splitting of the degenerate vibrational levels into two levels whose separation increases with increasing rotation about the top axis. Hence the formula for the rotational energy levels in a vibrational level of a symmetric top molecule in which a degenerate vibration ν_t is singly excited, may be represented by

$$E_{(v)}(J,K) = B_{(v)}J(J+1) + (A_{(v)}-B_{(v)})K^2 \mp 2A_{(v)}\zeta_i K\ell + ... \quad (2\text{-}67)$$

which differs from Eq. (2-42) only by the term $2A_{(v)}\zeta_i K\ell$.

Coriolis interactions due to rotation about the x, y axes appear as off-diagonal components:

$$\langle v_s-1, v_t, \ell_t; J, k | H_{cor} | v_s, (v_t-1), \ell_t \pm 1; J, k\pm 1\rangle$$
$$= -\Omega_{st}\zeta^y_{st}B_y[v_s(v_t \mp \ell_t)]^{1/2}[(J\mp k)(J\pm k+1)]^{1/2} \quad (2\text{-}68)$$

where

$$\Omega_{st} = [(\nu_s+\nu_t)/2(\nu_s\nu_t)^{1/2}] \quad . \quad (2\text{-}69)$$

For simplicity, let us consider states with $v_s = v_t = 1$. Since $\Delta k = \Delta\ell_t = \pm 1$, the matrix elements given in Eq. (2-68) connect only the state $|0,1^{+1};J,k+1\rangle$ with the state $|1,0;J,k\rangle$ which is further connected to the state $|0,1^{-1};J,k-1\rangle$ (Fig. 2-4). Thus for each value of J the energy

matrix factorizes in separate blocks, each block being characterized by a particular value of $(k-\ell_t)$. It is noticed that k is not a good quantum number any more whereas $(k-\ell_t)$ still remains as a good quantum number (17). We can obtain the eigenvalues by building and diagonalizing the following 3x3 matrix for given J and $k-\ell_t$;

$$\begin{array}{ccc} |0,1\ ;J,k+1\rangle & |1,0;J,k\rangle & |0,1\ \ ,J,k-1\rangle \\ \left[\begin{array}{ccc} \omega_t+F(J,k+1)-2B_z\zeta_t^z(k+1) & 2^{1/2}B_x\Omega_{st}\zeta_{st}^y[J,k] & 0 \\ & \omega_s+F(J,k) & -2^{1/2}B_x\Omega_{st}\zeta_{st}^y[J,k-1] \\ \text{(Hermitian)} & & \omega_t+F(J,k-1)+2B_z\zeta_t^z(k-1) \end{array}\right] & & \end{array} \qquad (2\text{-}70)$$

where

$$F(J,k) = B_xJ(J+1) + (B_z-B_x)k^2 , \qquad (2\text{-}71)$$

$$[J,k] = [J(J+1)-k(k+1)]^{1/2} . \qquad (2\text{-}72)$$

Because for each rotational state $|k| \leq J$, there are only two identical 2x2 blocks for the special case $(k-\ell_t) = \pm J$, and only two identical 1x1 blocks (unperturbed states) for $(k-\ell_t) = \pm(J+1)$. In addition, Garing et al (23) showed that for $k-\ell_t = 0$ the matrix given by Eq. (2-70) can be factorized by the transformation

$$|A_{\pm}\rangle = 2^{-1/2}[|0,1^{+1};J,1\rangle \pm |0,1^{-1};J,-1\rangle] . \qquad (2\text{-}73)$$

The transformed matrix has the form,

$$
\begin{array}{ccc}
|A^+\rangle & |1,0^o;J,0\rangle & |A_-\rangle \\
\left[\begin{array}{ccc}
\omega_t+F(J,1)-2B_z\zeta_t^z & 0 & 0 \\
 & \omega_s+F(J,0) & 2B_z\Omega_{st}\zeta_{st}^y[J(J+1)] \\
\text{(Hermitian)} & & \omega_t+F(J,1)-2B_z\zeta_t^z
\end{array}\right] &
\end{array}
\qquad (2\text{-}74)
$$

Thus the pair of degenerate levels with $k = \ell_t = \pm 1$ of the ν_t state splits into two components A_+ and A_-. The A_- sublevel interacts with the $k = 0$ level of ν_s but the A_+ sublevel is unperturbed, that is, only one of the two energy levels (A_1, A_2) is affected by the Coriolis interaction. Nielson called this splitting "giant ℓ-type doubling" (23). Since ℓ-type doublings provide a very good information source for Coriolis interactions, they have been probed to study existing Coriolis interactions (6,7). Note that for odd J the species of A_+ is A_1 and that of A_- is A_2, while for even J the species of A_+ is A_2 and A_- is A_1. The effects of ℓ-type doubling will be discussed in more detail in the following section.

II-2-3-3 Rotational ℓ-type Resonance Interaction

Wilson showed by symmetry considerations that rotation-vibration interaction might split degenerate rovibrational energy levels of symmetric top molecules into a number of components (24). For example, in a symmetric top molecule with C_{3v} symmetry, if $k-\ell \neq 3n$, then the

rotational and the vibrational wavefunctions belong to the degenerate species E and the total rovibrational wavefunctions should form bases for the irreducible representations of ExE = A_1+A_2+E. The splitting into an E level and A_1A_2 pair results from first order Coriolis coupling (see section II-2-3-2).

The splitting of the A_1A_2 pair into separate levels, however, is of higher order and explained by a more detailed treatment of vibration-rotation interaction (25). There are off-diagonal matrix elements in the quantum numbers ℓ and k which split and shift the zeroth-order energy levels. The most familiar example of the splitting of the A levels is ℓ-type doubling. The associated effects, which are called rotational ℓ-type doubling or ℓ-type resonance, were first discussed by Nielson (26,27) and later described in detail by Grenier-Besson (28). Selection rules for the matrix elements can be obtained from Amat's rule (29)

$$-\Delta k + \sum_t \eta_t \Delta \ell_t = pN \qquad (2\text{-}75)$$

where the value of N is determined by the N-fold principal symmetry axis of the point group; p is an arbitrary integer which is positive, negative or zero; and η_t=1 for E_1 (or E) species, η_t=2 for E_2 species etc. This relation gives off-diagonal matrix elements of three types which, in the notation of Cartwright and Mills (30), are given as follows:

$$\langle v_t, \ell_t+1; J, k+1 | \tilde{H}/hc | v_t, \ell_t-1, J, k-1 \rangle$$
$$= (\rho/4) q_t^{+} [(v_t+1)^2 - \ell_t^2]^{1/2} \{[J(J+1)-k(k+1)][J(J+1)-k(k-1)]\}^{1/2} \quad (2\text{-}76)$$

$$\langle v_t, \ell_t+1; J, k-1 | \tilde{H}/hc | v_t, \ell_t-1, J, k+1 \rangle$$
$$= (\rho/4) q_t^{-} [(v_t+1)_2 - \ell_t^2]^{1/2} \{[J(J+1)-k(k+1)][J(J+1)-k(k-1)]\}^{1/2} \quad (2\text{-}77)$$

$$\langle v_t, \ell_t; J, k | \tilde{H}/hc | v_t, \ell_t \pm 2; J, k \mp 1 \rangle$$
$$= \rho r_t [(v_t+1)^2 - (\ell_t \mp 1)^2]^{1/2} [J(J+1)-k(k+1)]^{1/2} (2k \pm 1) \ . \quad (2\text{-}78)$$

The Hamiltonian $\tilde{H}$ is obtained by the appropriate contact transformation and the constant ρ in Eqs. (2-76) - (2-78) is equal to either +1 or -1, depending on the sign of the constants q_t and r_t. Cartwright and Mills (30) refer to the effects associated with the matrix elements as q_t^{+} (or $\pm 2, \pm 2$)-type , q_t^{-} (or $\pm 2, \mp 2$)-type, and r_t (or $\pm 2, \mp 1$)-type interactions.

According to Eq. (2-75), q_t^{+} interactions occur for all E_1(or E, E_{1g}, E_{1u}, E'_1, etc) type vibrational species in all symmetric top molecules; the q_t^{-} interactions occur for all E_m species in symmetric top molecules with an even principal axis of symmetry (C_n or S_n with n even) when m=(n-2)/2 (E in D_{2d}, $E_{g,u}$ in D_{4h}, etc.); the r_t type interaction occurs for E_m species in molecules with an odd principal axis of symmetry C_n if m = (n-1)/2 (E in C_{3v}, E_2 in C_{5v}, etc). Since this thesis is concerned with C_{3v} molecules, q_t^{-} interactions will not be discussed further.

We will follow the sign convention that Cartwright and Mills introduced; $q_t > 0$ when the ℓ-type doubling in the $\ell_t = k = \pm 1$ levels leads to the rovibrational A_1 level lying above the rovibrational A_2

level for J even. In the $(v_t,\ell_t) = (1,\pm 1)$ vibrational state the doubling is thus given by the formula

$$T(A_1)-T(A_2) = q_t^+ J(J+1) \text{ for J even} \tag{2-79}$$

$$T(A_2)-T(A_1) = q_t^+ J(J+1) \text{ for J odd} \tag{2-80}$$

where $T(A_1)$, etc., denote the term values. The general formula for q_t^+ in terms of the vibration-rotation interaction parameters also has a definite sign if we follow these conventions (28,30). Thus,

$$q_t^+ = \frac{2B^2}{\nu_t}\{-\sum_s\left[\frac{3\nu_t^2+\nu_s^2}{\nu_s^2-\nu_t^2}\right]\zeta_{st}^{y\,2} + \sum_s\left[\frac{3\nu_t+\nu_s}{\nu_s^2-\nu_t^2}\right]\zeta_{st}^{x\,2}$$
$$-3a_t^{xz\,2}/4I_{zz}^o + 2\pi(c/h)^{1/2}\sum_{t'}\rho_{t,t,t'}a_{t'}^{yy}\nu_{t'}/\nu_t^{3/2}\} \tag{2-81}$$

where

$$\rho_{t,t,t'} = (hc)^{-1}(\partial^3 V/\partial q_t^2 \partial q_{t'}) \tag{2-82}$$

is a cubic anharmonic constant, q_r is a dimensionless normal coordinate, $q_r = 2\pi(\nu_r/\hbar)^{1/2}Q_r$, and $a_t^{yy} = (\partial I_{yy}/\partial Q_t)_o$.

The effects of ℓ-resonances are illustrated in Fig. 2-5. The reason that ℓ-type doubling is large compared to other A_1-A_2 splittings can be explained by the fact that the ℓ-resonances take place between the two degenerate levels ($k = \ell_t = \pm 1$). Finally, since subscripts s and t have been used here to denote the nondegenerate and degenerate vibrational states only for clarification, they will be dropped or switched with notation of the corresponding vibrational modes for convenience in the following sections.

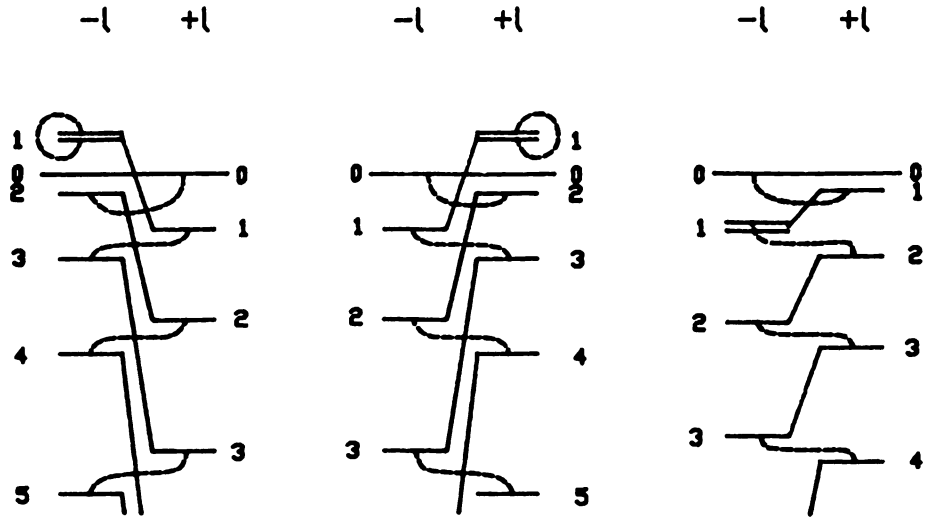

Figure 2-5. $q_t^{(+)}$, $q_t^{(-)}$, and r_t ℓ-resonance in an $\ell_t = \pm 1$ degenerate state of an oblate symmetric top. The levels are labeled by K, with $(+\ell)$ to the left of $(-\ell)$; interactions are shown by broken lines.

II-3 Experimental

II-3-1 White-Type Long Path Cell

White-type cells have been applied to a number of applications in spectroscopy to provide long absorbing paths (31,32). This type of cell is useful for many cases: (1) inherently weak transitions, for example, combination and overtone bands; (2) low concentration samples such as transient molecules and reaction intermediates; (3) high resolution spectroscopy that needs to keep the pressure low for small pressure broadening. In 1942, White introduced the design which accomplished the desired result (33). The essential parts of the equipment are three spherical, concave mirrors that all have the same radius of curvature. The setup is shown in Fig. 2-6, where two mirrors A and A' are placed close together at one end and the third mirror B at the other end. The centers of curvature of A and A' are located on the front surface of B, and the center of curvature of B is half way between A and A'. Later Bernstein and Herzberg introduced a useful variation in the shape of the front mirror (B), which, in the case where the size of the source is appreciable, doubles the number of traverses obtainable without overlapping images (34). Fig. 2-7 shows the shape of a front mirror of this type together with the image location on it.

In a multiple-reflection system, astigmatism can limit the maximum attainable number of passes even more than reflectivity. This aberration causes an increase of the size of each successive image and eventually image overlapping. In the double row alignment (Fig. 2-7), the tangential image elongation is the main result of the astigmatism. The general formula for the image increase has been derived by Edward

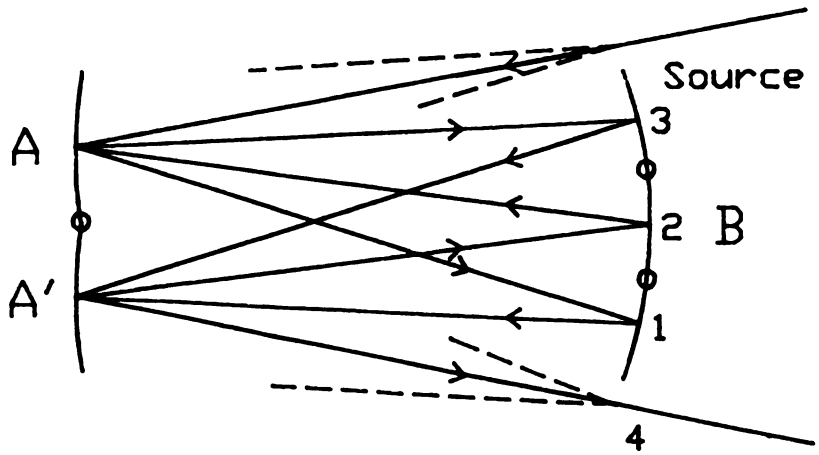

Figure 2-6. Mirror arrangement of a White-type cell. The small circles on mirror surface are the centers of curvature of the mirrors.

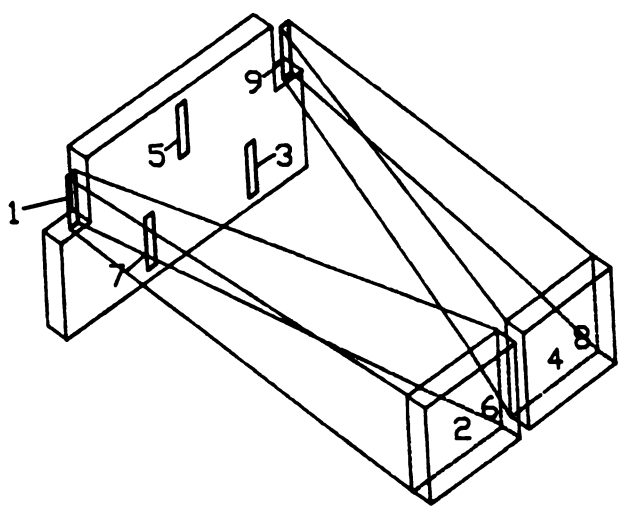

Figure 2-7. Modified optical arrangement for a White-type cell. The numbers show the sequence of reflection.

(35):

$$\Delta L_T = \frac{hb}{12R^2}(N - \frac{4}{N}) = \frac{b}{12Rf_v}(N - \frac{4}{N}) \qquad (2\text{-}83)$$

where b is the total separation between the entrance and exit images, N the number of traverses, h the height of mirror, R the radius of curvature, and f_v the vertical f number (h/R). From Eq. (2-83), it is clear that b should be as small as possible. For a source of width w_s the minimum value of b which will give distinct images on the front mirror and, will allow the entrance and exit images to clear the mirror edges, is $b_{min}=N/4w_s$ and the corresponding width of the upper portion of the front mirror is $(N/4-1)w_s$ (35). One may wish to cut down the wide front mirror to reduce ΔL_T. Reflectivities of mirrors also limit the number of traverses. For example, forty traverses with 98% reflectivity reduces energy to about 45% of that incident.

The homemade White type cell used in this work includes three spherical mirrors with 1 m radius of curvature, two one inch diameter mirrors and a two inch diameter front mirror. Three micrometers provide required fine adjustment for appropriate alignment of each mirror. The cell body consists of a 6 inch glass cylinder, 1 inch CaF_2 windows located horizontally at the level of the center of the front mirror, and aluminium end plates, which are tightened with O-rings for seals. The whole structure is supported by the customized aluminium frame, and the actual volume of the cell is estimated to be about 11 liters. The windows provide enough room to adjust the incoming and outgoing laser for double row alignment (Fig. 2-7). Without particular difficulty, a

24 m path-length can be obtained with a 2 mm diameter He/Ne laser beam entering parallel. Throughout the study of the $\nu_3 + \nu_6 - \nu_6$ band of CH_3F, the mirrors were arranged to give 8 m path-length, which is enough to provide the necessary signal to noise ratio when the cell is filled with CH_3F to 0.5 Torr pressure.

II-3-2 Infrared-Microwave Sideband Laser Spectrometer

Fig. 2-8 is a block diagram of the infrared microwave sideband laser spectrometer used to record the spectra for this work. It is very similar to the spectrometer used for previous studies from this laboratory (2,3) except for the use of the White-type long path sample cell. Since the instruments used in the spectrometer have been described in detail elsewhere (2,3), only a brief explanation of the components will be given. The semisealed CO_2 laser includes a 1.7 m plasma discharge tube with ZnSe Brewster angle windows in a 2.2 m laser cavity with a rotatable plane grating at one end and a partially transmitting (95% reflection) spherical concave mirror on a piezoelectric translator (PZT) at the other end. Microwave radiation was generated by a synthesizer (HP 8671B) and amplified by a traveling wave tube amplifier (Varian Model VZM-6991B1) at specific frequencies in the 8-18 GHz region. Approximately 1 W of CO_2 laser power (frequency ν_ℓ) is mixed with ~20 W of microwaves (frequency ν_m) in a CdTe electrooptic crystal that is mounted in an impedance-matched housing. A detailed description of the CdTe electrooptic crystal and the electrooptic effect can be found in Shin-Chu Hsu's thesis (36). Since the generated sidebands (frequency $\nu_\ell \pm \nu_m$) are polarized in a vertical

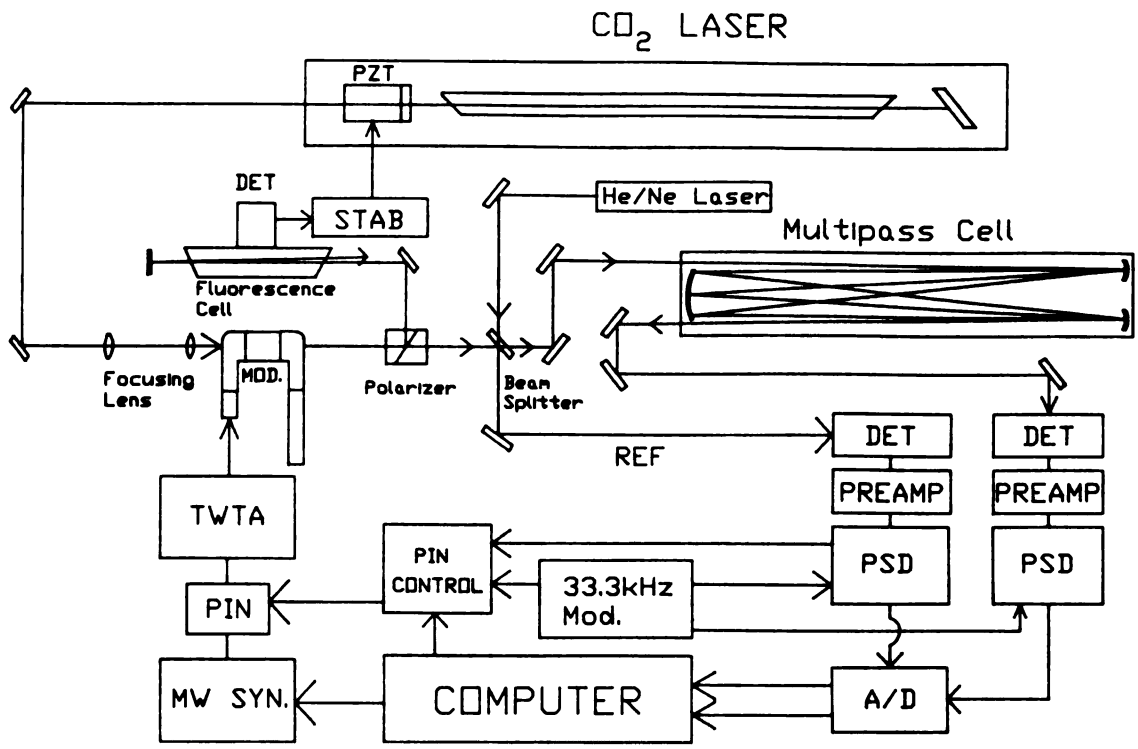

Figure 2-8. Block diagram of the infrared microwave sideband laser used in this study.

plane, they are efficiently separated from the horizontally-polarized carrier by means of a polarizer and later divided by a beam splitter into two portions. One of the beams is used as a reference while the other is allowed to pass through the White-type sample cell. Both beams are monitored by liquid N_2 cooled HgCdTe detectors (Infrared Associates, Inc. HCT-100) cooled by liquid N_2. The sidebands are 100% amplitude modulated by chopping the microwave power with a PIN diode, and the detector signals (signal and reference) are processed by lock-in amplifiers at the modulation frequency (33 kHz). The signal from the reference lock-in amplifier is sent to a feedback circuit to stabilize the total sideband power by controlling the microwave power. The CO_2 laser carrier reflected from the polarizer passes back and forth through a cell that contains CO_2 and the 4.3 μm fluorescence signal that results from the additional vibrational excitation is detected at 90^o angle to the beam by a liquid N_2 cooled InSb photovoltaic detector (Judson Infrared, Inc. J10D). The saturation dip in the fluorescence from this cell is used to stabilize the laser frequency. For this purpose the laser frequency is modulated at 100 Hz by means of a sinusoidal voltage applied to the PZT. The residual jitter in the laser frequency is estimated to be ~150 kHz, which is also the expected accuracy of the frequencies of the sidebands. The sidebands were not separated, but the spectra were recorded a second time with the CO_2 laser locked at the edge of the fluorescence saturation dip in a known direction. The shift in the apparent center frequency of each spectral line (5-10 MHz) was enough to identify whether the positive or negative sideband had been absorbed.

Figs. 2-9 and 2-10 are examples of spectra of the hot band of

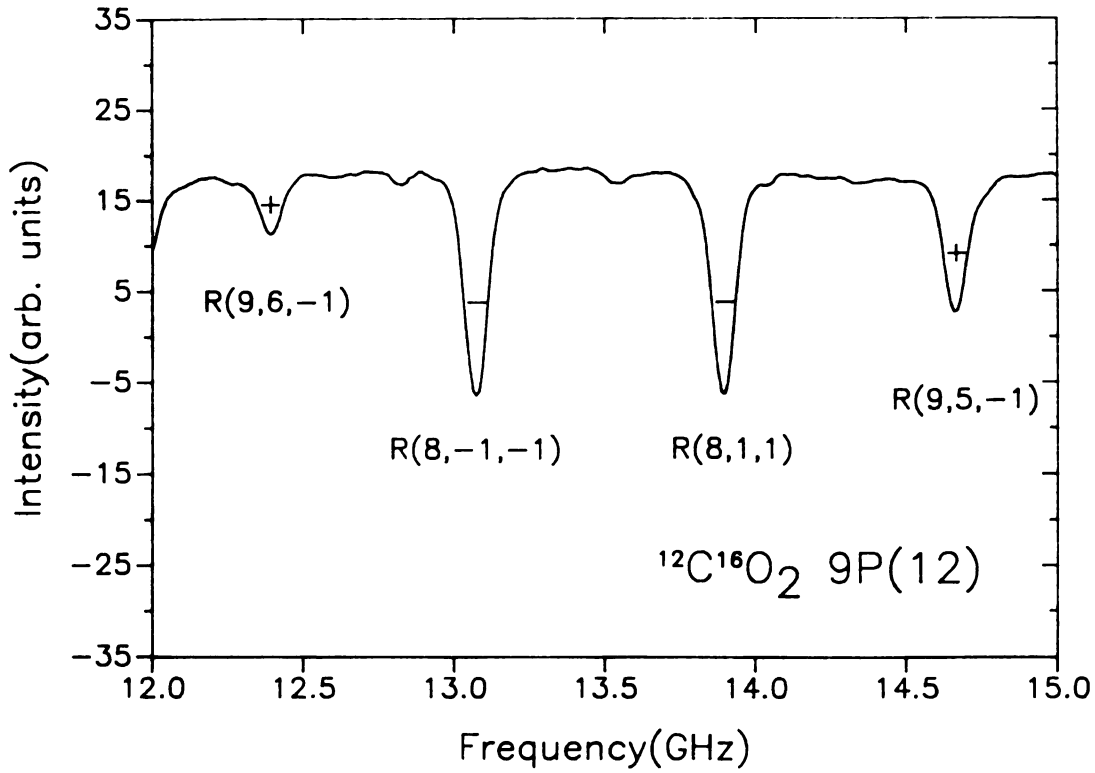

Figure 2-9. Portion of the spectrum of the $\nu_3+\nu_6-\nu_6$ band observed in the present work. The horizontal axis is the microwave frequency to be added to (+) or subtracted from (-) the frequency of the 9P(12) $^{12}C^{16}O_2$ laser to obtain the infrared frequency of the transition.

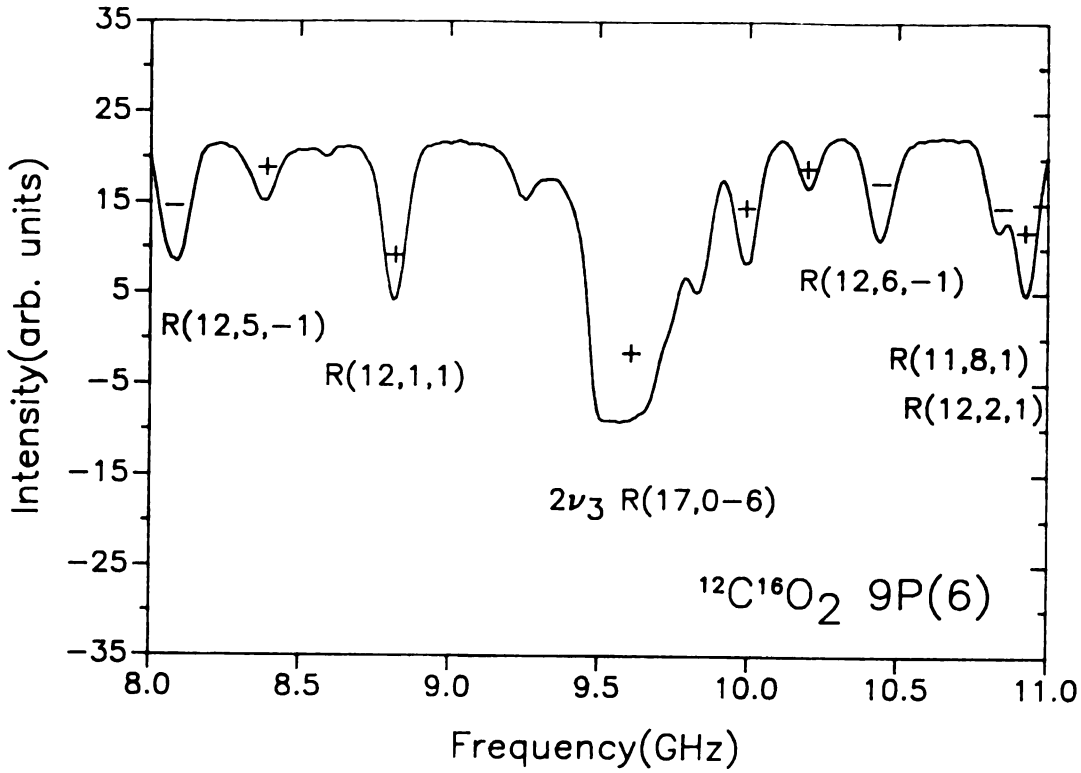

Figure 2-10. Portion of the spectrum of the $\nu_3+\nu_6-\nu_6$ band observed in the present work. The horizontal axis is the microwave frequency to be added to (+) or subtracted from (−) the frequency of the 9P(6) $^{12}C^{16}O_2$ laser to obtain the infrared frequency of the transition. The transition marked $2\nu_3$ is in the $2\nu_3-\nu_3$ band and completely absorbs the positive sideband power.

interest in this work plotted as a function of the microwave frequency, which must be added to or subtracted from the appropriate laser frequency to obtain the infrared frequency of the transition; the laser frequencies were obtained from the report of Freed et al. (37). Fig. 2-9 is an example of a relatively clear region of the spectrum that shows a well-resolved ℓ-doublet. Fig. 2-10 shows a portion of the spectrum that includes a $2\nu_3 \leftarrow \nu_3$ hot-band transition that is sufficiently strong to absorb the entire positive sideband power.

Spectra were recorded for microwave frequencies from 8 to 18 GHz in 4-MHz steps for more than 40 laser lines. The frequencies of the transitions were obtained by fitting the spectra by least squares to Gaussian lineshapes; for overlapped transitions, the Doppler halfwidths were constrained to the appropriate value (~34 MHz). A commercial sample of CH_3F from Peninsular Chemical Research was used as received with only the usual freeze-pump-thaw cycling. The spectra were recorded at room temperature (~297 K).

II-4 Results

II-4-1 Term Values and Selection Rules

As mentioned in the introduction, both the upper and the lower vibrational states of the $\nu_3 + \nu_6 - \nu_6$ band in CH_3F belong to E-type symmetry for C_{3v} point group. The spectra were analyzed by calculating the frequencies as differences in term values $E(v,J,k,\ell)$ for degenerate vibrational states (28,30) as follows:

$$E(v,J,k,\ell) = W(v,J,k,\ell) + w_q(v,J,k,\ell) \qquad (2\text{-}84)$$

where

$$\begin{aligned} W(v,J,k,\ell) = {} & \nu_o + B_v\, J(J+1) + (A_v - B_v)\, k^2 - 2A_v\, \zeta k\ell \\ & - D_J^v\, J^2(J+1)^2 - D_{JK}^v\, J(J+1)k^2 - D_k^v\, k^4 \\ & + \eta_J^v\, J(J+1)k\ell + \eta_K^v\, k^3\ell \\ & + H_J^v\, J^3(J+1)^3 + H_{JK}^v\, J^2(J+1)^2k^2 + H_{KJ}^v\, J(J+1)k^4 \\ & + H_K^v\, k^4 \quad . \end{aligned} \qquad (2\text{-}85)$$

In Eq. (2-85), ν_o is the vibrational band center; A_v and B_v are the rotational constants; D_J^v, D_{JK}^v, D_K^v, H_J^v, H_{JK}^v, H_{KJ}^v, and H_K^v are the quartic and sextic centrifugal distortion constants; and ζ, η_J^v, and η_K^v are Coriolis coupling constants. In Eq. (2-84), $w_q(v,J,k,\ell)$ is the ℓ-resonance contribution which, except when $k = \ell$, was taken into account explicitly as a second order perturbation:

$$w_q(v,J,k,\ell) = [q_v J(J+1) + q_v' J^2(J+1)^2]^2 f(v,J,k,\ell) \quad \text{for } k \neq \ell \qquad (2\text{-}86)$$

where

$$f(v,J,k,\ell=\pm 1) = \frac{(J\pm k)(J\pm k-1)(J\mp k+1)(J\mp k+2)}{4[W(v,J,k,\ell=\pm 1) - W(v,J,k\mp 2,\ell=\mp 1)]} \quad . \quad (2\text{-}87)$$

When $k = \ell = \pm 1$, the ℓ-resonance term becomes ℓ-type doubling:

$$w_q(v,J,k,\ell) = \frac{1}{2}\,[q_v J(J+1) + q_v' J^2(J+1)^2] \quad \text{for } k = \ell \; . \quad (2\text{-}88)$$

The ℓ-resonance term described above is referred as the $(\pm 2,\pm 2)$-interaction (30). Another possible ℓ-resonance in a C_{3v} symmetric top, the $(\pm 2,\mp 1)$ interaction, can not be included in the least squares fitting of the frequencies because of linear dependence. The details will be described later.

During the vibrational transition, $\nu_3 + \nu_6 \leftarrow \nu_6$, the dipole moment may be considered to change parallel to the principal axis of symmetry. Therefore the selection rules for allowed transitions were taken to be $\Delta J = 0$ or ± 1, $\Delta k = 0$, and $\Delta\ell = 0$ (17). Since off-diagonal ℓ-resonance elements mix the rotational levels ($\Delta k = \Delta\ell = \pm 2$ and $\Delta k = \pm 1$, $\Delta\ell = \mp 2$) of degenerate vibrational states, in principle, other transitions, ($\Delta k = \Delta\ell = \pm 2$, $\Delta(k-\ell) = \pm 3$), are also allowed, but they are expected to be much weaker and no attempt has been made to assign them. The primary selection rules were used for all of the transitions except those for which $k = \ell$, for which k and ℓ are not good quantum numbers because of the linear combination of the states. For these transitions, it was necessary to use the fundamental selection rule $A_1 \leftrightarrow A_2$, where the identification of A_1 and A_2 levels is shown in Fig. 2-11 for odd J and $q_v > 0$ for the ν_6 state (q_6 is known to be positive (8)) and for the two

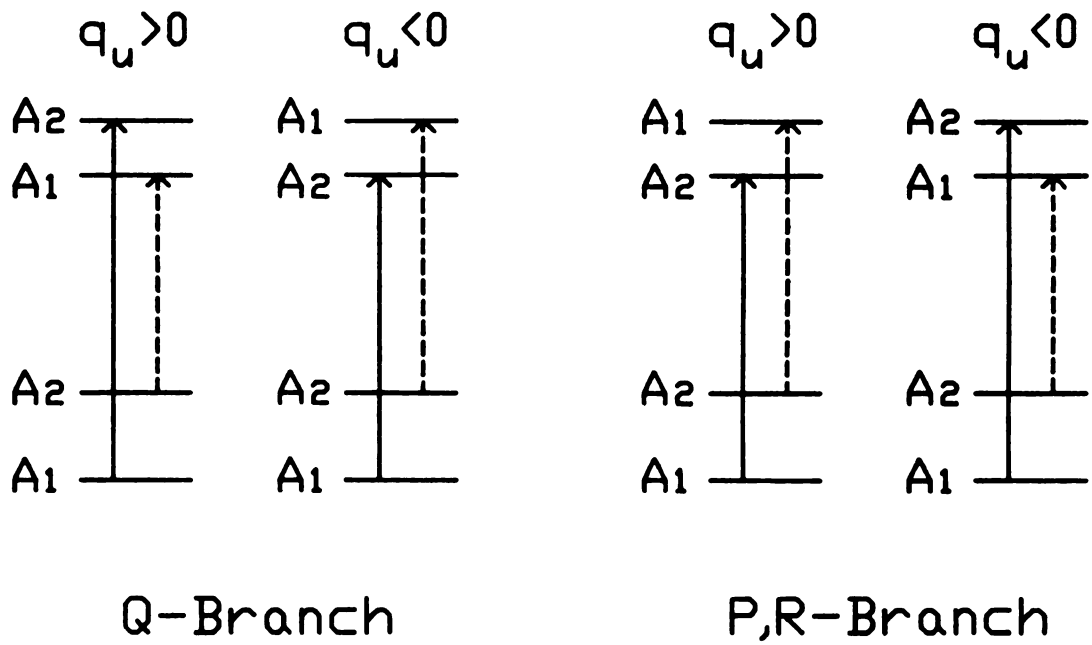

Figure 2-11. Energy-level diagrams showing higher frequency (solid lines) and lower frequency (dashed lines) allowed transitions between rotational levels belonging to two vibrational states of E symmetry for C_{3v}. For each of the diagrams, the J value of the levels in the lower state is assumed to be odd and the q_v value of the lower state is assumed to be positive; the sign of the q_v value (q_u) for the rotational levels of the upper state is indicated above each diagram.

possible signs of q_v for the $\nu_3+\nu_6$ state. As indicated in Fig. 2-11, we followed the sign convention suggested by Cartwright and Mills (30).

II-4-2 Analysis

The most tedious part of the assignment of the spectra was the identification and labeling of the many transitions from the ν_3 fundamentals of $^{12}CH_3F$ and $^{13}CH_3F$ and the $2\nu_3 - \nu_3$ hot band of $^{12}CH_3F$, all of which were considerably stronger than the transitions desired for the present study. Fortunately, we had precise constants available (2,3) for the interfering bands and were able to calculate the frequencies of the overlapping transitions to high accuracy (within few MHz). A first attempt at assignment was made by combining the reported frequencies of the ν_6 and $\nu_3+\nu_6$ bands, as reported by Hirota (8) and Nakagawa (9) et al., respectively. This method led to the assignment of three J = 6←5 transitions about 500 MHz from their predicted values. The Q(6,4) transition, in which Q denotes the transition J→J and the numbers are the J and K quantum numbers, was also found near the value reported by Duxbury and Kato (10), although it was seriously overlapped with another transition which was assigned later as the Q(10,10). However, assignment of higher J and k transitions by this method was not possible because a limited number of experimental frequencies were reported. We then calculated energy levels of the two states by using the parameters reported by these workers and obtained frequencies from differences in the energies. This procedure was also not useful because the calculated frequencies were far from the experimental values. The

problem was traced to the fact that rather different ground state constants were used in Refs. 8 and 9. Successful assignment of the $\nu_3 + \nu_6 - \nu_6$ band transitions was obtained when the constants in the paper by Hirota (8) were used to calculate frequencies of the ν_6 band and the constants in the paper by Nakagawa (9) were used to calculate frequencies in the $\nu_3+\nu_6$ combination band. Then the desired frequencies of the $\nu_3+\nu_6-\nu_6$ band were obtained as combination differences of the calculated frequencies. This procedure led to assignment of additional transitions for ℓ = +1, but the ℓ = -1 transitions could not be assigned with confidence until after several iterations of least-squares fittings of the ℓ = +1 frequencies with proposed assignments of the ℓ = -1 transitions gave better values of the constants. Strong correlations between $A\zeta$ and the centrifugal distortion constants D_K and D_{JK} could not be broken until the ℓ = -1 transitions were included. The Coriolis terms in the energy expression give contributions to the energies that are large enough to cause the transitions for adjacent k values for a given J to be separated by about 3 GHz. The ℓ = +1 and ℓ = -1 transitions spread out in different directions from the k = 0 transition for each J; the separation between ℓ = +1 components for adjacent k is somewhat larger than for the corresponding ℓ = -1 components. In case of oblate top molecules one can actually observe a series of doublets (ℓ = +1, -1) with k for a given J because the Coriolis interaction term, $|C\zeta|$ is smaller than the term, $|(C-B)k^2|$ (13).

As shown in Fig. 2-11, both components of the ℓ-type doublets occur for P, Q, and R transitions according to A_1-A_2 selection rule. It can be seen that the $\nu_3+\nu_6-\nu_6$ band frequencies are sensitive to the absolute

magnitudes and the relative signs of q_v for the upper and lower states, but cannot be used to determine the absolute signs of the q_v's. We took the sign of q_v for the ν_6 state from Ref. 8. Fig. 2-9 shows the ℓ-doublet pair for the $^{Q}R(8,1)$ transition, which was the first pair found. By using the splitting for this pair and constraining the q_v constant for the ν_6 state to that determined by Hirota (8) it was possible to identify one or both components of 13 P- or R-branch ℓ-type doublets for $3 \leq J \leq 20$ and one Q-branch pair, $^{Q}Q(4,1)$; the frequencies of these transitions are shown in Table 2-1. Additional Q-branch transitions were not identified because of the density of the Q-branch region and the low intensity of Q-branch transitions for k = 1. In the final fitting, which included the microwave frequencies for the direct ℓ-doublet transitions in the ν_6 state (7), the q_v constants for both states were adjusted (q_6 was constrained to be positive) and it was necessary to include the higher-order constant q_v' for high J ℓ-doubling transitions as shown in Eq. (2-88).

In principle, the contribution of ℓ-resonance to the energy includes r_v-dependent terms that result from the following matrix elements (28,30):

$$\langle v,J,k,\ell=+1| H |v,J,k+1,\ell=-1\rangle$$
$$= 2r_v(2k + 1)[(J - k)(J + k + 1)]^{1/2} \quad . \qquad (2\text{-}89)$$

An attempt was made to include the effect of these terms for both states at the level of second-order perturbation, but unstable fittings with unpredictable correlations were obtained. In order to trace the origin of the problem, the data were fit, including r_v for the ν_6 state only, by means of a least-squares routine that calculates the eigenvalues of

TABLE 2-1

Observed Transition Frequencies from ℓ-type Doublets of the $\nu_3 + \nu_6 - \nu_6$ Band of $^{12}CH_3F$

Trans.[a]	Laser[b]		ν_m[c]	ν/MHz	O-C[d]	Unc.[e]	ν/cm^{-1} [f]
P(17, 1, 1)	13C1602	9P(12)	-13 805.5	30 199 220.6	2.5	5.0	1007.337 57(8)
P(17,-1,-1)	13C1602	9P(12)	-10 667.9	30 202 358.2	2.1	5.0	1007.442 22(7)
P(15,-1,-1)	13C1602	9P(8)	9 081.4	30 324 127.7	0.2	5.0	1011.504 01(1)
P(7, 1, 1)	12C1602	9P(40)	-15 094.5	30 785 048.2	-0.3	5.0	1026.878 67(-1)
P(7,-1,-1)	12C1602	9P(40)	-14 513.9	30 785 628.8	4.4	10.0	1026.898 04(15)
P(5,-1,-1)	13C1602	9R(18)	-17 955.5	30 894 523.2	0.9	3.0	1030.530 36(3)
P(3, 1, 1)	13C1602	9R(22)	13 210.6	31 000 682.6	0.4	5.0	1034.071 45(1)
P(3,-1,-1)	13C1602	9R(22)	13 324.5	31 000 796.4	-3.4	5.0	1034.075 26(-11)
Q(4, 1, 1)	12C1602	9P(28)	-11 040.4	31 148 467.8	-3.4	5.0	1039.001 05(-11)
Q(4,-1,-1)	12C1602	9P(28)	-10 908.2	31 148 600.0	-0.2	5.0	1039.005 46(-1)
R(4, 1, 1)	12C1602	9P(20)	15 308.6	31 399 209.0	-3.7	5.0	1047.364 87(-12)
R(5,-1,-1)	12C1602	9P(18)	8 229.4	31 446 289.5	3.5	5.0	1048.935 31(12)
R(8, 1, 1)	12C1602	9P(12)	-13 892.7	31 581 939.0	2.8	3.0	1053.460 09(9)
R(8,-1,-1)	12C1602	9P(12)	-13 072.6	31 582 759.1	-0.1	3.0	1053.487 45(0)
R(11, 1, 1)	12C1602	9P(8)	14 634.8	31 711 696.3	1.1	5.0	1057.788 33(4)
R(11,-1,-1)	12C1602	9P(8)	16 115.8	31 713 177.2	1.1	5.0	1057.837 72(4)
R(12,-1,-1)	12C1602	9P(6)	8 815.6	31 755 299.4	0.3	3.0	1059.242 77(1)
R(18, 1, 1)	12C1602	9R(4)	-13 901.0	31 990 116.4	-1.9	5.0	1067.075 41(-6)
R(18,-1,-1)	12C1602	9R(4)	-10 192.3	31 993 825.1	-0.9	5.0	1067.199 12(-3)
R(19,-1,-1)	12C1602	9R(6)	-17 028.8	32 031 207.5	0.6	3.0	1068.446 06(2)
R(20, 1, 1)	12C1602	9R(6)	15 166.7	32 063 403.0	2.0	5.0	1069.519 99(7)

[a] Numbers are J, k, and ℓ of the lower vibrational state. Levels with k,ℓ = -1,-1 are the lower energy components of the ℓ-type doublets.

[b] Laser line used; laser frequencies were taken from Ref. 37.

[c] Microwave frequency in MHz. The signed microwave frequency was added to the laser frequency to obtain the absorption frequency.

[d] Observed minus calculated frequency in MHz; the parameters for the calculation are in Tables 2-3 and 2-4.

[e] Estimated uncertainty in the observed frequency in MHz.

[f] Observed wavenumber in cm^{-1}. The numbers in parentheses are observed minus calculated wavenumbers in units of 0.00001 cm^{-1}.

the normal equations matrix after scaling. It is known that the occurrence of one or more small eigenvalues in this procedure is evidence of linear dependence (38); we found one small eigenvalue for which the corresponding eigenvector contained a substantial contribution from the parameter r_6. The origin of this problem then became obvious when we expanded the second-order perturbation contribution from the matrix element in Eq. (2-89) and found that the contribution to the energy, w_r, could be written as

$$w_r(v,J,k,\ell) = r'[-J(J+1) + 3k^2 + k\ell - 2J(J+1)k\ell + 2k^3\ell] \qquad (2\text{-}90)$$

where

$$r' = \frac{4r_v^2}{A_v - B_v + 2A_v\zeta} \quad . \qquad (2\text{-}91)$$

The detailed derivation of this equation is in the Appendix. Apparently, at this level of approximation, by redefining the parameters B_v, A_v-B_v, $A_v\zeta$, η_J^v, and η_K^v to include a contribution from r_v, the effects of the matrix elements in Eq. (2-89) are included completely. It is therefore not surprising that a linear dependence was encountered when r_v was included as a parameter in the fitting. A linear dependence involving r_v was already implicit in the equation given by Grenier-Besson and Amat for the rotational frequencies in an E state of a C_{3v} molecule (39).

Ultimately, the measured frequencies of more than 220 transitions in the $\nu_3+\nu_6-\nu_6$ band were assigned and used to obtain vibration-rotation parameters for the two states. The final least squares fitting included

the rotational frequencies reported in Refs. (6,7), in which each data point was weighted by the inverse of the squares of the uncertainty. In order to avoid linear dependence, ν_o, (A_v-B_v), D_K, $A_v\zeta$, and η_K of the v_6=1 state were constrained to the values reported by Hirota (8), and H_K for this state was constrained to zero. The standard deviation for an object of unit weight and the root-mean-square deviation are calculated 1.05 and 8.05 MHz, respectively. The frequencies of assigned transitions are compared in Table 2-2 to calculated frequencies that were obtained from the determined vibration-rotation parameters in Tables 2-3 and 2-4.

TABLE 2-2

Comparison of Observed and Calculated Frequencies in the $\nu_3 + \nu_6 - \nu_6$ Band of $^{12}CH_3F$

Trans.[a]	Laser[b]		ν_a[c]	ν/MHz	O-C[d]	Unc.[e]	ν/cm^{-1} [f]
P(17, 1,-1)	13C1602	9P(12)	-17 765.8	30 195 260.3	-2.1	3.0	1007.205 46(-7)
P(17, 0, 1)	13C1602	9P(12)	-15 063.0	30 197 963.2	0.1	5.0	1007.295 62(0)
P(17, 1, 1)	13C1602	9P(12)	-13 805.5	30 199 220.6	2.5	5.0	1007.337 57(8)
P(17,-1,-1)	13C1602	9P(12)	-10 667.9	30 202 358.2	2.1	5.0	1007.442 22(7)
P(17, 2, 1)	13C1602	9P(12)	-9 277.2	30 203 748.9	5.3	5.0	1007.488 61(18)
P(16, 5,-1)	13C1602	9P(10)	-17 314.9	30 247 154.2	4.7	3.0	1008.936 46(16)
P(16, 4,-1)	13C1602	9P(10)	-15 158.6	30 249 310.5	4.7	5.0	1009.008 38(16)
P(16, 3,-1)	13C1602	9P(10)	-12 865.7	30 251 603.3	-2.2	3.0	1009.084 87(-7)
P(16, 2,-1)	13C1602	9P(10)	-10 431.8	30 254 037.3	-6.4	5.0	1009.166 06(-21)
P(16, 5, 1)	13C1602	9P(10)	10 431.8	30 274 900.8	-0.1	5.0	1009.861 98(0)
P(16, 7, 1)	13C1602	9P(10)	17 708.2	30 282 177.3	-11.7	5.0	1010.104 70(-39)
P(15, 9,-1)	13C1602	9P(8)	-14 201.7	30 300 844.6	0.1	5.0	1010.727 38(0)
P(15, 8,-1)	13C1602	9P(8)	-12 708.1	30 302 338.2	4.7	5.0	1010.777 19(16)
P(15, 7,-1)	13C1602	9P(8)	-11 039.2	30 304 007.1	1.5	5.0	1010.832 86(5)
P(15, 6,-1)	13C1602	9P(8)	-9 186.5	30 305 859.8	11.0	30.0	1010.894 67(37)
P(15,-1,-1)	13C1602	9P(8)	9 081.4	30 324 127.7	0.2	5.0	1011.504 01(1)
P(15, 2, 1)	13C1602	9P(8)	10 826.9	30 325 873.2	1.1	3.0	1011.562 23(4)
P(15, 3, 1)	13C1602	9P(8)	13 952.5	30 328 998.8	0.6	5.0	1011.666 50(2)
P(15, 4, 1)	13C1602	9P(8)	17 220.8	30 332 267.1	-0.8	5.0	1011.775 52(-3)
P(9, 5,-1)	12C1602	9P(44)	-16 006.7	30 658 439.0	-3.8	5.0	1022.655 44(-13)
P(9, 2,-1)	12C1602	9P(44)	-9 045.1	30 665 400.7	1.5	5.0	1022.887 65(5)
P(9, 4, 1)	12C1602	9P(44)	8 739.0	30 683 184.8	-22.1	30.0	1023.480 87(-74)
P(9, 5, 1)	12C1602	9P(44)	12 253.1	30 686 698.8	0.7	3.0	1023.598 08(2)
P(9, 6, 1)	12C1602	9P(44)	15 917.4	30 690 363.2	7.7	5.0	1023.720 32(26)
P(8, 3,-1)	13C1602	9R(8)	9 306.3	30 719 078.4	-2.7	3.0	1024.678 15(-9)
P(8, 1,-1)	12C1602	9P(42)	-13 484.1	30 724 172.6	3.2	20.0	1024.848 07(11)
P(8, 3, 1)	13C1602	9R(10)	-16 001.5	30 736 057.4	1.4	3.0	1025.244 51(5)
P(8, 4, 1)	13C1602	9R(10)	-12 664.1	30 739 394.8	-0.8	3.0	1025.355 83(-3)
P(8, 5, 1)	13C1602	9R(10)	-9 161.6	30 742 897.3	4.0	5.0	1025.472 67(13)
P(8, 6, 1)	12C1602	9P(42)	8 917.0	30 746 573.7	16.4	20.0	1025.595 29(55)
P(8, 7, 1)	12C1602	9P(42)	12 765.2	30 750 421.9	24.0	10.0	1025.723 66(80)
P(7, 6,-1)	13C1602	9R(10)	16 001.5	30 768 060.4	18.4	20.0	1026.312 02(61)
P(7, 2,-1)	13C1602	9R(12)	-16 422.5	30 777 049.4	0.6	3.0	1026.611 85(2)
P(7, 0, 1)	12C1602	9P(40)	-17 696.7	30 782 446.0	13.5	20.0	1026.791 87(45)
P(7, 1, 1)	12C1602	9P(40)	-15 094.5	30 785 048.2	-0.3	5.0	1026.878 67(-1)
P(7,-1,-1)	12C1602	9P(40)	-14 513.9	30 785 628.8	4.4	10.0	1026.898 04(15)
P(7, 2, 1)	12C1602	9P(40)	-11 743.0	30 788 399.7	16.3	20.0	1026.990 46(54)
P(7, 3, 1)	12C1602	9P(40)	-8 555.1	30 791 587.6	10.8	20.0	1027.096 80(36)
P(6, 3, 1)	12C1602	9P(38)	-15 467.0	30 846 430.5	-3.3	5.0	1028.926 16(-11)
P(6, 3, 1)	13C1602	9R(14)	12 421.6	30 846 433.6	-0.2	3.0	1028.926 26(-1)
P(6, 4, 1)	12C1602	9P(38)	-12 116.2	30 849 781.3	-0.7	5.0	1029.037 93(-2)
P(6, 4, 1)	13C1602	9R(14)	15 771.0	30 849 782.9	0.9	3.0	1029.037 99(3)
P(6, 5, 1)	12C1602	9P(38)	-8 608.0	30 853 289.5	1.7	5.0	1029.154 96(6)
P(5, 3,-1)	13C1602	9R(16)	9 876.0	30 883 556.4	-8.6	10.0	1030.164 55(-29)
P(5, 2,-1)	13C1602	9R(16)	12 375.5	30 886 055.9	1.9	3.0	1030.247 92(6)
P(5, 1,-1)	13C1602	9R(16)	15 003.6	30 888 684.0	-1.4	3.0	1030.335 58(-5)
P(5, 0, 1)	13C1602	9R(16)	17 778.0	30 891 458.4	0.8	3.0	1030.428 13(3)
P(5,-1,-1)	13C1602	9R(18)	-17 955.5	30 894 523.2	0.9	3.0	1030.530 36(3)
P(5, 3, 1)	13C1602	9R(18)	-11 855.8	30 900 622.9	-2.2	5.0	1030.733 82(-7)
P(5, 4, 1)	13C1602	9R(18)	-8 504.4	30 903 974.3	-1.3	5.0	1030.845 62(-4)

TABLE 2-2 (cont'd)

Trans.[a]	Laser[b]		ν_m[c]	ν/MHz	O-C[d]	Unc.[e]	ν/cm^{-1} f
P(4, 3,-1)	12C1602	9P(36)	14 150.8	30 937 066.3	1.1	5.0	1031.949 45(4)
P(4, 2,-1)	12C1602	9P(36)	16 647.5	30 939 562.9	2.7	5.0	1032.032 72(9)
P(4, 1,-1)	13C1602	9R(20)	-8 207.4	30 942 201.1	4.3	5.0	1032.120 73(15)
P(3, 2,-1)	12C1602	9P(34)	9 209.7	30 992 400.5	0.8	3.0	1033.795 20(3)
P(3, 1,-1)	12C1602	9P(34)	11 852.5	30 995 043.3	1.9	3.0	1033.883 36(6)
P(3, 0, 1)	12C1602	9P(34)	14 631.5	30 997 822.3	0.4	3.0	1033.976 05(1)
P(3, 1, 1)	13C1602	9R(22)	13 210.6	31 000 682.6	0.4	5.0	1034.071 45(1)
P(3,-1,-1)	13C1602	9R(22)	13 324.5	31 000 796.4	-3.4	5.0	1034.075 26(-11)
P(3, 2, 1)	13C1602	9R(22)	16 328.5	31 003 800.4	0.0	5.0	1034.175 45(0)
Q(17, 8,-1)	12C1602	9P(32)	-12 184.2	31 030 533.9	20.0	OMIT	1035.067 19(67)
Q(17, 7,-1)	12C1602	9P(32)	-10 201.3	31 032 516.8	10.2	20.0	1035.133 34(34)
Q(16, 9,-1)	13C1602	9R(24)	16 510.3	31 040 181.7	23.2	OMIT	1035.389 01(77)
Q(16, 7,-1)	13C1602	9R(26)	-15 065.0	31 043 944.3	-4.2	5.0	1035.514 51(-14)
Q(19, 7, 1)	13C1602	9R(26)	-12 374.6	31 046 634.6	0.7	5.0	1035.604 26(2)
Q(15,12,-1)	13C1602	9R(26)	-12 374.6	31 046 634.6	2.2	5.0	1035.604 26(7)
P(2, 1,-1)	13C1602	9R(26)	-11 791.9	31 047 217.4	-0.2	5.0	1035.623 70(-1)
Q(15,11,-1)	13C1602	9R(26)	-11 109.9	31 047 899.4	2.4	5.0	1035.646 44(8)
Q(16, 5,-1)	13C1602	9R(26)	-10 734.8	31 048 274.4	5.2	5.0	1035.658 95(17)
P(2, 0, 1)	13C1602	9R(26)	-9 011.5	31 049 997.7	-4.1	5.0	1035.716 43(-14)
Q(15, 5,-1)	12C1602	9P(32)	16 284.0	31 059 002.0	-6.5	10.0	1036.016 78(-22)
Q(14, 5,-1)	13C1602	9R(26)	10 063.5	31 069 072.8	-9.4	20.0	1036.352 72(-31)
Q(13,10,-1)	13C1602	9R(26)	10 063.5	31 069 072.8	13.1	20.0	1036.352 72(44)
Q(13, 8,-1)	13C1602	9R(26)	13 368.5	31 072 377.7	5.5	5.0	1036.462 96(18)
Q(13, 7,-1)	13C1602	9R(26)	15 261.1	31 074 270.3	0.7	5.0	1036.526 09(2)
Q(16, 5, 1)	13C1602	9R(28)	-17 173.7	31 076 314.8	-7.7	5.0	1036.594 28(-26)
Q(13, 6,-1)	13C1602	9R(28)	-17 173.7	31 076 314.8	2.9	3.0	1036.594 28(10)
Q(12,11,-1)	13C1602	9R(26)	17 532.7	31 076 541.9	-3.6	5.0	1036.601 85(-12)
Q(15, 4, 1)	12C1602	9P(30)	-17 664.3	31 083 827.9	8.2	10.0	1036.844 89(27)
Q(11,11,-1)	12C1602	9P(30)	-16 759.0	31 084 733.1	-6.3	5.0	1036.875 09(-21)
Q(12, 6,-1)	12C1602	9P(30)	-16 426.0	31 085 066.1	1.8	5.0	1036.886 19(6)
Q(11, 9,-1)	12C1602	9P(30)	-13 926.2	31 087 566.0	-16.9	20.0	1036.969 57(-56)
Q(12, 4,-1)	12C1602	9P(30)	-11 968.7	31 089 523.5	-0.2	5.0	1037.034 87(-1)
Q(15, 6, 1)	12C1602	9P(30)	-10 939.4	31 090 552.8	-8.5	5.0	1037.069 21(-28)
Q(16, 9, 1)	12C1602	9P(30)	-10 751.5	31 090 740.7	-37.2	40.0	1037.075 47(-124)
Q(11, 7,-1)	12C1602	9P(30)	-10 361.5	31 091 130.7	-6.2	5.0	1037.088 49(-21)
Q(12, 3,-1)	12C1602	9P(30)	-9 545.7	31 091 946.5	3.7	5.0	1037.115 70(12)
Q(11, 6,-1)	12C1602	9P(30)	-8 349.0	31 093 143.2	-4.3	5.0	1037.155 61(-14)
Q(9, 9,-1)	13C1602	9R(28)	8 337.1	31 101 825.6	-9.8	20.0	1037.445 23(-33)
Q(14, 7, 1)	13C1602	9R(28)	10 828.9	31 104 317.3	-6.9	3.0	1037.528 35(-23)
Q(10, 4,-1)	13C1602	9R(28)	11 489.4	31 104 977.9	-2.0	20.0	1037.550 37(-7)
Q(15,10, 1)	13C1602	9R(28)	12 313.9	31 105 802.4	28.0	OMIT	1037.577 88(94)
Q(13, 5, 1)	13C1602	9R(28)	13 235.3	31 106 723.8	-2.7	5.0	1037.608 61(-9)
Q(9, 6,-1)	13C1602	9R(28)	13 805.0	31 107 293.5	-8.6	10.0	1037.627 61(-29)
Q(9, 5,-1)	13C1602	9R(28)	15 941.1	31 109 429.6	-4.0	5.0	1037.698 86(-13)
Q(8, 8,-1)	13C1602	9R(28)	16 092.9	31 109 581.3	-6.0	5.0	1037.703 92(-20)
Q(13, 6, 1)	12C1602	9P(30)	8 719.7	31 110 211.9	-0.9	5.0	1037.724 96(-3)
Q(8, 7,-1)	12C1602	9P(30)	9 903.1	31 111 395.3	-4.2	3.0	1037.764 43(-14)
Q(9, 4,-1)	12C1602	9P(30)	10 208.8	31 111 700.9	-3.4	5.0	1037.774 64(-11)
Q(14, 9, 1)	12C1602	9P(30)	10 510.2	31 112 002.4	10.3	5.0	1037.784 68(35)
Q(12, 4, 1)	12C1602	9P(30)	10 654.3	31 112 146.5	-0.6	5.0	1037.789 50(-2)

TABLE 2-2 (cont'd)

Trans.[a]	Laser[b]		ν_0[c]	ν/MHz	O-C[d]	Unc.[e]	ν/cm^{-1} [f]
Q(8, 6,-1)	12C1602	9P(30)	11 877.5	31 113 369.7	-2.2	5.0	1037.830 30(-7)
Q(8, 5,-1)	12C1602	9P(30)	14 012.5	31 115 504.7	10.3	10.0	1037.901 51(34)
Q(7, 7,-1)	12C1602	9P(30)	15 307.5	31 116 799.7	-7.4	5.0	1037.944 70(-25)
Q(13, 8, 1)	12C1602	9P(30)	16 131.3	31 117 623.5	-4.3	5.0	1037.972 18(-14)
Q(8, 4,-1)	12C1602	9P(30)	16 265.2	31 117 757.4	-1.2	5.0	1037.976 66(-4)
Q(7, 6,-1)	12C1602	9P(30)	17 275.3	31 118 767.4	-1.8	3.0	1038.010 35(-6)
Q(5, 2,-1)	13C1602	9R(30)	9 699.6	31 136 811.7	4.3	10.0	1038.612 23(14)
Q(8, 3, 1)	13C1602	9R(30)	10 111.6	31 137 223.8	0.8	5.0	1038.625 99(3)
Q(4, 3,-1)	13C1602	9R(30)	10 542.3	31 137 654.5	6.6	5.0	1038.640 34(22)
Q(9, 5, 1)	13C1602	9R(30)	10 748.0	31 137 860.2	1.7	20.0	1038.647 22(6)
Q(10, 7, 1)	13C1602	9R(30)	11 239.1	31 138 351.3	9.0	5.0	1038.663 60(30)
Q(5, 1,-1)	13C1602	9R(30)	12 340.8	31 139 452.9	-11.0	5.0	1038.700 34(-37)
Q(7, 2, 1)	13C1602	9R(30)	12 340.8	31 139 452.9	0.9	5.0	1038.700 34(3)
Q(4, 2,-1)	13C1602	9R(30)	13 057.7	31 140 169.9	-1.4	20.0	1038.724 25(-5)
Q(3, 3,-1)	13C1602	9R(30)	13 248.8	31 140 360.9	20.6	20.0	1038.730 63(69)
Q(8, 4, 1)	13C1602	9R(30)	13 403.4	31 140 515.6	-3.5	5.0	1038.735 78(-12)
Q(9, 6, 1)	13C1602	9R(30)	14 322.3	31 141 434.5	6.5	5.0	1038.766 44(22)
Q(7, 3, 1)	12C1602	9P(28)	-16 891.7	31 142 616.5	-5.7	10.0	1038.805 86(-19)
Q(3, 2,-1)	12C1602	9P(28)	-16 644.0	31 142 864.2	1.3	10.0	1038.814 12(4)
Q(2, 2,-1)	12C1602	9P(28)	-14 625.1	31 144 883.1	1.3	5.0	1038.881 48(4)
Q(9, 7, 1)	12C1602	9P(28)	-14 338.9	31 145 169.3	15.5	5.0	1038.891 02(52)
Q(7, 4, 1)	12C1602	9P(28)	-13 579.8	31 145 928.4	-0.3	3.0	1038.916 33(-1)
Q(6, 3, 1)	12C1602	9P(28)	-12 163.1	31 147 345.0	-2.9	3.0	1038.963 60(-10)
Q(2, 1,-1)	12C1602	9P(28)	-11 970.7	31 147 537.4	-1.3	20.0	1038.970 01(-4)
Q(8, 6, 1)	12C1602	9P(28)	-11 970.7	31 147 537.4	-4.4	20.0	1038.970 01(-15)
Q(5, 2, 1)	12C1602	9P(28)	-11 293.4	31 148 214.8	-1.4	3.0	1038.992 61(-5)
Q(4, 1, 1)	12C1602	9P(28)	-11 040.4	31 148 467.8	-3.4	5.0	1039.001 05(-11)
Q(4,-1,-1)	12C1602	9P(28)	-10 908.2	31 148 600.0	-0.2	5.0	1039.005 46(-1)
Q(1, 1,-1)	12C1602	9P(28)	-10 615.6	31 148 892.5	7.6	30.0	1039.015 21(26)
Q(9, 8, 1)	12C1602	9P(28)	-10 426.2	31 149 082.0	34.7	30.0	1039.021 52(116)
Q(7, 5, 1)	12C1602	9P(28)	-10 130.8	31 149 377.4	-0.6	5.0	1039.031 39(-2)
Q(6, 4, 1)	13C1602	9R(32)	-9 213.6	31 150 670.0	6.6	10.0	1039.074 50(22)
Q(8, 7, 1)	12C1602	9P(28)	-8 207.8	31 151 300.4	14.0	10.0	1039.095 53(47)
Q(5, 3, 1)	12C1602	9P(28)	-8 113.1	31 151 395.0	-4.6	5.0	1039.098 69(-15)
Q(4, 2, 1)	13C1602	9R(32)	-8 293.9	31 151 589.8	1.6	5.0	1039.105 18(5)
R(0, 0, 1)	12C1602	9P(26)	-14 243.5	31 202 517.8	4.6	5.0	1040.803 95(15)
R(3, 3,-1)	12C1602	9P(22)	11 965.4	31 340 926.9	3.8	5.0	1045.420 78(13)
R(3, 2,-1)	12C1602	9P(22)	14 516.3	31 343 477.8	3.8	5.0	1045.505 87(13)
R(4, 1, 1)	12C1602	9P(20)	15 308.6	31 399 209.0	-3.7	5.0	1047.364 87(-12)
R(5,-1,-1)	12C1602	9P(18)	8 229.4	31 446 289.5	3.5	5.0	1048.935 31(12)
R(5, 2, 1)	12C1602	9P(18)	11 088.4	31 449 148.6	-1.6	3.0	1049.030 68(-5)
R(5, 3, 1)	12C1602	9P(18)	14 249.7	31 452 309.8	-3.9	3.0	1049.136 13(-13)
R(5, 4, 1)	12C1602	9P(18)	17 538.8	31 455 599.0	-5.3	3.0	1049.245 84(-18)
R(6, 6,-1)	12C1602	9P(16)	-17 196.3	31 474 241.1	20.4	20.0	1049.867 68(68)
R(6, 5,-1)	12C1602	9P(16)	-15 009.9	31 476 427.5	4.5	5.0	1049.940 61(15)
R(6, 4,-1)	12C1602	9P(16)	-12 678.5	31 478 758.9	3.2	3.0	1050.018 37(11)
R(6, 3,-1)	12C1602	9P(16)	-10 227.3	31 481 210.1	-2.0	5.0	1050.100 14(-7)
R(6, 4, 1)	12C1602	9P(16)	10 227.3	31 501 664.7	-6.1	5.0	1050.782 42(-20)
R(6, 5, 1)	12C1602	9P(16)	13 640.0	31 505 077.4	-0.4	5.0	1050.896 25(-1)
R(6, 6, 1)	12C1602	9P(16)	17 196.3	31 508 633.7	11.4	20.0	1051.014 88(38)

TABLE 2-2 (cont'd)

Trans.[a]	Laser[b]		ν_m[c]	ν/MHz	O-C[d]	Unc.[e]	ν/cm^{-1} [f]
R(7, 3,-1)	12C1602	9P(14)	-17 414.9	31 526 614.0	0.2	3.0	1051.614 64(1)
R(7, 2,-1)	12C1602	9P(14)	-14 825.3	31 529 203.6	5.5	5.0	1051.701 02(19)
R(7, 1,-1)	12C1602	9P(14)	-12 132.0	31 531 896.8	2.7	3.0	1051.790 86(9)
R(7, 0, 1)	12C1602	9P(14)	-9 329.4	31 534 699.5	-1.2	3.0	1051.884 35(-4)
R(7, 6, 1)	12C1602	9P(14)	9 938.3	31 553 967.1	4.3	3.0	1052.527 04(14)
R(8, 0, 1)	12C1602	9P(12)	-16 395.6	31 579 436.2	1.6	3.0	1053.376 61(5)
R(8, 1, 1)	12C1602	9P(12)	-13 892.7	31 581 939.0	2.8	3.0	1053.460 09(9)
R(8,-1,-1)	12C1602	9P(12)	-13 072.6	31 582 759.1	-0.1	3.0	1053.487 45(0)
R(8, 2, 1)	12C1602	9P(12)	-10 469.0	31 585 362.8	-5.8	5.0	1053.574 29(-19)
R(9, 8,-1)	12C1602	9P(12)	8 209.2	31 604 041.0	-34.4	OMIT	1054.197 32(-115)
R(9, 7,-1)	12C1602	9P(12)	10 247.7	31 606 079.4	-2.7	3.0	1054.265 32(-9)
R(8, 8, 1)	12C1602	9P(12)	10 247.7	31 606 079.4	42.5	OMIT	1054.265 32(142)
R(9, 6,-1)	12C1602	9P(12)	12 393.7	31 608 225.5	1.7	3.0	1054.336 90(6)
R(9, 5,-1)	12C1602	9P(12)	14 661.7	31 610 493.4	2.9	3.0	1054.412 55(10)
R(9, 4,-1)	12C1602	9P(12)	17 040.0	31 612 871.8	-3.1	3.0	1054.491 89(-10)
R(9, 2, 1)	12C1602	9P(10)	-17 439.9	31 629 403.5	-3.6	3.0	1055.043 33(-12)
R(9, 3, 1)	12C1602	9P(10)	-14 321.4	31 632 522.0	-4.6	3.0	1055.147 35(-15)
R(9, 4, 1)	12C1602	9P(10)	-11 091.2	31 635 752.2	-4.7	3.0	1055.255 11(-16)
R(10, 4,-1)	12C1602	9P(10)	9 373.4	31 656 216.8	2.5	3.0	1055.937 73(8)
R(10, 3,-1)	12C1602	9P(10)	11 883.3	31 658 726.7	3.1	3.0	1056.021 44(10)
R(10, 2,-1)	12C1602	9P(10)	14 494.1	31 661 337.5	2.5	5.0	1056.108 53(8)
R(10, 1,-1)	12C1602	9P(10)	17 204.6	31 664 047.9	2.7	3.0	1056.198 94(9)
R(10, 6, 1)	12C1602	9P(8)	-11 214.8	31 685 846.6	-0.5	3.0	1056.926 07(-2)
R(11, 1,-1)	12C1602	9P(8)	9 677.3	31 706 738.7	10.1	20.0	1057.622 95(34)
R(11, 0, 1)	12C1602	9P(8)	12 478.7	31 709 540.1	3.6	3.0	1057.716 40(12)
R(11, 1, 1)	12C1602	9P(8)	14 634.8	31 711 696.3	1.1	5.0	1057.788 33(4)
R(11,-1,-1)	12C1602	9P(8)	16 115.8	31 713 177.2	1.1	5.0	1057.837 72(4)
R(12, 8,-1)	12C1602	9P(6)	-14 767.6	31 731 716.2	1.1	3.0	1058.456 12(4)
R(11, 7, 1)	12C1602	9P(6)	-14 516.1	31 731 967.7	2.3	3.0	1058.464 51(8)
R(11, 8, 1)	12C1602	9P(6)	-10 832.4	31 735 651.4	13.2	10.0	1058.587 37(44)
R(12, 6,-1)	12C1602	9P(6)	-10 437.5	31 736 046.2	-10.8	10.0	1058.600 55(-36)
R(12, 5,-1)	12C1602	9P(6)	-8 080.2	31 738 403.6	6.6	5.0	1058.679 19(22)
R(12,-1,-1)	12C1602	9P(6)	8 815.6	31 755 299.4	0.3	3.0	1059.242 77(1)
R(12, 2, 1)	12C1602	9P(6)	10 927.2	31 757 410.9	0.2	5.0	1059.313 20(1)
R(12, 3, 1)	12C1602	9P(6)	14 002.6	31 760 486.4	-0.4	3.0	1059.415 79(-1)
R(12, 4, 1)	12C1602	9P(6)	17 174.2	31 763 657.9	-0.7	5.0	1059.521 58(-2)
R(13, 6,-1)	12C1602	9P(4)	-17 814.1	31 777 294.6	0.1	20.0	1059.976 45(0)
R(12, 8, 1)	12C1602	9P(4)	-17 653.5	31 777 455.2	7.6	5.0	1059.981 80(26)
R(13, 5,-1)	12C1602	9P(4)	-15 448.3	31 779 660.4	-0.4	3.0	1060.055 37(-1)
R(13, 4,-1)	12C1602	9P(4)	-12 991.0	31 782 117.7	-6.0	20.0	1060.137 33(-20)
R(13, 3,-1)	12C1602	9P(4)	-10 431.7	31 784 677.0	-0.4	3.0	1060.222 70(-1)
R(13, 4, 1)	12C1602	9P(4)	9 804.0	31 804 912.6	-3.0	5.0	1060.897 69(-10)
R(13, 5, 1)	12C1602	9P(4)	13 054.0	31 808 162.7	0.6	10.0	1061.006 10(2)
R(14,10,-1)	12C1602	9P(4)	14 245.1	31 809 353.8	8.5	5.0	1061.045 83(28)
R(14, 9,-1)	12C1602	9P(4)	16 182.4	31 811 291.1	2.9	5.0	1061.110 44(10)
R(13, 6, 1)	12C1602	9P(4)	16 398.6	31 811 507.3	-4.9	3.0	1061.117 65(-16)
R(16, 9, 1)	12C1602	9R(2)	-17 740.2	31 941 255.8	-15.4	5.0	1065.445 60(-51)
R(17, 3,-1)	12C1602	9R(2)	-15 986.7	31 943 009.4	-9.1	5.0	1065.504 10(-30)
R(16,10, 1)	12C1602	9R(2)	-14 069.6	31 944 926.5	-25.7	30.0	1065.568 05(-86)
R(17, 1,-1)	12C1602	9R(2)	-10 559.4	31 948 436.7	-5.7	3.0	1065.685 14(-19)

TABLE 2-2 (cont'd)

Trans.[a]	Laser[b]	ν_m[c]	ν/MHz	O-C[d]	Unc.[e]	ν/cm^{-1} [f]
R(18, 8,-1)	12C1602 9R(2)	9 385.3	31 968 381.4	18.9	30.0	1066.350 41(63)
R(17, 6, 1)	12C1602 9R(2)	10 380.0	31 969 376.0	5.3	3.0	1066.383 59(18)
R(18, 7,-1)	12C1602 9R(2)	11 749.6	31 970 745.7	22.5	30.0	1066.429 29(75)
R(18, 6,-1)	12C1602 9R(2)	14 169.2	31 973 165.3	2.0	5.0	1066.509 99(7)
R(18, 5,-1)	12C1602 9R(2)	16 674.9	31 975 671.0	-3.8	5.0	1066.593 57(-13)
R(17, 8, 1)	12C1602 9R(2)	17 041.8	31 976 037.9	-4.8	5.0	1066.605 81(-16)
R(18, 1,-1)	12C1602 9R(4)	-17 696.5	31 986 320.9	-5.9	5.0	1066.948 82(-20)
R(18, 0, 1)	12C1602 9R(4)	-14 902.2	31 989 115.2	-12.6	20.0	1067.042 03(-42)
R(18, 1, 1)	12C1602 9R(4)	-13 901.0	31 990 116.4	-1.9	5.0	1067.075 41(-6)
R(18,-1,-1)	12C1602 9R(4)	-10 192.3	31 993 825.1	-0.9	5.0	1067.199 12(-3)
R(18, 2, 1)	12C1602 9R(4)	-9 141.0	31 994 876.4	6.1	3.0	1067.234 20(20)
R(19, 5,-1)	12C1602 9R(4)	8 795.5	32 012 812.9	-1.6	3.0	1067.832 49(-5)
R(18, 8, 1)	12C1602 9R(4)	9 640.6	32 013 658.0	-11.3	10.0	1067.860 68(-38)
R(19, 3,-1)	12C1602 9R(4)	14 041.3	32 018 058.7	-11.1	10.0	1068.007 47(-37)
R(19, 2,-1)	12C1602 9R(4)	16 741.5	32 020 758.9	-14.5	20.0	1068.097 54(-49)
R(19,-1,-1)	12C1602 9R(6)	-17 028.8	32 031 207.5	0.6	3.0	1068.446 06(2)
R(19, 2, 1)	12C1602 9R(6)	-16 187.3	32 032 048.9	10.8	3.0	1068.474 14(36)
R(19, 3, 1)	12C1602 9R(6)	-13 240.9	32 034 995.4	15.3	5.0	1068.572 41(51)
R(20, 2,-1)	12C1602 9R(6)	9 030.6	32 057 266.8	-12.8	10.0	1069.315 31(-43)
R(20, 1,-1)	12C1602 9R(6)	11 788.4	32 060 024.6	-10.4	3.0	1069.407 31(-35)
R(20, 0, 1)	12C1602 9R(6)	14 588.8	32 062 825.1	-7.2	10.0	1069.500 72(-24)
R(20, 1, 1)	12C1602 9R(6)	15 166.7	32 063 403.0	2.0	5.0	1069.519 99(7)
R(20, 4, 1)	12C1602 9R(8)	-17 229.4	32 074 423.3	24.6	10.0	1069.887 60(82)
R(20, 5, 1)	12C1602 9R(8)	-14 222.9	32 077 429.8	17.9	10.0	1069.987 87(60)

[a] Numbers are J, k, and ℓ of the lower vibrational state. The k,ℓ = -1,-1 level is the lower energy component of an ℓ-type doublet.

[b] Laser line used; laser frequencies were taken from Ref. 37.

[c] Microwave frequency in MHz. The signed microwave frequency was added to the laser frequency to obtain the absorption frequency.

[d] Observed minus calculated frequency in MHz; the parameters for the calculation are in Tables 2-3 and 2-4.

[e] Estimated uncertainty in the observed frequency in MHz. An "OMIT" means that the frequency was omitted from the least squares fits.

[f] Observed wavenumber in cm^{-1}. The numbers in parentheses are observed minus calculated wavenumbers in units of 0.00001 cm^{-1}.

TABLE 2-3

Molecular Constants of the $v_6 = 1$ State of $^{12}CH_3F$[a]

Parameter[b]	This Work[c]	Hirota[d]
E_v /GHz	35 455.736 0[e]	35 455.736 0(240)
B_v /MHz	25 418.931 7(144)	25 418.92(48)[f]
(A_v-B_v) /MHz	130 491.1[e]	130 491.1(42)
D_J /kHz	61.613 5(4190)	59.869[g]
D_{JK} /kHz	457.251(4225)	440.27[g]
D_K /kHz	2 108.[e]	2 108.[g]
H_J /Hz	1.961(1061)	
H_{JK} /Hz	7.231(8791)	
H_{KJ} /Hz	-160.30(3447)	
H_K /Hz	0.[h]	
$A\zeta$ /MHz	46 279.[e]	46 279.(33)
η_J /kHz	1 146.40(454)	1 120.(60)[f]
η_K /kHz	-9 600.[e]	-9 600.(6600)
q_v /MHz	8.720 5(396)	8.70(13)[f]
q'_v /kHz	-2.147 7(258)	

[a]Values in parentheses are one standard deviation in multiples of the last digit in the parameter.

[b]Vibration-rotation parameters.

[c]Obtained from a fit of the vibration-rotation frequencies listed in Table 2-2.

[d]Ref. 8, Table 2-3.

[e]Constrained to the value reported in Ref. 8.

[f]Ref. 7, Table I.

[g]Assumed to be the same as in the ground state (Ref. 8).

[h]Constrained to zero.

TABLE 2-4

Molecular Constants of the v_3=1,v_6=1 Vibrational State of $^{12}CH_3F$[a]

Parameter[b]	This Work[c]	Nakagawa et al.[d]
E_v /GHz	66 608.085 00(109)	66 605.04(36)
B_v /MHz	25 082.214 8(305)	25 080.(39)
(A_v-B_v) /MHz	130 557.989 9(961)	127 452.(60)
D_J /kHz	58.076 9(4107)	55.2(45)
D_{JK} /kHz	519.867(3725)	528.(6)
D_K /kHz	2 039.099(2173)	2 370.(30)
H_J /Hz	1.166(855)	
H_{JK} /Hz	8.966(6712)	
H_{KJ} /Hz	-186.89(3241)	
ΔH_K /Hz	13.26(1270)	
$A\zeta$ /MHz	44 850.096(97)	41 800.(150)
η_J /kHz	942.86(433)	1 020.(60)
η_K /kHz	-9 479.44(41)	3 900.(300)
q_v /MHz	-2.204 7(50)	-90.[e]
q'_v /kHz	-0.959 8(207)	

[a]Values in parentheses are one standard deviation in multiples of the last digit in the parameter.

[b]Vibration-rotation parameters.

[c]Obtained from a fit of the vibration-rotation frequencies listed in Table 2-2.

[d]Ref. 9, Table I.

[e]Ref. 9, constrained.

II-5 Discussion

The frequencies of the transitions in Table 2-2 were fit without consideration of Coriolis interaction with other vibrational states. It is known that the levels of the $v_6 = 1$ state are in mild Coriolis resonance with the levels of $v_3 = 1$ (1,21) and presumably a similar resonance occurs between $(v_3,v_6)=(1,1)$, (2,0), and (0,2). As was discussed in the studies of the ν_3 band from this laboratory (1,2), the mild ν_3-ν_6 Coriolis resonance in CH_3F can be taken into account for reasonable J and k by adjustment of the rotational and centrifugal distortion constants for the states involved. As can be seen in Table 2-2, the transitions in the present work are limited to $J \leq 20$ and $K \leq 10$, and for K = 10 the residuals are beginning to show Coriolis effects that cannot be simulated by adjustment of the parameters. Since the necessary frequency information was not available for the $v_6 = 2$ vibrational state, we did not examine the Coriolis interaction with nearby vibrational states in detail. The comparisons in Table 2-2 show that the frequencies of the transitions in the $\nu_3+\nu_6-\nu_6$ band can be computed from the parameters in Tables 2-3 and 2-4 to within a few MHz for lower J and K and to within ±10 MHz for $J \leq 20$, $K \leq 10$.

In Tables 2-3 and 2-4 the parameters obtained in the present study are compared to previously-determined values. Except for the ℓ-doubling constant, the newly-determined constants agree with the older values to within the experimental accuracy of the latter. However, the new constants are much more precise, as the older data led to predictions of the frequencies that differed by as much as 1 GHz (0.03 cm^{-1}) from the experimental values. Coriolis parameters for $\nu_3+\nu_6$ have been also

determined from the frequencies of the assigned ℓ=-1 transitions of $\nu_3+\nu_6-\nu_6$ band. Finally, the parameters in Tables 2-3 and 2-4 have been used to predict coincidences within 100 MHz of laser lines for the various isotopes of CO_2. The predicted coincidences are in Table 2-5, which may be helpful for various studies such as infrared-infrared double resonance.

There are intriguing aspects of this work that suggest interesting topics for future study. First, there are unanswered questions about the effects of Coriolis coupling, or possibly Fermi resonance, in the $\nu_3+\nu_6$ state. Two pieces of evidence suggest that such effects should not be ignored: (1) the q_v constants in the ν_6 and $\nu_3+\nu_6$ states differ not only in magnitude, but in sign, whereas they are expected to be of similar value (Eq. (2-81)); and (2) the ratio of the intensities of the transitions in the $2\nu_3-\nu_3$ band to those in the $\nu_3+\nu_6-\nu_6$ band, although not measured, seemed to be greater than the value of ~2 that is inferred from the Boltzmann factor. A second interesting subject for future research would be an attempt to observe transitions in the $\nu_3+\nu_6-\nu_6$ band that obey selection rules other than the $\Delta k = 0$, $\Delta\ell = 0$ rules observed in this work. In principle, transitions with $\Delta k = \pm 2$, $\Delta\ell = \pm 2$ and with $\Delta k = \pm 1$, $\Delta\ell = \mp 2$ are allowed via the $(\pm 2,\pm 2)$ and $(\pm 2,\mp 1)$ type ℓ-resonances, respectively. However, their intensities may be as much as two orders of magnitude or more below the intensities observed in this study as inferred from the fact that frequency corrections due to ℓ-resonances are usually less than 20 MHz except for ℓ-type doublets. Nevertheless, the molecular constants reported here are sufficiently accurate to predict these frequencies to within a few MHz for low J and k, so that it may be possible to observe them if a region can be found

TABLE 2-5

Coincidences between Calculated Frequencies for the $\nu_3+\nu_6-\nu_6$ Band of $^{12}CH_3F$ and Laser Frequencies

Trans.[a]	Frequency[b]	$\nu_0-\nu_L$[c]	Laser[d]	
P(12, 8,-1)	30 480 581.7	54.7	12C1602 BAND II	P(50)
P(10, 3,-1)	30 606 125.4	14.9	12C160180 BAND II	P(58)
P(10, 7, 1)	30 637 314.3	-19.4	12C160180 BAND II	P(57)
P(8, 1, 1)	30 730 197.3	74.3	12C160180 BAND II	P(54)
Q(18, 3,-1)	31 029 621.8	-78.6	12C160180 BAND II	P(44)
Q(20, 6, 1)	31 029 700.6	0.3	12C160180 BAND II	P(44)
Q(17, 3,-1)	31 041 668.1	-35.1	13C1802 BAND II	R(12)
Q(18, 4, 1)	31 049 480.4	0.5	12C1802 BAND II	P(58)
Q(15, 5,-1)	31 059 008.1	-1.1	13C1602 BAND II	R(26)
Q(13, 1, 1)	31 093 513.9	25.4	13C1602 BAND II	R(28)
Q(10,10,-1)	31 093 552.5	64.0	13C1602 BAND II	R(28)
P(1, 0, 1)	31 101 511.4	19.2	12C1602 BAND II	P(30)
Q(13, 5, 1)	31 106 726.8	-25.7	12C1802 BAND II	P(56)
Q(9, 2,-1)	31 116 638.7	42.8	12C160180 BAND II	P(41)
Q(11, 6, 1)	31 127 170.8	58.6	13C1602 BAND II	R(30)
Q(9, 7, 1)	31 145 153.8	-96.6	12C160180 BAND II	P(40)
Q(5, 1, 1)	31 145 263.9	13.5	12C160180 BAND II	P(40)
Q(6, 4, 1)	31 150 663.4	1.7	13C1802 BAND II	R(18)
R(8, 6, 1)	31 598 614.4	58.3	12C1802 BAND II	P(38)
R(9, 5,-1)	31 610 490.6	-43.4	13C1802 BAND II	R(48)
R(10, 2,-1)	31 661 334.8	-96.8	13C1802 BAND II	R(52)
R(10, 9, 1)	31 696 998.2	-63.3	12C1602 BAND II	P(8)
R(15, 3, 1)	31 882 260.9	-45.9	12C160180 BAND II	P(12)
R(18, 5, 1)	32 003 944.4	-73.0	12C1602 BAND II	R(4)

[a] Transition in the $\nu_3+\nu_6-\nu_6$ band of $^{12}CH_3F$; $J \leq 20$, $k \leq 10$.

[b] Frequency of the $\nu_3+\nu_6-\nu_6$ band transition in MHz.

[c] Frequency of the $\nu_3+\nu_6-\nu_6$ band transition minus the laser frequency in MHz.

[d] Identification of the CO_2 laser; Band II is the 9 μm band. Laser frequencies were obtained from Ref. 37.

in which the transitions are not strongly overlapped.

II-6 Appendix

The contribution to the energy of the state $|v,J,k,\ell=+1\rangle$ from the $(\pm 2,\mp 1)$ interaction given in Eq. (2-89) can be represented by a second order perturbation,

$$W_r(v,J,k,\ell=+1) = \frac{4r_v^2(2k+1)^2[J(J+1)-k(k+1)]}{W(v,J,k,\ell=+1)-W(v,J,k+1,\ell=-1)} \quad . \tag{2-92}$$

The energy difference between the corresponding rotational levels may be calculated approximately by

$$W(v,J,k,\ell=+1) - W(v,J,k+1,\ell=-1)$$

$$= \nu_o+BJ(J+1)+(A-B)k^2-2A\zeta k$$
$$-[\nu_o+BJ(J+1)+(A-B)(k+1)^2+2A\zeta(k+1)]$$

$$= -(2k+1)(A-B+2A\zeta) \quad . \tag{2-93}$$

By substituting Eq. (2-93) into Eq. (2-92),

$$W_r(v,J,k,\ell=+1) = -\left(\frac{4r_v^2}{A-B+2A\zeta}\right)(2k+1)[J(J+1)-k(k+1)]$$
$$= r'[-J(J+1)-2kJ(J+1)+k+3k^2+2k^3] \quad . \tag{2-94}$$

where

$$r' = 4r_v^2/(A-B+2A\zeta) \tag{2-95}$$

If the contribution to the energy of the state $|v,J,k,\ell=-1\rangle$ is calculated in similar fashion, it will be seen that the result is the same except that the signs of the terms including odd powers of k are reversed. Therefore, since $\ell = \pm 1$ only for $v = 1$, we can write for the energy of either state,

$$W(v,J,k,\ell=\pm 1) = r'[-J(J+1)+3k^2+k\ell-2J(J+1)k\ell+2k^3\ell] \quad . \qquad (2\text{-}96)$$

II-7 References

1. P. Shoja-Chagervand and R. H. Schwendeman, J. Mol. Spectrosc. **98**, 27-40 (1983).

2. S. K. Lee, R. H. Schwendeman, and G. Magerl, J. Mol. Spectrosc. **117**, 416-434 (1986).

3. S. K. Lee, R. H. Schwendeman, R. L. Crownover, D. D. Skatrud, and F. C. DeLucia, J. Mol. Spectrosc. **123**, 145-160 (1987).

4. Y. Matsuo and R. H. Schwendeman, J. Chem. Phys. **91**, 3966-3975 (1989).

5. W. L. Smith and I. M. Mills, J. Mol. Spectrosc. **11**, 11-38 (1963).

6. T. Tanaka and E. Hirota, J. Mol. Spectrosc. **54**, 437-446 (1975).

7. E. Hirota, T. Tanaka, and S. Saito, J. Mol. Spectrosc. **63**, 478-484 (1976).

8. E. Hirota, J. Mol. Spectrosc. **74**, 209-216 (1979).

9. J. Nakagawa, I. Suzuki, T. Shimanouchi, and T. Fujiyama, Bull. Chem. Soc. Japan **47**, 1134-1138 (1974).

10. G. Duxbury and H. Kato, Chem. Phys. **66**, 161-167 (1982).

11. S. Yamamoto, R. Kuwabara, M. Takami, and K. Kuchitsu, J. Mol. Spectrosc. **115**, 333-352 (1986).

12. G. Graner, R. Anttila, and J. Kauppinen, Mol. Phys. **38**, 103-128 (1979).

13. Z. Yao, B. R. Foy, J. R. Hetzler, and J. I. Steinfeld, Spectrochim.Acta. **42A**, 1337-1339 (1986).

14. W. H. Shaffer, Rev. Mod. Phys. **16**, 245-259 (1944).

15. A. J. Merer, J. K. G. Watson, J. Mol. Spectrosc. **47**, 499-514 (1973).

16. G. Herzberg, "Molecular Spectra and Molecular Structure. II. Infrared and Raman Spectra of Polyatomic Molecules". D. Van Nostrand, Princeton, New Jersey 1959.

17. J. T. Hougen, J. Chem. Phys. **37**, 1433-1441 (1962).

18. H. H. Nielsen, Rev. Mod. Phys. **23**, 90-136 (1951).

19. H. H. Nielsen, in Handb. Physik, Vol. 37, Part I, Springer, Berlin 1959.

20. G. Amat, H. H. Nielsen, and G. Tarrago, "Rotation-Vibration of Polyatomic Molecules". M. Dekker, New York 1971.

21. C. DiLauro and I.M. Mills, J. Mol. Spectrosc. 21, 386-413 (1966).

22. H. A. Jahn, Phys. Rev. 56, 680-683 (1939).

23. J. S. Garing, H. H. Nielsen, and K. N. Rao, J. Mol. Spectrosc. 3, 496-527 (1959).

24. E. B. Wilson, Jr., J Chem. Phys. 3, 818-821 (1935).

25. T. Oka, J. Chem. Phys. 47, 5410-5426 (1967).

26. H. H. Nielsen, Phys. Rev. 75, 1961 (1949).

27. H. H. Nielsen, Phys. Rev. 77, 130-135 (1950).

28. M. L. Grenier-Besson, J. Phys. Radium 21, 555-565 (1960).

29. G. Amat, Compt. Rend. 250, 1439 (1960).

30. G. J. Cartwright and I. M. Mills, J. Mol. Spectrosc. 34, 415-439 (1970).

31. A. Biernacki, D. C. Moule, and J. L. Neale, Appl. Spectrosc. 26, 648-650 (1972).

32. D. Horn and G. C. Pimental, Appl. Opt. 10, 1892-1898 (1971).

33. J. U. White, J. Opt. Soc. Am. 32, 285-288 (1942).

34. H. J. Bernstein and G. Herzberg, J. Chem. Phys. 16, 30-39 (1948).

35. T. H. Edwards, J. Opt. Soc. Am. 51, 98-102 (1961).

36. S. C. Hsu, Ph. D. Thesis, Michigan State University, 1988.

37. C. Freed, L. C. Bradley, and R. G. O'Donnell, IEEE J. Quantum Electron. QE-16, 1195-1206 (1980).

38. R. M. Lees, J. Mol. Spectrosc. 33, 124-136 (1970).

39. M. L. Grenier-Besson and G. Amat, J. Mol. Spectrosc. 8, 22-29 (1962).

CHAPTER III

HIGH RESOLUTION INFRARED STUDY OF THE ν_2 BANDS OF CD_3I AND CD_3Br

III-1 Introduction

The fundamental halides, CD_3I and CD_3Br, have been the subject of a number of spectroscopic studies in the microwave and infrared regions. Especially the ν_2 bands are of importance because they occur in the CO_2 laser region and have therefore provided considerable spectroscopic information by means of linear and nonlinear spectroscopic techniques. The ν_2 band is identified to be the symmetric deformation of symmetry A_1, a parallel band, among the six fundamental bands of the C_{3v} prolate symmetric top. The ν_2 bands for both molecules appear in almost the same region ($\nu_2(CD_3I)$=949.4cm^{-1}, $\nu_2(CD_3Br)$=991.4cm^{-1}), and were reported to have sufficient intensity that a long path cell is not necessary for observation of the spectra as long as the sample pressure is higher than 0.1 Torr (1-7).

This chapter is concerned with high resolution infrared studies of the ν_2 bands of these molecules by means of an infrared-microwave sideband laser spectrometer. As for other methyl halide molecules, the Coriolis interactions between the ν_2 bands and the ν_5 bands (asymmetric deformation) of these molecules have been long-standing subjects of study (2,3,6,7). A question concerning the effects of the Coriolis coupling for these bands was one of the reasons for our interest in

studying the molecules. The main reason for studying them, however, was to determine the magnitude of the nuclear quadrupole coupling constants of the iodine and bromine atoms by the method of infrared-radiofrequency double resonance. The presence of a single nucleus of spin I > 1 in each of these molecules causes each rotational level to be split into 2I+1 sublevels. As a result, the lineshapes of transitions in the infrared spectra of these species are distorted and sometimes, especially in CD_3I spectra, even split. Direct observations of pure quadrupole transitions by means of infrared-radio frequency double resonance allowed us to determine the magnitude of the quadrupole interaction between the nuclear quadrupole and the electric field gradient at the I or Br nucleus. However, in order to perform the double-resonance study, it was first necessary to have accurate frequencies for linear infrared spectra for the vibration-rotation bands. The experimental frequencies and parameters are reported in this chapter; the infrared-radiofrequency double resonance results are described in the next chapter.

In this work, the ν_2 bands of CD_3I, $CD_3{}^{79}Br$, and $CD_3{}^{81}Br$ were recorded at Doppler-limited resolution. About 200 transitions for each species, including transitions of high J,K (higher than 40,8), were recorded and the frequencies measured to an accuracy of few MHz. The effect of the quadrupole interaction has been observed for some transitions in the infrared spectrum and the infrared frequencies have been converted to hypothetical unsplit frequencies where necessary. The frequencies in these parallel bands have been combined with frequencies reported from previous microwave, millimeter, and infrared studies and fit by least squares to an energy expression containing centrifugal

distortion parameters up to the eighth order. The Coriolis interaction with the ν_5 band has been taken into account in each case by using previously-reported parameters (2,7) for the interaction and for the ν_5 band. The resulting combination of the ν_2 parameters obtained in this work is sufficient to predict the frequencies within a few MHz for the appropriate range of J and K. The determined parameters have been used to calculate coincidences with CO_2 laser frequencies.

In a series of microwave studies of the ground vibrational state of CD_3I by Simmons and co-workers (8-10) the rotational constant B_0 and the centrifugal distortion constants D_J and D_{JK} were determined. Kuczkowski (11) extended this microwave work to transitions in the low-lying vibrational states ν_2, ν_3, ν_5, ν_6, $2\nu_3$, and $\nu_3+\nu_6$. More recently, higher J transitions have been recorded in the millimeter wave region and more accurate quadrupole constants were reported for low-lying vibrational states by Demaison et al. (12) and by Wlodarczak et al. (13).

The first vibration-rotation spectra of CD_3I were taken by Jones et al. (1) with grating spectrometers in the 500-5000 cm^{-1} region. A series of studies of several bands by different investigators followed (14-19). In 1976 Matsuura and Shimanouchi reported a study of Coriolis coupling of the ν_2, ν_5, and $2\nu_3$ bands (2). Then, as a result of laser-Stark and laser-microwave double resonance spectroscopy, Kawaguchi et al. (3) obtained the rotational constant B_2, the centrifugal distortion constants D_J and D_{JK}, and the quadrupole coupling constant eQq for the ν_2 vibrational state in a study in which they found no need to include Coriolis coupling to other states for the rather low J transitions that they recorded. In addition to the vibration-rotation parameters

obtained by infrared studies of deuterated methyl iodide, the rotational constant A_0 and the centrifugal distortion constant D_K were determined by studying the ν_4 band by Raman spectroscopy (20).

Sakai and Katayama (21,22) have performed level-crossing and level-anticrossing experiments in CD_3I by using the coincidence of the $^QP(4,1)$ transition of the ν_2 band with the CO_2 10P(16) laser line. They determined the dipole moments of the ground and ν_2 vibrational states in this laser Stark study. An intracavity cell and an external cavity White cell were used by Caldow et al. (23) to record laser Stark Lamb dips for this molecule. Infrared radio frequency double resonance at 1-MHz resolution was reported by Rackley and Butcher (24) as part of a study of Stark-tuned non-linear spectroscopy. More recently, Demaison et al. (12) used infrared-radiofrequency double resonance to measure the frequencies of pure quadrupole transitions in the ground state of this molecule with 100 kHz accuracy. Vibrational energy transfer has been studied in CD_3I by using coincidences with Q-switched CO_2 laser lines and detecting fluorescence from ν_1, ν_4, ν_6, and $2\nu_5$ levels (25). The influence of nuclear quadrupole coupling on rotational relaxation has been investigated by means of microwave double resonance (26). Finally, submillimeter wave laser emission has been observed from CD_3I pumped by a number of CO_2 laser lines (27).

Even with all of these spectroscopic studies, there has been no systematic study at Doppler-limited resolution of high J and K transitions in the very important ν_2 band region of CD_3I. Such a study would be expected to provide more precise frequency information and to allow investigation of the effect of Coriolis coupling in the calculations of the energies of the levels in the v_2=1 state. It would

also allow accurate calculation of possible coincidences between ν_2-band transitions and CO_2 laser lines.

The infrared and microwave spectra of CD_3Br are rather complicated compared with CD_3I for two reasons: First, CD_3Br consists of two isotopes with almost the same natural abundance ($CD_3{}^{79}Br$ = 50.54%, $CD_3{}^{81}Br$ = 49.46%); thus, the transitions of the two species with the same J,K appear about 500 MHz apart, depending on the value of J and K. Second, the Coriolis interaction between the ν_2 (991.4 cm^{-1}) and the ν_5 (1055.5 cm^{-1}) bands is much more serious than in CD_3I since the bands lie only 64 cm^{-1} apart and the Coriolis coupling constants are about 1.5 times larger than that of CD_3I. As a result, CD_3Br has not been studied previously in as much detail as CD_3I.

Infrared spectra of the ν_2 bands of $CD_3{}^{79}Br$ and $CD_3{}^{81}Br$ recorded with grating instruments have been reported by Morino and Nakamura (4) and by Jones et al. (5). More recently, Betrencourt-Stirnemann et al. (6) analyzed the ν_2 and ν_5 bands recorded by Fourier transform spectroscopy at a resolution of 0.01 cm^{-1}. Also, Harada et al. observed low J,K transitions and investigated the Coriolis coupling between the ν_2 and ν_5 bands by laser-Stark spectroscopy (7) and Edwards and Broderson determined the rotational constant A_0 by analysis of Raman spectra of the ν_4 band (28). Microwave spectra in the ground states of $CD_3{}^{79}Br$ and $CD_3{}^{81}Br$ have been reported by Garrison et al. (10) and have been extended to low-lying excited states by Morino and Hirose (29). Frequencies reported by these workers (6,7,10,29) were included in our analysis.

As implied by the studies performed to date, the ν_2 band of CD_3Br

has been one of the major concerns and the Coriolis interaction between the ν_2 and the ν_5 bands is very important for analyzing the corresponding rotational energy structure. However, for possible double resonance studies, the previous FT-IR (6) and laser-Stark (7) studies had not provided precise enough frequency information because of the limited resolution as well as a frequency calibration problem. Therefore, experimental frequencies and rovibrational parameters were obtained in this study and are reported for both species.

III-2 Theory

III-2-1 Term Values

The $v_2 = 1$ states of CD_3I and both $CD_3{}^{79}Br$ and $CD_3{}^{81}Br$ are nondegenerate, so the vibration-rotation energy levels of these states and the ground states of these species can be expressed as the usual power series in $J(J+1)$ and K^2, as follows:

$$\begin{aligned} W_R(v,J,K) &= \nu_v + B_v\, J(J+1) + (A_v - B_v)\, K^2 \\ &\quad - D_J^v\, J^2(J+1)^2 - D_{JK}^v\, J(J+1)K^2 - D_K^v\, K^4 \\ &\quad + H_J^v\, J^3(J+1)^3 + H_{JK}^v\, J^2(J+1)^2K^2 + H_{KJ}^v\, J(J+1)K^4 + H_K^v\, K^6 \\ &\quad + L_J^v\, J^4(J+1)^4 + L_{JJJK}^v\, J^3(J+1)^3\, K^2 + L_{JJKK}^v\, J^2(J+1)^2\, K^4 \\ &\quad + L_{JKKK}^v\, J(J+1)K^6 + L_K^v\, K^8 \quad . \end{aligned} \tag{3-1}$$

In this expression, ν_v is the vibrational energy of the state v ($\nu_0 = 0$), A_v and B_v are rotational constants for the state v, and the D's, H's, and L's are quartic, sextic, and octic centrifugal distortion constants for the state v, respectively. The frequencies corresponding to the experimental frequencies were computed by taking differences in energy levels calculated with the term value written above; the usual selection rules for a parallel band, $\Delta J = 0, \pm 1$ and $\Delta k = 0$ ($K = |k|$) were used.

III-2-2 Coriolis Interaction

In order to include the effect of the Coriolis coupling on the fitting of the frequencies reported here, we calculated the effect of

the coupling for each of the transitions in the fitting and subtracted these effects from the experimental frequencies before completing the fitting. For this purpose, the appropriate matrix was set up for each transition and the eigenvalue was obtained by diagonalizing each matrix; the second order perturbation method is considered not to be adequate because of the large Coriolis effect and the accuracy of frequency determination of this work. The zero-order energy was subtracted from the desired eigenvalue and the difference was subtracted from the experimental frequency. The coupling effects and the subtracted zero-order energies were calculated with the parameters, including the parameters for $v_2 = 1$, reported in previous works where the Coriolis interaction constants are derived. This was done to insure a treatment of the Coriolis effects that was equivalent to the previous analysis, since we do not have any additional data for the other vibrational states involved.

III-2-2-1 CD_3I

There are three vibrational states, v_2=1 (A_1, 949.4 cm^{-1}), v_5=1 (E, 1049.3 cm^{-1}), and v_3=2 (A_1, 999.0 cm^{-1}), involved in the mid-infrared Coriolis interaction system in CD_3I (2). In order to calculate the effect of the Coriolis interaction, the appropriate matrix was set up for each transition as discussed in Ref. (2):

$$
\begin{array}{cccc}
|0,0,1,-1;J,k-1\rangle & |1,0,0,0,J,k\rangle & |0,2,0,0;J,k\rangle & |0,0,1,+1;J,k+1\rangle \\
\left[\begin{array}{cccc}
E_o(v_5=1,\ell_5=-1;J,k-1) & -\xi_{25}f(J,k-1) & -\xi_{335}f(J,k-1) & -q_5f(J,k-1)f(J,k+1)/2 \\
 & E_o(v_2=1,J,k) & 0 & \xi_{25}f(J,k+1) \\
 & & E_o(v_3=2;J,k) & \xi_{335}f(J,k+1) \\
\text{(Hermitian)} & & & E_o(v_5=1,\ell_5=1;J,k+1)
\end{array}\right]
\end{array}
$$

. (3-2)

In this equation, E^o denotes the unperturbed energy, the "ket" notation is $|v_2,v_3,v_5,\ell_5;J,k\rangle$, the $-q_5f(J,k-1)f(J,k+1)/2$ term accounts for the $(\pm2,\pm2)$ interaction in the $v_5=1$ state, and

$$f(J,k\pm1) = [J(J+1)-k(k\pm1)]^{1/2} \quad . \tag{3-3}$$

For K=0, the matrix is reduced to 3x3 matrices; for the A_+ species

$$
\begin{array}{ccc}
|1,0,0,0;J,0\rangle & |0,2,0,0;J,0\rangle & |0,0,1,\pm1;J,1\rangle \\
\left[\begin{array}{ccc}
E_o(v_2=1;J,k=0) & 0 & \xi_{25}\{2[J(J+1)]\}^{1/2} \\
 & E_o(v_3=2;J,k=0) & \xi_{335}\{2[J(J+1)]\}^{1/2} \\
\text{(Hermitian)} & & E_o(v_5=1,\ell_5=1;J,k=1)+q_5J(J+1)/2
\end{array}\right]
\end{array}
\tag{3-4}
$$

and for A_- species that do not affect the $v_2=1$ state,

$$|0,0,1,\pm1;J,1\rangle = E^o(v_5=1,\ell_5=1;J,k=1)-q_5J(J+1)/2 \ . \tag{3-5}$$

The parameters used in our calculation are given in Table II of Ref. (2). The only ambiguity in this procedure was the specific value to

use for $B\zeta^{(y)}_{2,5}$ which affects the value of ξ_{25}. In Table II of Ref. (2) only the value of $|\zeta^{(y)}_{2,5}|$ is given; the value of B used to obtain the desired product is not mentioned. A value of 3106.495 MHz was used for the combined constant $B\zeta^{(y)}_{2,5}$ by using the B_2 rotational constant of the v_2=1 state in the following equation.

$$\xi_{25} = (1/2)^{1/2}[(\nu_5/\nu_2)^{1/2}+(\nu_2/\nu_5)^{1/2}]B\zeta^{(y)}_{2,5} \quad . \qquad (3\text{-}6)$$

The resulting value of ξ_{25} was 4398.7 MHz.

III-2-2-2 CD_3Br

The Coriolis coupling between the ν_2 and ν_5 bands in these molecules is, as indicated before, somewhat stronger than that between the same bands in CD_3I and it was necessary to include this interaction in order to obtain a satisfactory fitting of the frequencies. For this purpose, the effect of the coupling was calculated for each of the transitions by setting up, for the upper state of the transition, the appropriate matrix with elements defined by Eq. (4), (5) and (7) in Ref. (7). The matrix is essentially the same as the one in Eq. (3-2) except that the v_3=2 state (1154cm^{-1}) is not included because its effect has been considered to be satisfactorily included in the usual Coriolis contribution to the molecular constants (7). The energies needed to compute the Coriolis contribution were calculated with the parameters, including the parameters for the v_2 = 1 state, given in Table V of Ref. (7).

III-2-3 Effect of Nuclear Quadrupole Coupling

In order to obtain the frequencies of rotational and ro-vibrational transitions, it is necessary to subtract the effect of nuclear quadrupole interactions from the spectra. In order to calculate the effect of quadrupole coupling, the appropriate energy matrix was set up and diagonalized. In this matrix, we also included the effects of centrifugal distortion of the quadrupole coupling and the nuclear spin rotation interaction. To carry out this calculation the energy matrix was written

$$H = H_R + H_Q + H_D + H_S \quad . \tag{3-7}$$

The matrix H_R was assumed to be diagonal with diagonal elements equal to the rotational energies given in Eq. (3-1). The elements of H_Q, the nuclear quadrupole coupling, were taken to be the elements proportional to $eqQ = \chi_{zz}$ in the Appendix of the paper by Benz et al. (30); the matrix elements are listed in the Appendix of Chapter IV.

The matrices H_D and H_S were also assumed to be diagonal with non-zero matrix elements as follows:

$$\langle J,K,I,F|H_D|J,K,I,F\rangle = e_1\{[3K^2 - J(J+1)][\chi_J J(J+1) + \chi_K K^2] + \chi_d K^2(4K^2-1)\} \tag{3-8}$$

$$\langle J,K,I,F|H_S|J,K,I,F\rangle = -\frac{1}{2}\left[C_N + (C_K - C_N)\frac{K^2}{J(J+1)}\right] G \ . \tag{3-9}$$

In these equations F is the total angular momentum quantum number and e_1 is the Casimir function divided by J(J+1);

$$e_1 = [(3/4)G(G+1)-I(I+1)J(J+1)]/[2I(2I-1)J(J+1)(2J-1)(2J+3)] \quad (3\text{-}10)$$

with

$$G = F(F+1) - I(I+1) - J(J+1) \; . \quad (3\text{-}11)$$

The constants χ_J, χ_K, and χ_d are centrifugal distortion constants for the quadrupole coupling (31,32), whereas C_N and C_K are spin-rotation constants (33). The signs of the spin rotation constants are taken to be consistent with the signs in the previous work on CD_3I (12). Inclusion of the spin-rotation and the centrifugal distortion of the quadrupole coupling terms on the diagonal before the diagonalization was done for convenience. This is almost equivalent to what is desired - a first-order perturbation treatment of these terms in a zero-order basis which diagonalizes the quadrupole coupling effects. The only difference is that the distortion and spin-rotation terms have a small effect on the diagonalization. The matrix H, as defined, is diagonal in F, I, and K; therefore, submatrices with rows and columns indexed by J (usually 6x6 for CD_3I and 4x4 for CD_3Br) were set up and diagonalied to obtain the energy levels. The nuclear quadrupole coupling is discussed in greater detail in the next chapter.

III-2-4 Hypothetical Unsplit Frequencies

III-2-4-1 CD_3I

In order to obtain the experimental frequencies of the infrared transitions, each experimental lineshape as a function of microwave frequency was fitted by least squares to a sum of Gaussian functions. The relative intensities and separations of the Gaussians were

constrained to the values calculated with the highest quality set of quadrupole parameters available at the time of the fitting. Since there was little change in quadrupole parameters and since the quadrupole splittings of many of the transitions were rather small, the hypothetical unsplit frequencies obtained did not depend on the specific set of quadrupole parameters used. Each experimental infrared frequency was obtained by adding or subtracting the resonant microwave frequency to or from the appropriate laser frequency; the laser frequencies were obtained from the report of Freed et al. (34).

The microwave and millimeter-wave frequencies measured in previous studies were also converted into hypothetical unsplit frequencies by subtracting the frequency shifts caused by the quadrupole couplings. The frequency shifts were calculated with the same set of quadrupole parameters used for the frequency determination of infrared transitions. The rovibrational parameters were adjusted by a least squares fitting of the modified experimental frequencies including, in addition to the present measurements, microwave and millimeter wave frequencies from Refs. (8-13) and infrared frequencies from the laser-Stark study (3).

III-2-4-2 CD_3Br

In order to obtain the experimental frequencies of the infrared-micrave sideband-laser transitions, each experimental lineshape as a function of microwave frequency was fitted by least squares to a single Gaussian function. Because the shifts in frequency resulting from the hyperfine splitting were less than 5 MHz in nearly every case, it did not seem necessary to fit the lineshapes to a sum of Gaussians, one for

each hyperfine component, as was done for CD_3I (35); there was no apparent evidence of hyperfine splitting in the Doppler-limited spectra recorded in this work. Each experimental infrared frequency was obtained by adding or subtracting the resonant microwave frequency to or from the appropriate laser frequency, which was obtained from the report of Freed et al. (34).

On the other hand, the microwave and millimeter wave frequencies were converted into the corresponding hypothetical unsplit frequencies with the quadrupole coupling constants reported in Ref. (29). The rovibrational parameters were adjusted by a least squares fitting of the experimental frequencies including, in addition to the present measurements, converted microwave and millimeter wave frequencies from Refs. (10) and (29) and infrared frequencies from the FTIR (6) and laser-Stark (28) studies. Each experimental frequency was given a weight equal to the reciprocal of the square of its estimated uncertainty.

III-3 Experimental

All of the spectra in this work were recorded with an infrared microwave sideband laser spectrometer that has been assembled in our laboratory. Fig. 3-1 shows block diagram of the spectrometer used in this study. The design of the electrooptic modulator used is that of Magerl et al. (36) and a detailed description of our spectrometer has already been given in Chapter II. As examples, portions of the spectra of the ν_2 bands of CD_3I and CD_3Br are shown in Figs. 3-2 and 3-3. The horizontal axes of Figs. 3-2 and 3-3 are the microwave frequencies that must be added to or subtracted from the laser frequency to obtain the sideband frequency depending on the sign. The overall accuracy of the frequency scale is limited entirely by our ability to reproduce the known laser frequencies; we estimate this accuracy to be ±150 kHz. The accuracy of the reported frequencies of the transitions was limited by our ability to determine the center frequency of the Doppler-limited absorption lines ($\Delta\nu_D$ = ~18.5 MHz); this uncertainty ranges from 2-10 MHz.

The sample cell was a 1-meter glass tube with NaCl windows and the samples were obtained from Merck & Co. and used as received except for the usual freeze-pump-thaw cycles. Sample pressures, which were about 0.3 Torr for CD_3I and 0.5 Torr for CD_3Br, were measured with a capacitance manometer. All spectra were recorded at room temperature (~297 K).

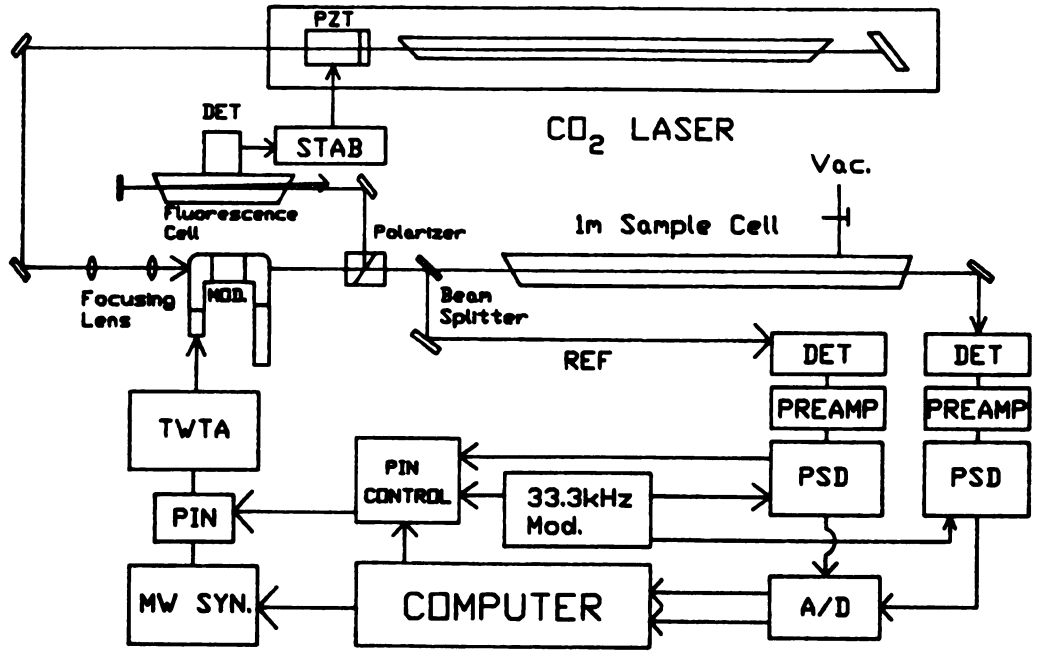

Figure 3-1. Block diagram of the infrared microwave sideband laser spectrometer used to record the Doppler-limited vibration-rotation spectra in this work.

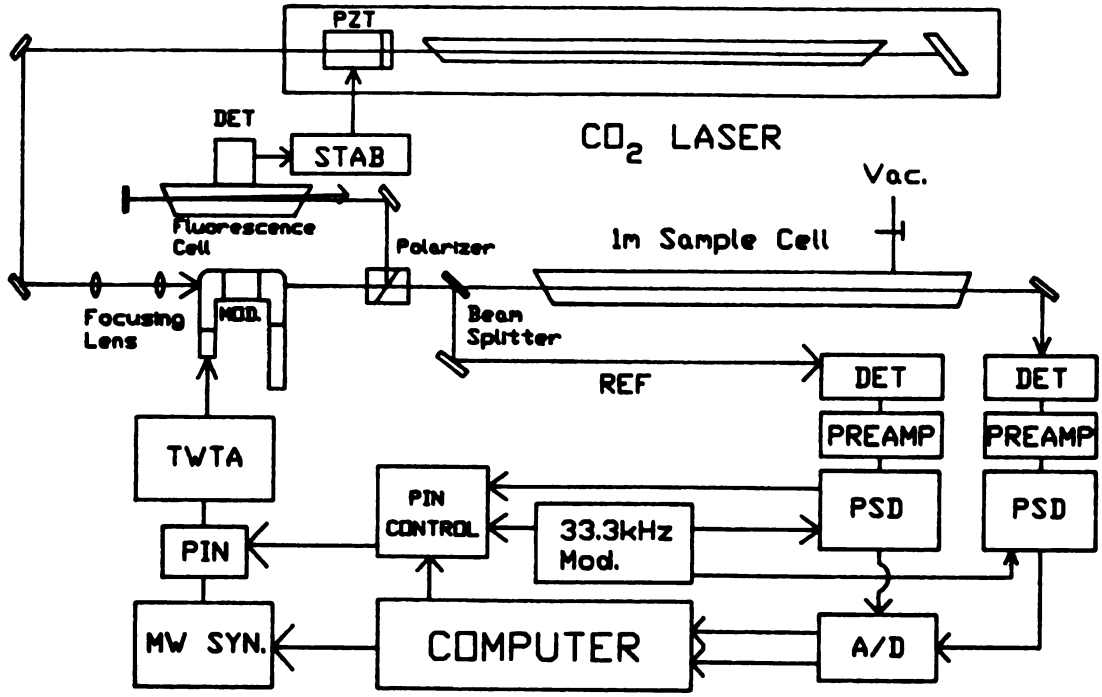

Figure 3-1. Block diagram of the infrared microwave sideband laser spectrometer used to record the Doppler-limited vibration-rotation spectra in this work.

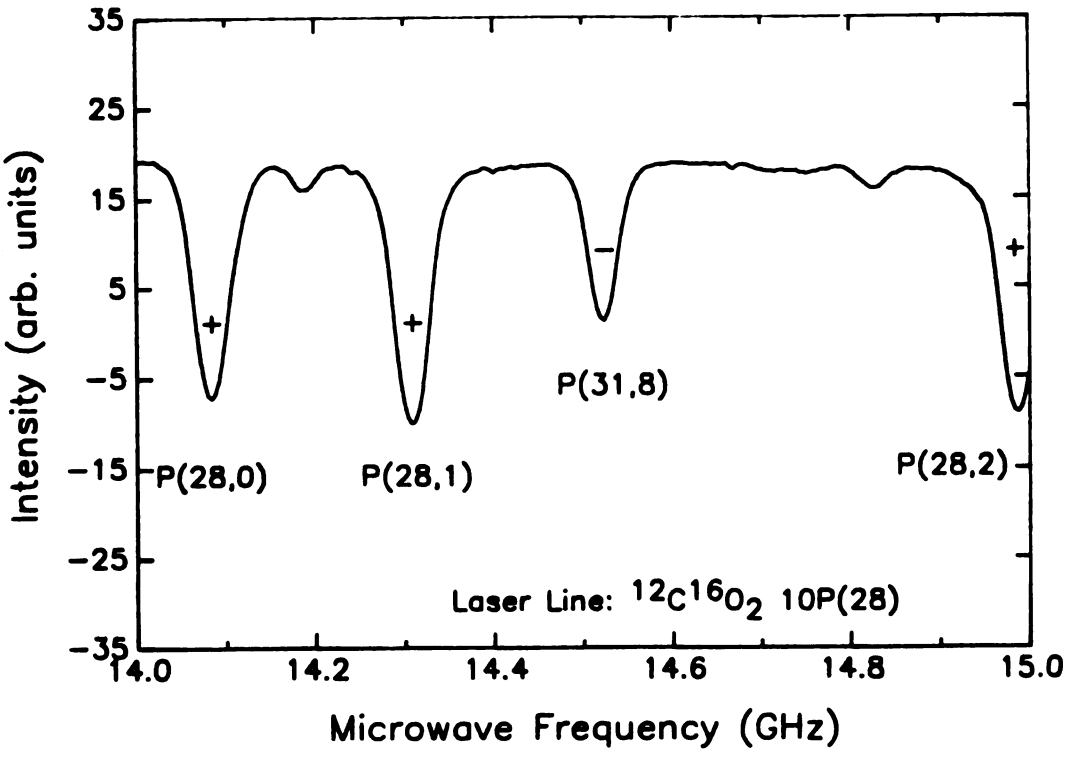

Figure 3-2. A portion of the infrared spectrum of the ν_2 band of CD_3I recorded by the infrared microwave sideband laser spectrometer. The microwave frequency on the horizontal axis is added to (+) or subtracted from (-) the frequency of the 10P(28) $^{12}C^{16}O_2$ laser to obtain the infrared frequency. The sample pressure was 0.3 Torr and a 1-m path length was used.

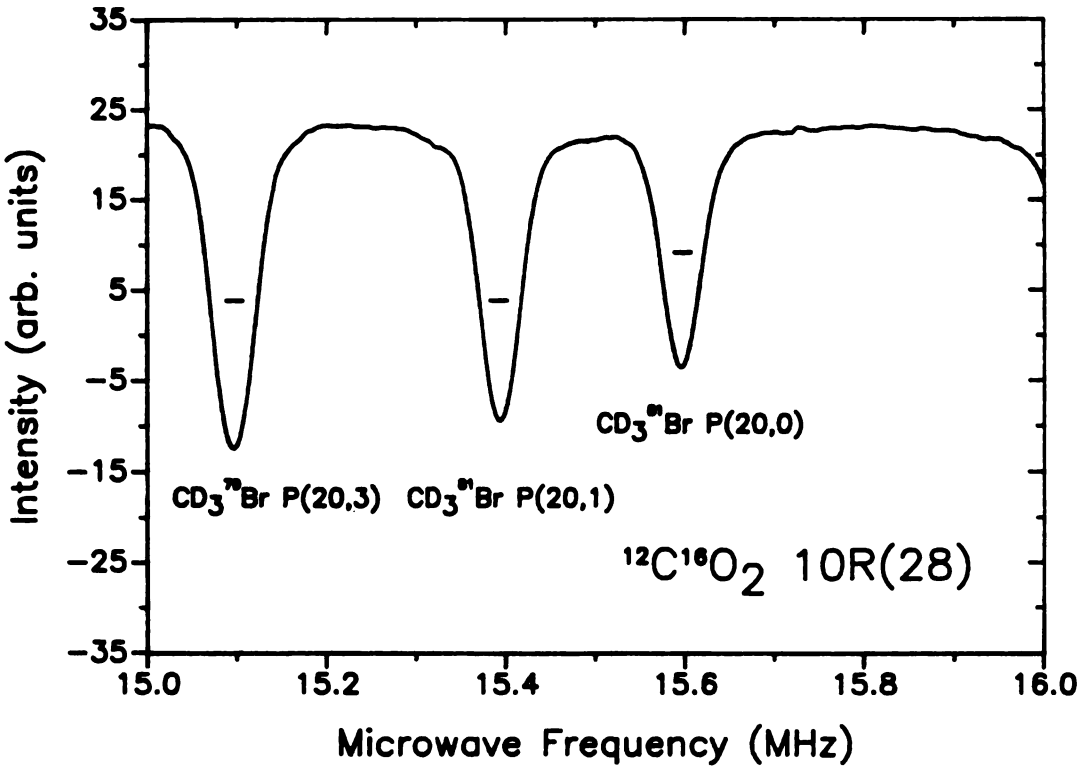

Figure 3-3. A small portion of the spectrum in the ν_2 band region of CD_3Br showing the typical lineshapes and signal/noise obtained for the spectra reported. The horizontal scale is the microwave frequency that must be subtracted from the frequency of the $^{12}C^{16}O_2$ 10(28) laser to obtain the infrared frequency of the transitions. Transitions of $CD_3{}^{79}Br$ and $CD_3{}^{81}Br$ occur approximately alternately everywhere in this region.

III-4 Results

The Coriolis effects were eliminated from all the experimental frequencies, including the new, more precise infrared frequencies for each species, and the modified frequencies were fit to the differences in energy levels calculated by Eq. (3-1). In the least squares fittings, the ground-state parameters A_o, D_K^o, H_K^o, and L_K^o were constrained to zero or to the previously-reported values. This was done to avoid the linear dependence, which is a result of the selection rule, $\Delta K=0$ for a parallel band. In addition, it was found that all of the L constants for the ground states were too small to affect the calculated frequencies significantly; consequently, these parameters were constrained to zero in the fittings for all three species.

III-4-1 CD_3I

Approximately 175 vibration-rotation transitions were recorded with J's up to 43 and K's up to 10. Some transitions of higher K were recorded, but these frequencies show the effects of a resonance that cannot be fully accounted for by a power series expansion in J(J+1) and K^2; this appears to be the Coriolis resonance with ν_5 and $2\nu_3$ reported by Matsuura and Shimanouchi (2). A small portion of the infrared spectrum is shown in Fig. 3-2.

The frequencies of the infrared transitions measured in this work are shown in Table 3-1 with their estimated uncertainties. Also shown in Table 3-1 are the observed minus calculated frequencies for the parameters derived in this work. The rotational and centrifugal

TABLE 3-1

Comparison of Observed and Calculated Frequencies in the ν_2 Band of CD_3I

Trans.	Laser[a]	ν_m[b]	ν/MHz	O-C[c]	Unc[d]	ν/cm^{-1} [e]
P(43, 8)	10P(34)	-16 281.8	27 894 439.0	-1.4	2.0	930.458 33(-4)
P(43, 9)	10P(34)	-14 549.9	27 896 170.9	1.2	2.0	930.516 10(4)
P(43,10)	10P(34)	-13 276.1	27 897 444.7	-0.8	2.0	930.558 59(-2)
P(42, 0)	10P(34)	-11 245.0	27 899 475.8	-0.1	2.0	930.626 34(0)
P(42, 1)	10P(34)	-11 065.0	27 899 655.8	0.0	2.0	930.632 34(0)
P(42, 2)	10P(34)	-10 523.8	27 900 197.0	1.8	2.0	930.650 40(5)
P(42, 4)	10P(34)	-8 427.0	27 902 293.8	0.3	2.0	930.720 34(1)
P(41, 7)	10P(34)	11 582.2	27 922 303.0	-1.7	2.0	931.387 77(-5)
P(41, 9)	10P(34)	15 616.4	27 926 337.2	3.0	2.0	931.522 34(9)
P(41,10)	10P(34)	17 209.9	27 927 930.7	0.2	2.0	931.575 49(0)
P(40, 0)	10P(34)	17 931.4	27 928 652.2	-0.2	2.0	931.599 56(0)
P(39, 8)	10P(32)	-15 410.7	27 954 039.1	-0.5	2.0	932.446 38(-1)
P(39, 9)	10P(32)	-13 208.4	27 956 241.4	0.8	2.0	932.519 84(2)
P(39,10)	10P(32)	-11 300.8	27 958 149.0	-1.9	2.0	932.583 47(-6)
P(38, 0)	10P(32)	-11 854.6	27 957 595.2	-0.3	2.0	932.564 99(-1)
P(38, 2)	10P(32)	-11 076.9	27 958 372.9	-1.5	2.0	932.590 94(-5)
P(38, 4)	10P(32)	-8 788.5	27 960 661.3	-0.2	2.0	932.667 27(0)
P(37, 6)	10P(32)	9 350.3	27 978 800.1	-0.9	10.0	933.272 31(-2)
P(37, 8)	10P(32)	14 007.1	27 983 456.9	-0.6	2.0	933.427 65(-2)
P(37, 9)	10P(32)	16 427.3	27 985 877.1	-7.7	OMIT	933.508 38(-25)
P(36, 0)	10P(32)	16 854.0	27 986 303.8	0.2	2.0	933.522 61(0)
P(36, 1)	10P(32)	17 055.9	27 986 505.7	0.2	2.0	933.529 35(0)
P(35, 7)	10P(30)	-17 386.1	28 010 045.8	1.0	2.0	934.314 56(3)
P(35, 8)	10P(30)	-14 815.2	28 012 616.7	-0.2	2.0	934.400 31(0)
P(35, 9)	10P(30)	-12 168.2	28 015 263.7	0.5	2.0	934.488 61(1)
P(35,10)	10P(30)	-9 654.9	28 017 777.0	-0.5	2.0	934.572 44(-1)
P(34, 0)	10P(30)	-12 657.9	28 014 774.0	-0.8	2.0	934.472 27(-2)
P(34, 1)	10P(30)	-12 448.6	28 014 983.3	-0.2	2.0	934.479 26(0)
P(34, 2)	10P(30)	-11 823.6	28 015 608.3	-0.1	2.0	934.500 10(0)
P(34, 3)	10P(30)	-10 789.0	28 016 642.9	1.2	2.0	934.534 61(4)
P(34, 4)	10P(30)	-9 363.5	28 018 068.4	-1.2	2.0	934.582 16(-3)
P(33, 6)	10P(30)	8 860.2	28 036 292.1	0.8	10.0	935.190 04(2)
P(33, 7)	10P(30)	11 352.8	28 038 784.7	0.2	2.0	935.273 18(0)
P(33, 9)	10P(30)	16 941.7	28 044 373.6	1.9	2.0	935.459 61(6)
P(32, 0)	10P(30)	15 576.1	28 043 008.0	0.5	2.0	935.414 06(1)
P(32, 1)	10P(30)	15 790.6	28 043 222.5	-0.1	2.0	935.421 21(0)
P(32, 2)	10P(30)	16 429.3	28 043 861.2	-5.4	2.0	935.442 52(-17)
P(32, 3)	10P(30)	17 502.3	28 044 934.2	1.5	2.0	935.478 31(5)
P(31, 7)	10P(28)	-17 404.3	28 067 265.5	-0.9	2.0	936.223 20(-2)
P(31, 8)	10P(28)	-14 522.9	28 070 146.9	-0.4	2.0	936.319 32(-1)

Table 3-1 (cont'd)

Trans.	Laser[a]	ν_m[b]	ν/MHz	O-C[c]	Unc[d]	ν/cm^{-1} e
P(31, 9)	10P(28)	-11 463.1	28 073 206.7	-0.1	2.0	936.421 38(0)
P(31,10)	10P(28)	-8 384.2	28 076 285.6	-0.5	2.0	936.524 08(-1)
P(30, 0)	10P(28)	-13 669.8	28 071 000.0	-0.1	2.0	936.347 77(0)
P(30, 1)	10P(28)	-13 448.8	28 071 221.0	-0.2	2.0	936.355 14(0)
P(30, 2)	10P(28)	-12 784.6	28 071 885.2	1.9	2.0	936.377 30(6)
P(30, 3)	10P(28)	-11 689.7	28 072 980.1	-0.3	2.0	936.413 82(-1)
P(30, 4)	10P(28)	-10 166.3	28 074 503.5	1.1	2.0	936.464 64(3)
P(30, 5)	10P(28)	-8 238.5	28 076 431.3	-1.7	2.0	936.528 94(-5)
P(29, 7)	10P(28)	10 818.0	28 095 487.8	-0.1	2.0	937.164 60(0)
P(29, 8)	10P(28)	13 843.1	28 098 512.9	0.4	2.0	937.265 50(1)
P(29, 9)	10P(28)	17 095.8	28 101 765.6	0.9	2.0	937.374 00(2)
P(28, 0)	10P(28)	14 084.6	28 098 754.4	3.4	2.0	937.273 56(11)
P(28, 1)	10P(28)	14 308.5	28 098 978.3	0.6	2.0	937.281 03(2)
P(28, 2)	10P(28)	14 987.7	28 099 657.5	0.7	2.0	937.303 68(2)
P(28, 3)	10P(28)	16 115.2	28 100 785.0	1.7	2.0	937.341 29(5)
P(28, 4)	10P(28)	17 678.4	28 102 348.2	-0.3	2.0	937.393 44(0)
P(27, 7)	10P(26)	-17 720.3	28 123 445.7	-0.9	2.0	938.097 17(-3)
P(27, 8)	10P(26)	-14 559.0	28 126 607.0	0.0	2.0	938.202 62(0)
P(27, 9)	10P(26)	-11 124.4	28 130 041.6	-0.4	2.0	938.317 19(-1)
P(26, 0)	10P(26)	-14 908.7	28 126 257.3	-1.2	2.0	938.190 96(-4)
P(26, 1)	10P(26)	-14 676.6	28 126 489.4	-1.1	2.0	938.198 70(-3)
P(26, 2)	10P(26)	-13 979.0	28 127 187.0	1.4	2.0	938.221 97(4)
P(26, 3)	10P(26)	-12 826.5	28 128 339.5	-0.1	2.0	938.260 41(0)
P(26, 4)	10P(26)	-11 221.0	28 129 945.0	-0.2	2.0	938.313 97(0)
P(26, 5)	10P(26)	-9 176.3	28 131 989.7	-1.4	2.0	938.382 17(-4)
P(25, 7)	10P(26)	9 975.2	28 151 141.2	1.0	2.0	939.020 99(3)
P(25, 9)	10P(26)	16 869.6	28 158 035.6	0.3	2.0	939.250 97(1)
P(24, 0)	10P(26)	12 355.6	28 153 521.6	0.4	2.0	939.100 40(1)
P(24, 1)	10P(26)	12 592.1	28 153 758.1	0.0	2.0	939.108 28(0)
P(24, 3)	10P(26)	14 480.2	28 155 646.2	-1.4	2.0	939.171 26(-4)
P(24, 4)	10P(26)	16 126.1	28 157 292.1	1.1	2.0	939.226 17(3)
P(24,11)	10P(24)	-16 992.6	28 179 930.0	-4.8	OMIT	939.981 29(-15)
P(23, 8)	10P(24)	-14 950.7	28 181 971.9	-1.3	2.0	940.049 40(-4)
P(23, 9)	10P(24)	-11 182.7	28 185 739.9	-1.3	2.0	940.175 08(-4)
P(22, 0)	10P(24)	-16 385.3	28 180 537.3	-0.3	2.0	940.001 54(0)
P(22, 1)	10P(24)	-16 143.2	28 180 779.4	0.4	2.0	940.009 62(1)
P(22, 2)	10P(24)	-15 421.2	28 181 501.4	-1.2	2.0	940.033 70(-4)
P(22, 3)	10P(24)	-14 215.7	28 182 706.9	1.0	2.0	940.073 91(3)
P(22, 5)	10P(24)	-10 388.8	28 186 533.8	3.6	2.0	940.201 56(11)
P(21, 7)	10P(24)	8 800.3	28 205 722.9	-0.1	2.0	940.841 64(0)

Table 3-1 (cont'd)

Trans.	Laser[a]	ν_m[b]	ν/MHz	O–C[c]	Unc[d]	ν/cm^{-1} e
P(21, 8)	10P(24)	12 316.7	28 209 239.3	-0.4	2.0	940.958 94(-1)
P(21, 9)	10P(24)	16 234.9	28 213 157.5	0.8	2.0	941.089 64(2)
P(20, 1)	10P(24)	10 628.1	28 207 550.7	-1.1	2.0	940.902 61(-3)
P(20, 2)	10P(24)	11 365.9	28 208 288.5	0.5	2.0	940.927 22(1)
P(20, 4)	10P(24)	14 301.8	28 211 224.4	1.4	2.0	941.025 15(4)
P(20, 5)	10P(24)	16 491.1	28 213 413.7	0.5	2.0	941.098 18(1)
P(19, 8)	10P(22)	-15 718.6	28 236 223.1	-2.1	2.0	941.859 02(-7)
P(19, 9)	10P(22)	-11 664.3	28 240 277.4	-1.4	2.0	941.994 26(-4)
P(18, 1)	10P(22)	-17 867.0	28 234 074.7	-0.3	2.0	941.787 36(-1)
P(18, 2)	10P(22)	-17 119.7	28 234 822.0	-0.6	2.0	941.812 29(-1)
P(18, 3)	10P(22)	-15 874.7	28 236 067.0	0.0	2.0	941.853 81(0)
P(18, 4)	10P(22)	-14 135.8	28 237 805.9	-0.1	2.0	941.911 82(0)
P(18, 5)	10P(22)	-11 905.3	28 240 036.4	0.1	2.0	941.986 22(0)
P(17, 9)	10P(22)	15 162.6	28 267 104.3	-0.3	2.0	942.889 11(-1)
P(16, 0)	10P(22)	8 153.0	28 260 094.7	-0.2	2.0	942.655 29(0)
P(16, 1)	10P(22)	8 406.6	28 260 348.3	0.8	2.0	942.663 75(2)
P(16, 2)	10P(22)	9 179.5	28 261 121.2	16.1	OMIT	942.689 53(53)
P(16, 3)	10P(22)	10 425.2	28 262 366.9	-0.1	2.0	942.731 08(0)
P(16, 4)	10P(22)	12 190.9	28 264 132.6	0.7	2.0	942.789 98(2)
P(16, 5)	10P(22)	14 456.3	28 266 398.0	0.2	2.0	942.865 55(0)
P(16, 6)	10P(22)	17 220.9	28 269 162.6	0.3	2.0	942.957 76(1)
P(15, 8)	10P(20)	-16 881.2	28 289 343.7	-0.4	2.0	943.630 93(-1)
P(15, 9)	10P(20)	-12 599.2	28 293 625.7	-6.0	2.0	943.773 77(-20)
P(14, 3)	10P(20)	-17 813.8	28 288 411.1	-0.5	2.0	943.599 83(-1)
P(14, 4)	10P(20)	-16 026.6	28 290 198.3	-0.8	2.0	943.659 44(-2)
P(14, 5)	10P(20)	-13 729.2	28 292 495.7	-0.8	2.0	943.736 07(-2)
P(14, 6)	10P(20)	-10 923.4	28 295 301.5	-1.7	2.0	943.829 66(-5)
P(12, 4)	10P(20)	9 781.8	28 316 006.7	0.3	2.0	944.520 32(0)
P(12, 5)	10P(20)	12 106.5	28 318 331.4	0.6	2.0	944.597 86(2)
P(12, 6)	10P(20)	14 948.9	28 321 173.8	-0.1	2.0	944.692 67(0)
P(10, 5)	10P(18)	-15 872.4	28 343 901.4	2.0	2.0	945.450 78(6)
P(9, 0)	10P(18)	-9 728.1	28 350 045.7	-1.5	2.0	945.655 73(-4)
P(9, 1)	10P(18)	-9 467.5	28 350 306.3	-1.9	2.0	945.664 43(-6)
P(9, 2)	10P(18)	-8 683.1	28 351 090.7	-0.6	2.0	945.690 59(-1)
P(7, 0)	10P(18)	15 400.3	28 375 174.1	-0.7	2.0	946.493 93(-2)
P(7, 1)	10P(18)	15 662.7	28 375 436.5	-0.7	2.0	946.502 68(-2)
P(7, 2)	10P(18)	16 450.7	28 376 224.5	-0.2	2.0	946.528 97(0)
P(7, 3)	10P(18)	17 764.3	28 377 538.1	-0.1	2.0	946.572 78(0)
P(5, 0)	10P(16)	-12 543.2	28 400 046.5	0.6	2.0	947.323 58(2)
P(5, 2)	10P(16)	-11 491.8	28 401 097.9	-1.9	4.0	947.358 65(-6)

Table 3-1 (cont'd)

Trans.	Laser[a]	ν_m[b]	ν/MHz	O-C[c]	Unc[d]	ν/cm^{-1} e
P(5, 3)	10P(16)	-10 167.9	28 402 421.8	3.1	2.1	947.402 81(10)
Q(16,10)	10P(14)	12 199.1	28 476 872.8	5.0	2.0	949.886 23(16)
Q(15, 9)	10P(14)	8 835.1	28 473 508.8	-0.5	2.0	949.774 02(-1)
Q(15,10)	10P(14)	13 516.7	28 478 190.4	0.5	2.0	949.930 18(1)
Q(14, 9)	10P(14)	10 001.5	28 474 675.2	1.9	10.0	949.812 93(6)
Q(14,10)	10P(14)	14 757.4	28 479 431.1	0.3	2.0	949.971 57(0)
Q(13, 9)	10P(14)	11 087.6	28 475 761.3	0.7	2.0	949.849 16(2)
Q(13,10)	10P(14)	15 918.9	28 480 592.6	2.2	2.0	950.010 31(7)
Q(12, 9)	10P(14)	12 096.0	28 476 769.7	-1.4	2.0	949.882 79(-4)
Q(12,10)	10P(14)	16 996.0	28 481 669.7	1.4	2.0	950.046 24(4)
Q(11, 8)	10P(14)	8 621.4	28 473 295.1	-1.9	2.0	949.766 89(-6)
Q(11,10)	10P(14)	17 990.2	28 482 663.9	-0.4	10.0	950.079 40(-1)
Q(10, 8)	10P(14)	9 438.0	28 474 111.7	-0.5	2.0	949.794 13(-1)
Q(10, 9)	10P(14)	13 886.2	28 478 559.9	-0.9	2.0	949.942 51(-3)
Q(9, 8)	10P(14)	10 177.8	28 474 851.5	-2.2	2.0	949.818 81(-7)
Q(9, 9)	10P(14)	14 666.1	28 479 339.8	0.0	2.0	949.968 52(0)
Q(8, 8)	10P(14)	10 848.7	28 475 522.4	1.1	2.0	949.841 19(3)
R(5, 1)	10P(12)	16 448.8	28 532 475.5	0.1	2.0	951.740 94(0)
R(5, 2)	10P(12)	17 233.2	28 533 259.9	0.8	2.0	951.767 10(2)
R(7, 0)	10P(10)	-11 252.3	28 555 396.9	-1.9	2.0	952.505 51(-6)
R(7, 1)	10P(10)	-10 992.5	28 555 656.7	-1.5	2.0	952.514 18(-4)
R(7, 2)	10P(10)	-10 211.9	28 556 437.3	0.9	2.0	952.540 22(3)
R(7, 3)	10P(10)	-8 915.9	28 557 733.3	-0.8	2.0	952.583 45(-2)
R(9, 0)	10P(10)	11 672.2	28 578 321.4	-0.4	2.0	953.270 19(-1)
R(9, 1)	10P(10)	11 929.9	28 578 579.1	0.2	2.0	953.278 79(0)
R(9, 2)	10P(10)	12 701.2	28 579 350.4	0.1	2.0	953.304 52(0)
R(9, 3)	10P(10)	13 986.8	28 580 636.0	-0.2	2.0	953.347 40(0)
R(9, 4)	10P(10)	15 789.5	28 582 438.7	1.1	2.0	953.407 53(3)
R(11, 0)	10P(8)	-15 560.0	28 600 981.8	-0.9	2.0	954.026 06(-3)
R(11, 1)	10P(8)	-15 306.5	28 601 235.3	-1.8	2.0	954.034 52(-6)
R(11, 2)	10P(8)	-14 542.2	28 601 999.6	-0.8	2.0	954.060 01(-2)
R(11, 3)	10P(8)	-13 269.7	28 603 272.1	-0.3	2.0	954.102 46(0)
R(11, 5)	10P(8)	-9 200.1	28 607 341.7	-1.2	2.0	954.238 21(-3)
R(13, 3)	10P(8)	9 100.3	28 625 642.1	-0.2	2.0	954.848 64(0)
R(13, 4)	10P(8)	10 860.5	28 627 402.3	3.0	2.0	954.907 35(10)
R(13, 5)	10P(8)	13 119.0	28 629 660.8	4.5	2.0	954.982 69(15)
R(13, 6)	10P(8)	15 877.0	28 632 418.8	7.0	2.0	955.074 69(23)
R(14, 0)	10P(8)	17 940.5	28 634 482.3	0.2	2.0	955.143 52(0)
R(14, 8)	10P(6)	-15 337.9	28 650 366.7	-0.8	2.0	955.673 36(-2)
R(14, 9)	10P(6)	-11 154.5	28 654 550.1	-0.8	2.0	955.812 91(-2)

Table 3-1 (cont'd)

Trans.	Laser[a]	ν_m[b]	ν/MHz	O-C[c]	Unc[d]	ν/cm^{-1} [e]
R(15, 3)	10P(6)	-17 959.0	28 647 745.6	-0.1	2.0	955.585 93(0)
R(15, 4)	10P(6)	-16 229.2	28 649 475.4	-0.3	2.0	955.643 63(-1)
R(15, 5)	10P(6)	-14 008.4	28 651 696.2	0.5	2.0	955.717 71(1)
R(15, 6)	10P(6)	-11 304.5	28 654 400.1	-1.7	2.0	955.807 90(-5)
R(16, 0)	10P(6)	-9 217.4	28 656 487.2	0.6	2.0	955.877 52(2)
R(16, 1)	10P(6)	-8 972.9	28 656 731.7	-0.8	2.0	955.885 68(-2)
R(16, 2)	10P(6)	-8 238.0	28 657 466.6	-3.3	2.0	955.910 19(-10)
R(16,10)	10P(6)	14 915.2	28 680 619.8	21.7	OMIT	956.682 50(72)
R(17, 6)	10P(6)	10 408.6	28 676 113.2	1.2	2.0	956.532 18(3)
R(17, 8)	10P(6)	17 084.6	28 682 789.2	-0.8	2.0	956.754 86(-2)
R(18, 0)	10P(6)	12 524.0	28 678 228.6	0.4	2.0	956.602 74(1)
R(18, 1)	10P(6)	12 766.5	28 678 471.1	1.2	2.0	956.610 83(3)
R(18, 3)	10P(6)	14 696.9	28 680 401.5	0.6	2.0	956.675 22(2)
R(18, 4)	10P(6)	16 381.8	28 682 086.4	1.7	2.0	956.731 42(5)

[a] CO_2 laser line used ($^{12}C^{16}O_2$); laser frequencies were taken from Ref. 34.

[b] Microwave frequency in MHz. The signed microwave frequency was added to the laser frequency to obtain the absorption frequency.

[c] Observed minus calculated frequency in MHz; the parameters for the calculation are in the second column in Table 3-2 and the second column of Table 3-4.

[d] Estimated uncertainty in the observed frequency in MHz. An "OMIT" means that the frequency was omitted from the least squares fits.

[e] Observed wavenumber in cm^{-1}. The numbers in parentheses are observed minus calculated wavenumbers in units of 0.00001 cm^{-1}.

distortion constants obtained by least squares fitting of the hypothetical unsplit rotation and vibration-rotation frequencies are given in Tables 3-2 and 3-3 for the ground and $v_2 = 1$ states, respectively. In Table 3-3 the Coriolis effects described above were ignored. Table 3-4 contains the corresponding parameters for $v_2 = 1$ for fittings in which the Coriolis coupling to ν_5 and $2\nu_3$ was included. Finally, the parameters in Tables 3-2 and 3-3 have been used to calculate coincidences within ±200 MHz of CO_2 laser frequencies for transitions with $J \leq 40$ and $K \leq 10$ in the ν_2 band of CD_3I, and these are listed in Table 3-5. For this calculation, the laser frequencies were taken from Refs. (34) and (38).

III-4-2 CD_3Br

The infrared frequencies measured in this work are given in Tables 3-6 and 3-7 for $CD_3{}^{79}Br$ and $CD_3{}^{81}Br$, respectively. The least squares fitting was done with more than 1200 experimental frequencies for each species, including approximately 230 and 190 new, more precise infrared frequencies for $CD_3{}^{79}Br$ and $CD_3{}^{81}Br$, respectively. For both species, ground state molecular parameters A_o and D_K were constrained to the values reported by Edwards and Broderson (28). H_K^o and L_K^o are constrained to zero so that only ΔH_K and ΔL_K for $v_2 = 1$ are reported. The determined molecular constants are shown in Tables 3-8 and 3-9 for $CD_3{}^{79}Br$ and $CD_3{}^{81}Br$, respectively. Although the values in these tables are approximations to deperturbed parameters, with the effects of the ν_2-ν_5 Coriolis coupling removed, until a complete fitting of both bands

TABLE 3-2

Comparison of Ground State Rotational Constants of CD_3I[a]

Parameter	This Work[b]	This Work[c]	Wlodarczak[d]
B_o /MHz	6 040.297 40 (47)	6 040.297 77 (22)	6 040.297 28 (38)
D_J /kHz	3.722 63 (60)	3.722 60 (32)	3.721 88 (30)
D_{JK} /kHz	48.294 8 (40)	48.294 5 (16)	48.296 3 (36)
H_J /Hz	-0.001 346(145)	-0.001 358(78)	-0.001 530(60)
H_{JK} /Hz	0.043 41 (320)	0.033 47(152)	0.037 75(192)
H_{KJ} /Hz	0.998 5 (108)	1.017 8 (38)	1.008 0 (63)

[a]Values in parentheses are one standard deviation in multiples of the last digit in the parameter.

[b]Obtained from fit of vibration-rotation frequencies listed in Table 3-1 and hypothetical unsplit rotational frequencies calculated from References (3,11-13).

[c]Obtained from fit of rotational frequencies from references (11-13) and pure quadrupole frequencies in Table V of Ref. 5 and in Table 4-1.

[d]From Table VI in Ref. 6.

TABLE 3-3

Molecular Constants of the v_2 = 1 State of CD_3I Without Coriolis Corrections[a]

Parameter[b]	This Work[c]	This Work[d]	Kawaguchi[e]
E_v /GHz	28 461.093 3 (9)	28 461.093 3 (15)	28 461.093 8(14)
B_v /MHz	6 007.878 0 (28)	6 007.878 4 (46)	6 007.873 (8)[f]
$\Delta(A_v-B_v)$ /MHz	264.71 (13)	264.71 (22)	266.4 (4)
D_J /kHz	3.557 4(171)	3.557 4(287)	3.6[g]
D_{JK} /kHz	102.265 (249)	102.263 (421)	106. (2)[f]
ΔD_K /kHz	19.6 (58)	19.6 (98)	121. (34)
H_{JK} /Hz	1.374 (182)	1.362 (309)	
H_{KJ} /Hz	-186.01 (400)	-185.95 (677)	
ΔH_K /Hz	1136. (93)	1136. (157)	
L_{JJJK} /mHz	-0.242 (57)	-0.242 (96)	
L_{JJKK} /mHz	48.77 (157)	48.78 (27)	
L_{JKKK} /mHz	-1988.5 (243)	-1988.4 (411)	
ΔL_K /mHz	-3562. (475)	-3563. (804)	

[a] Values in parentheses are one standard deviation in multiples of the last digit in the parameter.

[b] Vibration-rotation parameters. $\Delta P = P(v_2=1) - P(v_2=0)$. H_J and L_J were constrained to zero in both fits in this work.

[c] Obtained from a fit of the vibration-rotation frequencies listed in Table 3-3 and hypothetical unsplit rotational frequencies calculated from References (3,11-13).

[d] Obtained from a fit of the frequencies described in previous footnote with the ground state parameters constrained to the parameters in Table 3-2 (Column 2).

[e] Obtained from Table V in Ref. 3.

[f] Obtained from Ref. 11 (Tables VIII and X).

[g] Assumed to be the same as in the ground state.

TABLE 3-4

Molecular Constants of the v_2 = 1 State of CD_3I with Coriolis Correction[a]

Parameter[b]	This Work[c]	This Work[d]	Matsuura[e]
E_v /GHz	28 461.095 4 (6)	28 461.095 4 (14)	28 461.094 7 (18)
B_v /MHz	6 020.287 0 (33)	6 020.287 2 (75)	6 020.339 2 (180)
$\Delta(A_v-B_v)$ /MHz	252.328 (47)	252.328 (105)	250.600 (180)
D_J /kHz	3.692 3 (50)	3.692 1 (113)	4.197 1(8894)
D_{JK} /kHz	52.56 (16)	52.56 (37)	54.86 (60)
ΔD_K /kHz	13.8 (5)	13.8 (12)	8.1 (15)
H_J /Hz	-0.006 4 (20)	-0.006 5 (46)	
H_{JK} /Hz	0.454 (137)	0.439 (311)	
H_{KJ} /Hz	-13.46 (22)	-13.38 (50)	
L_{JJJK} /mHz	-0.059 (50)	-0.057 (113)	
L_{JJKK} /mHz	2.78 (106)	2.77 (240)	
L_{JKKK} /mHz	-77.9 (111)	-77.8 (251)	

[a]Effects of Coriolis interaction with v_5 and $2v_3$ states were subtracted from the experimental frequencies before fitting. The Coriolis parameters in Table II of Ref. 2 were used except that ζ_{25} = 4398.7 MHz. Values in parentheses are one standard deviation in multiples of the last digit in the parameter.

[b]Vibration-rotation parameters. $\Delta P = P(v_2=1) - P(v_2=0)$. ΔH_K, ΔL_K, and L_J were constrained to zero for both fittings in this work.

[c]Obtained from full fit of vibration-rotation frequencies listed in Table 3-1 and hypothetical unsplit rotational frequencies calculated from References (3,11-13).

[d]Obtained from fit of frequencies described in previous footnote with the ground state parameters constrained to the parameters in Table V (Column 2).

[e]Obtained from Table II in Ref. 2.

TABLE 3-5

Coincidences between Calculated Frequencies for the ν_2 Band of CD_3I and Laser Frequencies

Trans.[a]	Frequency[b]	$\nu_0-\nu_L$[c]	Laser[d]	
P(40,10)	27 943 074.3	-62.5	N20	P(8)
P(39, 0)	27 943 156.3	19.5	N20	P(8)
P(38, 8)	27 968 783.7	-79.4	N20	P(7)
P(34, 4)	28 018 067.4	-140.9	13C1802 BAND I	R(8)
P(34, 5)	28 019 870.2	-142.8	N20	P(5)
P(32, 6)	28 050 509.7	-15.6	12C160180 BAND I	P(36)
P(31, 1)	28 057 251.8	7.2	12C1802 BAND I	P(38)
P(27, 2)	28 113 451.9	-15.0	12C1802 BAND I	P(36)
P(25, 4)	28 143 652.0	-192.6	13C1602 BAND I	R(36)
P(24, 7)	28 164 886.5	-63.3	12C160180 BAND I	P(32)
P(23, 4)	28 170 871.8	-161.5	N20	R(0)
P(20, 5)	28 213 414.7	-90.7	13C1602 BAND I	R(40)
P(19, 0)	28 220 595.4	35.0	N20	R(2)
P(19, 1)	28 220 843.5	-135.5	12C160180 BAND I	P(30)
P(19, 8)	28 236 223.1	-98.7	13C1802 BAND I	R(20)
P(17, 1)	28 247 241.6	-145.5	13C1602 BAND I	R(42)
P(16, 8)	28 276 169.4	-53.6	12C160180 BAND I	P(28)
P(15, 4)	28 277 199.9	-89.9	12C1802 BAND I	P(30)
P(12, 5)	28 318 329.9	-59.0	N20	R(6)
P(9, 8)	28 366 860.0	171.8	N20	R(8)
P(8, 4)	28 366 837.5	149.3	N20	R(8)
P(4, 1)	28 412 648.0	58.3	12C1602 BAND I	P(16)
P(4, 3)	28 414 762.8	186.9	N20	R(10)
P(2, 1)	28 437 133.0	16.8	13C1602 BAND I	R(54)
Q(2, 2)	28 461 956.9	-94.1	N20	R(12)
Q(4, 4)	28 464 662.3	-11.5	12C1602 BAND I	P(14)
Q(6, 3)	28 462 093.1	42.1	N20	R(12)
Q(6, 5)	28 466 291.8	-138.9	13C1602 BAND I	R(56)
Q(7, 4)	28 463 462.3	41.6	12C160180 BAND I	P(21)
Q(9, 2)	28 459 216.0	-108.5	13C1802 BAND I	R(34)
Q(9, 5)	28 464 664.9	-8.8	12C1602 BAND I	P(14)
Q(11, 3)	28 459 132.4	-192.1	13C1802 BAND I	R(34)
Q(11, 5)	28 463 242.3	-178.4	12C160180 BAND I	P(21)
Q(13, 4)	28 459 266.8	-57.7	13C1802 BAND I	R(34)
Q(14, 6)	28 463 370.0	-50.7	12C160180 BAND I	P(21)
Q(17, 7)	28 463 223.4	-197.3	12C160180 BAND I	P(21)
Q(18, 7)	28 461 944.5	-106.6	N20	R(12)
Q(20, 7)	28 459 176.5	-148.0	13C1802 BAND I	R(34)
Q(20, 9)	28 466 547.9	117.2	13C1602 BAND I	R(56)

Table 3-5 (cont'd)

Trans.[a]	Frequency[b]	$\nu_0-\nu_L$[c]	Laser[d]	
Q(22, 8)	28 459 502.0	177.5	13C1802 BAND I	R(34)
Q(22, 9)	28 463 233.7	-187.0	12C160180 BAND I	P(21)
Q(24,10)	28 463 420.8	0.1	12C160180 BAND I	P(21)
Q(26,10)	28 459 271.3	-53.2	13C1802 BAND I	R(34)
Q(28, 4)	28 438 387.0	21.8	N20	R(11)
Q(29, 2)	28 433 887.0	1.6	12C1802 BAND I	P(24)
Q(29, 5)	28 438 378.2	13.0	N20	R(11)
Q(33, 8)	28 437 044.5	-71.7	13C1602 BAND I	R(54)
Q(34, 6)	28 429 733.7	160.7	13C1802 BAND I	R(32)
Q(34, 9)	28 437 165.9	49.7	13C1602 BAND I	R(54)
Q(35, 7)	28 429 619.7	46.8	13C1802 BAND I	R(32)
Q(36, 8)	28 429 459.2	-113.8	13C1802 BAND I	R(32)
Q(36,10)	28 433 976.2	90.8	12C1802 BAND I	P(24)
Q(39, 1)	28 411 108.9	198.8	12C160180 BAND I	P(23)
Q(39, 3)	28 412 554.7	-35.0	12C1602 BAND I	P(16)
Q(40, 5)	28 412 686.6	96.9	12C1602 BAND I	P(16)
Q(40, 6)	28 414 451.0	-124.9	N20	R(10)
R(3, 1)	28 509 030.3	-82.0	N20	R(14)
R(5, 1)	28 532 474.6	-12.7	N20	R(15)
R(7, 1)	28 555 657.3	-101.1	N20	R(16)
R(8, 4)	28 571 030.1	-156.3	13C1802 BAND I	R(42)
R(11, 2)	28 602 001.0	13.0	N20	R(18)
R(12, 4)	28 616 261.8	-31.4	12C160180 BAND I	P(15)
R(15, 3)	28 647 747.7	-52.3	N20	R(20)
R(17, 4)	28 671 284.9	-136.7	13C1802 BAND I	R(50)
R(18, 7)	28 689 934.8	-180.2	12C160180 BAND I	P(12)
R(19, 2)	28 689 958.4	-156.6	12C160180 BAND I	P(12)
R(21, 4)	28 714 089.3	-48.4	12C1602 BAND I	P(4)
R(22, 6)	28 729 166.7	132.0	13C1602 BAND II	P(60)
R(22, 9)	28 738 957.4	169.5	13C1802 BAND I	R(56)
R(26,10)	28 782 703.7	-12.0	N20	R(26)
R(30, 3)	28 805 022.6	190.4	N20	R(27)
R(31, 4)	28 816 383.4	-17.1	12C1802 BAND I	P(8)
R(32, 7)	28 832 413.2	-127.6	12C160180 BAND I	P(6)
R(35, 4)	28 855 419.2	-183.2	12C160180 BAND I	P(5)
R(36, 7)	28 870 580.4	36.0	N20	R(30)
R(37, 6)	28 877 919.1	16.7	12C1602 BAND I	R(2)
R(39, 3)	28 892 201.6	-33.9	N20	R(31)
R(31, 4)	28 816 383.4	-17.1	12C1802 BAND I	P(8)

[a] Transition in the ν_2 band of CD_3I; $J \leq 40$, $k \leq 10$.

[b] Frequency of the ν_2 band transition in MHz.

[c]Frequency of the ν_2 band transition minus the laser frequency in MHz.

[d]Identification of CO_2 or N_2O laser. Band I is 10 μm band; band II is 9 μm band. Laser frequencies were obtained from Refs. 34 and 38.

TABLE 3-6

Comparison of Observed and Calculated Frequencies in the ν_2 Band of $CD_3{}^{79}Br$

Trans.[a]	Laser[b]	ν_m[c]	ν/MHz	O-C[d]	Unc.[e]	ν/cm^{-1} [f]
P(45, 5)	12C1602 10R(4)	-15 854.1	28 907 192.3	-5.1	5.0	964.240 13(-17)
P(45, 4)	12C1602 10R(4)	-12 408.0	28 910 638.4	-2.7	5.0	964.355 09(-9)
P(45, 3)	12C1602 10R(4)	-10 318.5	28 912 728.0	1.8	5.0	964.424 79(6)
P(44, 7)	12C1602 10R(4)	-9 531.6	28 913 514.9	3.9	10.0	964.451 04(13)
P(45, 2)	12C1602 10R(4)	-9 098.0	28 913 948.4	1.9	5.0	964.465 50(6)
P(45, 1)	12C1602 10R(4)	-8 464.0	28 914 582.4	-0.7	5.0	964.486 65(-2)
P(45, 0)	12C1602 10R(4)	-8 269.5	28 914 776.9	-3.5	5.0	964.493 14(-12)
P(44, 4)	12C1602 10R(4)	8 086.2	28 931 132.7	-2.7	10.0	965.038 71(-9)
P(44, 3)	12C1602 10R(4)	10 029.2	28 933 075.6	3.2	5.0	965.103 52(11)
P(44, 1)	12C1602 10R(4)	11 729.7	28 934 776.1	1.4	20.0	965.160 24(5)
P(43, 7)	12C1602 10R(4)	11 769.3	28 934 815.7	10.5	20.0	965.161 56(35)
P(44, 0)	12C1602 10R(4)	11 909.3	28 934 955.8	2.0	5.0	965.166 23(7)
P(43, 4)	12C1602 10R(6)	-15 917.3	28 951 539.8	-1.1	5.0	965.719 42(-4)
P(43, 3)	12C1602 10R(6)	-14 125.6	28 953 331.4	1.3	5.0	965.779 17(4)
P(43, 2)	12C1602 10R(6)	-13 101.6	28 954 355.4	1.6	5.0	965.813 34(5)
P(42, 7)	12C1602 10R(6)	-11 435.7	28 956 021.3	4.1	5.0	965.868 91(14)
P(38,10)	12C1602 10R(6)	-9 085.6	28 958 371.5	0.9	5.0	965.947 30(3)
P(41, 7)	12C1602 10R(6)	9 691.5	28 977 148.6	4.0	10.0	966.573 62(13)
P(40, 8)	12C1602 10R(6)	17 369.9	28 984 826.9	1.4	10.0	966.829 75(5)
P(41, 6)	12C1602 10R(6)	17 513.5	28 984 970.6	-4.0	5.0	966.834 55(-13)
P(41, 3)	12C1602 10R(8)	-17 557.5	28 993 575.5	1.4	5.0	967.121 57(5)
P(41, 2)	12C1602 10R(8)	-16 730.1	28 994 402.9	0.3	10.0	967.149 18(1)
P(41, 1)	12C1602 10R(8)	-16 319.2	28 994 813.8	-1.5	10.0	967.162 87(-5)
P(41, 0)	12C1602 10R(8)	-16 191.9	28 994 941.1	1.3	10.0	967.167 13(4)
P(40, 7)	12C1602 10R(8)	-12 944.9	28 998 188.1	3.0	5.0	967.275 44(10)
P(39, 6)	12C1602 10R(8)	15 013.3	29 026 146.3	-5.2	20.0	968.208 02(-17)
P(37, 9)	12C1602 10R(8)	15 056.7	29 026 189.7	-194.7	OMIT	968.209 47(-649)
P(38, 8)	12C1602 10R(8)	16 622.2	29 027 755.2	0.0	5.0	968.261 69(0)
P(38, 7)	12C1602 10R(10)	-14 072.1	29 040 000.6	4.3	5.0	968.670 15(14)
P(37, 6)	12C1602 10R(10)	12 870.9	29 066 943.6	-3.0	5.0	969.568 86(-10)
P(36, 8)	12C1602 10R(10)	16 283.9	29 070 356.6	2.3	5.0	969.682 72(8)
P(33,10)	12C1602 10R(10)	17 030.5	29 071 103.2	-188.2	OMIT	969.707 62(-628)
P(37, 4)	12C1602 10R(10)	17 958.3	29 072 031.0	-0.3	5.0	969.738 56(-1)
P(36, 7)	12C1602 10R(12)	-14 840.2	29 081 434.2	2.4	5.0	970.052 23(8)
P(36, 6)	12C1602 10R(12)	-9 082.8	29 087 191.6	-4.4	5.0	970.244 28(-15)
P(35, 6)	12C1602 10R(12)	11 067.8	29 107 342.2	-1.8	5.0	970.916 42(-6)
P(35, 4)	12C1602 10R(12)	15 145.5	29 111 419.9	-1.3	5.0	971.052 44(-4)
P(35, 3)	12C1602 10R(12)	15 772.1	29 112 046.5	1.4	5.0	971.073 00(5)
P(34, 8)	12C1602 10R(12)	16 325.7	29 112 600.1	1.0	5.0	971.091 81(3)
P(33, 9)	12C1602 10R(12)	17 756.4	29 114 030.8	-6.6	5.0	971.139 53(-22)
P(34, 6)	12C1602 10R(14)	-10 350.5	29 127 385.6	-2.9	5.0	971.585 00(-10)
P(33, 6)	12C1602 10R(14)	9 590.9	29 147 327.0	-0.5	5.0	972.250 18(-2)
P(33, 5)	12C1602 10R(14)	11 737.2	29 149 473.3	7.8	5.0	972.321 77(26)
P(33, 4)	12C1602 10R(14)	12 662.6	29 150 398.8	-6.9	5.0	972.352 63(-23)
P(32, 8)	12C1602 10R(14)	16 727.7	29 154 463.8	0.1	5.0	972.488 23(0)
P(32, 7)	12C1602 10R(16)	-15 357.0	29 163 098.6	4.5	5.0	972.776 25(15)
P(32, 6)	12C1602 10R(16)	-11 301.0	29 167 154.7	-4.3	5.0	972.911 56(-14)
P(32, 5)	12C1602 10R(16)	-9 453.9	29 169 001.8	-2.5	5.0	972.973 16(-8)
P(32, 4)	12C1602 10R(16)	-8 714.9	29 169 740.8	-1.7	5.0	972.997 82(-6)
P(31, 5)	12C1602 10R(16)	9 978.9	29 188 434.6	-0.9	5.0	973.621 38(-3)

Table 3-6 (cont'd)

Trans.[a]	Laser[b]	ν_m[c]	ν/MHz	O-C[d]	Unc.[e]	ν/cm^{-1} [f]
P(30, 8)	12C1602 10R(16)	17 464.9	29 195 920.6	0.7	5.0	973.871 08(2)
P(30, 7)	12C1602 10R(18)	-15 150.1	29 203 280.6	2.1	5.0	974.116 58(7)
P(30, 6)	12C1602 10R(18)	-11 945.7	29 206 485.0	-5.8	5.0	974.223 47(-19)
P(28, 7)	12C1602 10R(20)	-14 656.4	29 243 002.1	0.1	5.0	975.441 55(0)
P(28, 3)	12C1602 10R(20)	-11 958.0	29 245 700.6	4.0	5.0	975.531 56(13)
P(26, 0)	12C1602 10R(22)	-14 206.7	29 281 929.7	-4.4	5.0	976.740 04(-15)
P(26, 1)	12C1602 10R(22)	-14 084.0	29 282 052.3	-4.0	5.0	976.744 13(-14)
P(26, 7)	12C1602 10R(22)	-13 892.5	29 282 243.8	2.4	5.0	976.750 52(8)
P(26, 2)	12C1602 10R(22)	-13 728.0	29 282 408.3	2.0	5.0	976.755 99(7)
P(26, 2)	12C1602 10R(22)	-13 728.0	29 282 408.4	2.1	5.0	976.756 00(7)
P(26, 3)	12C1602 10R(22)	-13 205.8	29 282 930.6	3.7	5.0	976.773 42(12)
P(26, 4)	12C1602 10R(22)	-12 632.3	29 283 504.1	1.0	5.0	976.792 55(3)
P(24, 8)	12C1602 10R(24)	-16 332.6	29 317 528.6	4.1	5.0	977.927 49(14)
P(24, 0)	12C1602 10R(24)	-15 405.9	29 318 455.2	-1.3	5.0	977.958 39(-4)
P(24, 1)	12C1602 10R(24)	-15 254.7	29 318 607.0	0.5	5.0	977.963 46(2)
P(22,10)	12C1602 10R(24)	-15 071.8	29 318 789.4	27.1	OMIT	977.969 55(90)
P(24, 2)	12C1602 10R(24)	-14 818.0	29 319 043.1	0.8	5.0	977.978 01(3)
P(24, 3)	12C1602 10R(24)	-14 143.3	29 319 717.9	1.7	5.0	978.000 52(6)
P(24, 7)	12C1602 10R(24)	-12 883.9	29 320 977.3	3.8	5.0	978.042 53(13)
P(24, 6)	12C1602 10R(24)	-12 175.4	29 321 685.8	-2.3	5.0	978.066 15(-8)
P(22, 0)	12C1602 10R(26)	-16 290.8	29 354 533.8	-11.6	OMIT	979.161 84(-39)
P(22, 1)	12C1602 10R(26)	-16 109.7	29 354 719.9	-1.5	5.0	979.168 05(-5)
P(22, 2)	12C1602 10R(26)	-15 589.6	29 355 240.0	2.1	5.0	979.185 41(7)
P(22, 3)	12C1602 10R(26)	-14 771.9	29 356 057.7	1.7	5.0	979.212 67(6)
P(22, 5)	12C1602 10R(26)	-12 622.9	29 358 206.7	-0.5	5.0	979.284 36(-2)
P(19,10)	12C1602 10R(26)	15 422.9	29 386 252.5	-28.8	OMIT	980.219 87(-96)
P(20, 0)	12C1602 10R(28)	-16 845.0	29 390 193.3	-0.9	5.0	980.351 31(-3)
P(20, 1)	12C1602 10R(28)	-16 643.4	29 390 394.8	0.4	5.0	980.358 05(1)
P(20, 2)	12C1602 10R(28)	-16 050.7	29 390 987.5	1.6	5.0	980.377 82(5)
P(20, 3)	12C1602 10R(28)	-15 096.5	29 391 941.8	3.3	5.0	980.409 65(11)
P(20, 4)	12C1602 10R(28)	-13 839.5	29 393 198.7	9.7	5.0	980.451 56(32)
P(20, 5)	12C1602 10R(28)	-12 422.2	29 394 616.1	-1.3	5.0	980.498 84(-4)
P(20, 7)	12C1602 10R(28)	-10 219.5	29 396 818.7	-1.3	5.0	980.572 31(-4)
P(19, 8)	12C1602 10R(28)	8 132.9	29 415 171.2	5.7	5.0	981.184 49(19)
P(19, 7)	12C1602 10R(28)	8 386.4	29 415 424.6	-2.8	5.0	981.192 94(-9)
P(18, 0)	12C1602 10R(30)	-17 088.7	29 425 394.6	-2.0	5.0	981.525 51(-7)
P(18, 1)	12C1602 10R(30)	-16 867.2	29 425 616.1	-2.9	5.0	981.532 90(-10)
P(18, 2)	12C1602 10R(30)	-16 201.1	29 426 281.8	2.2	5.0	981.555 11(7)
P(18, 3)	12C1602 10R(30)	-15 119.7	29 427 363.6	7.7	5.0	981.591 18(26)
P(18, 4)	12C1602 10R(30)	-13 678.7	29 428 804.6	3.7	5.0	981.639 26(12)
P(18, 5)	12C1602 10R(30)	-11 960.4	29 430 522.9	-0.4	5.0	981.696 56(-1)
P(18, 6)	12C1602 10R(30)	-10 144.3	29 432 339.0	-5.3	5.0	981.757 15(-18)
P(18, 7)	12C1602 10R(30)	-8 599.5	29 433 883.9	-3.5	5.0	981.808 67(-12)
P(17, 7)	12C1602 10R(30)	9 710.7	29 452 194.0	-3.0	5.0	982.419 44(-10)
P(16,10)	12C1602 10R(30)	11 564.0	29 454 047.4	-42.3	OMIT	982.481 26(-141)
P(16, 0)	12C1602 10R(30)	17 661.0	29 460 144.4	-2.4	5.0	982.684 63(-8)
P(16, 1)	12C1602 10R(32)	-16 774.0	29 460 386.9	-2.4	5.0	982.692 72(-8)
P(16, 4)	12C1602 10R(32)	-13 251.0	29 463 909.8	-13.5	10.0	982.810 24(-45)
P(16, 6)	12C1602 10R(32)	-9 019.6	29 468 141.3	-6.3	5.0	982.951 38(-21)
P(15, 6)	12C1602 10R(32)	8 671.3	29 485 832.1	-6.2	5.0	983.541 48(-21)

Table 3-6 (cont'd)

Trans.[a]	Laser[b]	ν_m[c]	ν/MHz	O-C[d]	Unc.[e]	ν/cm^{-1} [f]
P(15, 8)	12C1602 10R(32)	13 251.0	29 490 411.9	-6.4	20.0	983.694 25(-21)
P(15, 9)	12C1602 10R(32)	13 251.0	29 490 411.9	208.7	OMIT	983.694 25(696)
P(14, 0)	12C1602 10R(32)	17 277.9	29 494 438.6	-0.8	5.0	983.828 57(-3)
P(14, 1)	12C1602 10R(34)	-16 367.6	29 494 699.1	-0.8	5.0	983.837 26(-3)
P(14, 2)	12C1602 10R(34)	-15 593.2	29 495 473.4	-5.5	5.0	983.863 09(-18)
P(14, 3)	12C1602 10R(34)	-14 295.4	29 496 771.3	3.1	5.0	983.906 38(10)
P(14, 4)	12C1602 10R(34)	-12 516.2	29 498 550.5	2.0	5.0	983.965 73(7)
P(14,10)	12C1602 10R(34)	-11 422.7	29 499 644.0	-19.5	5.0	984.002 20(-65)
P(14, 5)	12C1602 10R(34)	-10 287.2	29 500 779.5	-1.3	5.0	984.040 07(-4)
P(13, 6)	12C1602 10R(34)	9 716.6	29 520 783.3	-6.3	5.0	984.707 34(-21)
P(13,10)	12C1602 10R(34)	11 588.8	29 522 655.5	1.1	5.0	984.769 78(4)
P(13, 7)	12C1602 10R(34)	12 807.3	29 523 874.0	-3.9	5.0	984.810 42(-13)
P(13, 8)	12C1602 10R(34)	15 922.6	29 526 989.3	10.1	OMIT	984.914 35(34)
P(12, 0)	12C1602 10R(34)	17 201.1	29 528 267.7	-1.7	5.0	984.956 99(-6)
P(12, 1)	12C1602 10R(36)	-15 652.7	29 528 543.6	-1.9	5.0	984.966 18(-6)
P(12, 2)	12C1602 10R(36)	-14 822.0	29 529 374.3	0.9	5.0	984.993 90(3)
P(12, 3)	12C1602 10R(36)	-13 444.4	29 530 751.9	1.6	5.0	985.039 85(5)
P(12, 5)	12C1602 10R(36)	-9 087.5	29 535 108.8	-4.4	5.0	985.185 19(-15)
P(11, 6)	12C1602 10R(36)	10 942.5	29 555 138.8	-18.6	OMIT	985.853 30(-62)
P(10, 0)	12C1602 10R(36)	17 433.5	29 561 630.1	-2.4	5.0	986.069 83(-8)
P(10, 1)	12C1602 10R(38)	-14 625.5	29 561 919.7	-2.2	5.0	986.079 50(-7)
P(10, 2)	12C1602 10R(38)	-13 754.1	29 562 791.0	0.0	5.0	986.108 56(0)
P(10, 4)	12C1602 10R(38)	-10 265.9	29 566 279.2	0.1	5.0	986.224 91(0)
R(3, 1)	13C1602 9P(28)	11 473.0	29 782 141.2	-0.9	10.0	993.425 29(-3)
R(5, 1)	13C1602 9P(26)	-17 264.2	29 811 661.3	-2.5	10.0	994.409 98(-8)
R(5, 2)	13C1602 9P(26)	-16 353.0	29 812 572.5	-2.8	10.0	994.440 38(-9)
R(5, 4)	13C1602 9P(26)	-12 653.6	29 816 271.9	7.0	20.0	994.563 77(23)
R(7, 0)	13C1602 9P(26)	11 476.3	29 840 401.9	-5.1	5.0	995.368 66(-17)
R(7, 1)	13C1602 9P(26)	11 770.9	29 840 696.4	-3.4	5.0	995.378 49(-11)
R(7, 2)	13C1602 9P(26)	12 653.6	29 841 579.1	-1.0	20.0	995.407 92(-3)
R(7, 3)	13C1602 9P(26)	14 127.1	29 843 052.6	0.1	5.0	995.457 08(0)
R(7, 4)	13C1602 9P(26)	16 201.4	29 845 127.0	2.2	20.0	995.526 28(7)
R(9, 0)	13C1602 9P(24)	-17 377.5	29 868 967.0	-3.8	5.0	996.321 50(-13)
R(9, 1)	13C1602 9P(24)	-17 105.1	29 869 239.4	-11.8	30.0	996.330 58(-39)
R(9, 2)	13C1602 9P(24)	-16 249.5	29 870 095.0	2.6	20.0	996.359 11(9)
R(9, 3)	13C1602 9P(24)	-14 849.0	29 871 495.5	0.8	10.0	996.405 84(3)
R(9, 4)	13C1602 9P(24)	-12 889.4	29 873 455.2	-1.0	10.0	996.471 19(-3)
R(9, 5)	13C1602 9P(24)	-10 380.1	29 875 964.5	-5.8	10.0	996.554 90(-19)
R(10, 7)	13C1602 9P(24)	9 719.0	29 896 063.5	9.2	20.0	997.225 33(31)
R(11, 0)	13C1602 9P(24)	10 709.4	29 897 053.9	-0.0	10.0	997.258 37(0)
R(11, 1)	13C1602 9P(24)	10 973.0	29 897 317.5	-1.8	5.0	997.267 16(-6)
R(11, 2)	13C1602 9P(24)	11 770.8	29 898 115.3	1.3	5.0	997.293 77(4)
R(10, 8)	13C1602 9P(24)	13 089.1	29 899 433.6	-137.4	OMIT	997.337 75(-525)
R(11, 3)	13C1602 9P(24)	13 089.1	29 899 433.6	1.1	20.0	997.337 75(4)
R(11, 4)	13C1602 9P(24)	14 918.9	29 901 263.4	1.4	10.0	997.398 78(5)
R(11, 5)	13C1602 9P(24)	17 229.2	29 903 573.7	-1.4	5.0	997.475 85(-5)
R(13, 2)	13C1602 9P(22)	-17 273.8	29 925 646.9	-0.2	5.0	998.212 13(-1)
R(13, 3)	13C1602 9P(22)	-16 043.1	29 926 877.6	8.7	5.0	998.253 19(29)
R(13, 4)	13C1602 9P(22)	-14 374.0	29 928 546.8	0.5	5.0	998.308 85(2)
R(13, 5)	13C1602 9P(22)	-12 290.6	29 930 630.1	2.1	5.0	998.378 36(7)

Table 3-6 (cont'd)

Trans.[a]	Laser[b]		ν_m[c]	ν/MHz	O-C[d]	Unc.[e]	ν/cm^{-1} f
R(13, 6)	13C1602	9P(22)	-9 917.0	29 933 003.8	-8.1	5.0	998.457 53(-27)
R(15, 0)	13C1602	9P(22)	8 864.7	29 951 785.4	-1.1	5.0	999.084 02(-4)
R(15, 1)	13C1602	9P(22)	9 093.6	29 952 014.3	-0.6	5.0	999.091 64(-2)
R(15, 2)	13C1602	9P(22)	9 774.0	29 952 694.8	-0.1	10.0	999.114 34(0)
R(15, 3)	13C1602	9P(22)	10 890.8	29 953 811.6	4.0	5.0	999.151 61(13)
R(15, 4)	13C1602	9P(22)	12 393.2	29 955 314.0	0.5	5.0	999.201 72(2)
R(15, 5)	13C1602	9P(22)	14 214.6	29 957 135.3	-0.0	5.0	999.262 47(0)
R(15, 6)	13C1602	9P(22)	16 195.5	29 959 116.3	-4.7	5.0	999.328 54(-16)
R(17, 4)	13C1602	9P(20)	-17 080.8	29 981 569.3	0.4	5.0	1000.077 49(1)
R(17, 5)	13C1602	9P(20)	-15 546.2	29 983 103.9	-0.6	5.0	1000.128 69(-2)
R(17, 6)	13C1602	9P(20)	-13 999.3	29 984 650.8	-2.9	5.0	1000.180 29(-10)
R(17, 8)	13C1602	9P(20)	-13 193.0	29 985 457.1	3.8	5.0	1000.207 18(13)
R(17, 7)	13C1602	9P(20)	-12 869.1	29 985 780.9	-4.2	5.0	1000.217 98(-14)
R(19, 4)	13C1602	9P(20)	8 672.2	30 007 322.3	4.0	5.0	1000.936 52(13)
R(19, 8)	13C1602	9P(20)	9 777.0	30 008 427.1	5.2	5.0	1000.973 38(17)
R(19, 5)	13C1602	9P(20)	9 894.8	30 008 544.9	1.5	5.0	1000.977 30(5)
R(19, 6)	13C1602	9P(20)	10 972.0	30 009 622.1	-0.1	5.0	1001.013 23(0)
R(19, 7)	13C1602	9P(20)	11 363.2	30 010 013.3	1.5	5.0	1001.026 29(5)
R(20, 9)	13C1602	9P(20)	12 280.8	30 010 930.9	-188.9	OMIT	1001.056 90(-630)
R(22, 8)	13C1602	9P(18)	-11 813.1	30 041 715.6	-0.1	5.0	1002.083 76(0)
R(22, 0)	13C1602	9P(18)	-10 504.2	30 043 024.5	-6.1	5.0	1002.127 43(-21)
R(22, 1)	13C1602	9P(18)	-10 355.1	30 043 173.7	-1.0	5.0	1002.132 39(-3)
R(22, 4)	13C1602	9P(18)	-8 519.7	30 045 009.1	1.0	5.0	1002.193 62(3)
R(22, 7)	13C1602	9P(18)	-8 275.9	30 045 252.9	-0.3	5.0	1002.201 76(-1)
R(24, 8)	13C1602	9P(18)	9 666.5	30 063 195.3	2.4	10.0	1002.800 25(8)
R(24, 7)	13C1602	9P(18)	14 530.0	30 068 058.7	12.5	10.0	1002.962 48(42)
R(24, 0)	13C1602	9P(18)	14 530.0	30 068 058.7	0.6	10.0	1002.962 48(2)
R(24, 1)	13C1602	9P(18)	14 644.2	30 068 172.9	-0.9	5.0	1002.966 28(-3)
R(24, 2)	13C1602	9P(18)	14 976.3	30 068 505.1	1.1	5.0	1002.977 36(4)
R(24, 3)	13C1602	9P(18)	15 467.2	30 068 995.9	4.4	5.0	1002.993 74(15)
R(26, 9)	13C1602	9P(18)	15 617.5	30 069 146.2	46.3	OMIT	1002.998 75(154)
R(24, 4)	13C1602	9P(18)	15 995.6	30 069 524.4	2.6	5.0	1003.011 37(9)
R(24, 6)	13C1602	9P(18)	16 131.0	30 069 659.7	-0.8	5.0	1003.015 88(-3)
R(24, 5)	13C1602	9P(18)	16 347.7	30 069 876.5	-3.5	5.0	1003.023 10(-12)
R(26, 7)	13C1602	9P(16)	-17 248.7	30 090 304.4	1.0	5.0	1003.704 52(3)
R(26, 0)	13C1602	9P(16)	-14 927.1	30 092 626.0	-4.4	5.0	1003.781 96(-15)
R(26, 2)	13C1602	9P(16)	-14 597.8	30 092 955.3	1.0	5.0	1003.792 94(3)
R(26, 4)	13C1602	9P(16)	-14 007.6	30 093 545.5	-8.8	5.0	1003.812 63(-29)
R(26, 5)	13C1602	9P(16)	-14 007.6	30 093 545.5	9.9	5.0	1003.812 63(33)
R(27, 8)	13C1602	9P(16)	-13 138.4	30 094 414.7	-2.0	5.0	1003.841 62(-7)
R(29, 9)	13C1602	9P(16)	-10 845.5	30 096 707.6	0.3	5.0	1003.918 09(1)
R(28, 2)	13C1602	9P(16)	9 396.3	30 116 949.4	0.3	5.0	1004.593 29(1)
R(28, 3)	13C1602	9P(16)	9 555.6	30 117 108.7	7.1	5.0	1004.598 61(24)
R(28, 4)	13C1602	9P(16)	9 555.6	30 117 108.7	-4.5	5.0	1004.598 61(-15)
R(30, 8)	13C1602	9P(16)	16 990.6	30 124 543.7	-2.2	5.0	1004.846 62(-7)
R(31, 7)	13C1602	9P(14)	-16 976.5	30 143 743.4	3.1	10.0	1005.487 04(10)
R(32, 8)	13C1602	9P(14)	-16 650.7	30 144 069.2	-2.8	5.0	1005.497 92(-9)
R(31, 5)	13C1602	9P(14)	-10 155.6	30 150 564.3	-2.6	5.0	1005.714 56(-9)
R(31, 4)	13C1602	9P(14)	-9 138.2	30 151 581.7	-0.3	5.0	1005.748 51(-1)
R(31, 3)	13C1602	9P(14)	-8 734.8	30 151 985.1	1.6	5.0	1005.761 96(5)

Table 3-6 (cont'd)

Trans.[a]	Laser[b]	ν_m[c]	ν/MHz	O-C[d]	Unc.[e]	ν/cm^{-1} [f]
R(31, 0)	13C1602 9P(14)	-8 618.4	30 152 101.5	-2.1	30.0	1005.765 84(-7)
R(31, 2)	13C1602 9P(14)	-8 618.4	30 152 101.5	2.0	30.0	1005.765 84(7)
R(31, 1)	13C1602 9P(14)	-8 618.4	30 152 101.5	-8.0	30.0	1005.765 84(-27)
R(33, 4)	13C1602 9P(14)	13 275.7	30 173 995.6	1.9	5.0	1006.496 14(6)
R(34, 7)	13C1602 9P(14)	13 675.0	30 174 394.9	3.9	5.0	1006.509 46(13)
R(33, 3)	13C1602 9P(14)	13 962.0	30 174 681.9	2.3	5.0	1006.519 04(8)
R(33, 0)	13C1602 9P(14)	14 383.5	30 175 103.4	-20.8	15.0	1006.533 10(-69)
R(33, 1)	13C1602 9P(14)	14 383.5	30 175 103.4	7.4	15.0	1006.533 10(25)
R(35, 4)	13C1602 9P(12)	-17 065.6	30 195 960.5	-1.1	5.0	1007.228 82(-4)
R(35, 2)	13C1602 9P(12)	-15 590.9	30 197 435.3	6.6	20.0	1007.278 01(22)
R(35, 1)	13C1602 9P(12)	-15 376.3	30 197 649.9	-1.4	10.0	1007.285 17(-5)
R(35, 0)	13C1602 9P(12)	-15 314.5	30 197 711.6	-2.7	10.0	1007.287 23(-9)
R(38, 8)	13C1602 9P(12)	-12 788.1	30 200 238.0	0.4	5.0	1007.371 50(1)
R(36, 6)	13C1602 9P(12)	-12 027.5	30 200 998.7	-2.4	5.0	1007.396 88(-8)
R(38, 5)	13C1602 9P(12)	12 587.3	30 225 613.4	-2.5	5.0	1008.217 93(-8)
R(38, 3)	13C1602 9P(12)	16 494.9	30 229 521.1	2.4	5.0	1008.348 28(8)
R(38, 2)	13C1602 9P(12)	17 276.7	30 230 302.9	2.0	5.0	1008.374 36(7)
R(38, 1)	13C1602 9P(12)	17 679.5	30 230 705.6	16.8	OMIT	1008.387 79(56)
R(38, 0)	13C1602 9P(12)	17 780.7	30 230 806.8	1.2	5.0	1008.391 16(4)
R(40, 4)	13C1602 9P(10)	-15 472.8	30 248 996.3	-1.5	5.0	1008.997 91(-5)
R(40, 3)	13C1602 9P(10)	-13 751.7	30 250 717.4	3.6	5.0	1009.055 32(12)
R(41, 6)	13C1602 9P(10)	-13 507.3	30 250 961.8	-4.1	5.0	1009.063 47(-14)
R(40, 1)	13C1602 9P(10)	-12 276.1	30 252 193.0	-0.3	5.0	1009.104 54(-1)
R(40, 0)	13C1602 9P(10)	-12 123.6	30 252 345.4	-1.1	5.0	1009.109 61(-4)
R(46, 6)	13C1602 9P(8)	-16 605.6	30 298 440.7	2.0	10.0	1010.647 19(7)
R(45, 1)	13C1602 9P(8)	-10 871.0	30 304 175.2	-6.3	10.0	1010.838 48(-21)
R(45, 0)	13C1602 9P(8)	-10 626.9	30 304 419.4	-8.3	10.0	1010.846 62(-28)
R(46, 5)	13C1602 9P(8)	-9 970.4	30 305 075.9	-0.3	5.0	1010.868 51(-1)
R(47, 2)	13C1602 9P(8)	8 340.0	30 323 386.2	0.2	5.0	1011.479 28(1)
R(48, 5)	13C1602 9P(8)	8 917.2	30 323 963.5	-1.4	10.0	1011.498 55(-5)
R(47, 1)	13C1602 9P(8)	9 239.5	30 324 285.8	-0.6	5.0	1011.509 30(-2)
R(47, 0)	13C1602 9P(8)	9 522.3	30 324 568.6	-1.4	5.0	1011.518 73(-5)
R(48, 4)	13C1602 9P(8)	13 507.2	30 328 553.5	1.8	5.0	1011.651 65(6)
R(48, 3)	13C1602 9P(8)	16 417.4	30 331 463.7	3.1	5.0	1011.748 72(10)

[a] Numbers are J and K of the lower vibrational state.

[b] Laser line used; laser frequencies were taken from Ref. 34.

[c] Microwave frequency in MHz. The signed microwave frequency was added to the laser frequency to obtain the absorption frequency.

[d] Observed minus calculated frequency in MHz; the parameters for the calculation are in Table 3-8 of this work and in Table V of Ref. 7.

[e] Estimated uncertainty in the observed frequency in MHz. An "OMIT" means that the frequency was omitted from the least squares fits.

[f] Observed wavenumber in cm^{-1}. The numbers in parentheses are observed minus calculated wavenumbers in units of 0.00001 cm^{-1}.

TABLE 3-7

Comparison of Observed and Calculated Frequencies in the ν_2 Band of $CD_3{}^{81}Br$

Trans.[a]	Laser[b]	ν_m[c]	ν/MHz	O-C[d]	Unc.[e]	ν/cm^{-1} f
P(45, 6)	12C1602 10R(4)	-17 835.0	28 905 211.4	9.4	5.0	964.174 07(31)
P(45, 5)	12C1602 10R(4)	-12 239.5	28 910 807.0	-6.2	5.0	964.360 72(-21)
P(45, 4)	12C1602 10R(4)	-8 825.6	28 914 220.8	-0.6	5.0	964.474 59(-2)
P(44, 5)	12C1602 10R(4)	8 365.5	28 931 411.9	-4.9	10.0	965.048 01(-16)
P(44, 4)	12C1602 10R(4)	11 571.6	28 934 618.1	1.1	5.0	965.154 97(4)
P(44, 3)	12C1602 10R(4)	13 485.0	28 936 531.4	1.0	5.0	965.218 79(3)
P(44, 2)	12C1602 10R(4)	14 588.7	28 937 635.1	-1.9	5.0	965.255 61(-6)
P(44, 1)	12C1602 10R(4)	15 162.4	28 938 208.8	0.2	5.0	965.274 73(1)
P(43, 7)	12C1602 10R(4)	15 282.0	28 938 328.4	-2.7	5.0	965.278 72(-9)
P(44, 0)	12C1602 10R(4)	15 336.6	28 938 383.1	-1.8	5.0	965.280 56(-6)
P(39,10)	12C1602 10R(4)	16 336.2	28 939 382.7	374.0	OMIT	965.313 89(1248)
P(43, 5)	12C1602 10R(6)	-15 531.4	28 951 925.7	-6.9	10.0	965.732 29(-23)
P(43, 3)	12C1602 10R(6)	-10 765.0	28 956 692.1	1.8	10.0	965.891 28(6)
P(43, 2)	12C1602 10R(6)	-9 756.6	28 957 700.4	1.4	10.0	965.924 90(5)
P(43, 1)	12C1602 10R(6)	-9 243.8	28 958 213.3	-1.4	10.0	965.942 01(-5)
P(42, 3)	12C1602 10R(6)	9 305.8	28 976 762.8	2.2	10.0	966.560 77(7)
P(42, 2)	12C1602 10R(6)	10 217.4	28 977 674.4	2.6	5.0	966.591 17(9)
P(42, 1)	12C1602 10R(6)	10 676.6	28 978 133.7	2.0	5.0	966.606 49(7)
P(42, 0)	12C1602 10R(6)	10 814.4	28 978 271.5	-0.1	20.0	966.611 08(0)
P(39, 9)	12C1602 10R(6)	17 944.3	28 985 401.3	-68.1	OMIT	966.848 92(-227)
P(41, 4)	12C1602 10R(8)	-15 867.4	28 995 265.6	-2.0	5.0	967.177 95(-7)
P(41, 3)	12C1602 10R(8)	-14 392.1	28 996 740.9	0.8	5.0	967.227 16(3)
P(41, 2)	12C1602 10R(8)	-13 577.9	28 997 555.1	0.9	5.0	967.254 32(3)
P(41, 1)	12C1602 10R(8)	-13 175.0	28 997 958.0	-0.6	5.0	967.267 75(-2)
P(41, 0)	12C1602 10R(8)	-13 052.4	28 998 080.6	0.1	5.0	967.271 84(0)
P(40, 7)	12C1602 10R(8)	-9 726.2	29 001 406.8	1.0	5.0	967.382 79(3)
P(39, 7)	12C1602 10R(8)	11 122.1	29 022 255.1	-0.8	5.0	968.078 22(-3)
P(39, 3)	12C1602 10R(10)	-17 650.7	29 036 422.0	0.6	5.0	968.550 78(2)
P(39, 2)	12C1602 10R(10)	-17 030.5	29 037 042.2	-0.7	5.0	968.571 46(-2)
P(38, 7)	12C1602 10R(10)	-11 059.2	29 043 013.5	-1.4	5.0	968.770 65(-5)
P(37, 7)	12C1602 10R(10)	9 608.9	29 063 681.6	1.2	5.0	969.460 05(4)
P(37, 6)	12C1602 10R(10)	15 733.9	29 069 806.6	-5.1	5.0	969.664 36(-17)
P(36, 7)	12C1602 10R(12)	-12 024.4	29 084 250.0	0.4	5.0	970.146 15(1)
P(35, 7)	12C1602 10R(12)	8 448.9	29 104 723.3	2.8	5.0	970.829 07(9)
P(35, 5)	12C1602 10R(12)	16 430.7	29 112 705.1	-1.0	5.0	971.095 31(-3)
P(35, 4)	12C1602 10R(12)	17 756.4	29 114 030.8	-1.5	5.0	971.139 53(-5)
P(34, 7)	12C1602 10R(14)	-12 661.9	29 125 074.3	-16.0	OMIT	971.507 89(-53)
P(33, 6)	12C1602 10R(14)	12 065.4	29 149 801.5	-0.4	5.0	972.332 71(-1)
P(33, 5)	12C1602 10R(14)	14 168.3	29 151 904.4	-4.9	5.0	972.402 86(-16)
P(33, 4)	12C1602 10R(14)	15 092.3	29 152 828.4	-0.2	5.0	972.433 67(-1)
P(32, 7)	12C1602 10R(16)	-12 937.8	29 165 517.9	1.9	5.0	972.856 95(6)
P(31, 6)	12C1602 10R(16)	10 706.9	29 189 162.6	-0.3	5.0	973.645 66(-1)
P(31, 5)	12C1602 10R(16)	12 234.5	29 190 690.1	-0.7	5.0	973.696 60(-2)
P(29, 9)	12C1602 10R(18)	-15 798.2	29 202 632.5	-228.0	OMIT	974.094 96(-760)
P(30, 7)	12C1602 10R(18)	-12 922.0	29 205 508.7	3.5	5.0	974.190 91(12)
P(28, 3)	12C1602 10R(20)	-10 010.6	29 247 648.0	-0.9	5.0	975.596 52(-3)
P(27, 2)	12C1602 10R(20)	8 125.6	29 265 784.1	3.1	5.0	976.201 47(10)
P(27, 3)	12C1602 10R(20)	8 566.9	29 266 225.4	-4.0	5.0	976.216 19(-13)
P(27, 6)	12C1602 10R(20)	8 876.0	29 266 535.1	0.5	5.0	976.226 53(2)
P(27, 4)	12C1602 10R(20)	9 033.0	29 266 691.5	0.2	5.0	976.231 75(1)

Table 3-7 (cont'd)

Trans.[a]	Laser[b]	ν_m[c]	ν/MHz	O-C[d]	Unc.[e]	ν/cm^{-1} [f]
P(26, 8)	12C1602 10R(22)	-16 756.9	29 279 379.5	-3.9	5.0	976.654 97(-13)
P(26, 3)	12C1602 10R(22)	-11 433.9	29 284 702.5	1.0	5.0	976.832 53(3)
P(26, 4)	12C1602 10R(22)	-10 849.5	29 285 286.9	0.5	5.0	976.852 02(2)
P(25, 9)	12C1602 10R(22)	-8 706.5	29 287 429.9	-229.0	OMIT	976.923 49(-764)
P(24, 3)	12C1602 10R(24)	-12 545.4	29 321 320.8	5.1	5.0	978.053 98(17)
P(24, 4)	12C1602 10R(24)	-11 723.6	29 322 137.6	0.1	5.0	978.081 23(0)
P(24, 7)	12C1602 10R(24)	-11 228.8	29 322 632.4	3.0	5.0	978.097 72(10)
P(24, 5)	12C1602 10R(24)	-10 940.9	29 322 920.2	0.9	5.0	978.107 34(3)
P(24, 6)	12C1602 10R(24)	-10 544.5	29 323 316.7	-0.5	5.0	978.120 55(-2)
P(22, 9)	12C1602 10R(24)	16 078.7	29 349 939.9	-226.3	OMIT	979.008 60(-755)
P(22, 2)	12C1602 10R(26)	-14 170.6	29 356 659.0	-1.2	5.0	979.232 74(-4)
P(22, 3)	12C1602 10R(26)	-13 345.8	29 357 483.8	0.5	5.0	979.260 25(2)
P(22, 4)	12C1602 10R(26)	-12 296.2	29 358 533.4	4.8	5.0	979.295 25(16)
P(22, 5)	12C1602 10R(26)	-11 183.8	29 359 645.8	0.0	5.0	979.332 36(0)
P(21, 6)	12C1602 10R(26)	8 143.5	29 378 973.2	2.4	5.0	979.977 06(8)
P(21, 7)	12C1602 10R(26)	8 623.0	29 379 452.6	4.6	5.0	979.993 05(15)
P(20, 9)	12C1602 10R(28)	-16 050.7	29 390 987.5	-228.7	OMIT	980.377 82(-763)
P(20, 0)	12C1602 10R(28)	-15 595.8	29 391 442.5	-1.2	5.0	980.392 99(-4)
P(20, 1)	12C1602 10R(28)	-15 393.5	29 391 644.7	-0.4	5.0	980.399 73(-1)
P(20, 2)	12C1602 10R(28)	-14 798.2	29 392 240.0	0.0	5.0	980.419 59(0)
P(20, 3)	12C1602 10R(28)	-13 839.5	29 393 198.7	2.2	5.0	980.451 56(7)
P(20, 4)	12C1602 10R(28)	-12 587.1	29 394 451.2	0.5	5.0	980.493 34(2)
P(20, 6)	12C1602 10R(28)	-9 773.0	29 397 265.2	3.4	5.0	980.587 22(11)
P(20, 8)	12C1602 10R(28)	-9 773.0	29 397 265.2	-4.5	5.0	980.587 22(-15)
P(20, 7)	12C1602 10R(28)	-8 926.7	29 398 111.6	1.9	5.0	980.615 45(6)
P(19, 8)	12C1602 10R(28)	9 362.8	29 416 401.1	-4.0	5.0	981.225 51(-13)
P(18, 0)	12C1602 10R(30)	-16 002.1	29 426 481.3	-0.1	5.0	981.561 76(0)
P(18, 1)	12C1602 10R(30)	-15 776.9	29 426 706.4	1.5	5.0	981.569 26(5)
P(18, 2)	12C1602 10R(30)	-15 119.7	29 427 363.6	-4.8	5.0	981.591 18(-16)
P(18, 3)	12C1602 10R(30)	-14 032.8	29 428 450.5	2.7	5.0	981.627 44(9)
P(18, 4)	12C1602 10R(30)	-12 585.1	29 429 898.3	3.4	5.0	981.675 74(11)
P(18, 5)	12C1602 10R(30)	-10 865.6	29 431 617.8	-0.6	5.0	981.733 08(-2)
P(18, 9)	12C1602 10R(30)	-10 865.2	29 431 618.1	-73.1	OMIT	981.733 11(-244)
P(18, 6)	12C1602 10R(30)	-9 041.3	29 433 442.0	-0.6	5.0	981.793 94(-2)
P(17, 8)	12C1602 10R(30)	11 705.3	29 454 188.6	-2.9	5.0	982.485 98(-10)
P(16, 1)	12C1602 10R(32)	-15 846.0	29 461 314.9	1.3	5.0	982.723 67(4)
P(16, 2)	12C1602 10R(32)	-15 121.4	29 462 039.5	0.2	5.0	982.747 84(1)
P(16, 3)	12C1602 10R(32)	-13 929.3	29 463 231.1	0.8	5.0	982.787 59(3)
P(16, 4)	12C1602 10R(32)	-12 314.9	29 464 845.9	-7.0	5.0	982.841 46(-23)
P(16, 5)	12C1602 10R(32)	-10 317.3	29 466 843.5	0.8	5.0	982.908 09(3)
P(15, 6)	12C1602 10R(32)	9 524.9	29 486 685.7	2.4	5.0	983.569 96(8)
P(15, 7)	12C1602 10R(32)	12 043.8	29 489 204.6	-1.5	5.0	983.653 99(-5)
P(15, 8)	12C1602 10R(32)	14 135.5	29 491 296.3	-2.2	5.0	983.723 75(-7)
P(15, 9)	12C1602 10R(32)	14 381.0	29 491 541.9	390.9	OMIT	983.731 94(1304)
P(14, 0)	12C1602 10R(34)	-15 861.5	29 495 205.1	1.0	5.0	983.854 14(3)
P(14, 1)	12C1602 10R(34)	-15 593.2	29 495 473.4	7.9	5.0	983.863 09(26)
P(14, 2)	12C1602 10R(34)	-14 817.9	29 496 248.8	2.1	5.0	983.888 95(7)
P(14, 3)	12C1602 10R(34)	-13 523.1	29 497 543.5	6.1	5.0	983.932 14(20)
P(14, 4)	12C1602 10R(34)	-11 750.1	29 499 316.6	-0.5	5.0	983.991 27(-2)
P(14, 5)	12C1602 10R(34)	-9 521.6	29 501 545.1	-1.0	5.0	984.065 61(-3)

Table 3-7 (cont'd)

Trans.[a]	Laser[b]	ν_m[c]	ν/MHz	O-C[d]	Unc.[e]	ν/cm^{-1} [f]
P(13, 7)	12C1602 10R(34)	13 523.1	29 524 589.8	28.0	OMIT	984.834 30(94)
P(12, 0)	12C1602 10R(36)	-15 318.3	29 528 878.0	-1.1	5.0	984.977 35(-4)
P(13, 9)	12C1602 10R(36)	-14 345.5	29 529 850.8	28.7	OMIT	985.009 80(96)
P(12, 2)	12C1602 10R(36)	-14 210.0	29 529 986.4	0.8	5.0	985.014 31(3)
P(12, 3)	12C1602 10R(36)	-12 833.6	29 531 362.7	-0.7	5.0	985.060 23(-2)
P(12, 4)	12C1602 10R(36)	-10 942.5	29 533 253.9	-26.5	OMIT	985.123 30(-88)
P(11, 7)	12C1602 10R(36)	15 071.5	29 559 267.9	-0.7	5.0	985.991 03(-2)
P(10, 0)	12C1602 10R(38)	-14 455.2	29 562 089.9	-0.5	5.0	986.085 18(-2)
P(10, 1)	12C1602 10R(38)	-14 156.9	29 562 388.2	7.7	5.0	986.095 13(26)
P(10, 2)	12C1602 10R(38)	-13 295.6	29 563 249.5	-1.5	5.0	986.123 86(-5)
P(10, 3)	12C1602 10R(38)	-11 843.0	29 564 702.2	-0.5	5.0	986.172 31(-2)
P(10, 4)	12C1602 10R(38)	-9 808.9	29 566 736.2	-0.2	5.0	986.240 15(-1)
R(3, 0)	13C1602 9P(28)	10 663.5	29 781 331.7	7.4	10.0	993.398 29(25)
R(3, 1)	13C1602 9P(28)	10 965.2	29 781 633.4	-1.9	10.0	993.408 36(-6)
R(7, 0)	13C1602 9P(26)	10 729.8	29 839 655.3	-0.2	5.0	995.343 75(-1)
R(7, 1)	13C1602 9P(26)	11 022.5	29 839 948.0	-1.2	5.0	995.353 52(-4)
R(7, 2)	13C1602 9P(26)	11 903.5	29 840 829.1	-1.9	5.0	995.382 91(-6)
R(7, 3)	13C1602 9P(26)	13 378.7	29 842 304.3	0.6	5.0	995.432 12(2)
R(9, 1)	13C1602 9P(24)	-17 961.6	29 868 382.9	-0.8	5.0	996.302 00(-3)
R(9, 2)	13C1602 9P(24)	-17 105.1	29 869 239.4	12.7	OMIT	996.330 58(42)
R(9, 3)	13C1602 9P(24)	-15 717.3	29 870 627.2	-2.7	5.0	996.376 87(-9)
R(9, 4)	13C1602 9P(24)	-13 757.9	29 872 586.6	-2.6	5.0	996.442 22(-9)
R(10, 7)	13C1602 9P(24)	8 775.9	29 895 120.4	-0.7	5.0	997.193 88(-2)
R(11, 0)	13C1602 9P(24)	9 719.0	29 896 063.5	-8.7	5.0	997.225 33(-29)
R(11, 1)	13C1602 9P(24)	9 991.2	29 896 335.7	-2.8	5.0	997.234 42(-9)
R(11, 3)	13C1602 9P(24)	12 089.1	29 898 433.6	-21.8	OMIT	997.304 39(-73)
R(11, 4)	13C1602 9P(24)	13 937.8	29 900 282.3	-1.6	5.0	997.366 05(-5)
R(13, 4)	13C1602 9P(22)	-15 470.0	29 927 450.8	-9.8	5.0	998.272 29(-33)
R(13, 5)	13C1602 9P(22)	-13 381.3	29 929 539.4	-0.9	10.0	998.341 96(-3)
R(13, 6)	13C1602 9P(22)	-10 998.9	29 931 921.9	-0.7	5.0	998.421 43(-2)
R(15, 3)	13C1602 9P(22)	9 693.5	29 952 614.2	-1.9	10.0	999.111 67(-6)
R(15, 4)	13C1602 9P(22)	11 203.2	29 954 124.0	0.2	5.0	999.162 02(1)
R(15, 5)	13C1602 9P(22)	13 023.3	29 955 944.0	-1.8	5.0	999.222 74(-6)
R(15, 6)	13C1602 9P(22)	15 013.9	29 957 934.6	1.8	5.0	999.289 13(6)
R(17, 5)	13C1602 9P(20)	-16 836.1	29 981 814.0	-2.7	5.0	1000.085 65(-9)
R(17, 6)	13C1602 9P(20)	-15 277.4	29 983 372.7	2.2	5.0	1000.137 65(7)
R(17, 8)	13C1602 9P(20)	-14 434.2	29 984 215.9	-5.5	5.0	1000.165 78(-18)
R(17, 7)	13C1602 9P(20)	-14 130.0	29 984 520.1	3.8	5.0	1000.175 92(13)
R(18, 1)	13C1602 9P(20)	-8 220.0	29 990 430.1	-5.4	5.0	1000.373 06(-18)
R(20, 0)	13C1602 9P(20)	17 434.5	30 016 084.6	-6.5	5.0	1001.228 80(-22)
R(20, 1)	13C1602 9P(20)	17 614.8	30 016 264.9	1.8	5.0	1001.234 82(6)
R(22, 0)	13C1602 9P(18)	-12 048.4	30 041 480.7	-1.5	5.0	1002.075 92(-5)
R(22, 2)	13C1602 9P(18)	-11 476.5	30 042 052.2	2.0	5.0	1002.095 00(7)
R(22, 3)	13C1602 9P(18)	-10 829.5	30 042 699.3	-1.1	5.0	1002.116 57(-4)
R(24, 2)	13C1602 9P(18)	13 341.8	30 066 870.5	0.8	5.0	1002.922 85(3)
R(24, 3)	13C1602 9P(18)	13 839.5	30 067 368.2	3.1	5.0	1002.939 44(10)
R(24, 4)	13C1602 9P(18)	14 374.9	30 067 903.6	-1.1	5.0	1002.957 31(-4)
R(26, 0)	13C1602 9P(16)	-16 656.4	30 090 896.6	-2.1	5.0	1003.724 27(-7)
R(26, 1)	13C1602 9P(16)	-16 566.2	30 090 986.9	0.1	5.0	1003.727 27(0)
R(26, 6)	13C1602 9P(16)	-16 458.0	30 091 095.0	4.6	5.0	1003.730 89(15)

Table 3-7 (cont'd)

Trans.[a]	Laser[b]	ν_0[c]	ν/MHz	O-C[d]	Unc.[e]	ν/cm^{-1} [f]
R(26, 2)	13C1602 9P(16)	-16 320.0	30 091 233.1	2.4	5.0	1003.735 49(8)
R(26, 3)	13C1602 9P(16)	-15 990.7	30 091 562.4	-0.9	5.0	1003.746 48(-3)
R(26, 4)	13C1602 9P(16)	-15 702.9	30 091 850.2	-0.4	10.0	1003.756 07(-1)
R(26, 5)	13C1602 9P(16)	-15 702.9	30 091 850.2	3.9	10.0	1003.756 07(13)
R(29, 7)	13C1602 9P(16)	13 442.1	30 120 995.2	8.2	5.0	1004.728 25(27)
R(30, 8)	13C1602 9P(16)	15 179.6	30 122 732.7	-95.4	OMIT	1004.786 20(-318)
R(29, 6)	13C1602 9P(16)	17 134.3	30 124 687.4	1.7	5.0	1004.851 40(6)
R(31, 6)	13C1602 9P(14)	-14 244.0	30 146 475.9	-5.9	5.0	1005.578 18(-20)
R(31, 5)	13C1602 9P(14)	-12 042.9	30 148 677.0	-3.8	5.0	1005.651 61(-13)
R(31, 4)	13C1602 9P(14)	-11 045.8	30 149 674.1	-0.5	5.0	1005.684 88(-2)
R(31, 3)	13C1602 9P(14)	-10 661.0	30 150 058.9	-1.6	5.0	1005.697 71(-5)
R(31, 2)	13C1602 9P(14)	-10 554.2	30 150 165.7	0.9	10.0	1005.701 27(3)
R(31, 1)	13C1602 9P(14)	-10 554.2	30 150 165.7	-1.9	10.0	1005.701 27(-6)
R(31, 0)	13C1602 9P(14)	-10 554.2	30 150 165.7	6.5	10.0	1005.701 27(22)
R(33, 8)	13C1602 9P(14)	-8 856.1	30 151 863.8	2.9	5.0	1005.757 92(10)
R(33, 5)	13C1602 9P(14)	9 884.2	30 170 604.1	-0.4	5.0	1006.383 02(-1)
R(35, 8)	13C1602 9P(14)	9 884.2	30 170 604.1	-102.5	OMIT	1006.383 02(-342)
R(33, 4)	13C1602 9P(14)	11 291.3	30 172 011.2	1.4	10.0	1006.429 96(5)
R(34, 7)	13C1602 9P(14)	11 763.4	30 172 483.3	4.9	5.0	1006.445 70(16)
R(33, 2)	13C1602 9P(14)	12 247.4	30 172 967.3	0.2	5.0	1006.461 85(1)
R(34, 6)	13C1602 9P(14)	17 591.5	30 178 311.4	1.1	5.0	1006.640 12(4)
R(35, 1)	13C1602 9P(12)	-17 472.9	30 195 553.2	0.9	10.0	1007.215 23(3)
R(35, 0)	13C1602 9P(12)	-17 413.8	30 195 612.3	-0.3	10.0	1007.217 21(-1)
R(36, 5)	13C1602 9P(12)	-10 373.5	30 202 652.7	-2.8	10.0	1007.452 04(-9)
R(38, 5)	13C1602 9P(12)	10 452.7	30 223 478.9	-3.4	10.0	1008.146 74(-11)
R(38, 4)	13C1602 9P(12)	12 919.2	30 225 945.4	8.5	5.0	1008.229 01(28)
R(38, 2)	13C1602 9P(12)	15 076.6	30 228 102.7	2.2	5.0	1008.300 97(7)
R(38, 1)	13C1602 9P(12)	15 454.1	30 228 480.2	0.5	10.0	1008.313 56(2)
R(38, 0)	13C1602 9P(12)	15 590.9	30 228 617.0	23.4	OMIT	1008.318 12(78)
R(40, 4)	13C1602 9P(10)	-17 703.0	30 246 766.1	-0.5	5.0	1008.923 52(-2)
R(40, 3)	13C1602 9P(10)	-16 008.0	30 248 461.0	1.7	5.0	1008.980 05(6)
R(41, 6)	13C1602 9P(10)	-15 695.1	30 248 773.9	-6.9	10.0	1008.990 49(-23)
R(40, 1)	13C1602 9P(10)	-14 555.0	30 249 914.1	-0.1	5.0	1009.028 51(0)
R(41, 5)	13C1602 9P(10)	-10 533.6	30 253 935.5	-2.8	5.0	1009.162 65(-9)
R(48, 9)	13C1602 9P(10)	-9 498.1	30 254 970.9	520.1	OMIT	1009.197 19(1735)
R(43, 5)	13C1602 9P(10)	9 263.4	30 273 732.5	-2.5	10.0	1009.823 02(-8)
R(47, 8)	13C1602 9P(10)	12 123.6	30 276 592.7	162.0	OMIT	1009.918 41(540)
R(45, 7)	13C1602 9P(10)	12 123.6	30 276 592.7	0.3	10.0	1009.918 41(1)
R(44, 6)	13C1602 9P(10)	12 980.5	30 277 449.5	-13.3	OMIT	1009.947 00(-44)
R(43, 3)	13C1602 9P(10)	14 917.0	30 279 386.1	1.3	5.0	1010.011 60(4)
R(43, 1)	13C1602 9P(10)	16 835.9	30 281 304.9	-2.1	5.0	1010.075 60(-7)
R(45, 2)	13C1602 9P(8)	-14 084.9	30 300 961.3	-2.7	5.0	1010.731 27(-9)

Table 3-7 (cont'd)

[a]Numbers are J and K of the lower vibrational state.

[b]Laser line used; laser frequencies were taken from Ref. 34.

[c]Microwave frequency in MHz. The signed microwave frequency was added to the laser frequency to obtain the absorption frequency.

[d]Observed minus calculated frequency in MHz; the parameters for the calculation are in Table 3-9 of this work and in Table V of Ref. 7.

[e]Estimated uncertainty in the observed frequency in MHz. An "OMIT" means that the frequency was omitted from the least squares fits.

[f]Observed wavenumber in cm^{-1}. The numbers in parentheses are observed minus calculated wavenumbers in units of 0.00001 cm^{-1}.

TABLE 3-8

Molecular Constants of $CD_3{}^{79}Br$[a]

Parameter[b]	$v_2 = 0$[c]	$v_2 = 1$[c]
E_v /GHz	0.[e]	29 721.322 4(12)
B_v /MHz	7 714.650 1(68)	7 690.278 7(90)
(A_v-B_v) /MHz	70 243.4[d]	70 527.91(16)
D_J /kHz	5.797 8(96)	5.567 7(107)
D_{JK} /kHz	65.026(452)	69.722(558)
D_K /kHz	450.[d]	382.742 5(68497)
H_J /Hz	-0.002 30(303)	-0.017 39(425)
H_{JK} /Hz	0.174(121)	2.462(262)
H_{KJ} /Hz	-18.52(746)	-27.58(924)
ΔH_K /Hz	0.[e]	-1410.(115)
L_J /mHz	0.[e]	0.00325(76)
L_{JJJK} /mHz	0.[e]	-0.2999(533)
L_{JJKK} /mHz	0.[e]	18.34(218)
L_{JKKK} /mHz	0.[e]	-435.3(291)
ΔL_K /mHz	0.[e]	6677.(633)

[a]Values in parentheses are one standard deviation in multiples of the last digit in the parameter.

[b]Vibration-rotation parameters. $\Delta P = P(v_2=1) - P(v_2=0)$.

[c]Obtained from a fit of the vibration-rotation frequencies listed in Table 3-6 and hypothetical unsplit rotational frequencies calculated from the experimental frequencies reported in References 10 and 29.

[d]Constrained to the value reported in Ref. 28.

[e]Constrained to zero.

TABLE 3-9

Molecular Constants of $CD_3{}^{81}Br$[a]

Parameter[b]	$v_2 = 0$[c]	$v_2 = 1$[c]
E_v /GHz	0.[e]	29 721.073 2(12)
B_v /MHz	7 681.278 0(106)	7 657.050 4(121)
(A_v-B_v) /MHz	70 276.8[d]	70 562.22(19)
D_J /kHz	5.580 2(124)	5.595 8(153)
D_{JK} /kHz	63.030(1188)	67.955(1237)
D_K /kHz	450.[d]	455.3(83)
H_J /Hz	0.013 15(394)	-0.000 44(579)
H_{JK} /Hz	0.053(282)	2.227(384)
H_{KJ} /Hz	-18.85(1790)	-23.86(2144)
ΔH_K /Hz	0.[e]	-284.(120)
L_J /mHz	0.[e]	0.002 40(73)
L_{JJJK} /mHz	0.[e]	-0.416 5(518)
L_{JJKK} /mHz	0.[e]	15.03(324)
L_{JKKK} /mHz	0.[e]	-984.9(874)
ΔL_K /mHz	0.[e]	3 441.(492)

[a]Values in parentheses are one standard deviation in multiples of the last digit in the parameter.

[b]Vibration-rotation parameters. $\Delta P = P(v2=1) - P(v2=0)$.

[c]Obtained from a fit of the vibration-rotation frequencies listed in Table II and hypothetical unsplit rotational frequencies calculated from the experimental frequencies reported in References 10 and 29.

[d]Constrained to the value reported in Ref 28.

[e]Constrained to zero.

is performed, the parameters are best interpreted as constants for frequency calculation only. The parameters have been used to predict coincidences between CO_2 and N_2O laser frequencies (34,38) and the frequencies of the ν_2 bands of both species of CD_3Br. The predicted coincidences are shown in Tables 3-10 and 3-11.

The differences between the observed and calculated frequencies are shown in Tables 3-6 and 3-7, where it may be seen that the residuals are usually well within the estimated experimental uncertainties; this is confirmed by the values of the standard deviations for an observation of unit weight, which were 0.86 and 0.83 for the ^{79}Br and ^{81}Br species, respectively.

TABLE 3-10

Coincidences between Calculated Frequencies for the ν_2 Band of $CD_3{}^{79}Br$ and Laser Frequencies

Trans.[a]	Frequency[b]	$\nu_0-\nu_L$[c]	Laser[d]	
P(38,1)	29054033.96	-38.74	12C1602 BAND I	R(10)
P(38,0)	29054105.00	32.30	12C1602 BAND I	R(10)
P(32,6)	29167161.93	48.06	12C1802 BAND I	R(8)
P(27,3)	29264366.87	183.54	N20	R(49)
		-141.27	13C1802 BAND II	P(60)
P(27,6)	29264630.76	122.62	13C1802 BAND II	P(60)
P(26,6)	29283772.83	-31.46	N20	R(50)
P(26,5)	29283920.64	116.35	N20	R(50)
P(23,5)	29339816.89	3.99	13C1602 BAND II	P(42)
P(19,5)	29412634.09	36.19	12C1802 BAND I	R(22)
P(15,0)	29477350.60	189.74	12C1602 BAND I	R(32)
P(13,7)	29523877.89	-103.50	12C160180 BAND I	R(28)
P(12,2)	29529373.37	21.92	13C1602 BAND II	P(36)
P(12,5)	29535113.27	40.78	12C1802 BAND I	R(30)
P(11,6)	29555157.45	90.70	13C1802 BAND II	P(50)
P(10,6)	29572119.06	115.97	12C160180 BAND I	R(31)
Q(37,2)	29638806.15	-74.04	12C1602 BAND I	R(42)
Q(37,1)	29639068.83	188.64	12C1602 BAND I	R(42)
P(5,2)	29644222.22	-179.72	12C1802 BAND I	R(38)
Q(35,5)	29644480.38	78.44	12C1802 BAND I	R(38)
P(5,4)	29648033.64	41.04	12C160180 BAND I	R(36)
Q(31,4)	29662655.62	76.51	12C160180 BAND I	R(37)
Q(27,2)	29676834.52	-126.07	12C160180 BAND I	R(38)
Q(22,0)	29691147.43	10.93	12C160180 BAND I	R(39)
Q(23,5)	29691209.84	73.34	12C160180 BAND I	R(39)
Q(22,1)	29691307.70	171.20	12C160180 BAND I	R(39)
Q(21,1)	29693916.35	-158.96	12C1802 BAND I	R(42)
Q(20,3)	29697831.03	-198.32	12C1602 BAND I	R(46)
Q(21,6)	29698196.81	166.33	12C1602 BAND I	R(46)
Q(17,3)	29704927.13	-179.16	12C160180 BAND I	R(40)
Q(16,0)	29705012.72	-93.57	12C160180 BAND I	R(40)
Q(19,7)	29705092.29	-11.00	12C160180 BAND I	R(40)
Q(16,1)	29705243.25	136.96	12C160180 BAND I	R(40)
Q(13,2)	29711418.23	-158.86	13C1602 BAND II	P(30)
Q(17,8)	29711677.82	100.75	13C1602 BAND II	P(30)
Q(11,4)	29717755.86	106.03	12C1802 BAND I	R(44)
Q(6,0)	29718790.12	-79.26	12C160180 BAND I	R(41)
Q(7,4)	29722778.40	119.92	13C1802 BAND II	P(44)

Table 3-10 (cont'd)

Trans.[a]	Frequency[b]	$\nu_0-\nu_L$[c]	Laser[d]	
Q(9,6)	29726342.55	-52.21	12C1602 BAND I	R(48)
Q(11,7)	29726432.03	37.27	12C1602 BAND I	R(48)
Q(6,5)	29726532.18	137.42	12C1602 BAND I	R(48)
Q(10,8)	29732378.36	-46.81	12C160180 BAND I	R(42)
R(3,3)	29784647.36	84.16	12C160180 BAND I	R(46)
R(4,1)	29796963.69	-109.55	12C160180 BAND I	R(47)
R(6,5)	29833516.22	182.26	12C160180 BAND I	R(50)
R(7,4)	29845124.76	129.35	12C160180 BAND I	R(51)
R(8,2)	29855897.74	26.03	12C1602 BAND I	R(58)
R(13,5)	29930628.03	107.09	12C160180 BAND I	R(59)
R(26,3)	30093278.81	58.56	13C1802 BAND II	P(30)
R(31,7)	30143745.44	-10.96	13C1802 BAND II	P(28)

[a] Transition in the ν_2 band of $CD_3{}^{79}Br$; $J < 40$, $K < 8$.

[b] Frequency of the ν_2 band transition in MHz.

[c] Frequency of the ν_2 band transition minus the laser frequency in MHz.

[d] Identification of the CO_2 laser; Band II is the 9 μm band. Laser frequencies were obtained from Refs. 34 and 38.

TABLE 3-11

Coincidences between Calculated Frequencies for the ν_2 Band of $CD_3{}^{81}Br$ and Laser Frequencies

Trans.[a]	Frequency[b]	$\nu_0-\nu_L$[c]	Laser[d]	
P(39,5)	29033085.68	-52.19	12C160180 BAND I	R(2)
P(37,3)	29075724.25	137.89	12C160180 BAND I	R(4)
P(37,2)	29076156.12	151.68	13C1602 BAND II	P(50)
P(36,6)	29089962.67	198.43	12C1802 BAND I	R(4)
P(30,8)	29198208.41	-63.44	12C160180 BAND I	R(10)
P(27,7)	29264622.06	113.92	13C1802 BAND II	P(60)
P(26,0)	29283694.97	-109.32	N20	R(50)
P(26,1)	29283819.06	14.77	N20	R(50)
P(25,7)	29303421.72	108.04	N20	R(51)
P(24,7)	29322629.33	-81.88	N20	R(52)
P(23,6)	29341996.45	-0.11	N20	R(53)
P(16,5)	29466842.77	-134.00	13C1602 BAND II	P(38)
P(12,1)	29529159.04	-195.42	13C1602 BAND II	P(36)
P(10,7)	29576373.04	-172.09	12C1602 BAND I	R(38)
P(7,1)	29611334.75	-167.81	13C1802 BAND II	P(48)
P(5,2)	29644317.12	-84.83	12C1802 BAND I	R(38)
P(5,4)	29648123.20	130.59	12C160180 BAND I	R(36)
Q(34,2)	29651565.78	-91.33	13C1602 BAND II	P(32)
Q(34,1)	29651660.14	3.03	13C1602 BAND II	P(32)
Q(34,0)	29651681.13	24.29	13C1602 BAND II	P(32)
Q(29,6)	29668792.27	-63.56	12C1602 BAND I	R(44)
Q(27,6)	29676880.16	-79.78	12C160180 BAND I	R(38)
Q(27,2)	29676910.92	-49.67	12C160180 BAND I	R(38)
Q(22,0)	29691114.52	-21.98	12C160180 BAND I	R(39)
Q(23,5)	29691224.34	87.83	12C160180 BAND I	R(39)
Q(22,1)	29691276.38	139.88	12C160180 BAND I	R(39)
Q(21,6)	29698177.00	147.66	12C1602 BAND I	R(46)
Q(19,7)	29705050.18	-56.11	12C160180 BAND I	R(40)
Q(16,1)	29705113.37	7.08	12C160180 BAND I	R(40)
Q(17,8)	29711623.55	46.48	13C1602 BAND II	P(30)
Q(12,0)	29711761.59	184.52	13C1602 BAND II	P(30)
Q(11,4)	29717566.62	-83.21	12C1802 BAND I	R(44)
Q(7,0)	29717722.63	72.80	12C1802 BAND I	R(44)
Q(6,1)	29718863.80	-5.58	12C160180 BAND I	R(41)
Q(7,2)	29718923.38	54.00	12C160180 BAND I	R(41)
Q(10,4)	29719007.12	137.74	12C160180 BAND I	R(41)
Q(7,4)	29722552.17	-106.31	13C1802 BAND II	P(44)
Q(4,3)	29722696.93	38.45	13C1802 BAND II	P(44)

Table 3-11 (cont'd)

Trans.[a]	Frequency[b]	$\nu_0-\nu_L$[c]	Laser[d]	
Q(11,7)	29726232.07	-161.94	12C1602 BAND I	R(48)
Q(6,5)	29726290.57	-104.19	12C1602 BAND I	R(48)
R(8,3)	29856529.51	86.61	12C160180 BAND I	R(52)
R(10,4)	29886501.57	157.06	13C1602 BAND II	P(24)
R(14,2)	29938089.58	110.22	13C1802 BAND II	P(36)
R(14,5)	29942810.38	-110.36	13C1602 BAND II	P(22)
R(18,0)	29990238.92	-89.20	13C1802 BAND II	P(34)
R(18,1)	29990435.49	107.38	13C1802 BAND II	P(34)
R(22,2)	30042050.23	-26.08	13C1802 BAND II	P(32)
R(32,4)	30160897.88	177.99	13C1602 BAND II	P(14)
R(37,5)	30213122.03	95.90	13C1602 BAND II	P(12)

[a] Transition in the ν_2 band of $CD_3{}^{81}Br$; $J < 40$, $K < 8$.

[b] Frequency of the ν_2 band transition in MHz.

[c] Frequency of the ν_2 band transition minus the laser frequency in MHz.

[d] Identification of the CO_2 laser; Band II is the 9 μm band. Laser frequencies were obtained from Refs. 34 and 38.

III-5 Discussion

III-5-1 CD_3I

As seen in Table 3-1, the vibration-rotation parameters for the ground and $v_2 = 1$ states, including the Coriolis coupling, predict the infrared frequencies for $J \leq 43$ and $K \leq 10$ to an accuracy of a few MHz. As shown in the first two numerical columns of Table 3-4, the resulting parameters are quite reasonable and convergent. In fact, ΔH_K, ΔL_K, and L_J were so close to zero that they could be constrained to zero in the fitting without significant effect on the standard deviation for an observation of unit weight, which was ~0.7 for both fittings. The corresponding fitting in which explicit Coriolis effects were omitted also gave calculated frequencies that were in good agreement with the experimental values (standard deviation = 1.5), but, as shown in Table 3-3, the higher-order parameters, especially those that multiply higher powers of K, are rather large. This is the typical result of an attempt to mimic the effect of substantial Coriolis coupling by means of a power series expansion in $J(J+1)$ and K^2. An important conclusion is that it is possible to predict the vibration-rotation frequencies for $J \leq 43$ and $K \leq 10$ in the v_2 band of CD_3I to within a few MHz with the parameters in Table 3-4 in a simple power series expansion without Coriolis interaction. Above $K = 10$ the frequencies of the P, Q, and R branch transitions for a given J, which increase in frequency as K increases for lower K, reach a maximum and begin to decrease with increasing K. A small number of higher K transitions have been assigned and their frequencies agree much better with the Coriolis-corrected calculated values than with the values obtained with the simple power series

expansion. It appears that many higher K transitions can be recorded and assigned, but this was judged to be beyond the scope of the present study. Combination of such frequencies with those for the ν_5 band given in Ref. (3) should lead to an improved set of Coriolis parameters.

The parameters in Tables 3-2 and 3-4 were used to calculate the vibration-rotation frequencies of the ν_2 band and the rotational frequencies in the $v_2 = 1$ state for $J \leq 50$ and $K \leq 15$ for an attempt to assign the submillimeter laser transitions reported in Ref. (27). It was possible to give a definite assignment for two of the transitions and a provisional assignment for a third. The two assigned transitions are pumped by the 10P(38) CO_2 laser at 27851242 MHz (reported at 10.764 μm in Ref. (27)). This laser frequency is only 8 MHz above the calculated frequency of the P(46,10) transition in the ν_2 band. In addition, the two reported submillimeter wave frequencies (538347.3 MHz and 526434.4 MHz) are only 0.9 and 2.7 MHz above the calculated values for the R(44,10) and R(43,10) transitions in the $v_2 = 1$ state, respectively. Since these calculated values should be within a few MHz of the experimental frequencies, these assignments are probably definite. The provisional assignment involves a submillimeter wave laser pumped by the 10P(36) CO_2 at 27791010 MHz (reported as 10.787 μm in Ref. (27)). This frequency is ~426 MHz below the calculated frequency of the P(49,13) transition in the ν_2 band. The reported submillimeter wave frequency is 572772.1 MHz, which is ~19 MHz below the calculated value for the R(48,13) transition in $v_2 = 1$. This agreement is probably satisfactory considering the fact that the J and K values for the transitions is outside the range of J and K for which the parameters are known to be valid. For this reason and because of the

strange behavior of the levels in $v_2 = 1$ for $k > 10$, this last assignment must be viewed as provisional.

The ground state vibration rotation parameters obtained as a result of this study are compared to the values obtained by microwave and millimeter wave spectroscopy in Table 3-2, where it may be seen that there is good agreement between the results of our fittings and that obtained previously (13). Comparison in Table 3-3 of the parameters derived in this work with the best previous infrared values, obtained from a laser Stark study of a relatively small number of transitions, shows that a much more complete set of centrifugal distortion constants has been obtained in the present study. As mentioned above, the inclusion of the effects of Coriolis coupling to the ν_5 and $2\nu_3$ states improves the fit of the rotation and vibration-rotation frequencies; the standard deviation for an observation of unit weight is reduced from 1.5 to 0.75. The resulting parameters are compared to the results given by Matsuura and Shimanouchi (2) in Table 3-4, where it is seen that the agreement is very good considering the small number of experimental frequencies for the ν_2 band that were available to these authors. The Corilis effects on the energy are substantial for this molecule, reaching almost 30 GHz for the highest J and K studied in this work. Therefore, the calculated vibration-rotation frequencies are very sensitive to the values assumed for the Coriolis and vibration-rotation constants. It is essential that the two sets of parameters be consistent. The parameters in Table 3-3 do not include the effects of the Coriolis coupling discussed in this paper. Comparison of the B values for $v_2 = 1$ in Tables 3-3 and 3-4, for example, show the large

contribution of this Coriolis coupling to the rotational constants.

III-5-2 CD_3Br

A substantial number of frequencies in the ν_2 bands of $CD_3{}^{79}Br$ and $CD_3{}^{81}Br$ have been measured to an accuracy of a few MHz by the method of infrared-microwave sideband laser spectroscopy and have been used to evaluate vibration-rotation parameters for the ground and $v_2 = 1$ states for both species. The new parameters together with previously-reported vibration-rotation constants for $v_5 = 1$ and the ν_2-ν_5 Coriolis coupling are sufficiently accurate to reproduce the experimental frequencies for $J \leq 48$ and $K \leq 8$ to within ~ 5 MHz. The parameters have been used to predict coincidences between CO_2 and N_2O laser frequencies (34,37) and the frequencies of the ν_2 bands of both species of CD_3Br. The predicted coincidences are shown in Tables 3-10 and 3-11.

The frequencies of a number of transitions for $K > 8$ have been omitted from the fittings and, as can be seen in Tables 3-6 and 3-7, these show rather large residuals. We interpret this to be the result of some problem with the accuracy of the Coriolis parameters and/or the parameters for the $v_5 = 1$ state used in the fitting. Since the Coriolis corrections are very large, relatively small changes in these parameters, perhaps even within the round-off errors, would be sufficient to cause the difficulties observed. Since we do not have any data of our own for the ν_5 band, we did not pursue this problem any further.

III-6 References

1. E. W. Jones, R. L. Popplewell, and H. W. Thompson, Proc. Roy. Soc. London **A288**, 39-49 (1965).

2. H. Matsuura and T. Shimanouchi, J. Mol. Spectrosc. **60**, 93-110 (1976).

3. K. Kawaguchi, C. Yamada, T. Tanaka, and E. Hirota, J. Mol. Spectrosc. **64**, 125-138 (1977).

4. Y. Morino and J. Nakamura, Bull. Chem. Soc. Japan **38**, 443-458 (1965).

5. E. W. Jones, R. J. L. Popplewell, and H. W. Thompson, Spectrochim. Acta **22**, 639-646 (1966).

6. C. Betrencourt-Stirnemann, R. Paso, J. Kauppinen, and R. Anttila, J. Mol. Spectrosc. **87**, 506-521 (1981).

7. K. Harada, K. Tanaka, and T. Tanaka, J. Mol. Spectrosc. **98**, 349-374 (1983).

8. J. W. Simmons, Phys. Rev. **76**, 686 (1949).

9. J. W. Simmons and J. H. Goldstein, J. Chem. Phys. **20**, 122-124 (1952).

10. A. K. Garrison, J. W. Simmons, and C. Alexander, J. Chem. Phys. **45**, 413-415 (1966).

11. R. L. Kuczkowski, J. Mol. Spectrosc. **45**, 261-270 (1973).

12. J. Demaison, D. Boucher, G. Piau, and P. Glorieux, J. Mol. Spectrosc. **107**, 108-118 (1984).

13. G. Wlodarczak, D. Boucher, R. Bocquet, and J. Demaison, J. Mol. Spectrosc. **124**, 53-65 (1987).

14. Y. Morino and L. Nakamura, Bull. Chem. Soc. Jap. **38**, 443-459 (1965).

15. C. Joffrin, N. Van Thanh, and P. Bardewitz, J. Phys. Paris **27**, 15-23 (1966).

16. R. W. Peterson and T. H. Edwards, J. Mol. Spectrosc. **38**, 1-15 (1971).

17. H. Kurlat, M. Kurlat, and W. E. Blass, J. Mol. Spectrosc. **38**, 197-213 (1971).

18. D. R. Anderson and J. Overend, Spectrochim. Acta. **A28**, 1231-1251

(1972).

19. D. R. Anderson and J. Overend, Spectrochim. Acta. **A28**, 1637-1647 (1972).

20. C. Poulsen and S. Brodersen, J. Raman Spectrosc. **14**, 77-82 (1983).

21. J. Sakai and M. Katayama, Chem. Phys. Lett. **35**, 395-398 (1975).

22. J. Sakai and M. Katayama, Appl. Phys. Lett. **28**, 119-121 (1975).

23. G. L. Caldow, G. Duxbury, and L. A. Evans, J. Mol. Spectrosc. **69**, 239-253 (1978).

24. S. A. Rackley and R. J. Butcher, Mol. Phys. **39**, 1265-1272 (1980).

25. Y. Langsam, S. M. Lee and A. M. Ronn, Chem. Phys. **15**, 43-48 (1976).

26. W. Schrepp and H. Dreizler, Z. Naturforsch. **36a**, 654-661 (1981).

27. S. F. Dyubko, L. D. Fesenko, O. I. Baskakov, and V. A. Svich, Zhurnal Prikladnoi Spektroskopii **23**, 317-320 (1975).

28. T. H. Edwards and S. Brodersen, J. Mol. Spectrosc. **54**, 121-131 (1975).

29. Y. Morino and C. Hirose, J. Mol. Spectrosc. **24**, 204-224 (1967).

30. H. P. Benz, A. Bauder, and Hs. H. Gunthard, J. Mol. Spectrosc. **21**, 156-164 (1966).

31. J. T. Hougen, J. Chem. Phys. **57**, 4207-4217 (1972).

32. M. R. Aliev and J. T. Hougen, J. Mol. Spectrosc. **106**, 110-123 (1984).

33. C. H. Townes and A. L. Schawlow, "Microwave Spectroscopy," Chap. 8, McGraw-Hill, New York, 1955.

34. C. Freed, L. C. Bradley,and R. G. O'Donnell, IEEE J. Quantum Electron. **QE-16**, 1195-1206 (1980).

35. H.-G. Cho and R. H. Schwendeman, J. Mol. Spectrosc. **133**, 383-405 (1989).

36. G. Magerl, W. Schupita, and E. Bonek, IEEE J. Quantum Electron. **QE-18**, 1214-1220 (1982).

37. S. K. Lee, R. H. Schwendeman, and G. Magerl, J. Mol. Spectrosc. **117**, 416-434 (1986).

38. B. G. Whitford, K. J. Siemsen, H. D. Riccius, and G. R. Hanes, Opt. Commun. **14**, 70-74 (1975).

CHAPTER IV

INFRARED-RADIOFREQUENCY DOUBLE RESONANCE OF CD_3I AND CD_3Br

IV-1 Introduction

The radiofrequency spectroscopy provides a powerful tool for investigation of various hyperfine energy structures such as nuclear quadrupole splittings, A_1-A_2 splittings, λ-doubling, K-doubling, hyperfine rotational levels of tetrahedral molecules, and so on. However, the scope of the technique is seriously limited by the density of the spectrum, the poor signal-to-noise ratio caused by the negligible population difference, and the low photon energy due to the small energy gap between the levels. As a result, radiofrequency spectra are often too weak to record properly or too complicated to analyze. In order to overcome the limitations, the radiofrequency double resonance technique has been invented which is a combination with another radiation of much higher energy photons. By detecting a photon with much higher energy than the radiofrequency photon, sensitivity and signal-to-noise ratio are greatly enhanced; and, by requiring two near-resonant photons for signal detection, the spectra are greatly simplified.

The radiofrequency-microwave (RF-MW) double-resonance method was introduced by Autler and Townes (1). In their experiment, ℓ-type doublets in the J=1 and 2 rotational levels of the v_2=1 vibrational

state of OCS were probed while the corresponding rotational transition J=1→2 was pumped by microwave radiation. The RF-MW double resonance technique was further developed by Wodarczyk and Wilson (2) for assignment purposes in microwave spectroscopy. When the RF double resonance method was later extended to the infrared region (IR-RF double resonance), it became possible to observe RF resonances for higher rotational quantum numbers and higher-energy vibrational states than had been possible with RF-MW spectra.

Infrared-radiofrequency (IR-RF) double resonance was first used by Shimizu to observe the Stark splittings of the P(3,2) transition of the ν_2 excited state of PH_3 by pumping the transition with the R(33) N_2O laser line (3). This technique was further developed and applied to various studies, mostly by workers at the Herzberg Institute of Astrophysics. Curl and his coworkers studied hyperfine rotational energy structures of CH_4 by means of the laser coincidence of the ν_3 band and He-Ne 3.39 μm laser line and intracavity radiofrequency cells (4,5). The IR-RF double resonance technique is sensitive enough that they succeeded in observing two rotational transitions weakly allowed by the centrifugally induced electric dipole moment. Later, the 9P(36) $C^{18}O_2$ laser line was used for the investigation of the rotational energy levels of CD_4 by Kreiner (6). Kreiner and Oka extended this technique to observe forbidden rotational transitions of SiH_4 with P(5), R(4), and R(6) N_2O laser lines (7). Arimondo and his coworkers applied the technique to the observation of pure quadrupole transitions in CD_3I by using CO_2 and N_2O laser coincidences (8) and later analyzed energy transfer between rotational levels by means of collision-induced resonances in the radiofrequency region (9). Dale et al. and Lowe et al

used their CO laser to study Λ-doublings of NO utilizing the close coincidences of ν_1 band transitions of NO in the 5.4 μm region (10,11). They also applied the spectrometer to investigation of the spin-rotation hyperfine structure of NO_2 (12) and of the Stark effect of H_2O (13). Recently Sakai and his coworkers observed A_1-A_2 splittings in the ground state (K=3) and ν_5 state (Kℓ=-2) of CDF_3 by pumping the ν_5 band with a CO_2 laser (14). Mito et al. employed the coincidence of P(8,0) transition of ν_7 band of CH_3CN and 9P(30) CO_2 laser line to search for ℓ-type doubling transitions including collisionally transferred resonances and determined the effective ℓ-type doubling constants q_7 and q_7' (15). Ioli and his coworkers performed radiofrequency triple resonance for CH_3OH in order to study the K-doubling (16). Some ℓ-type doublets of the ν_6 state of CH_3I were observed by Arimondo and P. Glorieux (17). Man and Butcher studied pure quadrupole transitions (18-20) of halide compounds and K-doublings (21) of formic acid by means of CO_2 laser coincidences. Their precise experiment allowed determination of quadrupole coupling constants including the centrifugal distortion parameters and the spin-rotation constants.

The early IR-RF double-resonance measurements were performed with the sample cell inside the laser cavity in order to apply the highest available powers to the samples. As a result, the line broadening caused by the power of the pump laser seriously restricted the accuracy of the frequency measurement. Among the first demonstration of IR-RF double resonance outside the laser cavity were studies of CF_3I and CF_3Br in our laboratory (22,23). The lower pumping power still provides sufficient signal-to-noise ratio and many nuclear hyperfine structures are well resolved as a result of the considerably smaller linewidth.

Line-tunable infrared lasers provide accurate frequency and enough radiant power for saturating vibrational transitions; however, they restrict the method to accidental coincidences between the laser frequencies and the vibration-rotation frequencies of the molecule under study; this severely limits the performance of the technique. More recently, it has been shown that tunable infrared sources could be used for IR-RF double resonance. Takami introduced IR-RF double resonance by means of diode lasers in studying forbidden rotational transitions of v_3=1 state of CF_4 (24). The diode laser was intentionally focused inside the coaxial radiofrequency cell used in the experiment in order to overcome the low radiant power of the laser. In a series of works, he and his coworkers investigated the hyperfine rotational energy structure of CF_4 (25), $^{13}CF_4$ (26), SiH_4 (27,28), and SnH_4 (29) and determined the rotational parameters. The infrared-microwave sideband laser was first used by Oka to observe forbidden rotational transitions of OsO_4 (30) and SiH_4 (31). A color center laser was used to observe ℓ-type doubling in HCN by DeLeon et al. (32). Oka also employed a color center laser to search for A_1-A_2 splittings of CH_3F (33).

In recent studies, we discovered that our infrared microwave sideband laser system operating in the cavity mode (34) had sufficient power to saturate vibration-rotation transitions. In this thesis we describe the use of our infrared-microwave sideband laser for the measurement of pure nuclear quadrupole transitions in the ground and v_2=1 vibrational states of CD_3I and CD_3Br by the method of IR-RF double resonance. Before carrying out the double resonance measurements, it was necessary to determine the frequencies of the infrared transitions in the ν_2 vibrational bands of these molecules. Frequencies of

transitions with J,K up to higher than 40,8 were measured and fit to energy expressions for symmetric top molecules with centrifugal distortion. The measured IR frequencies and spectroscopic analyses have been described in Chapter III. The tunability of the infrared-microwave-sideband laser source allows the selection of vibration-rotation transitions over a wide range of J and k, which permits the evaluation of centrifugal distortion effects on the quadrupole coupling constants and spin-rotation interaction parameters, as well as the precise measurement of the quadrupole coupling constant itself. In addition to the advantages of tunability, the spectrometer is found to have sufficient sensitivity to work at very low RF power, which together with the very low power of the infrared-microwave sideband laser source substantially increases the resolution compared to direct CO_2 laser-pumped double resonance. As a result, it is possible to determine the spin rotation constants as well as the centrifugal distortion constants for the quadrupole coupling in these molecules.

IV-1-1 CD_3I

In a series of microwave studies of the ground vibrational state of CD_3I Simmons and co-workers (35-37) resolved quadrupole components and determed the primary quadrupole coupling constant as well as rotational constants. Kuczkowski (38) extended this microwave work to transitions in the low-lying vibrational states ν_2, ν_3, ν_5, ν_6, $2\nu_3$, and $\nu_3+\nu_6$. More recently, higher J transitions have been recorded in the millimeter wave region and more accurate quadrupole constants were reported for low-lying vibrational states by Demaison et al. (39) and by

Wlodarczak et al. (40). Infrared radio frequency double resonance at 1-MHz resolution was reported by Rackley and Butcher (41) as part of a study of Stark-tuned non-linear spectroscopy. Demaison et al. (39) used infrared radio frequency double resonance to measure the frequencies of pure quadrupole transitions in the ground state of this molecule with 100 kHz accuracy. The influence of nuclear quadrupole coupling on rotational relaxation has been investigated by means of microwave double resonance (42).

In the present study, about 150 radio frequency resonances, half each in the ground and $v_2 = 1$ states, have been recorded at 70 kHz resolution and few kHz accuracy by using the infrared microwave sideband system as a pumping source for infrared radio frequency double resonance. In addition to demonstrating the usefulness of this technique for systematic infrared radio frequency double resonance, the radio frequencies have been combined with previous measurements of microwave, millimeter wave, and infrared radio frequency double resonance spectra to determine nuclear quadrupole coupling parameters, including centrifugal distortion effects, and spin rotation parameters for the iodine nucleus.

IV-1-2 CD_3Br

The splittings caused by Br quadrupole coupling in $CD_3{}^{79}Br$ and $CD_3{}^{81}Br$ have been studied in the microwave region for the ground state by Garrison et al. (43) and in low-lying vibrational states by Morino and Hirose (44). Consequently, values of the quadrupole coupling constants for the ground and $v_2 = 1$ states of the two species have been

reported. However, we are not aware of any previous measurements that are sufficiently precise to include the effects of the centrifugal distortion of the quadrupole coupling or of the spin-rotation interaction.

An infrared microwave sideband laser source operating in the 10 μm region has been used with the method of infrared radiofrequency double resonance to record radiofrequency spectra in the ground and $v_2 = 1$ vibrational states of CD_3Br. The frequencies of ~ 200 and ~ 160 pure quadrupole transitions have been observed for $CD_3{}^{79}Br$ and $CD_3{}^{81}Br$, respectively, approximately half in the ground state and half in the $v_2 = 1$ vibrational state of each species. The frequencies have been used to determine the quadrupole coupling constants, including centrifugal distortion parameters, and spin-rotation constants for the bromine nucleus in each species.

During the fitting of the frequencies of the pure quadrupole spectra, it became apparent that some effect was causing an apparent shift in frequency for each of a pair of closely spaced double resonance transitions that occur at low RF frequencies. This shift has been traced to a double-resonance effect that appears in calculations when four interacting levels are taken into account, but is not evident in calculations based on the usual three-level system employed for double-resonance theory. The nature of the shifts, a description of the theory used to interpret them, and a comparison of observed and calculated lineshapes is described separately in Chapter V.

The theory of vibration-rotation-quadrupole interaction is outlined in the next section, whereas the experimental details of this study are presented in the subsequent section. The last two sections

include a description of the spectra and a discussion of the results of this work, respectively.

IV-2 Theory

IV-2-1 IR-RF Double Resonance

The mechanism of IR-RF double resonance is easily understood by considering a three-level system excited by laser and radiofrequency fields. We assume that two levels in the excited state form the hyperfine structure and that the laser frequency is much larger than kT/h. An example of a three-level system is shown in Fig. 4-1, where state $|1\rangle$ is a rotational level in the ground vibrational state and states $|2\rangle$ and $|3\rangle$ are rotational levels in an excited vibrational state. The laser radiation will interact with a group of molecules with velocity v, which satisfies the Doppler shifted resonance condition $\nu_{12} = \nu_{IR}(1-v/c)$. If the infrared radiation is strong and the gas pressure low, molecules with the correct velocity will be "pumped" from state $|1\rangle$ to $|2\rangle$. This occurs when the infrared Rabi frequency, $x_{Rabi(IR)} = \mu_{12}E_{IR}/h$, is comparable to or larger than the collisional frequency, $\nu_{collision} = (\Delta\nu)_p \cdot p$. Here μ_{12} is the transition dipole moment matrix element, E_{IR} is the laser electric field, $(\Delta\nu)_p$ is the pressure broadening parameter, and p is the gas pressure.

Due to the pumping, "holes" are burned in the Maxwellian velocity profile of state $|1\rangle$ and transferred to state $|2\rangle$ as "spikes." When the radiofrequency radiation with sufficient power for saturation comes into resonance with the transition between levels, the "spikes" in level $|2\rangle$ are transferred to level $|3\rangle$. This causes an increase in infrared absorption and is detected as a decrease in the infrared radiation reaching the detector. The condition for saturation by the

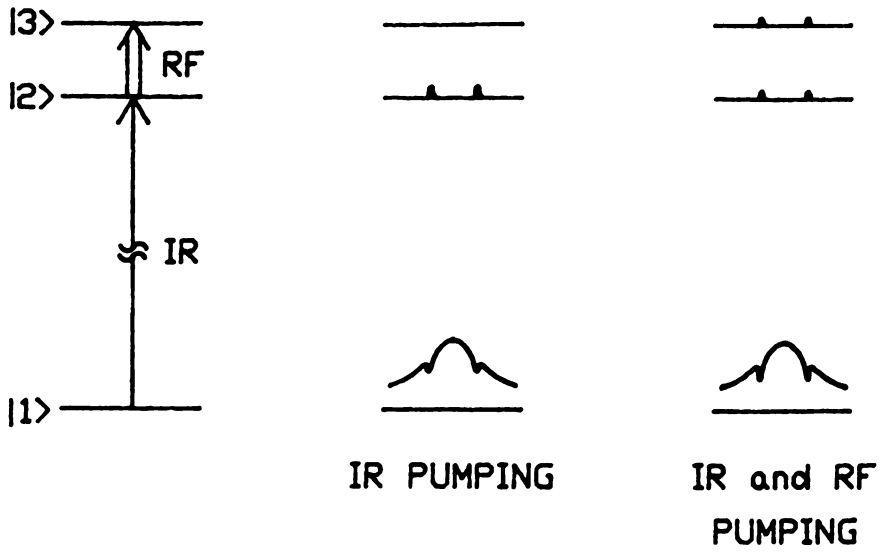

Figure 4-1. Three level system showing double resonance technique. The infrared radiation pumps molecules from |1> to |2> according to the Doppler shift resonance condition $\nu_{12} = \nu_{IR}(1 \pm v/c)$ which appears as "holes" in the Maxwellian velocity profile of |1> and "spikes" in |2>. The radiofrequency will then transfer the "spikes" from |2> to |3> creating deeper "holes" in |1>. This causes an increase in the molecular absorption. The radiofrequency transition from |2> to |3> can thus be observed by detecting the infrared radiation.

radiofrequency is that its Rabi frequency, $x_{Rabi(RF)} = \mu_{23} \cdot E_{RF}/h$, needs to be comparable to or larger than the collisional frequency, where μ_{23} is the transition dipole moment matrix element in the excited state, and E_{RF} is the radiofrequency electric field.

In terms of the absorption coefficient, the maximum value is obtained when the saturation parameter $\mu E/h\nu_{collision} \approx 1$ (3). According to Shimizu, the maximum attainable rf-induced absorption coefficient in this technique is 13% of the linear absorption coefficient for a Doppler-limited three-level system (3). The linewidth increases with increasing field intensities. The best operating condition is usually obtained when the saturation parameters of both fields are around one. In case the saturation parameter of the rf field is larger than that of the laser, the resonance line splits into a doublet.

IV-2-2 Nuclear Quadrupole Coupling

Atomic nuclei have radii near 10^{-12} cm, and hence are very small compared with the size of electron orbits, which are approximately 10^{-8} cm in diameter. Nuclei are also some 10^4 times heavier than electrons. To a good approximation, therefore, electronic energies can be obtained by considering nuclei to be positive point charges of infinite mass. However, effects on electronic energy levels due to the finite size and mass of nuclei, although small, often appear on observation of atomic and molecular spectra. These effects are called "hyperfine structure" because they produce a very small splitting of spectral lines.

If a nucleus is to be considered other than a point charge, it must be recognized that the nuclear particles may be in motion, producing a magnetic field and giving the nucleus an angular momentum. The interaction energy between a nuclear charge distribution $\rho_i(x_i, y_i, z_i)$ and an electron charge distribution $\rho_e(x_e,y_e,z_e)$ is

$$W = \int \frac{\rho_i \rho_e \, d\underset{\sim}{r}_i d\underset{\sim}{r}_e}{R} \qquad (4\text{-}1)$$

where

$$R = (r_i^2+r_e^2-2r_i r_e \cos\omega)^{1/2} .$$

Here, $\underset{\sim}{r}_i$=vector from the origin of the coordinates of the nuclear center of mass to the volume element $d\underset{\sim}{r}_i$, $\underset{\sim}{r}_e$ the vector from the origin to the volume element $d\underset{\sim}{r}_e$ and ω the angle between $\underset{\sim}{r}_i$ and $\underset{\sim}{r}_e$.

Only s electrons have non-negligible charge distribution inside the nucleus. However, the contribution of s electrons to the quadrupole coupling energy vanishes because of the spherical symmetry of the electron orbital. We therefore expand 1/R in powers of r_i/r_e to obtain

$$\frac{1}{R} = \frac{1}{r_e} \sum_{\ell=0}^{\infty} \left(\frac{r_i}{r_e}\right)^{\ell} P_{\ell}(\cos\omega) . \qquad (4\text{-}2)$$

Where $P_{\ell}(\cos\omega)$ is the Legendre polynomial of order ℓ. It is convenient to use the spherical harmonic addition theorem in the form,

$$P_{\ell}(\cos\omega) = \sum_{m=-\ell}^{\ell} (-1)^{m} \left(\frac{4\pi}{2\ell+1}\right) Y_{\ell m}(\theta_{\ell}, \phi_{\ell}) Y_{\ell,-m}(\theta_i, \phi_i) \ . \qquad (4\text{-}3)$$

Substitution of Eq. (4-2) in Eq. (4-1) gives W as a series of integrals, as follows:

$$W = W_0 + W_1 + W_2 + \ldots . \qquad \text{for } \ell = 0, 1, 2, \ldots . \qquad (4\text{-}4)$$

Then,

$$W_o = \iint \frac{\rho_i \rho_e}{r_e} d\underset{\sim}{r}_i d\underset{\sim}{r}_e = Ze \int \frac{\rho_e}{r_e} dr_e \qquad (4\text{-}5)$$

where Z = atomic number. This is the Coulomb interaction between the nucleus and the electrons, which is independent of the nuclear orientation and would be included in the determination of the electronic energy.

The second term in the series of W is

$$W_1 = \iint \frac{r_i}{r_e^2} \cos\omega \ \rho_i \rho_e d\underset{\sim}{r}_i d\underset{\sim}{r}_e$$

$$= \int \frac{\rho_e \underset{\sim}{r}_e}{r_e^3} \left[\int \rho_i \underset{\sim}{r}_i d\underset{\sim}{r}_i\right] d\underset{\sim}{r}_e \ . \qquad (4\text{-}6)$$

The quantity in square bracket is the nuclear electric dipole moment; hence W_1 is the nuclear dipole interaction energy. However, if the

nucleus has a dipole moment in one direction with respect to its angular momentum, there must be a degenerate nuclear state, or one of the same energy, with an oppositely directed dipole. Normally, such identical or degenerate states of the nucleus are not encountered. Hence the nucleus has no inherent dipole moment, and no effects from nuclear dipole moments have been observed, so that we can assume that this term vanishes. The rule is rather more general as all electronic multipole moments of odd order are zero for a nucleus.

The third term in the series for W is the quadrupole interaction,

$$H_Q = W = \iint \frac{r_i^2}{r_e^3} \rho_e \rho_i P_2(\cos\omega)\, d\underset{\sim}{r}_e d\underset{\sim}{r}_i$$

$$= \sum_{m=-2}^{+2} (-1)^m \left(\frac{4\pi}{5}\right) \int \rho_i r_i^2\, Y_{2,-m}(\theta_i,\phi_i) d\underset{\sim}{r}_i \int \frac{\rho_e}{r_e^3}\, Y_{2,m}(\theta_e,\phi_e) d\underset{\sim}{r}_e \quad (4\text{-}7)$$

or $$H_Q = \sum_{m=-2}^{+2} (-1)^m V_m Q_{-m}$$

where $$V_m = \left(\frac{4\pi}{5}\right)^{1/2} \int \frac{\rho_e}{r_e^3}\, Y_{2,m}(\theta_e,\phi_i)\, d\underset{\sim}{r}_i$$

$$Q_{-m} = \left(\frac{4\pi}{5}\right)^{1/2} \int \rho_i r_i^2\, Y_{2,-m}(\theta_i,\phi_i)\, d\underset{\sim}{r}_i \,.$$

V_m and Q_{-m} are components of second-rank irreducible spherical tensors since they are integrals of a spherical factor ($\sim r^n$) times a spherical harmonic (ref. (45), P. 115). They are characterized by $\underset{\sim}{I}$ in the nuclear space and $\underset{\sim}{J}$ in the molecular space.

The quadrupole moment may be considered as a measure of the

deviation of the nuclear charge from the spherical shape. If the charge distribution is somewhat elongated along the nuclear axis z_n, then Q is positive; if it is flattened along the nuclear axis, Q is negative.

IV-2-3 Irreducible Tensor Method

If the interaction energy of two parts of any quantum mechanical system is invariant under arbitrary rotations of the space-fixed axes, then it can be written most generally as a contraction of two irreducible tensors (45). Usually, the system may be divided into two distinct parts, characterized by their angular momenta J_1 and J_2, so that one tensor depends exclusively on one set of variables and the other tensor on a set of variables in a different space. The matrix elements of such a contraction of two commuting irreducible tensors A and B of rank K are given in the irreducible representation where the angular momenta of the two parts are coupled to form the resultant $J=J_1+J_2$ as

$$\langle J_1, J_2, J, M|A:B|J_1', J_2', J', M'\rangle$$

$$=(-1)^{J_2+J_1'+J}\delta_{JJ'}\delta_{MM'}\begin{Bmatrix} J & J_2 & J_1 \\ k & J_1' & J_2' \end{Bmatrix}\langle J_1||A||J_1'\rangle\langle J_2||B||J_2'\rangle \quad . \qquad (4\text{-}8)$$

The symbol in curly brackets is the Wigner 6j symbol. Eq.(4-8) expresses the fact that each matrix element is proportional to constants $(J_1||A||J_1')$ and $(J_2||B||J_2')$ called reduced matrix elements which may be determined by using the Wigner-Eckart theorem, as follows;

$$\langle j,m|T_q^{(i)}|j',m'\rangle=(-1)^{j-m}\begin{pmatrix} j & k & j' \\ -m & q & m' \end{pmatrix}\langle j||T^{(i)}||j'\rangle \ . \qquad (4\text{-}9)$$

If any one of the matrix elements of an irreducible set of spherical tensors $T_q^{(i)}$ of rank i is known in the representation with the angular momentum quantum number j and the projection quantum number m, the remaining elements can be determined. The symbol in parenthesis is the Wigner 3j symbol, which contains the entire dependence of the matrix elements on the projection quantum number.

The relation of a quantity, which refers to only one of the interacting systems, between its reduced matrix element in the coupled representation and in the original uncoupled representation is expressed as

$$\langle J_1,J_2,J||T^{(i)}||J_1',J_2,J'\rangle = (-1)^{J_1+J_2+J'+i} \cdot[(2J+1)(2J'+1)]^{1/2}\begin{Bmatrix} J_1 & J & J_2 \\ J' & J_1' & i \end{Bmatrix}\langle J_1||T^{(i)}||J_1'\rangle \qquad (4\text{-}10)$$

where the tensor operator $T^{(i)}$ acts only in the J_1 space. It is therefore possible to calculate the matrix elements of any observable in the coupled representation using Eq. (4-9) and (4-10).

IV-2-4 Quadrupole Interaction Energy

As shown above, the quadrupole interaction energy can be expressed as a contraction of two irreducible tensors of rank 2: the electric field gradient tensor V and the nuclear quadrupole moment tensor Q.

$$H_Q = \sum_{-2}^{2} (-1)^m V_m Q_{-m} \quad . \tag{4-7}$$

The quantity Q_{-m} is the -m component of the nuclear quadrupole tensor, $\underset{\sim}{Q}$. The nuclear quadrupole moment, Q, is defined conventionally to be the I, m_I=i diagonal matrix element of the m=0 component of $\underset{\sim}{Q}$ i.e.;

$$eQ = 2\langle II|Qo|II\rangle \tag{4-11}$$

where e is the electric charge. The matrix elements of H_Q in the coupled representation F = J+I are given according to Eq. (4-8). It turns out that H_Q may be factorized into blocks for the different quantum numbers of the total angular momentum F and is independent of the projection quantum number M_F. From the Wigner-Eckart theorem

$$\langle II|Q_o|II\rangle = \begin{pmatrix} I & I & 2 \\ I & -I & 0 \end{pmatrix} \langle I||Q||I\rangle$$

or

$$\langle I||Q||I\rangle = \frac{[(2I+3)(2I+2)(2I+1)(2I)(2I-1)]^{1/2}}{2[3I^2-I(I+1)]} \frac{eQ}{2} \quad . \tag{4-12}$$

The symbol in parenthesis is the Wigner 3j symbol, and $\langle I||Q||I\rangle$ called the reduced matrix elements.

The electric field gradient tensor V has constant components V'_q in the molecular frame. Hence it is necessary to transform one component of V to the principal inertial axes

$$V_0 = \sum_{q=-2}^{2} D^{(2)}_{0q}(\alpha,\beta,\gamma)V'_{-q}, \qquad (4\text{-}13)$$

where $D^{(2)}_{0q}(\alpha,\beta,\gamma)$ is a matrix element of the five-dimensional irreducible representation of the three-dimensional rotation group, which depends on the Eulerian angles α, β, γ locating the molecular frame in the space-fixed axes system. The matrix elements of $D^{(2)}_{0q}$ in the symmetric rotor basis $\psi^{(J)}_{MK}(\alpha,\beta,\gamma) \propto (2J+1)^{1/2}D^{(J)}_{MK}(\alpha,\beta,\gamma)$ are given as

$$\langle J,k,m|D^{(2)}_{0q}|j',k',m\rangle = (-1)^{m+k+q}\,[(2J+1)(2J'+1)]^{1/2} \cdot \begin{pmatrix} J & 2 & J' \\ -m & 0 & m \end{pmatrix} \begin{pmatrix} J & 2 & J' \\ -k & -q & k' \end{pmatrix} \qquad (4\text{-}14)$$

using k for the projection quantum number in the molecular frame and m for the same in the space-fixed system. Then, the reduced matrix element of the V tensor is calculated with the aid of Eqs. (4-10), (4-13), and (4-14) to yield

$$\langle J,k||V||J',k'\rangle = (-1)^{J+k}[(2J+1)(2J'+1)]^{1/2} \begin{pmatrix} J & 2 & J' \\ -k & -q & k' \end{pmatrix} V'_{-q}/2\,. \qquad (4\text{-}15)$$

The matrix elements of the quadrupole Hamiltonian can be expressed in the specified representation by introducing the reduced matrix elements (4-12) and (4-15) into Eq. (4-8) for each F block

$$\langle J,k,I,F|H_Q|J',k',I,F\rangle = (-1)^{J+J'+k+I+F+1}$$

$$\cdot[(2J+1)(2J'+1)]^{1/2} \begin{Bmatrix} F & I & J \\ 2 & J' & I \end{Bmatrix} \frac{\begin{pmatrix} J & 2 & J' \\ -k & -q & k' \end{pmatrix}}{\begin{pmatrix} I & 2 & I \\ -I & 0 & I \end{pmatrix}} \chi_{-q}/4 \qquad (4\text{-}16)$$

with the abbreviation $\chi_q = eQV'_q$ for the quadrupole coupling tensor. The irreducible quadrupole coupling tensor may also be expressed in the Cartesian axes

$$\begin{aligned} \chi_0 &= \chi_{zz}, \\ \chi_{\pm 1} &= \mp(2/3)^{1/2}(\chi_{xz} \pm i\chi_{yz}), \\ \chi_{\pm 2} &= (1/6)^{1/2}(\chi_{xx} - \chi_{yy} \pm 2i\chi_{xy}). \end{aligned} \qquad (4\text{-}17)$$

The explicit expressions for the matrix elements of the quadrupole interaction have been derived by Benz et al. (46). The matrix elements used in this study are listed in the Appendix of this chapter.

IV-2-5 Quadrupole Coupling of CD_3I and CD_3Br

The interaction between a nuclear quadrupole and an electric field gradient splits the rotational level into 2I+1 hyperfine levels if $J \geq I$, where I is the nuclear spin number. The complete Hamiltonian for quadrupole interaction includes the rotation of the molecules since J is no longer a good quantum number. Especially the quadrupole couplings of Iodine ($eqQ[CD_3I]$ = ~-1930 MHz) and Bromine ($eqQ[CD_3Br^{79}]$ = ~576 MHz, $eqQ[CD_3Br^{81}]$ = ~481 MHz) are large enough that calculation to the accuracy of 1 kHz requires inclusion of the effect of centrifugal

distortion on the quadrupole interaction and the spin-rotation interaction and diagonalization of the appropriate energy matrices. The method used to calculate the quadrupole interaction energy has been described in Chapter III in the discussion of the effect on the vibration-rotation energies of the molecules. As mentioned, the matrix H, as defined, is diagonal in F, I, and k; therefore, submatrices indexed by the possible J's (usually 6x6 for CD_3I and 4x4 for CD_3Br) were set up and diagonalized to obtain the energy levels; the eigenvalues were indexed by the J value of the closest diagonal element.

For CD_3I, all of the microwave(35-40) and radio frequency data for the ground vibrational state(39) were combined and used in a least squares adjustment of the rotational, centrifugal distortion, quadrupole coupling, distortion quadrupole, and spin rotation constants for the ground state (21 parameters). In this calculation the unresolved microwave data were included, but were assumed to have no quadrupole or spin rotation contribution. In the corresponding fitting for the $v_2 = 1$ state the centrifugal distortion constants and the rotational constants, except the B value, were constrained to the values obtained from the fitting of the vibration-rotation spectra because only a small number of rotational frequencies in the $v_2 = 1$ state have been measured.

For CD_3Br, the least squares fitting was performed by adjusting only the six quadrupole and spin-rotation parameters eqQ, χ_J, χ_K, χ_D, C_N, and C_K; the vibration-rotation parameters were constrained to the values determined in the analysis of the infrared spectra (Chapter III). This was done because of a limited number of reported microwave frequencies. The experimental data for the fitting included the previously-reported microwave frequencies (43,44), in addition to all of

the measured IR-RF double resonance spectra. The calculated frequencies of the IR-RF double-resonance spectra were obtained from the computed energy levels by using the selection rules $\Delta J = 0$, $\Delta k = 0$, and $\Delta F = \pm 1$.

IV-3 Experimental

Fig. 4-2 is a block diagram of the infrared radiofrequency double resonance spectrometer used in the present study. The infrared microwave sidebands are generated in a CdTe electrooptic crystal that is irradiated simultaneously with the output of a frequency-controlled CO_2 laser and the output of a 20-W traveling wave tube amplifier. For IR-RF double resonance, the sideband generator was operated in the "cavity mode" (34), in which the electrooptic crystal is made part of a tunable microwave cavity. In order to provide a cavity resonance, a tunable short was used which is adjustable anywhere in the 8-18 GHz range. In this mode the sideband output was ~1 mW per W of infrared power. Since we normally used 2 W of CO_2 laser power, the typical sideband power was 2 mW, which is sufficient to saturate partially an infrared transition in the molecules. In order to maintain highest power, the beam splitter and reference detector used in traveling mode operation (34), are not employed in the cavity mode of operation. Also, the PIN diode is set for maximum transmission. The sidebands were directed through a radiofrequency cell which is made of a 1-meter piece of X-band waveguide with a centered septum in a stripline design (47). The RF cell was matched to a 50 Ω transmission line impedance and has BaF_2 windows. The infrared power was detected by a liquid-N_2 cooled Hg-Cd-Te photoconductive detector (Santa Barbara Research Center Model 40742), whose signal was processed at the modulation frequency by means of a lock-in amplifier and recorded by a computer. The frequency of the infrared source was set at the center frequency of the Doppler-limited infrared transition, especially for CD_3Br. Because of the relatively

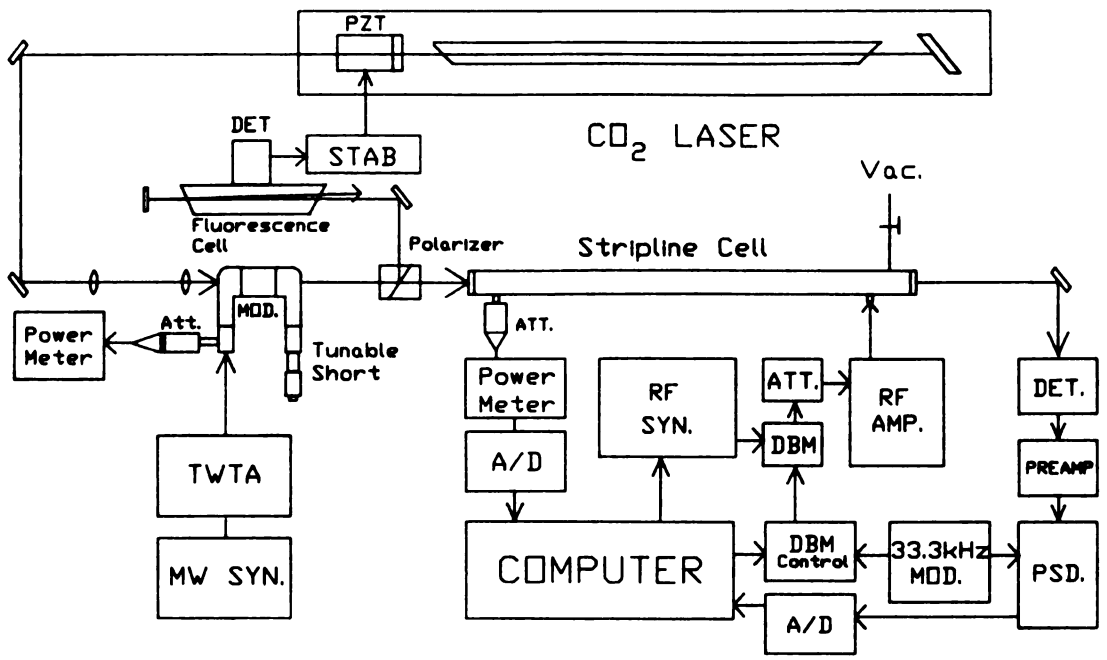

Figure 4-2. Block diagram of the infrared radiofrequency double-resonance spectrometer used to record the pure quadrupole transitions in this work. An infrared microwave sideband laser in the cavity mode serves as the infrared pumping source. A radiofrequency synthesizer whose output is chopped by a double-balanced mixer and amplified serves as the radiofrequency source.

small hyperfine splitting of the vibration-rotation transitions, all of the expected double resonances could be recorded without retuning the infrared frequency. However, when the frequency difference between the component and the hypothetical unsplit frequency was calculated to be more than 10 MHz, the frequency of the infrared sideband laser was fixed at the frequency of the desired hyperfine component. We estimate the accuracy of the time averaged infrared pump frequency to be ±150 kHz. The frequency jitter of this source is also ~150 kHz, which is mostly the intentional laser modulation for the frequency stabilization.

The radiofrequency was generated by an RF-synthesizer (Programmed Test Sources Model PTS 500) operating in the range 1-500 MHz with +3 to +13 dBm output. The frequency and the power of the radiowaves were controlled by the computer through an interface built at MSU. The radiowave was 100 % amplitude modulated at 33 kHz (Hewlett Packard 8428 C Modulator Control) by means of a double balanced mixer (DBM, Mini-Circuit Laboratory Model ZAD-1SH) at the output of the synthesizer. The switched RF output from the DBM was amplified by broadband power amplifier (Electronic and Navigation Industries, Inc. Model 525 LA). The amplified radiofrequency power from the computer-controlled synthesizer was applied to the central electrode of the cell. The power of the radiowave was monitored at the exit of the cell by a thermister detector (Hewlett Packard 8478 Thermister Mount) and a power meter (Hewlett Packard Model 432) after 30 dB attenuation. The signal of the power meter was fed into the computer, which in turn sent a correction voltage to the synthesizer in order to maintain constant power of the radiowave. The computer increased the radiofrequency in steps of 20 kHz within the range 1-500 MHz and recorded the output of the lock-in

amplifier, which consisted entirely of double-resonance effects. The RF power at the sample cell was kept as low as is consistent with reasonably good signal to noise ratio, because the spectra are easily RF power broadened at the low sample pressures used. Typical RF powers were of the order of a few milliwatts for CD_3I and 5-50 milliwatts for CD_3Br. An example of an infrared radio frequency double resonance spectrum of CD_3I is shown in Fig. 4-3, where it is seen that the half width at half maximum for the transitions is about 70 kHz. Figs. 4-4 and 4-5 show typical IR-RF double resonance spectra for $CD_3{}^{79}Br$ and $CD_3{}^{81}Br$, respectively, where it may be seen that the half width at half-maximum for the transitions is about 100 kHz. The center frequencies of the RF transitions were determined by fitting the observed lineshapes to a Lorentz function or to a sum of Lorentz functions for overlapped transitions; we estimate the RF accuracy of well-resolved transitions to be 1-5 kHz.

The methyl iodide and the methyl bromide were fully-deuterated samples obtained from Merck & Co. and used as received except for the usual freeze-pump-thaw cycling. Sample pressures were 3-5 mTorr for the double resonance measurements. All spectra were recorded at room temperature (~297 K).

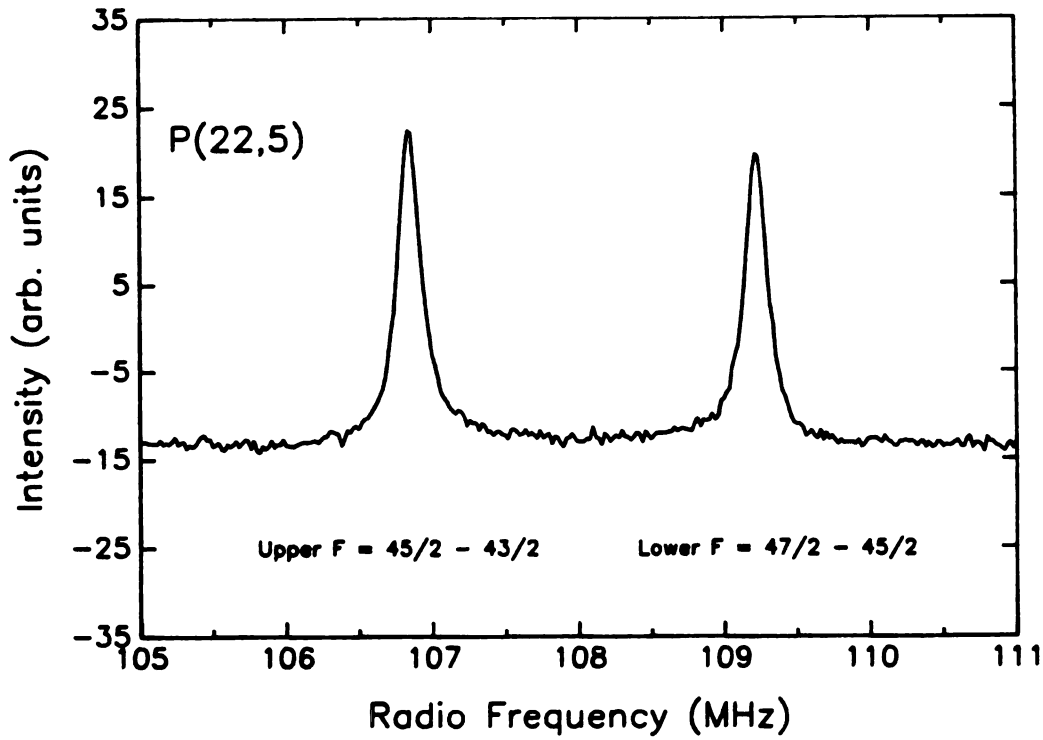

Figure 4-3. A portion of the infrared radiofrequency double resonance spectrum obtained by pumping the P(22,5) transition in the ν_2 band of CD_3I. The F quantum numbers of the transitions in the upper and lower states of the vibration-rotation transition are shown. The horizontal axis is the absolute radiofrequency. the sample pressure was 3 mTorr and 1-m path length was used.

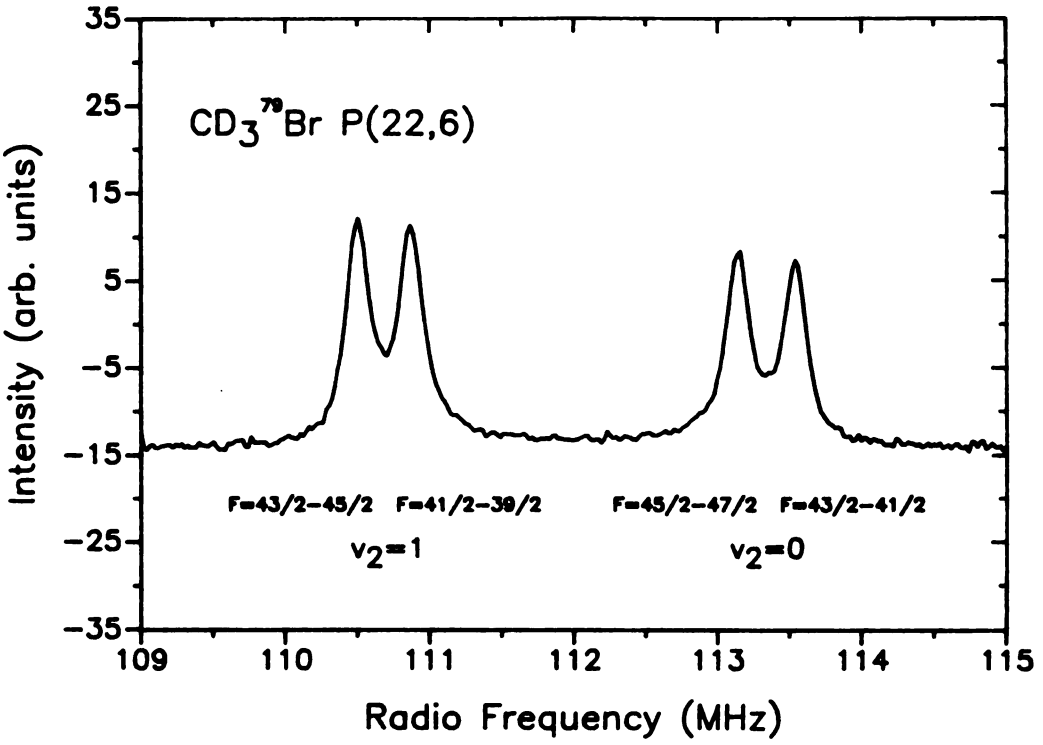

Figure 4-4. Example of infrared radiofrequency double resonance spectra obtained in the present study for $CD_3{}^{79}Br$. For these transitions, the infrared sideband laser source was tuned to the center frequency of the Doppler-limited lineshape of the P(22,6) transition in the ν_2 band. For the infrared microwave sideband laser source, the 10R(26) $^{12}C^{16}O_2$ laser was used with a microwave frequency of 11726 MHz; the lower frequency sideband was used.

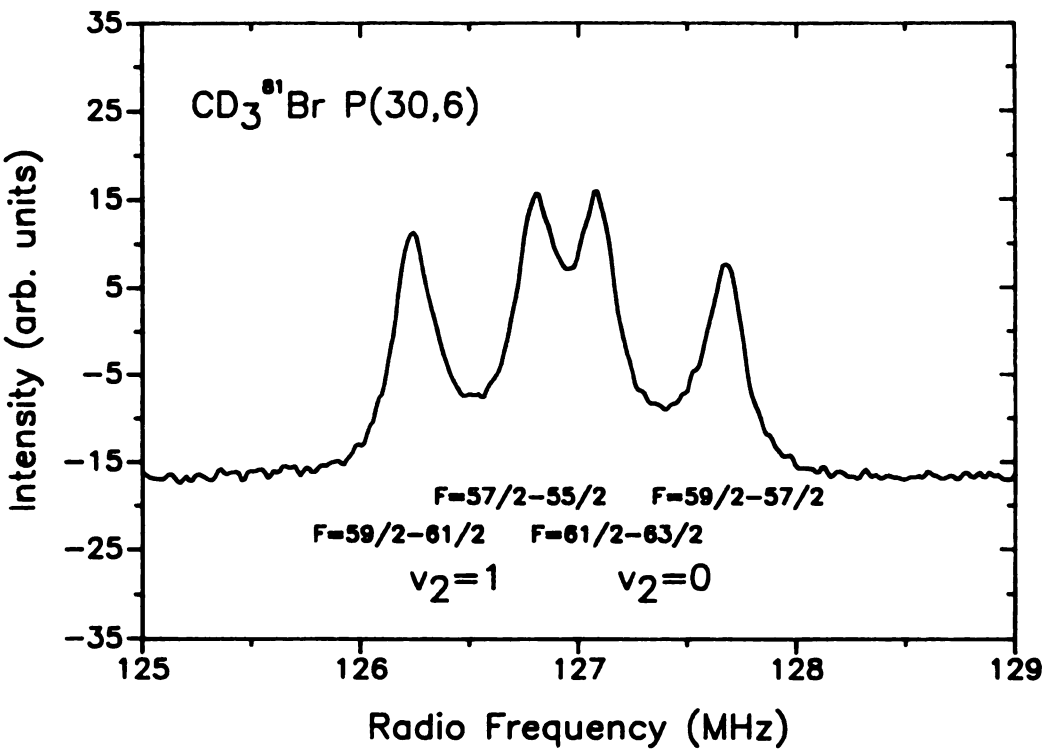

Figure 4-5. Example of infrared radiofrequency double resonance spectra obtained in the present study for $CD_3{}^{81}Br$. For these transitions, the infrared sideband laser source was tuned to the center frequency of the Doppler-limited lineshape of the P(30,6) transition in the ν_2 band. For the infrared microwave sideband laser source, the 10R(18) $^{12}C^{16}O_2$ laser was used with a microwave frequency of 9747 MHz; the lower frequency sideband was used.

IV-4 Results and Discussion

IV-4-1 CD_3I

About 150 radio-frequency resonances in CD_3I were recorded by the IR-RF double resonance technique; 19 vibration-rotation transitions with J's between 4 and 31 and K's between 1 and 9 were pumped. In many cases all 10 of the possible RF resonances were measured. It was often possible to observe all of the RF resonances with a single infrared pumping frequency. This can be explained by the fact that each quadrupole component is in resonance for some velocity group within the Doppler profile for the transition frequency (Fig. 4-6), though the intensities of the transitions vary because they depend on the Maxwellian (Gaussian) weight. The results show that the IR-RF double resonance method is very powerful for studying pure quadrupole transitions, especially for high J transitions. For these transitions, the quadrupole hyperfine splittings in the infrared spectrum are usually very small (a few MHz), because the hyperfine shifts in the energies of the upper and lower states are almost the same. However, the shifts in energy for the hyperfine components of a single vibration-rotation level are still very large for high J (up to 300 MHz). The $\Delta F = \pm 1$ selection rules for the RF resonances allows the differences in these large shifts to be observed directly. An example of RF transitions observed by IR-RF double resonance is shown in Fig. 4-3.

Previously reported microwave and radiofrequency transitions are also included in the least squares fittings with their estimated uncertainties. The frequencies of the radiofrequency transitions measured in this work are shown in Table 4-1 with their estimated

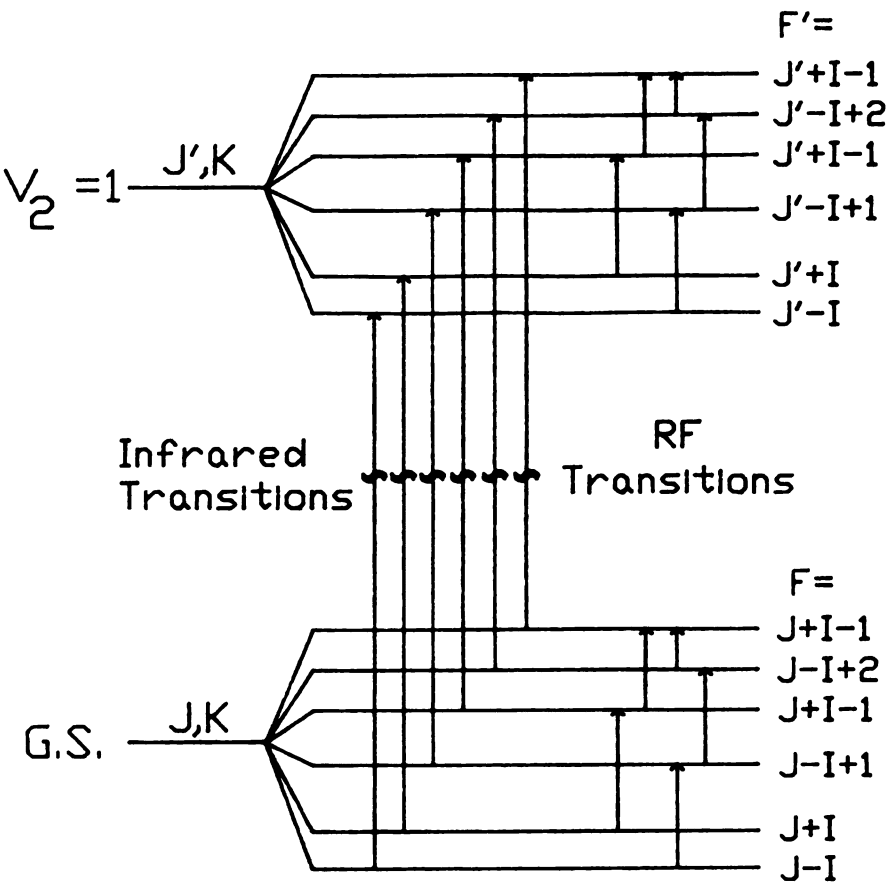

Figure 4-6. Typical energy level pattern for the infrared radiofrequency double resonances observed for CD_3I. In most cases, a single infrared frequency pumps all of the allowed infrared transitions by interacting with molecules in different velocity groups.

Table 4-1

Pure Quadrupole Frequencies of CD_3I

v = 0							v_2 = 1						
J	K	2F'	2F"	ν/MHz	O-C[a]	UC[b]	J	K	2F'	2F"	ν/MHz	O-C[c]	UC[b]	Pump[d]
5	1	15	13	300.357	4	5	4	1	13	11	290.458	-17	5	1
		13	11	57.337	-3	5			11	9	34.653	36	20	1
		7	9	180.203	-29	20			5	7	179.019	18	5	2
									3	5	175.569	0	5	2
5	2	15	13	199.185	2	5								3
		13	11	38.939	-2	5	4	2	11	9	17.739	33	20	3
		9	11	65.409	4	5			7	9	54.518	10	5	3
		7	9	120.597	-1	5			5	7	85.115	20	5	4
									3	5	82.945	-8	20	4
7	1	19	17	306.174	-29	20	6	1	17	15	304.872	20	20	5
		17	15	83.897	-3	5			15	13	72.909	8	5	5
		13	15	74.580	0	5			11	13	85.015	-1	5	6
		11	13	177.165	12	5			9	11	179.245	-2	5	6
9	1	21	19	98.493	-8	5	8	1	19	17	92.246	8	5	7
		15	17	173.113	7	20			13	15	175.258	-4	5	7
10	5	25	23	99.386	0	5	9	5	23	21	51.889	-17	5	8
		23	21	34.354	-4	5			21	19	17.630	3	5	8
									17	19	9.922	6	20	9
		17	19	56.233	-1	5			15	17	30.194	-3	5	9
12	5	29	27	161.095	-8	5	11	5	27	25	134.665	0	5	10
		27	25	59.083	0	5			25	23	48.010	0	5	10
		23	25	23.960	-18	20			21	23	21.696	21	20	11
		21	23	89.114	3	5			19	21	75.192	-7	5	11
		19	21	137.522	-7	5			17	19	113.662	-2	5	11
14	6	33	31	149.473	-6	5	13	6	31	29	125.666	-2	5	12
		31	29	57.578	-12	5			29	27	47.495	1	5	12
		27	29	19.206	-21	5			25	27	17.297	21	20	13
		25	27	81.652	-5	5			23	25	69.150	-8	5	13
		23	25	130.498	-2	5			21	23	108.844	-17	5	13
							14	9	31	33	48.795	5	5	14
									29	31	17.907	-33	20	14
									27	25	26.241	35	20	15
									25	23	41.181	5	5	15
							17	4	39	37	257.732	-5	5	16
18	4	39	37	106.818	3	5			37	35	103.820	4	5	16
		35	37	26.871	33	20			33	35	27.868	-12	20	16
		33	35	140.217	-8	5			31	33	138.556	12	5	16
		31	33	234.447	2	5			29	31	229.373	-2	5	16

Table 4-1 (cont'd)

v = 0							v_2 = 1							
J	K	2F'	2F"	ν/MHz	O-C[a]	UC[b]	J	K	2F'	2F"	ν/MHz	O-C[c]	UC[b]	Pump[d]
18	5	41	39	237.778	4	5	17	5	39	37	230.746	-10	5	17
		39	37	97.078	7	5			37	35	93.033	2	5	17
		35	37	24.368	42	20			33	35	24.890	-20	20	17
		33	35	127.363	0	5			31	33	124.079	4	5	17
		31	33	213.015	5	5			29	31	205.491	-5	5	17
19	9	43	41	109.599	0	5	18	9	41	39	88.375	10	5	18
		41	39	45.591	0	5			39	37	36.483	12	5	18
		37	39	10.393	-6	20			35	37	8.788	22	20	18
		35	37	58.573	7	5			33	35	47.445	7	5	19
		33	35	99.173	4	5			31	33	79.736	6	5	19
22	4	49	47	273.529	8	5	21	4	47	45	271.567	-6	5	20
		47	45	116.014	2	5			45	43	114.244	6	5	20
		43	45	23.167	25	20			41	43	24.018	-6	20	20
		41	43	144.731	-8	5			39	41	144.096	17	20	20
		39	41	249.583	4	5			37	39	246.786	-2	5	20
22	5	49	47	257.427	10	5	21	5	47	45	253.879	-14	5	21
		47	45	109.225	4	5			45	43	106.848	1	5	21
		43	45	21.780	33	20			41	43	22.412	-14	20	21
		41	43	136.217	-4	5			39	41	134.716	8	5	21
		39	41	234.937	3	5			37	39	230.775	-10	5	21
23	9	51	49	169.077	-1	5	22	9	49	47	157.529	3	5	22
		49	47	72.494	4	5			47	45	67.079	5	5	23
		43	45	89.245	3	5			41	43	83.373	8	5	23
		41	43	155.101	1	5			39	41	144.034	-7	20	22
26	3	57	55	288.894	-22	20	25	3	55	53	288.699	17	5	24
		55	53	125.810	-10	5			53	51	125.002	10	5	24
		51	53	20.816	22	20			49	51	21.568	-14	20	24
		49	51	151.591	37	20			47	49	151.691	-24	5	24
									45	47	266.084	6	5	24
26	4	57	55	279.957	3	5	25	4	55	53	278.978	-10	5	25
		55	53	121.934	-4	5			53	51	120.819	3	5	25
		51	53	20.155	25	20			49	51	20.821	-17	20	25
		49	51	146.817	-32	20			47	49	146.647	26	20	25
		47	49	258.814	-2	5			45	47	257.162	-5	5	25
27	9	57	55	89.464	-2	5	26	9	55	53	86.024	6	5	26
		51	53	106.722	-10	5			49	51	103.352	12	5	26
		49	51	189.161	-2	5			47	49	182.346	-3	5	27

Table 4-1 (cont'd)

v = 0							v_2 = 1						
J	K	2F'	2F"	ν/MHz	O-C[a]	UC[b]	J	K	2F'	2F"	ν/MHz	O-C[c]	UC[b]	Pump[d]
30	4	65	63	283.814	-4	5	29	4	63	61	283.358	-4	5	28
		63	61	126.027	-5	5			61	59	125.297	5	5	28
		59	61	17.743	34	20			57	59	18.261	-17	20	28
31	9	67	65	226.064	4	5	30	9	65	63	221.747	-8	5	29
		65	63	100.904	-2	5			63	61	98.602	2	5	29
		59	61	117.536	-10	20			57	59	115.485	10	5	29
		57	59	211.477	2	5			55	57	207.037	-7	5	29

[a]Observed minus calculated frequency in kHz. The parameters for the calculation are in the second column of Table 3-2 and in the first column of Table 4-3.

[b]Estimated uncertainty in the observed frequency in kHz.

[c]Observed minus calculated frequency in kHz. The parameters for the calculation are in the first column of Table 3-3 and the third column of Table 4-2.

[d]Pump transitions and frequencies are listed in Table 4-2.

uncertainties. Also shown in Table 4-1 are the observed minus calculated frequencies for the parameters derived in this work. Table 4-2 lists the infrared transitions that were pumped for the RF double resonances listed in Table 4-1. The quadrupole and spin rotation parameters obtained from the radio frequencies and the resolved microwave frequencies for both vibrational states are in Table 4-3. As shown in the table, the centrifugal distortion parameters for the quadrupole coupling and the spin-rotation parameters are well determined in the present work although the previous microwave and radiofrequency data could not determine all of these constants. This is a result of the accuracy of the present radiofrequency data as well as the tunability of our pump source which allowed selection of a wide range of J and K for the double resonances.

Comparison of the observed and calculated radio frequencies in Table 4-1 shows that the quadrupole and spin-rotation parameters in Table 4-3 predict the combined quadrupole-spin-rotation splittings to a few kHz. A comparison of the predicted uncertainties of the microwave and radio frequencies with the observed residuals indicates that the predicted uncertainties are approximately equal to the expected accuracies for resolved transitions by each technique; the standard deviations for an observation of unit weight are all within a factor of 2 of unity. Also, although the previous microwave and radiofrequency data could not determine all of the centrifugal distortion parameters for the quadrupole coupling, these parameters are all well determined in the present work.

Table 4-2

Infrared Pumping Frequencies for IR-RF Double Resonance

Index[a]	Transition[b]	ν/MHz[c]	Laser[d]	ν_P/MHz[e]
1	P(5,1)	-12 289.2	10P(16)	28 400 300.5
2	P(5,1)	-12 249.3	10P(16)	28 400 340.4
3	P(5,2)	-11 466.0	10P(16)	28 401 123.7
4	P(5,2)	-11 444.0	10P(16)	28 401 144.9
5	P(7,1)	15 655.5	10P(18)	28 375 429.3
6	P(7,1)	15 678.9	10P(18)	28 375 452.7
7	P(9,1)	-9 458.0	10P(18)	28 350 315.8
8	P(10,5)	-15 861.2	10P(18)	28 343 912.6
9	P(10,5)	-15 878.1	10P(18)	28 343 895.7
10	P(12,5)	12 111.0	10P(20)	28 318 335.9
11	P(12,5)	12 105.8	10P(20)	28 318 330.7
12	P(14,6)	-10 919.4	10P(20)	28 295 305.5
13	P(14,6)	-10 923.9	10P(20)	28 295 301.0
14	P(15,9)	-12 582.9	10P(20)	28 293 642.0
15	P(15,9)	-12 596.1	10P(20)	28 293 628.8
16	P(18,4)	-14 138.4	10P(22)	28 237 803.3
17	P(18,5)	-11 905.3	10P(22)	28 240 036.4
18	P(19,9)	-11 659.0	10P(22)	28 240 282.9
19	P(19,9)	-11 662.8	10P(22)	28 240 278.9
20	P(22,4)	-12 539.3	10P(24)	28 184 383.3
21	P(22,5)	-10 395.9	10P(24)	28 186 526.7
22	P(23,9)	-11 191.1	10P(24)	28 185 731.5
23	P(23,9)	-11 180.3	10P(24)	28 185 742.3
24	P(26,3)	-12 825.8	10P(26)	28 128 340.2
25	P(26,4)	-11 220.7	10P(26)	28 129 945.3
26	P(27,9)	-11 123.1	10P(26)	28 130 042.9
27	P(27,9)	-11 130.1	10P(26)	28 130 035.9
28	P(30,4)	-10 167.5	10P(28)	28 074 502.3
29	P(31,9)	-11 463.8	10P(28)	28 073 206.0

[a] Index number in Table 4-1.

[b] Vibration-rotation transition pumped for IR-RF double resonance.

[c] Microwave frequency in MHz; the signed microwave frequency was added to the laser frequency to obtain the pumping frequency.

[d] CO_2 laser line used; laser frequencies taken from Ref. 51.

[e] Pumping frequency in MHz.

Table 4-3

Quadrupole and Spin-Rotation Interaction Parameters of CD_3I[a]

Parameter	v = 0		v_2 = 1	
	This Work[b]	Wlodarczak[c]	This Work[d]	Kuczkowski[e]
eqQ/MHz	-1 929.008(14)	-1 928.918(86)	-1 930.886(31)	-1 930.30(26)
χ_J/KHz	-1.098(33)	-1.615(19)	-1.342(72)	
χ_K/KHz	-32.86 (40)	-8.16(184)	-45.81 (88)	
χ_D/KHz	19.27 (27)		26.58 (35)	
C_N/KHz	-13.64 (6)	-14.94 (42)	-14.03 (11)	
C_K/KHz	-9.57 (52)	-11.3 (63)	-7.09 (87)	

[a]Values in parentheses are one standard deviation in multiples of the last digit in the parameter.

[b]Obtained from a fit of the rotational frequencies of the ground state from the references shown in Table 4-1 and pure quadrupole frequencies in Table III and in Table V of Ref. 39.

[c]Obtained from Table VI in Ref. 40.

[d]Obtained from a fit of the rotational frequencies of the v_2 = 1 state from Table II in Ref. 38 and pure quadrupole frequencies in Table IV.

[e]Obtained from Table VIII in Ref. 38.

IV-4-2 CD_3Br

More than 160 IR-RF double resonances have been observed for each of the two naturally-occurring isotopic species of CD_3Br; it has been possible to measure pure quadrupole frequencies for $10 \leq J \leq 38$ and $3 \leq K \leq 8$. The experimental values of the pure quadrupole frequencies measured in this work are given in Tables 4-4 and 4-5. In each table the $v_2 = 0$ transitions are given on the left side and the $v_2 = 1$ transitions are given on the right side. The pumped vibration-rotation transition is identified by the J,K quantum numbers in the two vibrational states. Since most of the quadrupole splittings in the infrared spectra of CD_3Br are within 5 MHz and the Doppler width is ~18.5 MHz, it was not necessary to adjust pump frequencies to observe all of the pure quadrupole transitions for a given infrared transition. Hence, the infrared frequency was set at the center frequency of the Doppler-limited vibration-rotation transition. The infrared frequencies were calculated from the parameters given in Chapter III and the appropriate CO_2 laser transition and microwave frequency for the IMSL source were determined from the calculated frequency. The experimental frequencies in Tables 4-4 and 4-5 were fit separately by least squares to differences in energies calculated by diagonalization of Hamiltonian matrices with different parameters for the two isotopic species. The resulting parameters are shown in Tables 4-6 and 4-7 for $CD_3{}^{79}Br$ and $CD_3{}^{81}Br$, respectively. Also shown in Tables 4-6 and 4-7 are the values of eqQ determined by Morino and Hirose (44). It is seen that the newer values are in good agreement with the less accurate values previously reported. The observed minus calculated frequencies for the parameters

Table 4-4

Pure Quadrupole Frequencies of $CD_3{}^{79}Br$[a]

v = 0							v_2 = 1						
J	K	2F'	2F"	ν/MHz	O-C[b]	UC[c]	J	K	2F'	2F"	ν/MHz	O-C[b]	UC[c]
10	3	19	17	108.683	9	50	9	3	17	15	100.987	108	100
		21	23	108.517	-62	50			19	21	100.807	-35	100
10	4	19	17	81.161	-6	50	9	4	17	15	67.508	170	200
		21	23	81.161	10	50			19	21	67.272	-127	200
12	4	23	21	99.742	-10	40	11	4	21	19	91.853	31	50
		25	27	99.568	-55	40			23	25	91.674	-69	50
14	3	27	25	125.543	-37	50	13	3	25	23	122.841	35	50
		29	31	125.326	-9	40			27	29	122.629	36	50
14	4	27	25	111.183	-4	20	13	4	25	23	106.224	-22	30
		29	31	110.979	2	20			27	29	106.056	-17	30
14	5	27	25	92.688	8	30	13	5	25	23	84.932	-51	30
		29	31	92.515	4	30			27	29	84.788	-70	30
15	7	29	27	55.883	-63	OMIT							
		31	33	55.883	68	OMIT							
15	8	29	27	28.928	-19	OMIT							
		31	33	28.928	73	OMIT							
16	4	31	29	118.728	4	20	15	4	29	27	115.457	-3	20
		33	35	118.451	2	20			31	33	115.214	-2	20
16	5	31	29	104.449	5	20	15	5	29	27	99.298	-51	30
		33	35	104.201	3	20			31	33	99.092	-48	30
18	4	35	33	123.958	2	10	17	4	33	31	121.722	15	10
		37	39	123.628	3	10			35	37	121.420	16	10
18	5	35	33	112.606	0	10	17	5	33	31	109.059	-25	20
		37	39	112.297	0	10			35	37	108.784	-22	20
18	6	35	33	98.737	7	20	17	6	33	31	93.618	-63	50
		37	39	98.453	6	20			35	37	93.372	-59	50
20	4	39	37	127.736	-2	10	19	4	37	35	126.154	11	10
		41	43	127.355	-2	10			39	41	125.803	15	10
20	5	39	37	118.501	-0	10	19	5	37	35	115.977	-12	10
		41	43	118.135	-3	10			39	41	115.641	-11	10
20	6	39	37	107.212	1	20							
		41	43	106.866	0	20							

Table 4-4 (cont'd)

v = 0							v_2 = 1						
J	K	2F'	2F"	ν/MHz	O-C[b]	UC[c]	J	K	2F'	2F"	ν/MHz	O-C[b]	UC[c]
20	7	39	37	93.866	3	20	19	7	37	35	88.962	-21	20
		41	43	93.542	2	20			39	41	88.673	-19	20
20	8	39	37	78.456	0	10							
		41	43	78.152	-5	10							
22	5	43	41	122.907	5	10	21	5	41	39	121.062	-6	10
		45	47	122.489	2	10			43	45	120.674	-4	10
22	6	43	41	113.537	0	10	21	6	41	39	110.874	-15	10
		45	47	113.138	0	10			43	45	110.503	-13	10
24	3	47	45	137.747	-3	20	23	3	45	43	137.310	-10	50
		49	51	137.310	43	20			47	49	136.893	32	30
24	5	47	45	126.277	2	10	23	5	45	43	124.912	-5	10
		49	51	125.814	2	10			47	49	124.474	-4	10
24	6	47	45	118.384	0	10	23	6	45	43	116.397	-11	10
		49	51	117.932	0	10			47	49	115.976	-6	10
24	7	47	45	109.052	-2	10	23	7	45	43	106.410	39	10
		49	51	108.616	-1	10			47	49	105.995	34	10
26	3	51	49	138.717	-0	5	25	3	49	47	138.449	24	10
		53	55	138.190	-3	5			51	53	137.947	23	10
26	4	51	49	134.434	3	10	25	4	49	47	133.815	-5	20
		53	55	133.930	16	20			51	53	133.327	1	10
26	5	51	49	128.928	9	10	25	5	49	47	127.892	-14	20
		53	55	128.419	9	10			51	53	127.424	3	20
26	6	51	49	122.180	0	10	25	6	49	47	120.689	-1	10
		53	55	121.675	-6	10			51	53	120.215	0	10
26	7	51	49	114.210	2	10	25	7	49	47	112.220	42	30
		53	55	113.722	-3	10			51	53	111.758	42	20
28	3	55	53	139.483	-12	20	27	3	53	51	139.325	17	30
		57	59	138.923	-6	20			55	57	138.783	17	30
28	4	55	53	135.773	-20	30	27	4	53	51	135.347	-8	50
		57	59	135.229	-3	30			55	57	134.846	28	30
28	5	55	53	131.029	-2	10	27	5	53	51	130.255	-23	10
		57	59	130.485	7	10			55	57	129.745	-3	10
30	4	59	57	136.910	10	30	29	4	57	55	136.609	10	10
		61	63	136.291	-6	30			59	61	136.011	-9	10

Table 4-4 (cont'd)

v = 0							v_2 = 1						
J	K	2F'	2F"	ν/MHz	O-C[b]	UC[c]	J	K	2F'	2F"	ν/MHz	O-C[b]	UC[c]
30	5	59	57	132.724	-23	30	29	5	57	55	132.221	26	20
		61	63	132.126	-24	20			59	61	131.637	16	40
30	6	59	57	127.670	0	10	29	6	57	55	126.811	-9	10
		61	63	127.078	-2	10			59	61	126.240	-14	10
32	6	63	61	129.668	-26	30	31	6	61	59	129.097	35	50
		65	67	128.984	-76	60			63	65	128.455	3	40
34	6	67	65	131.369	-13	20	33	6	65	63	130.883	-42	50
		69	71	130.721	16	40			67	69	130.259	-13	30
35	6	69	67	132.128	5	20	34	6	67	65	131.719	-23	40
		71	73	131.432	8	30			69	71	131.040	-27	20

[a]Obtained by infrared radiofrequency double resonance. The infrared transition was between the J and K values across from each other in the left and right halves of the table. For example, the infrared transition for the first four double resonances was from (J,K) = (10,3) in v = 0 to (J,K) = (9,3) in v_2 = 1. The infrared frequency used was the center frequency of the Doppler-limited transition, as calculated from the parameters in Table 3-8.

[b]Observed minus calculated frequency in kHz. The parameters for the calculation are in Tables 4-6 and 3-8.

[c]Estimated uncertainty in the observed frequency in kHz. An "OMIT" means that the frequency was omitted from the least squares fits.

Table 4-5

Pure Quadrupole Frequencies of $CD_3{}^{81}Br$[a]

v = 0							v_2 = 1						
J	K	2F'	2F"	ν/MHz	O–C[b]	UC[c]	J	K	2F'	2F"	ν/MHz	O–C[b]	UC[c]
12	2	23	21	111.089	-26	40	11	2	21	19	109.546	33	40
		25	27	110.854	-13	30			23	25	109.322	26	40
12	3	23	21	99.547	-6	20	11	3	21	19	95.872	16	30
		25	27	99.323	-9	20			23	25	95.667	0	30
14	3	27	25	104.945	9	20	13	3	25	23	102.633	-25	20
		29	31	104.669	14	20			27	29	102.395	-10	20
14	4	27	25	92.890	-27	30	13	4	25	23	88.839	40	40
		29	31	92.622	-36	30			27	29	88.579	12	40
14	5	27	25	77.466	9	30	13	5	25	23	71.005	44	40
		29	31	77.221	-4	30			27	29	70.787	35	40
16	3	31	29	108.499	11	20	15	3	29	27	106.992	-16	30
		33	35	108.161	7	30			31	33	106.692	-9	20
16	4	31	29	99.228	13	50	15	4	29	27	96.518	4	20
		33	35	98.913	16	50			31	33	96.239	19	20
16	5	31	29	87.274	-14	30	15	5	29	27	83.029	22	30
		33	35	86.986	-3	30			31	33	82.750	22	30
18	3	35	33	110.959	2	10	17	3	33	31	109.977	16	10
		37	39	110.572	-2	10			35	37	109.610	4	10
18	4	35	33	103.585	-3	20	17	4	33	31	101.716	-28	30
		37	39	103.223	7	30			35	37	101.381	-16	10
18	5	35	33	94.123	14	30	17	5	33	31	91.120	-48	50
		37	39	93.768	17	30			35	37	90.818	-12	20
20	3	39	37	112.742	-2	10	19	3	37	35	112.069	8	20
		41	43	112.322	8	10			39	41	111.669	9	10
20	4	39	37	106.755	6	10	19	4	37	35	105.444	-13	20
		41	43	106.329	1	10			39	41	105.047	-14	10
22	2	43	41	117.640	8	50	21	2	41	39	117.514	34	50
		45	47	117.167	15	40			43	45	117.054	22	30
22	3	43	41	114.067	-15	10	21	3	41	39	113.661	50	20
		45	47	113.570	-37	10			43	45	113.192	26	20
22	4	43	41	109.116	5	10	21	4	41	39	108.175	-15	10
		45	47	108.648	6	10			43	45	107.735	-12	10

Table 4-5 (cont'd)

v = 0							v_2 = 1						
J	K	2F'	2F"	ν/MHz	O-C[b]	UC[c]	J	K	2F'	2F"	ν/MHz	O-C[b]	UC[c]
22	5	43	41	102.715	0	20	21	5	41	39	101.190	-22	30
		45	47	102.225	-30	20			43	45	100.750	-23	20
24	3	47	45	115.118	6	10	23	3	45	43	114.799	9	10
		49	51	114.591	0	10			47	49	114.307	6	10
24	4	47	45	110.923	0	10	23	4	45	43	110.237	-26	10
		49	51	110.427	19	10			47	49	109.771	-5	10
24	5	47	45	105.539	4	10	23	5	45	43	104.419	-17	10
		49	51	105.032	6	10			47	49	103.931	-20	10
24	6	47	45	98.948	1	10	23	6	45	43	97.310	7	20
		49	51	98.443	-1	10			47	49	96.830	10	10
26	3	51	49	115.932	10	20	25	3	49	47	115.727	16	20
		53	55	115.373	16	20			51	53	115.191	12	20
26	4	51	49	112.354	8	30	25	4	49	47	111.876	0	20
		53	55	111.805	20	30			51	53	111.327	-18	20
28	3	55	53	116.586	14	40	27	3	53	51	116.457	11	20
		57	59	115.970	7	50			55	57	115.864	-8	20
31	5	61	59	111.576	11	20	30	5	59	57	111.211	-3	20
		63	65	110.885	-11	20			61	63	110.556	-19	20
31	6	61	59	107.548	-48	50	30	6	59	57	107.003	-16	20
		63	65	106.883	-47	50			61	63	106.396	17	20
33	6	65	63	109.122	-17	20	32	6	63	61	108.720	-7	20
		67	69	108.424	-4	20			65	67	108.041	-3	20
34	7	67	65	105.895	-13	30	33	7	65	63	105.400	26	20
		69	71	105.170	-8	30			67	69	104.714	46	20
36	7	71	69	107.506	-13	20	35	7	69	67	107.166	21	20
		73	75	106.736	-8	20			71	73	106.416	21	20
38	7	75	73	108.888	0	30	37	7	73	71	108.635	-11	20
		77	79	108.089	20	20			75	77	107.854	0	20

Table 4-5 (cont'd)

[a]Obtained by infrared radiofrequency double resonance. The infrared transition was between the J and K values across from each other in the left and right halves of the table.

[b]Observed minus calculated frequency in kHz. The parameters for the calculation are in Tables 4-7 and 3-9.

[c]Estimated uncertainty in the observed frequency in kHz. An "OMIT" means that the frequency was omitted from the least squares fits.

Table 4-6

Quadrupole and Spin-Rotation Interaction Parameters of $CD_3{}^{79}Br$

Parameter	v = 0		v_2 = 1	
	This Work[a]	Morino & Hirose[b]	This Work[c]	Morino & Hirose[b]
eqQ/MHz	575.718(35)[d]	575.4(10)	575.811(41)	576.2(10)
x_J/kHz	0.224(53)		0.946(74)	
x_K/kHz	14.75(132)		26.01(243)	
x_D/kHz	4.19(154)		-52.76(402)	
C_N/kHz	-10.02(15)		-10.00(22)	
C_K/kHz	-9.12(259)		-9.04(391)	

[a]Obtained from a fit of the pure quadrupole frequencies in Table 4-4 and the rotational frequencies for the ground state reported in Refs. 43 and 44.

[b]Ref. 44.

[c]Obtained from a fit of the pure quadrupole frequencies in Table 4-4 and the rotational frequencies for the v_2 = 1 state reported in Ref. 44.

[d]Values in parentheses are one standard deviation in multiples of the last digit in the parameter.

Table 4-7

Quadrupole and Spin-Rotation Interaction Parameters of $CD_3{}^{81}Br$

Parameter	v = 0		v_2 = 1	
	This Work[a]	Morino & Hirose[b]	This Work[c]	Morino & Hirose[b]
eqQ/MHz	480.922(24)[d]	479.5(10)	481.206(25)	478.5(10)
χ_J/kHz	0.064(56)		0.480(64)	
χ_K/kHz	14.73(127)		35.15(153)	
χ_D/kHz	0.[e]		0.[e]	
C_N/kHz	-10.75(22)		-10.45(25)	
C_K/kHz	-11.12(588)		-17.61(612)	

[a]Obtained from a fit of the pure quadrupole frequencies in Table 4-5 and the rotational frequencies for the ground state reported in Ref. 44.

[b]Ref. 44.

[c]Obtained from a fit of the pure quadrupole frequencies in Table 4-5 and the rotational frequencies for the v_2 = 1 state reported in Ref. 44.

[d]Values in parentheses are one standard deviation in multiples of the last digit in the parameter.

[e]Constrained to zero.

in Tables 4-6 and 4-7 are shown in Tables 4-4 and 4-5, respectively, where it is seen that the theoretical frequencies agree with the experimental values for well-resolved transitions to within the experimental uncertainty.

Examination of the centrifugal distortion terms for the quadrupole coupling (Tables 4-6 and 4-7) shows that both χ_J and χ_D are quite small in the ground state. The residual for χ_D for $CD_3{}^{81}Br$ was larger than the value obtained, and it was therefore constrained to zero. The centrifugal distortion terms for the quadrupole coupling in $v_2 = 1$ are larger than in the ground state for both species. This may be the result of the Coriolis interaction between the $v_2 = 1$ and $v_5 = 1$ states (48), which should lead to some sharing of quadrupole effects between the two vibrational states. Since this is a Coriolis interaction involving states of A and E symmetry, the coupled levels differ by ± 1 in k. Therefore, even if the quadrupole coupling is very similar in the two vibrational states, an effect of the mixing is expected. The result is that caution should be used in interpretation of the vibrational dependence of the quadrupole parameters.

Since the values of eqQ obtained are quite precise, it is expected that the ratio of these values should be nearly equal to the ratio of the quadrupole moments of the two bromine isotopes. The experimental value of $eqQ(CD_3{}^{79}Br)/eqQ(CD_3{}^{81}Br)$ obtained in the present work for the ground vibrational state is 1.19711(9), which is the same within our experimental error as the molecular beam values of 1.1971005(24) for LiBr (49) and 1.1970568(15) for atomic bromine (50). The corresponding ratio obtained by us for $v_2 = 1$ in CD_3Br is 1.19660(9). The difference

between this value and that for the ground vibrational state may result from the effect of the Coriolis coupling.

As stated before, it has been found that some effect was causing an apparent shift of the transitions especially at low RF frequencies. In contrast to the residuals shown in Tables 4-4 and 4-5, the observed-minus- calculated frequencies for the low radiofrequency transitions shown in Tables 4-8 and 4-9 are often greater than the experimental uncertainty and nearly always the same sign for a given vibrational state; the residuals for $v_2 = 0$ are positive while the residuals for $v_2 = 1$ are negative. The reason has been traced to the result of a four-interacting-level double-resonance effect that causes the lower frequency transition of a pair to be shifted to higher frequency while the higher frequency component is shifted to lower frequency. In fact, the same effect has been observed in low frequency quadrupole transitions of CD_3I, however, it is much more serious in CD_3Br since the transitions are located much closer (within 1 MHz). The details are discussed in the next chapter. Since the low frequency transitions were most strongly affected by the four-interacting-level double resonance effect, they have been omitted from the least squares fittings.

V-4-3 Other Aspects

This is the first systematic application of an infrared microwave sideband laser system to the use of IR-RF double resonance for studying quadrupole transitions; previous studies of a few rotational transitions in OsO_4 and SiH_4 have been reported (30,31). Some unresolved questions

Table 4-8

F=J+1/2 ← F=J-1/2 transitions of $CD_3{}^{79}Br$[a]

v = 0							v_2 = 1						
J	K	2F'	2F"	ν/MHz	O-C[b]	UC[c]	J	K	2F'	2F"	ν/MHz	O-C[b]	UC[c]
10	3	21	19	15.834	95	50	9	3	19	17	16.110	-76	50
14	3	29	27	13.225	81	60	13	3	27	25	13.741	-62	60
16	4	33	31	11.047	89	100	15	4	31	29	11.283	-55	100
18	4	37	35	10.292	71	30	17	4	35	33	10.545	-53	30
18	5	37	35	9.362	51	60	17	5	35	33	9.512	-17	60
20	5	41	39	8.915	54	60	19	5	39	37	9.067	-40	60
20	6	41	39	8.036	-8	100	19	6	39	37	8.142	-23	100
							19	8	39	37	5.744	-26	30
22	5	45	43	8.446	49	40	21	5	43	41	8.608	-35	40
22	6	45	43	7.820	41	20	21	6	43	41	7.922	-19	20
24	3	49	47	8.686	42	30	23	3	47	45	8.934	-31	30
24	6	49	47	7.513	40	40	23	6	47	45	7.625	-22	40
24	7	49	47	6.930	22	160	23	7	47	45	7.019	5	160
26	2	53	51	8.294	41	30	25	2	51	49	8.524	-28	30
26	3	53	51	8.129	39	30	25	3	51	49	8.331	-20	30
26	4	53	51	7.889	47	30	25	4	51	49	8.060	-34	30
26	5	53	51	7.587	53	60	25	5	51	49	7.722	-29	60
26	6	53	51	7.175	18	80	25	6	51	49	7.292	-40	80
28	2	57	55	7.766	37	20	27	2	55	53	7.954	-34	20
28	3	57	55	7.630	39	30	27	3	55	53	7.797	-39	30
28	4	57	55	7.445	46	60	27	4	55	53	7.588	-36	60
28	5	57	55	7.188	37	40	27	5	55	53	7.325	-25	40
30	4	61	59	7.039	35	50	29	4	59	57	7.172	-34	50
30	5	61	59	6.847	45	50	29	5	59	57	6.973	-12	50
30	6	61	59	6.590	35	50	29	6	59	57	6.704	-11	50
34	6	69	67	6.047	20	70	33	6	67	65	6.153	-13	70
35	6	71	69	5.943	35	50							

[a]Obtained by infrared radiofrequency double resonance. The infrared transition was between the J and K values across from each other in the left and right halves of the table.

[b]Observed minus calculated frequency in kHz. The parameters for the calculation are in Tables 4-6 and 3-8.

[c]Estimated uncertainty in the observed frequency in kHz.

Table 4-9

F=J+1/2 ← F=J-1/2 transitions of $CD_3{}^{81}Br$[a]

v = 0							v_2 = 1						
J	K	2F'	2F"	ν/MHz	O-C[b]	UC[c]	J	K	2F'	2F"	ν/MHz	O-C[b]	UC[c]
12	2	25	23	13.591	94	50	11	2	23	21	14.383	-75	50
12	3	25	23	12.212	93	40	11	3	23	21	12.607	-82	40
16	3	33	31	10.147	114	100	15	3	31	29	10.437	-84	100
16	4	33	31	9.282	84	60	15	4	31	29	9.506	-11	60
18	3	37	35	9.272	93	40	17	3	35	33	9.537	-62	40
20	3	41	39	8.523	76	30	19	3	39	37	8.755	-52	30
20	4	41	39	8.062	48	50	19	4	39	37	8.248	-59	50
22	3	45	43	7.878	57	50	21	3	43	41	8.082	-47	50
22	4	45	43	7.569	75	50	21	4	43	41	7.708	-49	50
22	5	45	43	7.147	75	50	21	5	43	41	7.259	-20	50
24	3	49	47	7.333	50	50	23	3	47	45	7.510	-38	50
24	4	49	47	7.074	44	50	23	4	47	45	7.218	-46	50
24	5	49	47	6.753	49	50	23	5	47	45	6.888	-11	50
24	6	49	47	6.341	36	50	23	6	47	45	6.480	28	50
26	3	53	51	6.872	55	30	25	3	51	49	7.026	-21	30
26	4	53	51	6.665	48	50	25	4	51	49	6.798	-28	50
28	3	57	55	6.472	60	50	27	3	55	53	6.606	-6	50
30	7	61	59	5.349	40	50							
31	5	63	61	5.647	22	60	30	5	61	59	5.792	25	60
31	6	63	61	5.456	18	100	30	6	61	59	5.616	50	100
33	6	67	65	5.248	26	50	32	6	65	63	5.405	65	50

[a]Obtained by infrared radiofrequency double resonance. The infrared transition was between the J and K values across from each other in the left and right halves of the table.

[b]Observed minus calculated frequency in kHz. The parameters for the calculation are in Tables 4-7 and 3-9.

[c]Estimated uncertainty in the observed frequency in kHz.

have arisen as a result of this work. For example, the narrowest lines that we have obtained have a half width at half height of ~70 kHz for CD_3I and ~100 kHz for CD_3Br. We have not yet analyzed sources of the broadening, although the most likely candidates are some combination of RF power broadening, beam transit time broadening, and pressure broadening. It is also necessary to investigate the effect of the nuclear quadrupole coupling of the deuterium nuclei in these molecules, which could give additional linebroadening; however, further study may require more theoretical development for the effect of interaction of quadrupoles between different nuclei. In order to analyze the source of line-broadening, CH_3I is a very good candidate since the molecule provides a strong vibrational band (ν_2) in CO_2 laser region (8), and is free from the perturbation of deuterium nuclei.

A second unresolved question is the source of the many weak satellite lines that accompany the RF transitions. These could be the result of collisional double resonance (9,15), but have not yet been assigned. Probing the intensity and the frequencies of the satellite lines may also shed additional light on energy transfer between rotational levels as well as uusual double resonance effects. An additional interesting subject for future work is observation of A_1-A_2 splittings in the ν_5 doubly-degenerate vibrational bands of CD_3I and CD_3Br. Pure quadrupole transitions of $k = \ell = \pm 1$ states are not allowed due to the single parity of the hyperfine levels, however, A_1-A_2 transitions are allowed for all of the quadrupole components by the opposite parity and may provide further information about the Coriolis interaction between the ν_2 and the ν_5 vibrational states.

IV-5 Appendix

For a symmetric top molecule the principal axes of the quadrupole coupling tensor χ lie along the principal inertial axes of the molecule. Also, $\chi_{xx}=\chi_{yy}$. Therefore, for χ_q, only $\chi_o \neq 0$, and the only non-zero matrix elements of the quadrupole interaction are as follows:

$$\langle J,k,I,F|H_Q|J,k,I,F\rangle = e_1[3k^3-J(J+1)]\chi_{zz} \quad (4\text{-A1})$$

$$\langle J,k,I,F|H_Q|J+1,k,I,F\rangle = -3e_2k[(J+1)^2-k^2]^{1/2}\chi_{zz} \quad (4\text{-A2})$$

$$\langle J,k,I,F|H_Q|J+2,k,I,F\rangle = 3e_3[(J+1)^2-k^2)((J+2)^2-k^2)]^{1/2}\chi_{zz} \quad (4\text{-A3})$$

The abbreviations are

$$e_1 = [3G(G+1)/4-I(I+1)J(J+1)]/2I(2I-1)J(J+1)(2J-1)(2J+1), \quad (4\text{-A4})$$

$$G = F(F+1)-I(I+1)-J(J+1), \quad (4\text{-A5})$$

$$e_2 = \frac{[F(F+1)-I(I+1)-J(J+2)][(F+I+J+2)\cdot(J+I-F+1)(F+J-I+1)(F+I-J)/(2J+1)(2J+3)]^{1/2}}{8I(2I-1)J(J+1)(J+2)}, \quad (4\text{-A6})$$

$$e_3 = \frac{[(F+I+J+2)(F+I+J+3)(I-F+J+1)(I-F+J+2)\cdot(F-I+J+1)(F-I+J+2)(F+I-J-1)(F+I-J)]^{1/2}}{16I(2I-1)(J+1)(J+2)(2J+3)[(2J+1)(2J+5)]^{1/2}}, \quad (4\text{-A7})$$

χ_{zz} is equal to eqQ for a symmetric-top molecule.

IV-6 References

1. S. H. Autler and C. H. Townes, Phys. Rev. **100**, 703-722 (1955).

2. F. J. Wodarczyk and E. B. Wilson, J. Mol. Spectrosc. **37**, 445-463 (1971).
3. F. Shimizu, Chem. Phys. Lett. **17**, 620-622 (1972).

4. R. F. Curl, Jr., T. Oka, and D. S. Smith, J. Mol. Spectrosc. **46**, 518-520 (1973).

5. R. F. Curl, Jr., J. Mol. Spectrosc. **48**, 165-173 (1973).

6. W. A. Kreiner, H. D. Rudolph, and A. G. Robiette, J. Mol. Spectrosc. **91**, 499-502 (1982).

7. W. A. Kreiner and T. Oka, Can. J. Phys. **53**, 2000-2006 (1975).

8. E. Arimondo, P. Glorieux, and T. Oka, Phys. Rev. **A17**, 1375-1393 (1978).

9. P. Glorieux, E. Arimondo, and T. Oka, J. Phys. Chem. **87**, 2133-2141 (1983).

10. D. M. Dale, J. W. C. Johns, A. R. W. McKellar, and M. Riggin, J. Mol. Spectrosc. **67**, 440-458 (1977).

11. R. S. Lowe, A. R. W. McKellar, P. Veillette, and W. L. Meerts, J. Mol. Spectrosc. **88**, 372-377 (1981).

12. M. Allegrini, A. R. W. McKellar, and P. Pinson, J. Chem. Phys. **73**, 6086-6089 (1980).

13. M. Herman, J. W. C. Johns, and A. R. W. McKellar, Can J. Phys. **57**, 397-401 (1979).

14. J. Sakai, A. Mito, M. Katayama, Chem. Phys. Lett. **118**, 600-603 (1985).

15. A. Mito, K. Adomi, J. Sakai, and M. Katayama, J. Mol. Spectosc. **109**, 412-414 (1985).

16. N. Ioli, A. Moretti, G. Moruzzi, P. Roselli, and F. Strumia, J. Mol. Spectrosc. **105**, 284-298 (1984).

17. E. Arimondo and P. Glorieux, J. Mol. Spectrosc. **84**, 559-561 (1980).

18. H.-T. Man and R. J. Butcher, J. Mol. Spectrosc. **110**, 19-26 (1985).

19. H.-T. Man and R. J. Butcher, J. Mol. Spectrosc. **113**, 54-62 (1985).

20. H.-T. Man and R. J. Butcher, J. Mol. Spectrosc. **119**, 51-55 (1986).

21. H.-T. Man and R. J. Butcher, J. Mol. Spectrosc. **107**, 284-291 (1984).

22. W. Fawzy and R. H. Schwendeman, J. Mol. Spectrosc. **120**, 233-235 (1986).

23. W. Fawzy and R. H. Schwendeman, J. Mol. Spectrosc. **130**, 193-203 (1988).

24. M. Takami, J. Chem. Phys. **71**, 4164-4165 (1979).

25. M. Takami, J. Chem. Phys. **73**, 2665-2672 (1980).

26. M. Takami, J. Chem. Phys. **76**, 1670-1676 (1982).

27. M. Takami, J. Chem. Phys. **93**, 250-252 (1982).

28. M. Takami, J. Mol. Spectrosc. **93**, 250-252 (1982).

29. Y. Ohshima, Y Matsumoto, M. Takami, and K. Kuchitsu, J. Chem. Phys. **85**, 5519-5523 (1986).

30. F. Scappini, W. A. Kreiner, J. M. Frye, and T. Oka, J. Mol. Spectrosc. **106**, 436-440 (1984).

31. L. Joerissen, W. A. Kreiner, Y. T. Chen, and T. Oka, J. Mol. Spectrosc. **120**, 233-235 (1986).

32. R. L. DeLeon, P. H. Jones, and J. S. Muenter, Appl. Opt. **20**, 525-527 (1981).

33. C. Pursell, W. C. Ho, F. Scappini, and T. Oka, J. Mol. Spectrosc., **131**, 241-249 (1988).

34. G. Magerl, W. Schupita, and E. Bonek, IEEE J. Quantum Electron. **QE-18**, 1214-1220 (1982).

35. J. W. Simmons, Phys. Rev. **76**, 686 (1949).

36. J. W. Simmons and J. H. Goldstein, J. Chem. Phys. **20**, 122-124 (1952).

37. A. K. Garrison, J. W. Simmons, and C. Alexander, J. Chem. Phys. **45**, 413-415 (1966).

38. R. L. Kuczkowski, J. Mol. Spectrosc. **45**, 261-270 (1973).

39. J. Demaison, D. Boucher, G. Piau, and P. Glorieux, J. Mol. Spectrosc. **107**, 108-118 (1984).

40. G. Wlodarczak, D. Boucher, R. Bocquet, and J. Demaison, J. Mol. Spectrosc. **124**, 53-65 (1987).

41. S. A. Rackley and R. J. Butcher, Mol. Phys. **39**, 1265-1272 (1980).

42. W. Schrepp and H. Dreizler, Z. Naturforsch. **36a**, 654-661 (1981).

43. A. K. Garrison, J. W. Simmons, and C. Alexander, J. Chem. Phys. **45**, 413-415 (1966).

44. Y. Morino and C. Hirose, J. Mol. Spectrosc. **24**, 204-224 (1967).

45. A. R. Edmonds, "Angular Momentum in Quantum Mechnics," McGraw-Hill, New York, 1955.

46. H. P. Benz, A. Bauder, and Hs. H. Gunthard, J. Mol. Spectrosc. **21**, 156-164 (1966).

47. H. Dreizler, W. Schrepp, and R. Schwarz, Z. Naturforsch. **A34**, 571-574 (1979).

48. K. Harada, K. Tanaka, and T. Tanaka, J. Mol. Spectrosc. **98**, 349-374 (1983).

49. R. C. Hilborn, T. F. Gallagher, Jr., and N. F. Ramsey, J. Chem. Phys. **56**, 855-81 (1972).

50. H. H. Brown and J. G. King, Phys. Rev. **142**, 53-59 (1966).

51. C. Freed, L. C. Bradley, and R. G. O'Donnell, IEEE J. Quantum Electron. **QE-16**, 1195-1206 (1980).

CHAPTER V

FOUR-INTERACTING-LEVEL DOUBLE RESONANCE

V-1 Introduction

As mentioned in the previous chapter, the preliminary fittings of the pure quadrupole transitions of CD_3Br revealed some problem with the low-frequency RF spectra. The nature of the problem may be seen by reference to the energy-level diagram in Fig. 5-1, which shows a typical hyperfine pattern for a single J and k in the ground vibrational state coupled by the infrared radiation to a typical hyperfine pattern for J' and k' in the $v_2 = 1$ state. It may be seen that the allowed RF transitions include two transitions of relatively high frequency and one transition of relatively low frequency for each of the two vibrational states. Because the hyperfine splittings in the upper state are not greatly different from those in the lower state for the double resonances in this work and because of the near symmetry of the patterns, the four upper frequencies are comparable and the two lower frequencies are comparable. Generally, the two lower frequencies are more severely overlapped than the higher frequencies. Finally, each pair of comparable frequencies has an energy level pattern similar to that shown in Fig. 5-2, in which it may be seen that both the upper and lower states of both RF transitions are pumped by the infrared radiation. The least squares adjustment of the hyperfine constants to fit the experimental frequencies showed that the experimental values for

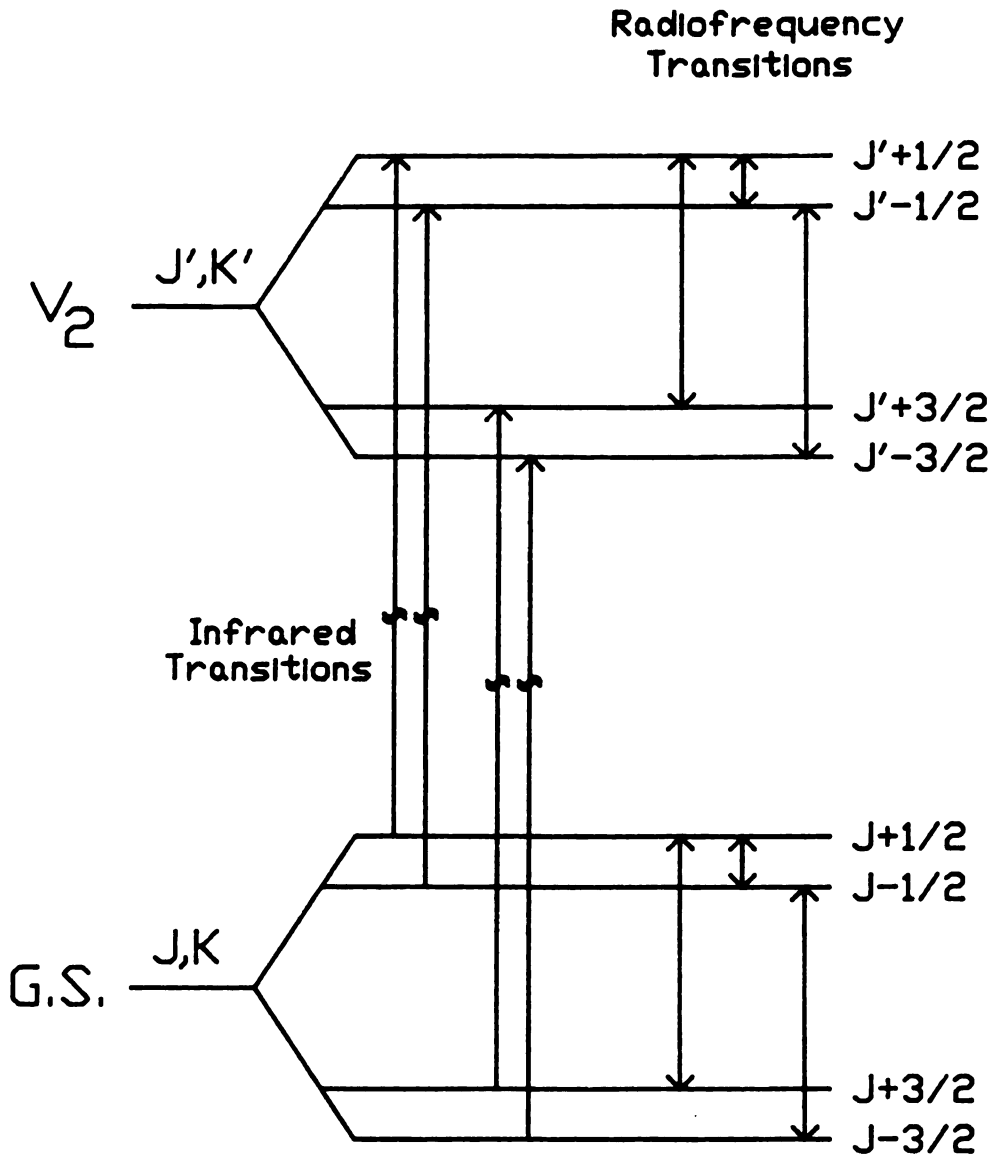

Figure 5-1. Typical energy level pattern for the infrared radiofrequency double resonance observed for CD_3Br. A single infrared frequency pumps all of the allowed infrared transitions by interacting with molecules in different velocity groups. In general, four high-frequency and two low-frequency double resonances were observed for each infrared transition.

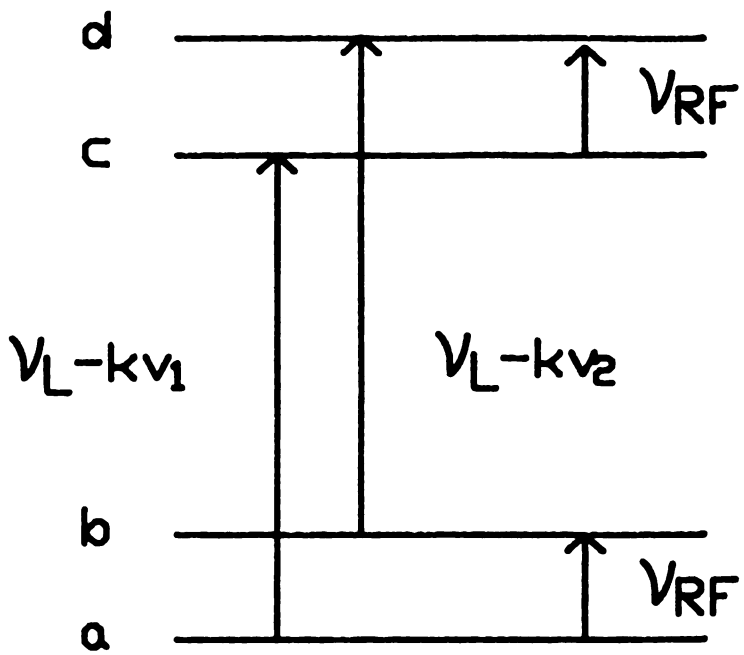

Figure 5-2. Energy level diagram for the four-interacting-level double resonance system.

the two lowest radiofrequency transitions were too close together; the lower frequency of the pair almost always showed a positive residual (observed - calculated) while the upper frequency showed a negative residual. This was finally traced to a double-resonance effect that appears to be unique to an energy-level pattern like that in Fig. 5-2, a pattern that we refer to as a "four-interacting-level double resonance". Double resonance for the four-level system in Fig. 5-2 has been treated by Small *et al.* (1), but in their case the millimeter wave frequency (corresponding in our case to the IR frequency) was scanned while the RF was fixed. In our study, it has been found that the magnitude of the shift in frequencies depends on the difference in frequency of the two overlapped lines, the Rabi frequencies for the IR and RF radiation, and the pressure broadening.

V-2 Theory

The purpose of this section is to describe the density matrix treatment used to calculate the lineshape of the double-resonance spectra obtained for the case of four interacting levels. The energy levels and allowed transitions for the four levels are shown in Fig. 5-2. The procedure followed is to set up and solve numerically the density matrix equations for the four levels in the presence of two radiation fields. The equations are solved for a sequence of values for the component of the velocity in the direction of the two beams and the resulting lineshapes are weighted by the appropriate Boltzmann factor and summed. Only the infrared frequencies are assumed to be affected by the Doppler averaging, since the Doppler shifts at the radiofrequencies involved are much smaller than the Lorentz widths of the double resonances. The density matrix equation is as follows:

$$\frac{d\rho}{dt} = -\frac{i}{\hbar}[H,\rho] - K(\rho - \rho^{o}) \quad . \tag{5-1}$$

Here, ρ is the density matrix, ρ^{o} is the density matrix at thermal equilibrium, and K is a supermatrix of relaxation coefficients. The Hamiltonian H is in two parts,

$$H = H^{(0)} + H^{(1)} , \tag{5-2}$$

in which $H^{(0)}$ is the Hamiltonian for the rovibrational energy including the quadrupole coupling, and $H^{(1)}$ describes the interaction with the two

radiation fields. A matrix element of $H^{(1)}$ is

$$H^{(1)}_{jk} = H^{(1)}_{kj} = -\mu_{jk}(\varepsilon_1 \cos 2\pi\nu_1 t + \varepsilon_2 \cos 2\pi\nu_2 t) . \quad (5\text{-}3)$$

In this expression, ε_1 and ε_2 are the peak electric fields and ν_1 and ν_2 are the frequencies of the laser and radiofrequency fields, respectively; it is assumed that $\nu_1 = \nu_L - k\nu_1 \approx E_c - E_a \approx E_d - E_b$ and $\nu_2 \approx \nu_1 \approx E_b - E_a \approx E_d - E_c$ in which the E_j are eigenvalues of $H^{(0)}$ for the energy levels shown in Fig. 5-2, ν_L the infrared laser frequency, $k = (\nu_L/c)$ and v is the component of molecular velocity in the direction of the beam; Doppler effects are assumed to be negligible at the radiofrequency ν_R. Of the dipole transition moments, we assume that μ_{ba}, μ_{ca}, μ_{db}, and μ_{dc} are all real and are the only non-zero elements.

For the four levels in Fig. 5-2, the density matrix contains 4 real diagonal elements and 6 complex elements above the diagonal that are complex conjugates of the elements below the diagonal as follows;

$$\dot{\rho}_{aa} = -(i/\hbar)(H^{(1)}_{ab}\rho_{ba} + H^{(1)}_{ac}\rho_{ca} - \rho_{ab}H^{(1)}_{ba} - \rho_{ac}H^{(1)}_{ca}) - k_{aa}\Delta\rho_{aa} \quad (5\text{-}4)$$

$$\dot{\rho}_{bb} = -(i/\hbar)(H^{(1)}_{ba}\rho_{ab} + H^{(1)}_{bd}\rho_{db} - \rho_{ba}H^{(1)}_{ab} - \rho_{bd}H^{(1)}_{db}) - k_{bb}\Delta\rho_{bb} \quad (5\text{-}5)$$

$$\dot{\rho}_{cc} = -(i/\hbar)(H^{(1)}_{ca}\rho_{ac} + H^{(1)}_{cd}\rho_{dc} - \rho_{ca}H^{(1)}_{ac} - \rho_{cd}H^{(1)}_{dc}) - k_{cc}\Delta\rho_{cc} \quad (5\text{-}6)$$

$$\dot{\rho}_{dd} = -(i/\hbar)(H^{(1)}_{db}\rho_{bd} + H^{(1)}_{dc}\rho_{cd} - \rho_{db}H^{(1)}_{bd} - \rho_{dc}H^{(1)}_{cd}) - k_{dd}\Delta\rho_{dd} \quad (5\text{-}7)$$

$$\dot{\rho}_{ba} = -(i/\hbar)(H^{(1)}_{ba}\rho_{aa} + H^{(1)}_{bd}\rho_{da} - \rho_{bc}H^{(1)}_{ca} - \rho_{bb}H^{(1)}_{ba}) - (i\nu_{ba} + k_{ba})\rho_{ba} \quad (5\text{-}8)$$

$$\dot{\rho}_{ca} = -(i/\hbar)(H^{(1)}_{ca}\rho_{aa} + H^{(1)}_{cd}\rho_{da} - \rho_{cc}H^{(1)}_{ca} - \rho_{cb}H^{(1)}_{ba}) - (i\nu_{ca} + k_{ca})\rho_{ca} \quad (5\text{-}9)$$

$$\dot{\rho}_{da} = -(i/\hbar)(H^{(1)}_{db}\rho_{ba} + H^{(1)}_{dc}\rho_{ca} - \rho_{dc}H^{(1)}_{ca} - \rho_{db}H^{(1)}_{ba}) - (i\nu_{da} + k_{da})\rho_{da} \quad (5\text{-}10)$$

$$\dot{\rho}_{cb}=-(i/\hbar)(H^{(1)}_{ca}\rho_{ab}+H^{(1)}_{ad}\rho_{db}-\rho_{ca}H^{(1)}_{ab}-\rho_{cd}H^{(1)}_{db})-(i\nu_{cb}+k_{cb})\rho_{cb} \quad (5\text{-}11)$$

$$\dot{\rho}_{db}=-(i/\hbar)(H^{(1)}_{db}\rho_{bb}+H^{(1)}_{dc}\rho_{cb}-\rho_{da}H^{(1)}_{ab}-\rho_{dd}H^{(1)}_{db})-(i\nu_{db}+k_{db})\rho_{db} \quad (5\text{-}12)$$

$$\dot{\rho}_{dc}=-(i/\hbar)(H^{(1)}_{db}\rho_{bc}+H^{(1)}_{dc}\rho_{cc}-\rho_{da}H^{(1)}_{ac}-\rho_{dd}H^{(1)}_{dc})-(i\nu_{dc}+k_{dc})\rho_{dc} \ . \quad (5\text{-}13)$$

To write Eq. (5-4) to (5-13), the relaxation supermatrix K has been assumed to have a particularly simple form.

In preparation for using the rotating-wave approximation, which assumes that the oscillating electric field of the radiation is too fast to be detected by experimental apparatus, we make the following substitution for the off-diagonal elements of ρ:

$$\rho_{jk} = \bar{\rho}_{jk}\exp(-2\pi i\nu_n t) \ . \quad (5\text{-}14)$$

Here, ν_n is ν_2, ν_1, $\nu_1+\nu_2$, $\nu_1-\nu_2$, ν_1, and ν_2 for jk = ba, ca, da, cb, db, and dc, respectively. After this substitution and elimination of common factors of $\exp(-2\pi i\nu_n t)$, all terms that oscillate at radiofrequencies or higher are eliminated. The resulting equations are;

$$\dot{\rho}_{aa}=(i/2)[x_2(d_{ba}-d_{ab})+x_1(d_{ca}-d_{ac})]-k_{aa}\Delta\rho_{aa} \quad (5\text{-}15)$$

$$\dot{\rho}_{bb}=(i/2)[x_2(d_{ab}-d_{ba})+x_3(d_{db}-d_{bd})]-k_{bb}\Delta\rho_{bb} \quad (5\text{-}16)$$

$$\dot{\rho}_{cc}=(i/2)[x_1(d_{ac}-d_{ca})+x_4(d_{dc}-d_{cd})]-k_{cc}\Delta\rho_{cc} \quad (5\text{-}17)$$

$$\dot{\rho}_{dd}=(i/2)[x_3(d_{bd}-d_{db})+x_4(d_{cd}-d_{dc})]-k_{dd}\Delta\rho_{dd} \quad (5\text{-}18)$$

$$\dot{\bar{\rho}}_{ba}=(i\delta_{ba}-k_{ba})d_{ba}+(i/2)[x_2(\rho_{aa}-\rho_{bb})+x_3d_{da}-x_1d_{bc})] \quad (5\text{-}19)$$

$$\dot{\bar{\rho}}_{ca}=(i\delta_{ca}-k_{ca})d_{ca}+(i/2)[x_1(\rho_{aa}-\rho_{cc})+x_4d_{da}-x_2d_{cb})] \quad (5\text{-}20)$$

$$\dot{\bar{\rho}}_{da}=(i\delta_{da}-k_{da})d_{da}+(i/2)[x_3\rho_{ba}+x_4\rho_{ca})-x_1d_{dc}-x_2d_{db})] \quad (5\text{-}21)$$

$$\dot{\bar{\rho}}_{db}=(i\delta_{db}-k_{db})d_{db}+(i/2)[x_3(\rho_{bb}-\rho_{dd})+x_4d_{cb}-x_2d_{da})] \quad (5\text{-}22)$$

$$\dot{\bar{\rho}}_{dc}=(i\delta_{dc}-k_{dc})d_{ba}+(i/2)[x_3d_{bc}+x_4(\rho_{cc}-\rho_{dd})-x_1d_{da})] \quad (5\text{-}23)$$

$$\dot{\bar{\rho}}_{cb}=(i\delta_{cb}-k_{cb})d_{cb}+(i/2)[x_1\rho_{ab}+x_4\rho_{db}-x_2d_{ca}-x_3d_{cd})] \ . \quad (5\text{-}24)$$

In these equations, the non-oscillating part of each off-diagonal element ($\bar{\rho}_{jk}$) has been represented by

$$\bar{\rho}_{jk}= d'_{jk} + i\ d''_{jk} \ , \quad (5\text{-}25)$$

where d'_{jk}, and d''_{jk} are real numbers that account the real and imaginary parts of the off-diagonal element. There are, therefore, 16 real numbers that must be specified to define the density matrix. It is possible to write the 4 diagonal elements and the 6 real and 6 imaginary parts of the off-diagonal elements as a column matrix, in which case the supermatrix K in Eq. (5-1) becomes an ordinary two-dimensional matrix, which is diagonal for the form of the relaxation elements in Eq. (5-15) - (5-24). For simplicity, we have made the further assumption that the diagonal elements are k_d and k_o for the relaxation rates for the diagonal and off-diagonal elements of ρ, respectively. For the calculations here, it was further assumed that $k_d = k_o$. The next step is to make the steady-state approximation in which the time derivatives of the ρ_{jj}'s and the d_{jk}'s are set equal to zero. The result is a

linear system, as follows:

$$A\,D = B \qquad (5\text{-}26)$$

in which D is a vector of the diagonal elements of the density matrix and the real and imaginary parts of the ρ_{jk}. The order of the elements in D is such that the transposes of D and B are

$$\tilde{D} = (\rho_{aa}\ d'_{ba}\ d''_{ba}\ \rho_{bb}\ d'_{ca}\ d''_{ca}\ \rho_{cc}\ d'_{db}\ d''_{db}\ \rho_{dd}\ d'_{dc}\ d''_{dc}\ d'_{cb}\ d''_{cb}\ d'_{da}\ d''_{da}) \ . \qquad (5\text{-}27)$$

$$\tilde{B} = -k_d\,(\rho^{o}_{aa}\ 0\ 0\ \rho^{o}_{bb}\ 0\ 0\ \rho^{o}_{cc}\ 0\ 0\ \rho^{o}_{dd}\ 0\ 0\ 0\ 0\ 0\ 0) \ . \qquad (5\text{-}28)$$

Finally, the matrix A is the following:

$$A = \begin{bmatrix}
-k_d & 0 & -x_2 & 0 & 0 & -x_1 & 0 & 0 & 0 & 0 & 0 & 0 & 0 & 0 & 0 & 0 \\
0 & -k_o & -\delta_2 & 0 & 0 & 0 & 0 & 0 & 0 & 0 & 0 & 0 & 0 & -x_1/2 & 0 & -x_3/2 \\
x_2/2 & \delta_2 & -k_o & -x_2/2 & 0 & 0 & 0 & 0 & 0 & 0 & 0 & 0 & -x_1/2 & 0 & x_3/2 & 0 \\
0 & 0 & x_2 & -k_d & 0 & 0 & 0 & 0 & -x_3 & 0 & 0 & 0 & 0 & 0 & 0 & 0 \\
0 & 0 & 0 & 0 & -k_o & -\delta_1 & 0 & 0 & 0 & 0 & 0 & 0 & 0 & x_2/2 & 0 & -x_4/2 \\
x_1/2 & 0 & 0 & 0 & \delta_1 & -k_o & -x_1/2 & 0 & 0 & 0 & 0 & 0 & -x_2/2 & 0 & x_4/2 & 0 \\
0 & 0 & 0 & 0 & 0 & x_1 & -k_d & 0 & 0 & 0 & 0 & -x_4 & 0 & 0 & 0 & 0 \\
0 & 0 & 0 & 0 & 0 & 0 & 0 & -k_o & -\delta_3 & 0 & 0 & 0 & 0 & -x_4/2 & 0 & x_2/2 \\
0 & 0 & 0 & x_3/2 & 0 & 0 & 0 & \delta_3 & -k_o & -x_3/2 & 0 & 0 & x_4/2 & 0 & -x_2/2 & 0 \\
0 & 0 & 0 & 0 & 0 & 0 & 0 & 0 & x_3 & -k_d & 0 & x_4 & 0 & 0 & 0 & 0 \\
0 & 0 & 0 & 0 & 0 & 0 & 0 & 0 & 0 & 0 & -k_o & -\delta_4 & 0 & x_3/2 & 0 & x_1/2 \\
0 & 0 & 0 & 0 & 0 & 0 & x_4/2 & 0 & 0 & -x_4/2 & \delta_4 & -k_o & x_3/2 & 0 & -x_1/2 & 0 \\
0 & 0 & x_1/2 & 0 & 0 & x_2/2 & 0 & 0 & -x_4/2 & 0 & 0 & -x_3/2 & -k_o & \delta_2-\delta_1 & 0 & 0 \\
0 & x_1/2 & 0 & 0 & -x_2/2 & 0 & 0 & x_4/2 & 0 & 0 & -x_3/2 & 0 & \delta_1-\delta_2 & -k_o & 0 & 0 \\
0 & 0 & -x_3/2 & 0 & 0 & -x_4/2 & 0 & 0 & x_2/2 & 0 & 0 & x_1/2 & 0 & 0 & -k_o & -\delta_2-\delta_3 \\
0 & x_3/2 & 0 & 0 & x_4/2 & 0 & 0 & -x_2/2 & 0 & 0 & -x_1/2 & 0 & 0 & 0 & \delta_2+\delta_3 & -k_o
\end{bmatrix} \qquad (5\text{-}29)$$

In the matrix, $x_1 = \mu_{ca}\varepsilon_1/h$, $x_2 = \mu_{ba}\varepsilon_2/h$, $x_3 = \mu_{db}\varepsilon_1/h$, and $x_4 = \mu_{dc}\varepsilon_2/h$. Also, $\delta_1 = \nu_1(1-v/c) - \nu_{ca}$, $\delta_2 = \nu_2 - \nu_{ba}$, $\delta_3 = \nu_1(1-v/c) - \nu_{db}$, and $\delta_4 = \nu_2 - \nu_{dc}$. In these equations v is the component of the molecular velocity in the direction of the laser beam, c is the speed of light, and $\nu_{jk} = (E_j - E_k)/h$.

In order to calculate the spectrum, the linear system is solved for a fixed value of the laser frequency, ν_1, and sequences of values of the velocity component v and the RF frequency ν_2. For each of these solutions, the contribution to a quantity α, which is proportional to the absorption of the laser radiation, is calculated as

$$\alpha = x_1 d''_{ca} + x_3 d''_{db} . \qquad (5\text{-}30)$$

This equation is set by the fact that the infrared absorption is proportional to the product of the Rabi-frequency (x_i) and the imaginary part of the corresponding off-diagonal element of the density matrix. The calculation is repeated for $x_2 = x_4 = 0$ in which case Eq. (5-26) becomes a 6x6 linear system since the hyperfine levels are not connected any more. It is then possible to derive an analytical expression for α, as follows:

$$\alpha_o = x_1 d''^{o}_{ca} + x_3 d''^{o}_{db}$$

$$= \frac{\frac{1}{2}\frac{k_o}{k_d}\{x_1^2 D_1[(\delta_3^2+k_o^2)+x_3^2\frac{k_o}{k}] + x_1^2 D_3(\delta_3^2+k_o^2) + x_3^2 D_3[(\delta_1^2+k_o^2)+x_1^2\frac{k_o}{k_d}] + x_3^2 D_1(\delta_1^2+k_o^2)\}}{\{[(\delta_1^2+k_o^2)+x_1^2\frac{k_o}{k_d}][(\delta_3^2+k_o^2)+x_3^2\frac{k_o}{k_d}]-(\delta_3^2+k_o^2)(\delta_1^2+k_o^2)} , \qquad (5\text{-}31)$$

where $D_1 = \rho^o_{aa} - \rho^o_{cc}$ and $D_3 = \rho^o_{bb} - \rho^o_{dd}$. The intensities of the double-resonance spectra are then proportional to the differences, $\Delta\alpha = \alpha - \alpha_o$. The values of $\Delta\alpha$ for the v values for a given ν_2 are multiplied by the Boltzmann weight factor $\exp(-v^2/u^2)$ and summed. Here, $u^2 = 2k_BT/m$ where k_B is the Boltzmann constant and m is the molecular mass. For the numerical integration, it is necessary to insure that the interval in v is sufficiently small and that the range of v includes the important contributions to the integral. It has been found that the interval in $\nu_1 v/c$ must be smaller than the smaller of k_d or k_o and that the range of $\nu_1 v/c$ must include at least several times the larger of k_d or k_o on either side of the v values for the resonant velocity groups (there are in general two resonant values of v in the four-interacting-level case).

V-3 Results and Discussion

The effect of the four-interacting-level double-resonance was discovered by calculating the lineshape for a selected doublet by means of Eq. (5-9) under conditions as close as could be estimated to the experimental conditions. An example of the comparison of observed and calculated lineshapes is shown in Fig. 5-3. The conditions used for the calculation are given in the caption for the figure. We have no value for the transition moment for the infrared transition and could only estimate the Rabi frequency to be about 20 kHz by assuming 0.01 Debye as the transition dipole moment (2,3). The Rabi frequency for the radiofrequency transition was calculated from the measured value of the amplitude of the RF field and the known permanent dipole moment for CD_3Br (1.83 D (4)) by using the dipole moment matrix elements given by Benz et al. (5). The only questionable point in this calculation is the method used to average over the spatial degeneracy. We used an average over the m states weighted by the expected intensity of the double resonance and obtained values of 5-80 kHz for the various transitions. Also needed for the double resonance calculation are the effective relaxation parameters; we used the halfwidth at half-maximum for the double resonances, 100 kHz.

The observed and calculated lineshapes in Fig. 5-3 were each fit by least squares to a sum of two Lorentz functions and the resulting residuals are plotted below each line. The agreement between the two plots of the residuals in both appearance and magnitude provides strong confirmation of the proposed four-interacting-level double resonance effect. If conventional 3-level double resonance equations (3,6) are

Figure 5-3. Comparison of observed and calculated infrared radiofrequency double resonance spectra for a four-interacting-level double resonance system. The upper trace is the calculated spectrum and the lower trace is the observed spectrum. The points below each trace are the residuals obtained when the lineshape is fitted by least squares to a sum of two Lorentz lineshapes. The experimental spectrum was observed with a sample pressure of 4 mTorr, infrared power ~2 mW, and radiofrequency power ~20 mW. The theoretical spectrum was calculated by means of Equation (5-26) with all x_i = 20 kHz and with $k_d = k_o$ = 100 kHz. For the experimental spectrum, the infrared frequency was set at the center frequency of the Doppler-limited lineshape of the P(26,4) transition in the ν_2 band of $CD_3{}^{79}Br$; the 10R(22) $^{12}C^{16}O_2$ laser was used with the lower frequency sideband generated by a microwave frequency of 12632 MHz.

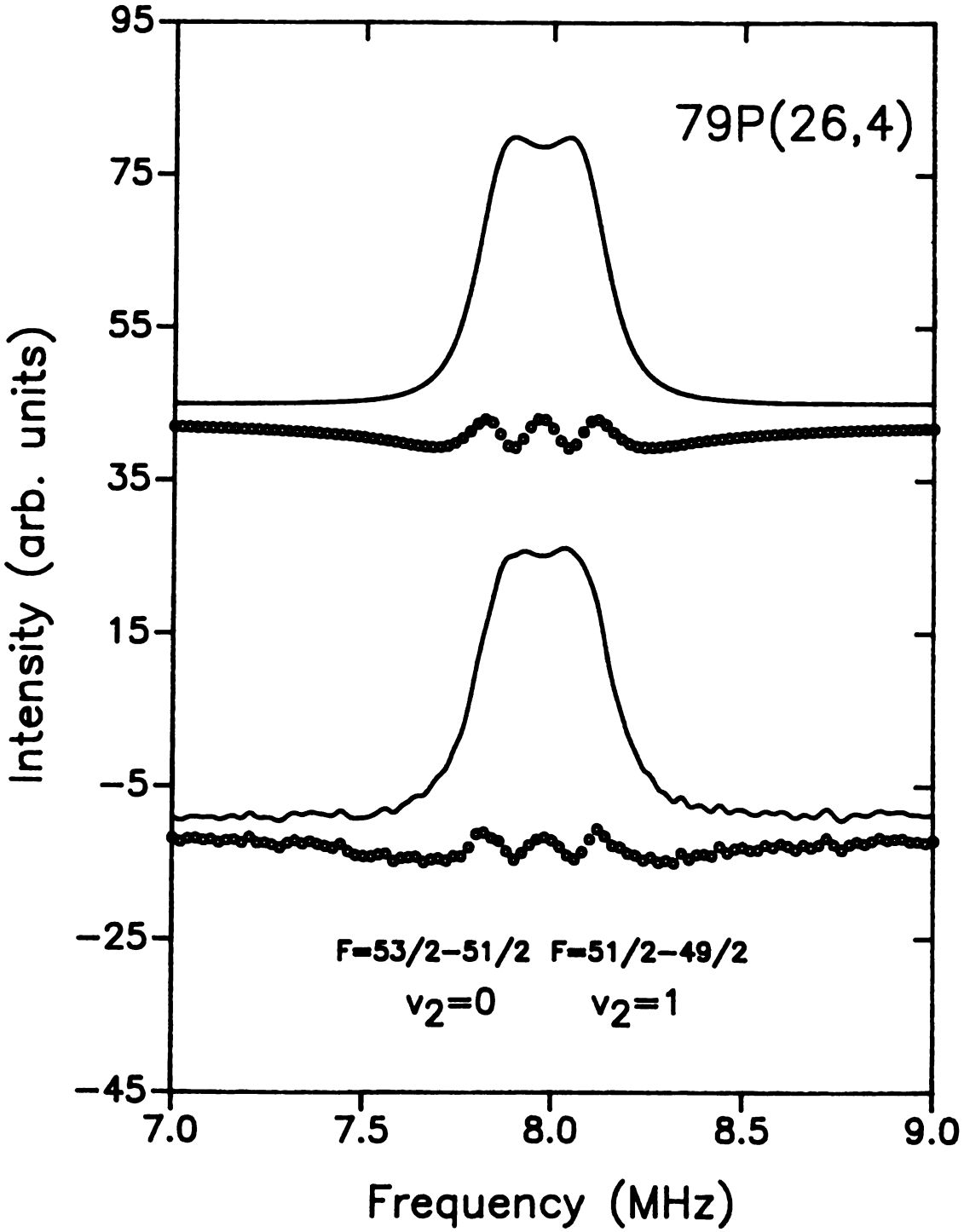
79P(26,4)
95
75
55
35
15
-5
-25
-45
Intensity (arb. units)
F=53/2-51/2 F=51/2-49/2
v2=0 v2=1
7.0
7.5
8.0
8.5
9.0
Frequency (MHz)

used to calculate the spectra, it is found for the conditions in this work that the lineshapes are almost perfect Lorentz functions centered at the predicted frequency. The two Lorentz functions obtained from the fitting of the calculated lineshape in Fig. 5-3 are each shifted by 40 kHz from their expected value; the lower frequency transition is shifted to higher frequency and vice-versa. Examination of the residuals in Tables 4-8 and 4-9 shows that 40 kHz is of the correct order of magnitude to explain the observed frequency shifts.

After discovering this effect, the next question was whether there was a corresponding shift in frequency for the other double resonances, because, as mentioned above, both the upper and lower levels of every RF transition are pumped. Such a difficulty did not seem probable because the residuals for the high-frequency double resonances were much smaller than for the low-frequency transitions, even when the low-frequency transitions were included in the fit. Nevertheless, a series of lineshape calculations have been carried out with 20 kHz for Rabi frequencies, with 100 kHz for the Lorentz widths, and with varying values of the separation in frequency of the two double-resonance transitions. The computed lineshapes were fit to a sum of two Lorentz functions and the difference between the center frequency of the lower frequency Lorentz component and the expected value is plotted in Fig. 5-4 as a function of the separation of the two peaks. It may be seen that the shift ranges from about 45 kHz for a separation of 0.3 MHz to less than 5 kHz for separations greater than 4 MHz. These values were surprising to us in view of the rather small Rabi frequencies involved.

A final point is that examination of the radiofrequencies obtained for a single pumping frequency shown in Tables 4-4 and 4-5 will reveal a

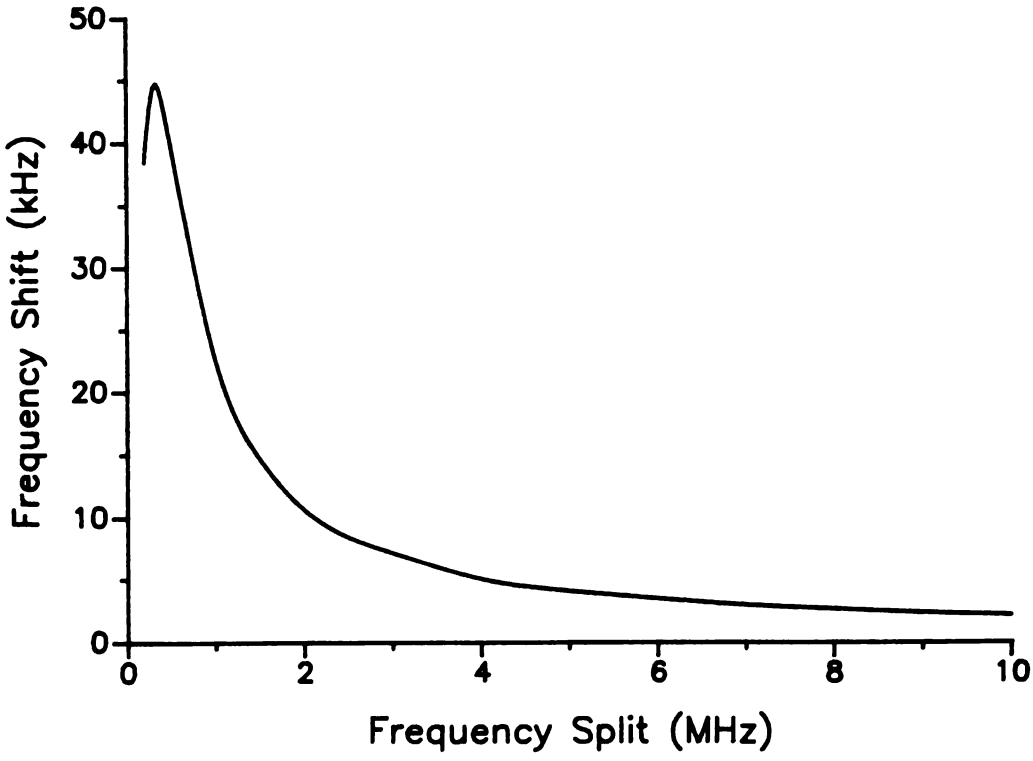

Figure 5-4. Plot of the frequency shift caused by the four-interacting-level double resonance effect against the assumed frequency splitting between the two lower frequency hyperfine transitions for the conditions described in Fig. 5-3. The vertical axis is the difference in frequency between the center of the best Lorentz line approximation to the calculated lineshape and the assumed hyperfine frequency for the lower-frequency component of the infrared radiofrequency double resonance doublet. All of the conditions for the calculated lineshape in Fig. 5-3 apply, except that the difference between the hyperfine frequency in the upper vibrational state (ν_{cd}) and that in the lower vibrational state (ν_{ba}) is varied. This difference is plotted on the horizontal axis.

number of strongly overlapped lines, which might be expected to be shifted. In these cases, however, the overlapped lines do not involve four interacting levels, as shown in Fig. 5-1. We believe, and the residuals in Tables 4-4 and 4-5 seem to confirm our belief, that the shifts occur only when the two transitions occur between four interacting levels. The calculation should probably be done for the eight-level system, but the necessary algebra and computer time are both formidable.

As has been shown, the frequency shifts of RF-transitions in low frequency region have been traced to a result of a four-interacting-level double-resonance. The amount of frequency shift and the distorted lineshape were calculated numerically by the use of density matrix; the calculated frequency shift and lineshape with the estimated input parameters show good agreements with the experimentally obtained values. Considering the amount of shift in frequency, the four-interacting-level double-resonance effect must be taken into account in the assessment of measured frequencies, especially for overlapped transitions in the low frequency region.

V-4 References

1. C. E. Small, J. G. Smith, and D. H. Whiffen, Mol. Phys. **37**, 681-688 (1979).

2. J. W. Russell, C. D. Needham, and J. Overend, J Chem. Phys. **45**, 3383-3398 (1966).

3. S. T. Sandholm and R. H. Schwendeman, J. Chem. Phys. **78**, 3476-3482 (1983).

4. K. Harada, K. Tanaka, and T. Tanaka, J. Mol. Spectrosc. **98**, 349-374 (1983).

5. H. P. Benz, A. Bauder, and Hs. H. Gunthard, J. Mol. Spectrosc. **21**, 156-164 (1966).

6. M. Takami, Jpn. J. Appl. Phys. **15**, 1063-1071 (1976); Jpn. J. Appl. Phys. **15**, 1889-1897 (1976).